



U.S. Department
of Transportation
**National Highway
Traffic Safety
Administration**



DOT HS 811 492C

September 2011

Vehicle Safety Communications – Applications (VSC-A)

Final Report: Appendix Volume 2 Communications and Positioning



DISCLAIMER

This publication is distributed by the U.S. Department of Transportation, National Highway Traffic Safety Administration, in the interest of information exchange. The opinions, findings, and conclusions expressed in this publication are those of the authors and not necessarily those of the Department of Transportation or the National Highway Traffic Safety Administration. The United States Government assumes no liability for its contents or use thereof. If trade names, manufacturers' names, or specific products are mentioned, it is because they are considered essential to the object of the publication and should not be construed as an endorsement. The United States Government does not endorse products or manufacturers.

Technical Report Documentation Page

1. Report No. DOT HS 811 492C	2. Government Accession No.	3. Recipient's Catalog No.	
4. Title and Subtitle Vehicle Safety Communications – Applications (VSC-A) Final Report: Appendix Volume 2 Communications and Positioning		5. Report Date September 2011	
		6. Performing Organization Code	
7. Authors Ahmed-Zaid, F., Bai, F., Bai, S., Basnayake, C., Bellur, B., Brovold, S., Brown, G., Caminiti, L., Cunningham, D., Elzein, H., Hong, K., Ivan, J., Jiang, D., Kenney, J., Krishnan, H., Lovell, J., Maile, M., Masselink, D., McGlohon, E., Mudalige, P., Popovic, Z., Rai, V., Stinnett, J., Tellis, L., Tirey, K., VanSickle, S.		8. Performing Organization Report No.	
		10. Work Unit No. (TRAIS)	
9. Performing Organization Name and Address Crash Avoidance Metrics Partnership on behalf of the Vehicle Safety Communications 2 Consortium 27220 Haggerty Road, Suite D-1 Farmington Hills, MI 48331		11. Contract or Grant No. DTNH22-05-H-01277	
		13. Type of Report and Period Covered Final Report Dec. 8, 2006, through Dec. 7, 2009	
12. Sponsoring Agency Name and Address NHTSA Headquarters 1200 New Jersey Avenue, SE West Building Washington, DC 20590 Research and Innovative Technology Administration U.S. Department of Transportation 1200 New Jersey Avenue, SE East Building Washington, DC 20590		14. Sponsoring Agency Code	
		15. Supplementary Notes	
16. Abstract The Vehicle Safety Communications – Applications (VSC-A) Project was a three-year project (December 2006 - December 2009) to develop and test communications-based vehicle-to-vehicle (V2V) safety systems to determine if Dedicated Short Range Communications (DSRC) at 5.9 GHz, in combination with vehicle positioning, can improve upon autonomous vehicle-based safety systems and/or enable new communications-based safety applications. The VSC-A Project was conducted by the Vehicle Safety Communications 2 Consortium (VSC2). Members of VSC2 are Ford Motor Company, General Motors Corporation, Honda R & D Americas, Inc., Mercedes-Benz Research and Development North America, Inc., and Toyota Motor Engineering & Manufacturing North America, Inc. This document presents the second volume set of appendices for the Final Report of the VSC-A Project which contains technical content for the Communications Power Testing, Multi-Channel Operations, Relative Positioning Software Performance Analysis, GPS Service Availability Study Literature Review and Final Report, and Multiple-OBE Scalability Testing Results.			
17. Key Word		18. Distribution Statement Document is available to the public from the National Technical Information Service www.ntis.gov	
19. Security Classif. (of this report) Unclassified	20. Security Classif. (of this page) Unclassified	21. No. of Pages 339	22. Price

Table of Contents

Appendix D-1	Communications Power Testing
Appendix D-2	Multi-Channel Operations
Appendix E-1	Relative Positioning Software Performance Analysis
Appendix E-2	<i>Prepared by: PLAN Group University of Calgary</i>
Appendix E-3	GPS Service Availability Study Final Report <i>Prepared by: PLAN Group University of Calgary</i>
Appendix I	Multiple-OBE Scalability Testing Results

VSC-A Final Report: Appendix D-1
Communications Power Testing

List of Acronyms

BSW	Blind Spot Warning
CAMP	Crash Avoidance Metrics Partnership
CLW	Control Loss Warning
dBm	Decibels relative to 1 Milliwatt
DGPS	Differential GPS
DNPW	Do Not Pass Warning
DSRC	Dedicated Short Range Communications
EEBL	Emergency Electronic Brake Lights
EIRP	Equivalent Isotropically Radiated Power
EVM	Error Vector Magnitude
FCW	Forward Collision Warning
GPS	Global Positioning System
IMA	Intersection Movement Assist
ITS	Intelligent Transportation Systems
LCW	Lane Change Warning
LOS	Line Of Sight
Mbps	MegaBits Per Second (10^6 bits/second)
NHTSA	National Highway Traffic Safety Administration
NLOS	Non Line Of Sight
PER	Packet Error Rate
RF	Radio Frequency
RSSI	Received Signal Strength Indication
VSC2	Vehicle Safety Communications 2
VSC-A	Vehicle Safety Communications – Applications
V-V or V2V	Vehicle-to-Vehicle
WSU	Wireless Safety Unit

Table of Contents

List of Acronyms.....	D-1-iv
1 Overview.....	D-1-1
2 Testing Overview	D-1-1
2.1 Relevant VSC-A Applications	D-1-1
3 Hardware Setup	D-1-2
3.1 Calibration	D-1-3
4 Test Results and Summary.....	D-1-6
4.1 Interpreting Data Graphs	D-1-7
5 Baseline Line-of-Sight Scenario Tests	D-1-8
5.1 Location Overview	D-1-9
5.2 Data Analysis	D-1-9
5.3 Baseline LOS Scenario Observations.....	D-1-11
6 Baseline Shadowing Scenario Test	D-1-12
6.1 Data Analysis	D-1-12
6.2 Baseline Shadowing Scenario Observations	D-1-15
7 Urban-Straight-Line Scenario Test.....	D-1-16
7.1 Location Overview	D-1-16
7.2 Data Analysis	D-1-17
7.3 Urban-Straight-Line Scenario Observations	D-1-19
8 Urban-Closed-Intersection Scenario Test	D-1-20
8.1 Location Overview	D-1-20
8.2 Data Analysis	D-1-21
8.3 Observations for Urban-Closed-Intersection Scenario.....	D-1-27
9 Urban-³/₄-Open-Intersection Scenario Test	D-1-28
9.1 Location Overview	D-1-28
9.2 Data Analysis	D-1-30
9.3 Observations for Urban- ³ / ₄ -Open-Intersection Scenario.....	D-1-35
9.4 Comparison of Urban-Closed-Intersection and Urban- ³ / ₄ -Open-Intersection Scenarios	D-1-36
10 Suburban-Closed-Intersection Scenario Test.....	D-1-37
10.1 Location Overview	D-1-37
10.2 Data Analysis	D-1-39

10.3 Observations for Suburban-Closed-Intersection Scenario	D-1-43
11 Suburban-¾-Open-Intersection Scenario Test.....	D-1-43
11.1 Location Overview	D-1-44
11.2 Data Analysis	D-1-44
11.3 Observations for Suburban-¾-Open-Intersection Scenario	D-1-49
11.4 Comparison of Suburban-Closed-Intersection and Suburban-Open-Intersection Scenarios	D-1-49
12 Rural-Closed-Intersection Scenario Test.....	D-1-51
12.1 Location Overview	D-1-51
12.2 Data Analysis	D-1-51
12.3 Observations for Rural-Closed-Intersection Scenario.....	D-1-54
13 Rural-¾-Open-Intersection Scenario Test	D-1-55
13.1 Location Overview	D-1-55
13.2 Data Analysis	D-1-55
13.3 Observations for Rural-¾-Open-Intersection Scenario	D-1-59
14 Curved-Road Scenario Test.....	D-1-59
14.1 Location Overview	D-1-59
14.2 Data Analysis	D-1-61
14.3 Observations for Curved-Road Scenario Test.....	D-1-66
15 Freeway-Line-of-Sight Scenario Test.....	D-1-66
15.1 Location Overview	D-1-67
15.2 Data Analysis	D-1-67
15.3 Observations for Freeway LOS Scenario Testing.....	D-1-70
16 Rural-Highway, Line-of-Sight Scenario Test	D-1-70
16.1 Location Overview	D-1-71
16.2 Data Analysis	D-1-71
16.3 Observations for Rural-Highway-LOS Scenario Test.....	D-1-74
17 Freeway-Shadowing Scenario Test.....	D-1-74
17.1 Location Overview	D-1-74
17.2 Data Analysis	D-1-75
17.3 Observations for Freeway-Shadowing Scenario Test.....	D-1-79
18 Rural-Highway-Shadowing Scenario Test.....	D-1-79
18.1 Location Overview	D-1-79

18.2 Data Analysis	D-1-80
18.3 Observations for Rural-Highway-Shadowing Scenario	D-1-82
19 Arterial–Road-Shadowing Scenario-Test	D-1-82
19.1 Location Overview	D-1-83
19.2 Data Analysis	D-1-83
19.3 Observations for Arterial-Road-Shadowing Scenario.....	D-1-85
20 Expressway-Shadowing Scenario Test	D-1-85
20.1 Location Overview	D-1-85
20.2 Data Analysis	D-1-86
20.3 Observations for Expressway–Shadowing Scenario	D-1-88
21 Power Test Conclusions	D-1-88
22 Observations of Reduced Range in Some Baseline LOS Tests	D-1-89

List of Figures

Figure 1: Transmitter Setup	D-1-2
Figure 2: Receiver Setup.....	D-1-3
Figure 3: Transmit Vehicle Antenna Placement: DSRC (2, Black) and GPS (White Sphere).....	D-1-3
Figure 4: Calibration Using Power Meter.....	D-1-4
Figure 5: EVM Measure for WSU Only.....	D-1-5
Figure 6: EVM Measure for WSU Connected to Power Amplifier.....	D-1-6
Figure 7: Alameda Test Site	D-1-8
Figure 8: View of the Ships at the Test Site	D-1-9
Figure 9: PER Versus Distance for Various Power Levels at 3 Mbps in Baseline-LOS Scenario.....	D-1-10
Figure 10: RSSI versus Distance for Various Power Levels at 3 Mbps in Baseline-LOS Scenario.....	D-1-11
Figure 11: PER versus Distance at Various Power Levels at 3 Mbps for the Baseline- Truck Scenario.....	D-1-12
Figure 12: RSSI versus Distance at Various Power Levels at 3 Mbps for the Baseline- Truck Scenario	D-1-13
Figure 13: PER versus Distance for 33 dBm and 20 dBm Transmissions at 3 Mbps and 6 Mbps	D-1-14
Figure 14: RSSI versus Distance for 33 dBm and 20 dBm Transmissions at 3 Mbps and 6 Mbps	D-1-15
Figure 15: Looking East on Santa Clara Street.....	D-1-16
Figure 16: Looking West on Santa Clara Street	D-1-17
Figure 17: PER versus Distance Curves at Various Power Levels at 3 Mbps for the Urban-Straight-Line Scenario.....	D-1-17
Figure 18: RSSI versus Distance Curves at Various Power Levels at 3 Mbps for the Urban-Straight-Line Scenario.....	D-1-18
Figure 19: Comparison of PER Curves for 33 dBm and 20 dBm at 3 Mbps and 6 Mbps	D-1-18
Figure 20: Comparison of RSSI Curves for 33 dBm and 20 dBm at 3 Mbps and 6 Mbps	D-1-19
Figure 21: Looking South on Market Street toward the Intersection from 150 Meters	D-1-20
Figure 22: PER versus Distance Curve at 33 dBm and 3 Mbps for all the Different Transmitter Positions	D-1-21
Figure 23: RSSI versus Distance Curve at 33 dBm and 3 Mbps for all the Different Transmitter Positions	D-1-22
Figure 24: PER versus Distance Curve at 20 dBm and 3 Mbps for all the Different Transmitter Positions	D-1-23
Figure 25: RSSI versus Distance Curve at 20 dBm and 3 Mbps for all the Different Transmitter Positions	D-1-24
Figure 26: Comparison of PER versus Distance Curves for Various Power Levels when the Transmitter was 100 Meters from the Intersection and Set to Transmit at 3 Mbps	D-1-25

Figure 27: Comparison of RSSI versus Distance Curves for Various Power Levels when the Transmitter was 100 Meters from the Intersection and Set to Transmit at 3 Mbps	D-1-25
Figure 28: PER Curves in Urban-Closed-Intersection Scenario for 20 dBm and 33 dBm at 3 Mbps and 6 Mbps	D-1-26
Figure 29: RSSI Curves in Urban-Closed-Intersection Scenario for 20 dBm and 33 dBm at 3 Mbps and 6 Mbps	D-1-27
Figure 30: One Open Corner of the 4th Street and Santa Clara Street Intersection ..	D-1-28
Figure 31: Closed Corner of the 4th Street and Santa Clara Street Intersection.....	D-1-29
Figure 32: PER versus Distance Curve at 33 dBm and 3 Mbps for all the Different Transmitter Positions	D-1-30
Figure 33: RSSI versus Distance Curve at 33 dBm and 3 Mbps for all the Different Transmitter Positions	D-1-31
Figure 34: Comparison of PER versus Distance Curves for Various Power Levels when the Transmitter was 100 Meters from the Intersection and Set to Transmit at 3 Mbps	D-1-32
Figure 35: Comparison of RSSI versus Distance Curves for Various Power Levels when the Transmitter was 100 Meters from the Intersection and Set to Transmit at 3 Mbps	D-1-33
Figure 36: Comparison of PER versus Distance Curves in Urban-Open-Intersection at 33 dBm and 20 dBm for 3 Mbps and 6 Mbps.....	D-1-34
Figure 37: Comparison of RSSI versus Distance Curves in Urban-Open-Intersection at 33 dBm and 20 dBm for 3 Mbps and 6 Mbps.....	D-1-35
Figure 38: PER Comparison of Urban-Closed-Intersection Scenario and Urban-Open-Intersection Scenario for 33 dBm at 3 Mbps	D-1-36
Figure 39: RSSI Comparison of Urban-Closed-Intersection Scenario and Urban-Open-Intersection Scenario for 33 dBm at 3 Mbps	D-1-37
Figure 40: West Corner of Santa Rita Avenue and Byron Street	D-1-38
Figure 41: Propagation Environment along Santa Rita Avenue.....	D-1-38
Figure 42: PER versus Distance Curves for Various Transmitter Locations at 33 dBm and 3 Mbps.....	D-1-39
Figure 43: RSSI versus Distance Curves for Various Transmitter Locations at 33 dBm and 3 Mbps.....	40
Figure 44: Comparison of PER versus Distance Curves between 20 dBm and 33 dBm when the Transmitter was 100 Meters from the Intersection and Set to Transmit at 3 Mbps	D-1-40
Figure 45: Comparison of RSSI versus Distance Curves between 20 dBm and 33 dBm when the Transmitter as 100 Meters from the Intersection and Set to Transmit at 3 Mbps	D-1-41
Figure 46: PER Comparison for Suburban-Closed-Intersection Scenario for 33 dBm and 20 dBm at 3 Mbps and 6 Mbps	D-1-42
Figure 47: RSSI Comparison for Suburban-Closed-Intersection Scenario for 33 dBm and 20 dBm at 3 Mbps and 6 Mbps	D-1-43
Figure 48: PER versus Distance Curves for Various Transmitter Locations at 33 dBm and 3 Mbps.....	D-1-45

Figure 49: RSSI versus Distance Curves for Various Transmitter Locations at 33 dBm and 3 Mbps.....	D-1-45
Figure 50: Comparison of PER versus Distance Curves Between 20 dBm, 26 dBm, and 33 dBm when the Transmitter was 85 Meters from the Intersection and Set to Transmit at 3 Mbps.....	D-1-46
Figure 51: Comparison of RSSI versus Distance Curves between 20 dBm, 26 dBm, and 33 dBm when the Transmitter was 85 Meters from the Intersection and Set to Transmit at 3 Mbps.....	D-1-47
Figure 52: PER Comparison for Suburban-3/4-Open-Intersection Scenario for 33 dBm and 20 dBm at 3 Mbps and 6 Mbps.....	D-1-48
Figure 53: RSSI Comparison for Suburban-3/4-Open-Intersection Scenario for 33 dBm and 20 dBm at 3 Mbps and 6 Mbps.....	D-1-48
Figure 54: PER Comparison of Suburban-Closed-Intersection and Suburban-Open-Intersection Scenarios for 33 dBm at 3 Mbps.....	D-1-50
Figure 55: RSSI Comparison of Suburban-Closed-Intersection and Suburban-Open-Intersection Scenarios for 33 dBm at 3 Mbps.....	D-1-50
Figure 56: PER versus Distance Curves for Various Transmitter Locations at 33 dBm and 3 Mbps.....	D-1-52
Figure 57: RSSI versus Distance Curves for Various Transmitter Locations at 33 dBm and 3 Mbps.....	D-1-52
Figure 58: Comparison of PER versus Distance Curves between 20 dBm, 26 dBm, and 33 dBm when the Transmitter was 100 Meters from the Intersection and Set to Transmit at 3 Mbps.....	D-1-53
Figure 59: Comparison of RSSI versus Distance Curves between 20 dBm, 26 dBm, and 33 dBm when the Transmitter was 100 Meters from the Intersection and Set to Transmit at 3 Mbps.....	D-1-54
Figure 60: Comparison of PER versus Distance Curves between 33 dBm, 26 dBm, and 20 dBm when the Transmitter was 100 Meters from the Intersection and Set to Transmit at 3 Mbps.....	D-1-56
Figure 61: Comparison of RSSI versus Distance Curves between 33 dBm, 26 dBm, and 20 dBm when the Transmitter was 100 Meters from the Intersection and Set to Transmit at 3 Mbps.....	D-1-57
Figure 62: Comparison of PER Curves in Rural-3/4-Open-Intersection for 33 dBm and 20 dBm at 3 Mbps and 6 Mbps.....	D-1-58
Figure 63: Comparison of RSSI Curves in Rural-3/4-Open-Intersection for 33 dBm and 20 dBm at 3 Mbps and 6 Mbps.....	D-1-58
Figure 64: Heading South on Stevens Canyon Road.....	D-1-60
Figure 65: Negotiating the Curve.....	D-1-60
Figure 66: Comparison of PER Curves for Curved-Road Scenario at 50 Meters and 100 Meters for 33 dBm Transmission.....	D-1-61
Figure 67: Comparison of RSSI Curves for Curved-Road Scenario at 50 Meters and 100 Meters for 33 dBm Transmission.....	D-1-62
Figure 68: Comparison for PER Curves for a Curved-Road Scenario for 33 dBm, 26 dBm, and 20 dBm Transmissions.....	D-1-63
Figure 69: Comparison for RSSI Curves for a Curved-Road Scenario for 33 dBm, 26 dBm, and 20 dBm Transmissions.....	D-1-64

Figure 70: Comparison of PER Curves in a Curved-Road Scenario for 33 dBm and 20 dBm at 3 Mbps and 6 Mbps.....	D-1-65
Figure 71: Comparison of RSSI Curves in a Curved-Road Scenario Test for 33 dBm and 20 dBm at 3 Mbps and 6 Mbps	D-1-66
Figure 72: Heading South on US-101.....	D-1-67
Figure 73: Comparison of PER versus Distance Curves for Various Power Levels in a Freeway-LOS Scenario when Transmitter is Set to 3 Mbps.....	D-1-68
Figure 74: Comparison of RSSI versus Distance Curves for Various Power Levels in a Freeway-LOS Scenario when Transmitter is Set to 3 Mbps.....	D-1-69
Figure 75: Comparison of PER Curves in a Freeway-LOS Scenario for 20 dBm and 10 dBm at 3 Mbps and 6 Mbps	D-1-69
Figure 76: Comparison of RSSI Curves in a Freeway-LOS Scenario for 33 dBm and 20 dBm at 3 Mbps and 6 Mbps.....	D-1-70
Figure 77: Comparison of PER versus Distance Curves for Various Power Levels in a Rural-Highway-LOS Scenario when Transmitter is Set to 3 Mbps	D-1-71
Figure 78: Comparison of RSSI versus Distance Curves for Various Power Levels in a Rural-Highway-LOS Scenario when Transmitter is Set to 3 Mbps	D-1-72
Figure 79: Comparison of PER Curves in a Rural-Highway-LOS Scenario for 33 dBm and 20 dBm at 3 Mbps and 6 Mbps	D-1-73
Figure 80: Comparison of RSSI Curves in a Rural-Highway-LOS Scenario for 33 dBm and 20 dBm at 3 Mbps and 6 Mbps	D-1-73
Figure 81: Receiver Behind the Truck Along I-880	D-1-75
Figure 82: Comparison of PER versus Distance Curves for Various Power Levels in a Freeway-Shadowing Scenario when Transmitter is Set to 3 Mbps	D-1-76
Figure 83: Comparison of RSSI versus Distance Curves for Various Power Levels in a Freeway-Shadowing Scenario when Transmitter is Set to 3 Mbps ..	D-1-77
Figure 84: Comparison of PER Curves in a Freeway-Shadowing Scenario Test for 33 dBm and 20 dBm at 3 Mbps and 6 Mbps	D-1-78
Figure 85: Comparison of RSSI Curves in a Freeway-Shadowing Scenario Test for 33 dBm and 20 dBm at 3 Mbps and 6 Mbps	D-1-78
Figure 86: Driving Down Highway 156.....	D-1-80
Figure 87: Comparison of PER versus Distance Curves for Various Power Levels in a Rural Highway Shadowing Scenario when Transmitter is Set to 3 Mbps.....	80
Figure 88: Comparison of PER versus Distance Curves for a Rural-Highway-Shadowing Scenario when Transmitting at 33 dBm and Different Data Rates.....	D-1-81
Figure 89: Comparison of RSSI versus Distance Curves for a Rural-Highway-Shadowing Scenario when Transmitting at 33 dBm and Different Data Rates	D-1-82
Figure 90: Driving North Along El Camino Real.....	D-1-83
Figure 91: Comparison of PER versus Distance Curves for Various Power Levels in an Arterial-Road-Shadowing Scenario when Transmitter is Set to 3 Mbps.....	84
Figure 92: Comparison of RSSI versus Distance Curves for Various Power Levels in an Arterial-Road-Shadowing Scenario when Transmitter is Set to 3 Mbps.....	D-1-84
Figure 93: Driving East on Central Expressway.....	86
Figure 94: Comparison of PER versus Distance Curves for Various Power Levels in an Expressway-Shadowing Scenario when Transmitter is Set to 3 Mbps.....	87

Figure 95: Comparison of RSSI versus Distance Curves for Various Power Levels in an
Expressway-Shadowing Scenario when Transmitter is Set to 3 Mbps.....D-1-88

Figure 96: RSSI versus Distance at 20 dBm and 3 Mbps for the Baseline-LOS-
Scenario Test.....D-1-90

Figure 97: RSSI versus Distance for 33 dBm and 3 Mbps in Baseline LOS.....D-1-91

List of Tables

Table 1: Power Test Scenarios.....	D-1-7
Table 2: Test Cases for the Baseline LOS Scenario	D-1-9
Table 3: Test Cases for the Urban-Straight-Line Scenario Test	D-1-16
Table 4: Test Cases for the Urban-Closed-Intersection-Scenario	D-1-20
Table 5: Test Cases for the Urban-¾-Open-Intersection Scenario Test	D-1-28
Table 6: Test Cases for Suburban-Closed-Intersection Scenario	D-1-37
Table 7: Test Cases for the Suburban-¾-Open-Intersection Scenario	D-1-44
Table 8: Test Cases for the Rural-Closed-Intersection Scenario	D-1-51
Table 9: Test Cases for the Rural-¾-Open-Intersection Scenario	D-1-55
Table 10: Test Cases for the Curved-Road Scenario	D-1-59
Table 11: Test Cases for the Freeway-LOS Scenario	D-1-67
Table 12: Test Cases for the Rural-Highway-LOS Scenario	D-1-71
Table 13: Test Cases for the Freeway-Shadowing Scenario Test.....	D-1-74
Table 14: Test Cases for the Rural-Highway-Shadowing Scenario	D-1-79
Table 15: Test Cases for the Arterial-Road-Shadowing Scenario Test	D-1-83
Table 16: Test Cases for the Expressway-Shadowing Scenario Test.....	D-1-85

1 Overview

The purpose of the VSC-A Power Testing activity is to measure the relationship between transmission power and packet reception performance in the Dedicated Short Range Communication (DSRC) band. Sending messages with greater power has the potential to improve message reception at far ranges or around obstructions. However, increasing transmission power has potential problems as well. Higher transmission power generally leads to a larger interference range and, thereby, increases channel loading and congestion. High power transmissions are also subject to a tighter spectral mask.

Transmission characteristics with reduced power are also of interest. As the transmission range decreases, the scope of the shared wireless “channel” shrinks, which can be an effective tool in alleviating packet congestion. This advantage must be balanced, however, against any reduced effectiveness of safety applications that results from the smaller transmission range.

These tests provided the VSC-A team with a robust understanding of how transmission power, fading, and obstacles affect message reception. Various propagation environments were considered: urban, suburban, rural, and highway.

The principal work item of this activity is to fully characterize packet reception probability as a function of transmission power, occlusions (e.g., trucks, buildings, etc.), distance, multi-path environment, and bit rate.

This report documents the test setup, test scenarios, and associated power testing results.

2 Testing Overview

The test cases for are designed to address two specific issues:

1. Identify environments in which the improved reception performance associated with higher transmission powers may be useful for the VSC-A applications
2. Improve our understanding of the limitations of communication performance for both high power and lower power communications

For these tests 20 dBm is defined as the “nominal” transmission power for DSRC messages. Transmission levels above 20 dBm are defined as “high” power, and transmission levels below 20 dBm are defined as “low” power.

2.1 Relevant VSC-A Applications

The VSC-A Project has defined 6 safety applications to be developed.

1. Emergency Electronic Brake Lights (EEBL)
2. Forward Collision Warning (FCW)
3. Do No Pass Warning (DNPW)
4. Control Loss Warning (CLW)
5. Intersection Movement Assist (IMA)

6. Blind Spot Warning+Lane Change Warning (BSW+LCW)

From a power testing perspective, a number of these applications are primarily concerned with traffic traveling along a single axis. It follows that the test scenarios motivated by these applications individually are largely overlapping. This point is reinforced by the observation that a single lane of lateral offset between two vehicles will not produce a notably different power test result than a same-lane alignment. Thus, if an application is concerned with AHEAD-LEFT, AHEAD, and AHEAD-RIGHT alignments, each of these alignments need not be tested separately.

The curved track geometry also applies to a number of these applications but in a more limited set of environments (e.g., rural setting versus freeway setting).

The intersecting geometry is unique in the sense that it must be tested in specific intersection situations.

3 Hardware Setup

The Federal Communications Commission (FCC) allows for a maximum equivalent isotropically radiated power (EIRP) transmission level of 33 dBm. The DENSO Wireless Safety Units (WSUs) used for these tests are capable of transmitting up to almost 20 dBm. In order to boost the signal strength to the maximum permissible value, the VSC-A team used a solid state power amplifier to generate a 33 dBm signal. The VSC-A team decided to use a General Dynamics Solid State Power Amplifier (Model LPCD6025R). Figure 1 depicts the transmitter setup, while Figure 2 shows the receiver.

These tests employed an antenna with 7 dB gain in the direction of maximum radiation and 0 dB gain in the horizontal direction. The antennas were mounted on the flat part of the roofs of the transmitting and receiving vehicles (see Figure 3), respectively, at the same height on each vehicle. Therefore, the horizontal plane transmission power is of primary interest. The transmission power reported for each test (e.g., 33 dBm) is the signal power into the antenna, which is equal to the power in the horizontal plane out of the antenna, and is, thus, 7 dB less than the EIRP.

The packet size in all tests was 400 bytes (including all overhead). For test efficiency, the sending WSU was configured to transmit as many packets per second as possible.

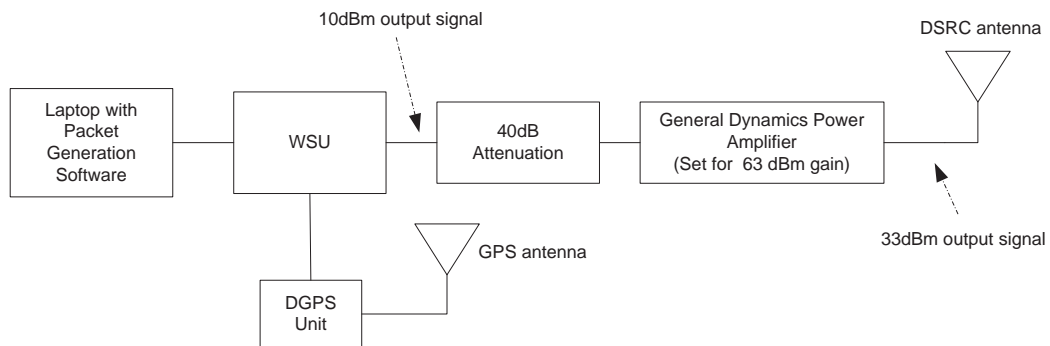
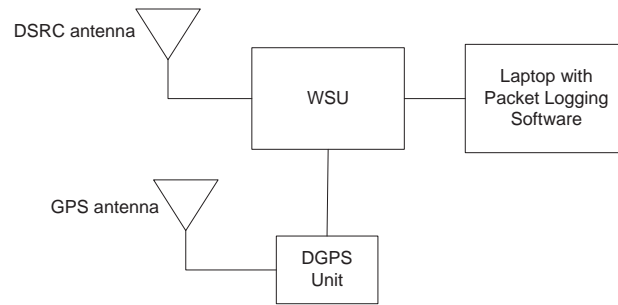


Figure 1: Transmitter Setup

**Figure 2: Receiver Setup****Figure 3: Transmit Vehicle Antenna Placement: DSRC (2, Black) and GPS (White Sphere)**

3.1 Calibration

In order to validate the transmit power level, the setup was calibrated using a power meter. Figure 4 depicts how this was done. To ensure the validity of the results, the setup was recalibrated every time a new power level was chosen.

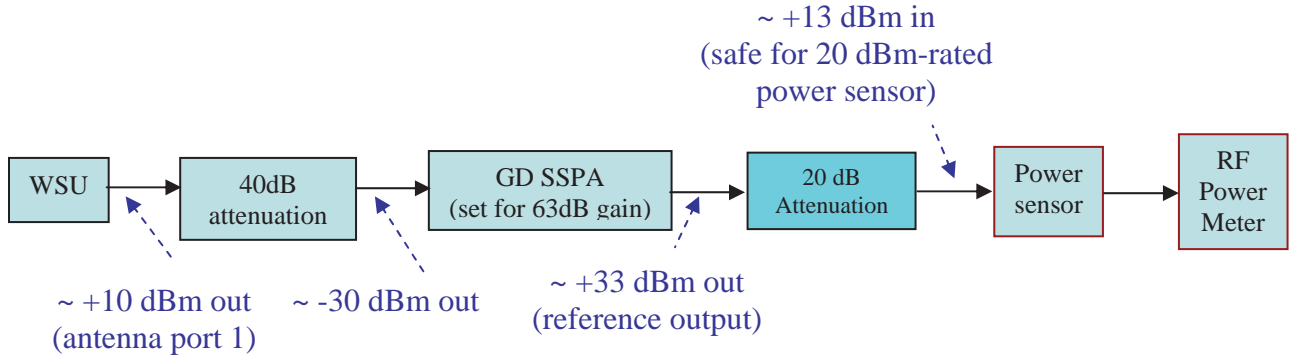


Figure 4: Calibration Using Power Meter

The use of a power amplifier on a signal induces nonlinearity. The Error Vector Magnitude (EVM) was measured in the transmitter setup both with and without the power amplifier. The setup and results are shown below in Figure 5 and Figure 6. Based on similar measurements reported to the VSC-A team by outside experts, EVMs in the range of 5-8 percent were expected. The team's EVM measurements, conducted both with and without the power amplifier attached to the WSU output, fell within that range.

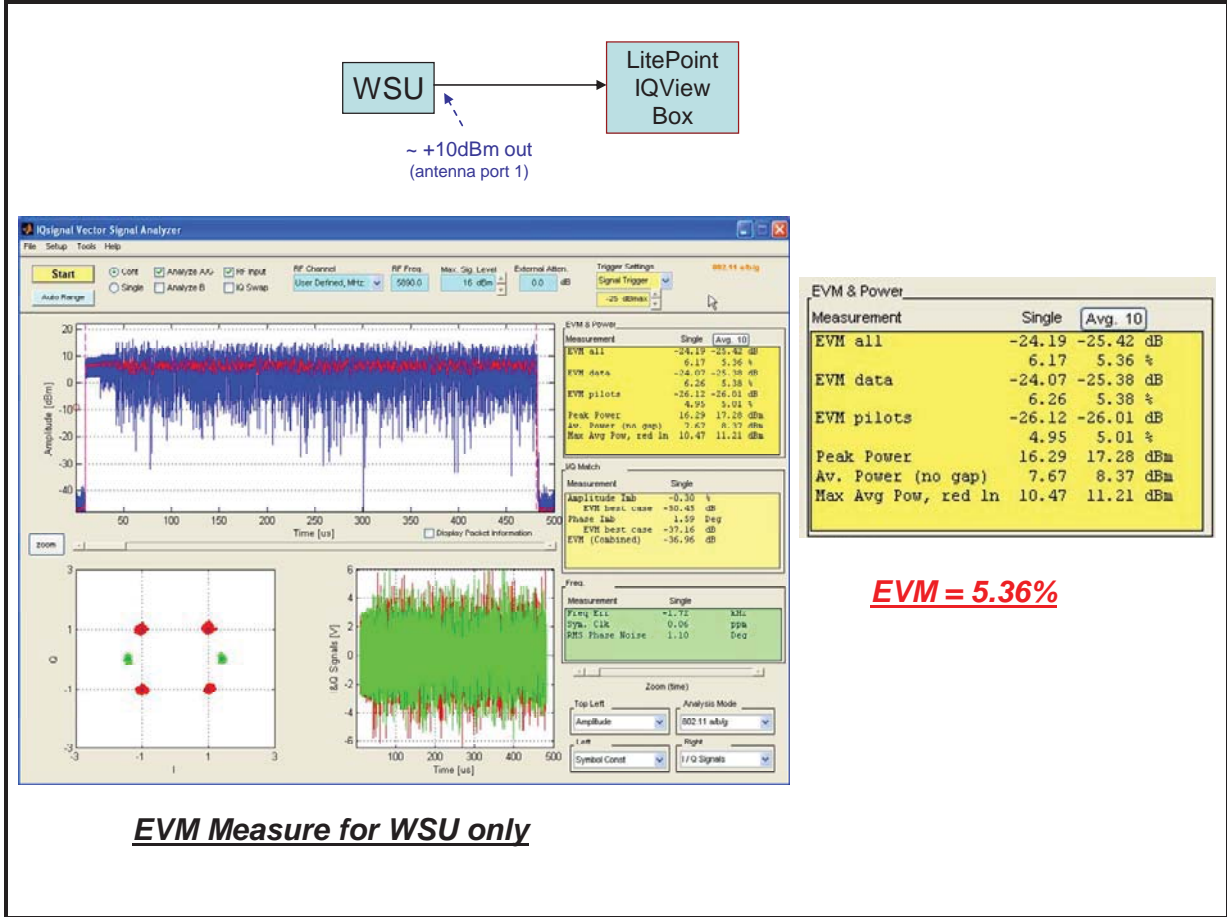


Figure 5: EVM Measure for WSU Only

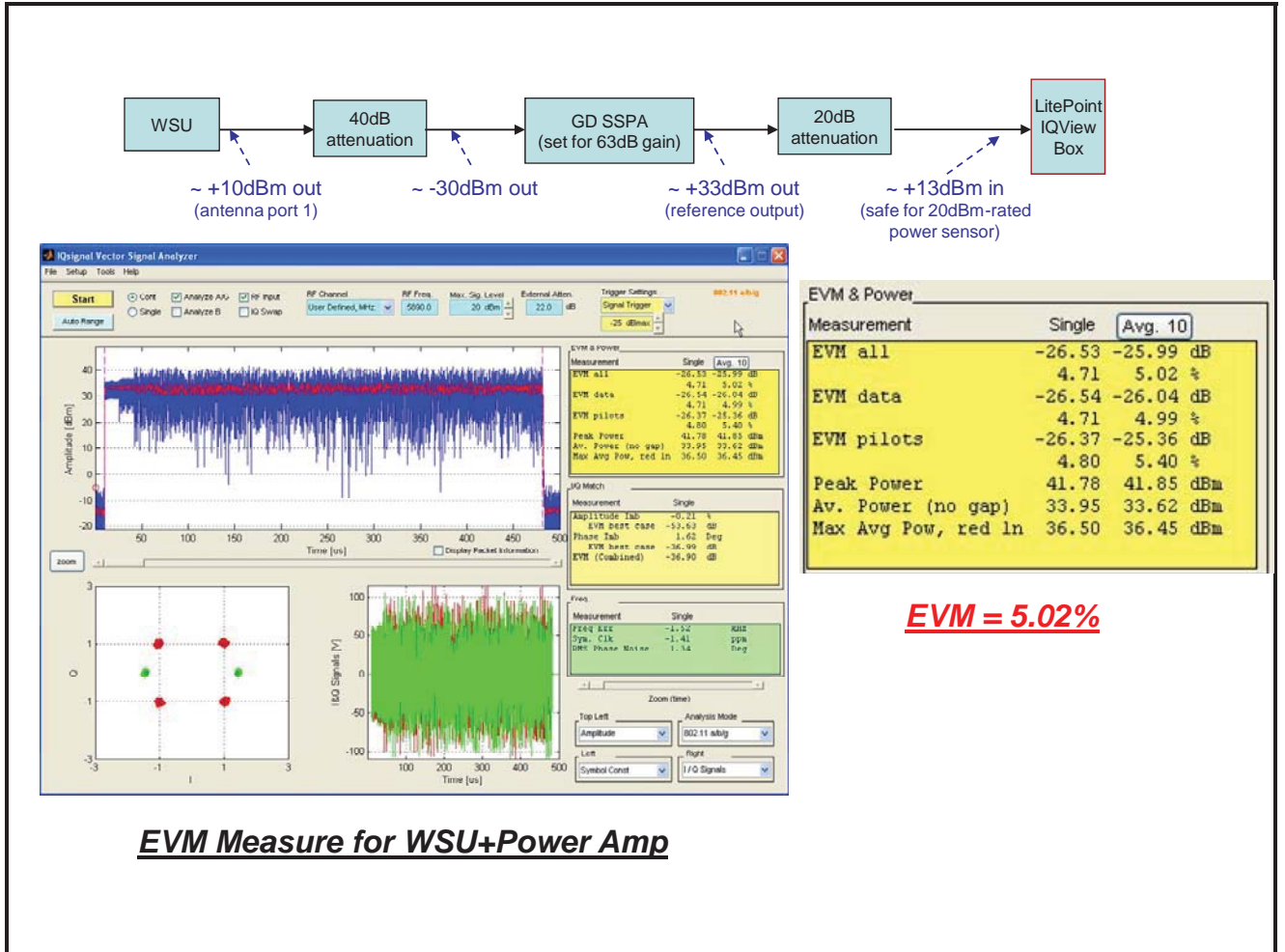


Figure 6: EVM Measure for WSU Connected to Power Amplifier

4 Test Results and Summary

The hardware setup was kept constant throughout the tests. Sixteen scenarios were tested. These are listed in Table 1. Each test scenario is reported in one of the sections 4.1-20 below. For each scenario the following details are presented:

1. Test location
2. Test settings and configuration
3. Description of any testing discrepancies
4. Graphical plots of the relationship between Packet Error Rate (PER) and distance, and Received Signal Strength Indication (RSSI) and distance
5. Observations that can be drawn from that test scenario

Table 1: Power Test Scenarios

Scenario
Baseline Line-of-Sight
Baseline Shadowing
Urban Straight Line
Urban Closed Intersection
Urban $\frac{3}{4}$ Open Intersection
Suburban Closed Intersection
Suburban $\frac{3}{4}$ Open Intersection
Rural Closed Intersection
Rural $\frac{3}{4}$ Open Intersection
Curved Road
Freeway Line of Sight
Rural Highway Line of Sight
Freeway Shadowing
Rural Highway Shadowing
Arterial Road Shadowing
Expressway Shadowing

4.1 Interpreting Data Graphs

PER is the primary performance metric used in this report. It is defined as the ratio of unsuccessful packet transmissions to total packet transmissions within a single test. A packet transmission is unsuccessful if the packet is either not received at all or is received with uncorrectable bit errors. PER plots tend to have high variance so it is hard to define a precise range of successful transmission. However, in each case PER tends to increase with increasing distance, and in most cases, there is a point beyond which communication is clearly unreliable.

The performance graphs in this report all use distance as the x-axis variable, either vehicle-to-vehicle distance or vehicle-to-intersection distance. In some cases a specific curve does not span the entire distance range of the x-axis. There are two reasons why this might be true for a given plot:

- Communication was not attempted for the particular configuration shown by the plot, but the distance was used in other tests reported in the same figure. An example of this can be seen in Figure 79. The PER curve labeled “ruralLOS-33dBm-6Mbps-1” stops between 300 m and 400 m, and the PER value never exceeds 4% below 300 m. In these cases it is not possible to say what the PER would be for distances greater than those included in the plot, except that PER generally grows with distance.
- The receive vehicle was unable to receive any packets from the transmit vehicle for distances beyond a certain threshold. An example of this can be seen in Figure 9. The PER curve labeled “var-LOS-5dBm-3Mbps-1” stops between 400 m and 600 m, after experiencing a rapid rise toward 100% between 200 m and

400 m. In these cases the PER should be considered 100% for distances greater than those included in the plot.

The tests reported in Sections 5-14 involve one stationary vehicle and one moving vehicle. In those tests, which are easy to repeat, the distance range tested is the same for all plots included in a given figure. So, in these sections a curve that stops before reaching the right edge of the graph could be explained only by the second reason above.

The tests reported in Sections 15-20 involve two vehicles moving in traffic. The varying distance between the vehicles was achieved by varying their relative speed (usually by varying the speed of the transmit vehicle), and tests were not easy to repeat. In particular, it was not always possible to exercise the same distance ranges for all tests plotted in a given figure. So, in these sections a curve that stops before reaching the right edge of the graph could be explained by either of the above reasons.

5 Baseline Line-of-Sight Scenario Tests



Figure 7: Alameda Test Site

Figure 7 shows the site for the baseline tests. The tests were conducted at an abandoned naval airstrip in Alameda, California. The runway was approximately 1 mile in length. The transmitter was kept stationary at the same location for all the tests. The receiver was initially placed at a distance beyond communication range. It moved toward the transmitter at a constant speed (10 mph or 20 mph)¹ for each of the test cases. Table 2

¹ In each test the WSU transmitter was configured to send approximately 1000 packets per second. At 10 mph relative vehicle speed, the inter-vehicle distance changes by about 5 meters per second.

below outlines the various test cases that were conducted for the Baseline Line-of-Sight (LOS) Scenario.

Table 2: Test Cases for the Baseline LOS Scenario

TX Power Data Rate	5dBm	10dBm	15dBm	20dBm	26dBm	33dBm
3Mbps	Test 1	Test 4	Test 7	Test 10	Test 13	Test 16
6Mbps	Test 2	Test 5	Test 8	Test 11	Test 14	Test 17
12Mbps	Test 3	Test 6	Test 9	Test 12	Test 15	Test 18

5.1 Location Overview

The airstrip served as a good location to conduct the baseline tests. There was clear LOS propagation between the transmitter and receiver from opposite ends of the air strip, and minimal sources of reflection. The team did note the presence of cargo ships in a channel adjacent to the airfield (see Figure 8) and recorded the movement of ships during the various tests. No correlation was found between ship presence and test outcomes. The nearest point between the channel and the transmit vehicle was about 1/2 mile. The nearest point between the channel and the receive vehicle was about 1/4 mile, which occurred when the transmit and receive vehicles were at their maximum separation.



Figure 8: View of the Ships at the Test Site

5.2 Data Analysis

The results of the Baseline LOS tests conducted with a 3 Mbps bit rate are shown in Figure 9 and Figure 10. The first figure shows PER versus inter-vehicle distance for the

six transmit powers. At 33 dBm transmission power, communication becomes sporadic or worse beyond about 1300 meters. At 20 dBm, the packet error rate is high for distances greater than about 900 meters. At 5 dBm, PER is significant for distances greater than 200 meters.

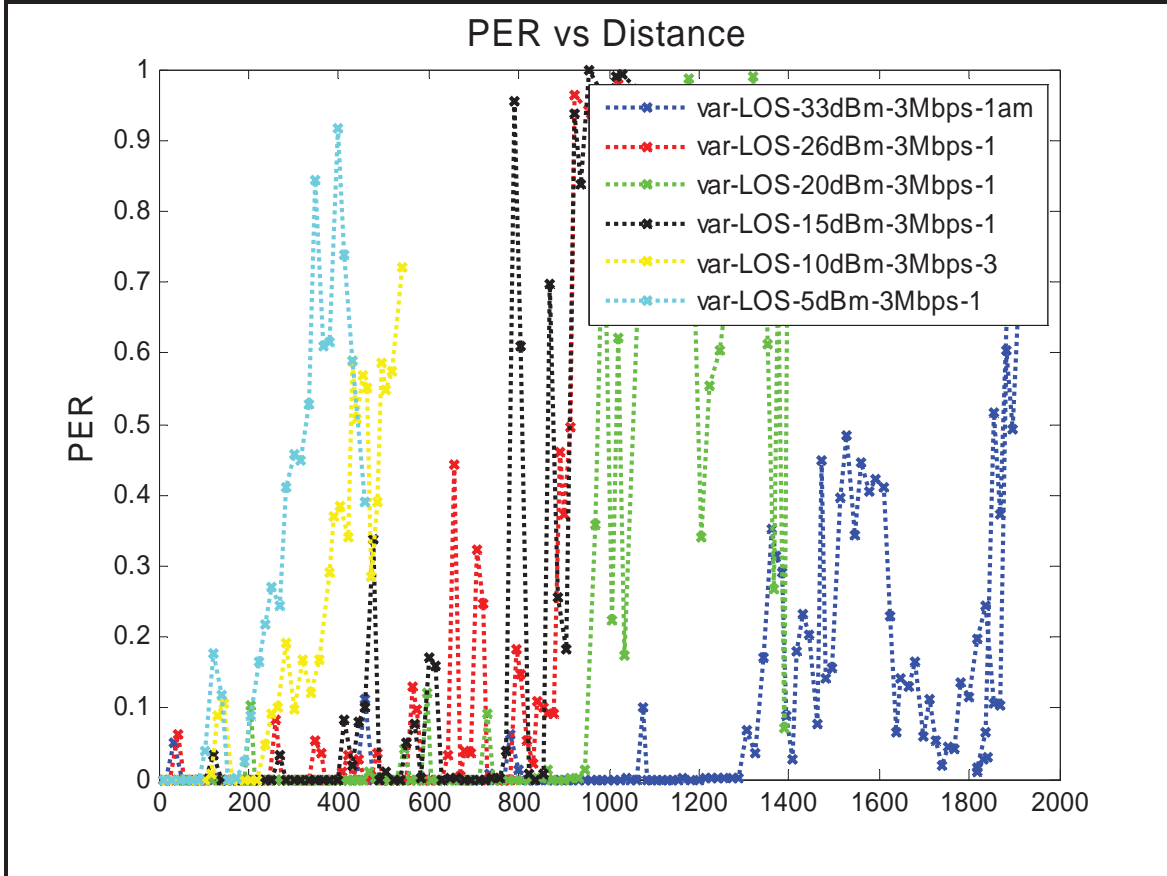


Figure 9: PER Versus Distance for Various Power Levels at 3 Mbps in Baseline-LOS Scenario

Figure 10 shows RSSI versus distance. In each case, the RSSI decays approximately exponentially with distance. Both plots show worse performance for 26 dBm than for 20 dBm. This anomaly was observed during testing and is discussed in Section 22.

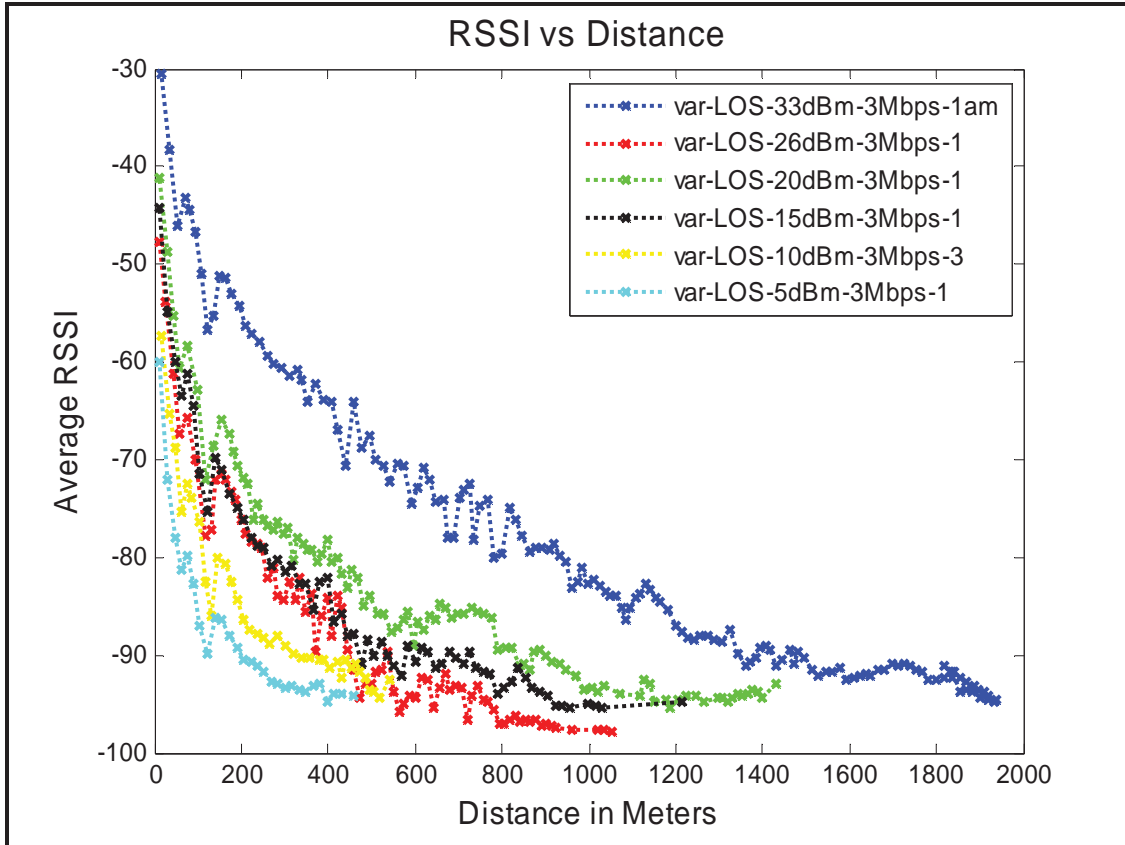


Figure 10: RSSI versus Distance for Various Power Levels at 3 Mbps in Baseline-LOS Scenario

5.3 Baseline LOS Scenario Observations

Figure 9 and Figure 10, along with other data collected in the Baseline LOS Scenario tests, lead to the following observations:

1. There is a clear dependence between power and range, with greater power leading to greater transmission range
2. Transmissions at higher data rates (6 Mbps and 12 Mbps) result in a drop in transmission range (6 Mbps and 12 Mbps baseline LOS results are not shown; similar results for 6 Mbps are shown in several sections below)
3. It is clear from Figure 9 that the PER curves exhibit high variability. This characteristic is inherent to the dynamic nature of the Radio Frequency (RF) propagation environment.
4. The PER curves make it difficult to identify a specific “reliable transmission range” for a given power. The range can be identified qualitatively as a region of rapid increase in PER, ignoring PER “bumps.”
5. The RSSI curves are smoother and are representative of a 2-Ray Rayleigh fading environment. This is evident from the consistent dips in RSSI in the 100-200 meter range, which is a result of destructive interference at 5.9 GHz between the LOS wave and the wave reflected from the ground.

6 Baseline Shadowing Scenario Test

The Baseline Shadowing Scenario Tests were conducted at the same site as the Baseline LOS Scenario reported in the previous section (see Figure 7). In this test, the transmitter and receiver were initially placed at a distance out of communication range, and a semi-truck with 45 foot trailer was placed midway between the two vehicles. The transmitter was kept stationary at the same location for all the tests. The receiver moved toward the transmitter at a constant speed (20 mph) for each of the test cases, while the truck moved at roughly ½ the speed (10 mph). The 18 test cases shown in Table 2 were repeated for this scenario.

6.1 Data Analysis

Four graphs are shown in this section. The first two graphs (Figure 11 and Figure 12) show PER and RSSI, respectively, versus distance for various transmission powers. The second pair of graphs (Figure 13 and Figure 14) show PER and RSSI, respectively, for two powers and two bit rates (four total combinations).

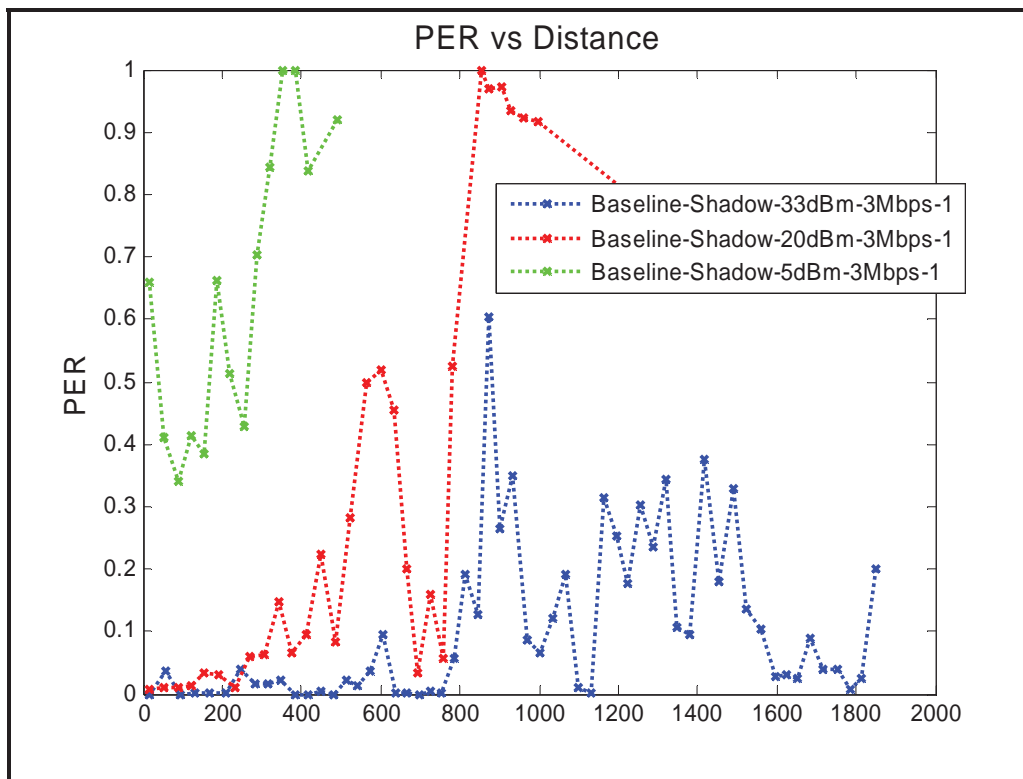


Figure 11: PER versus Distance at Various Power Levels at 3 Mbps for the Baseline-Truck Scenario

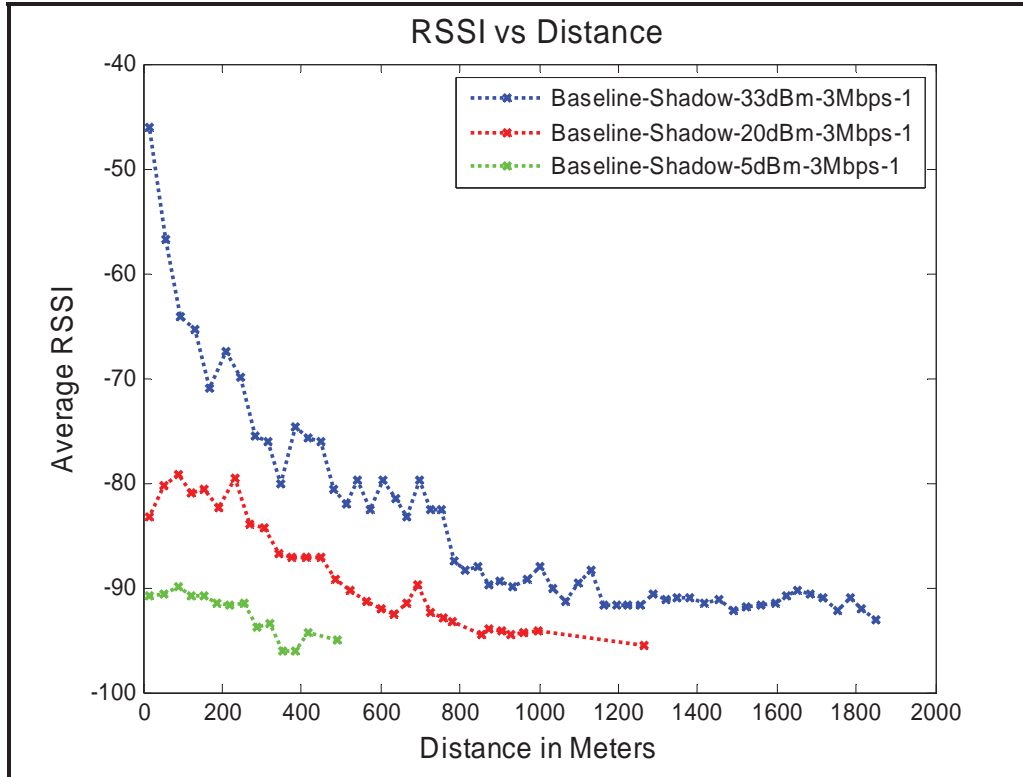


Figure 12: RSSI versus Distance at Various Power Levels at 3 Mbps for the Baseline-Truck Scenario

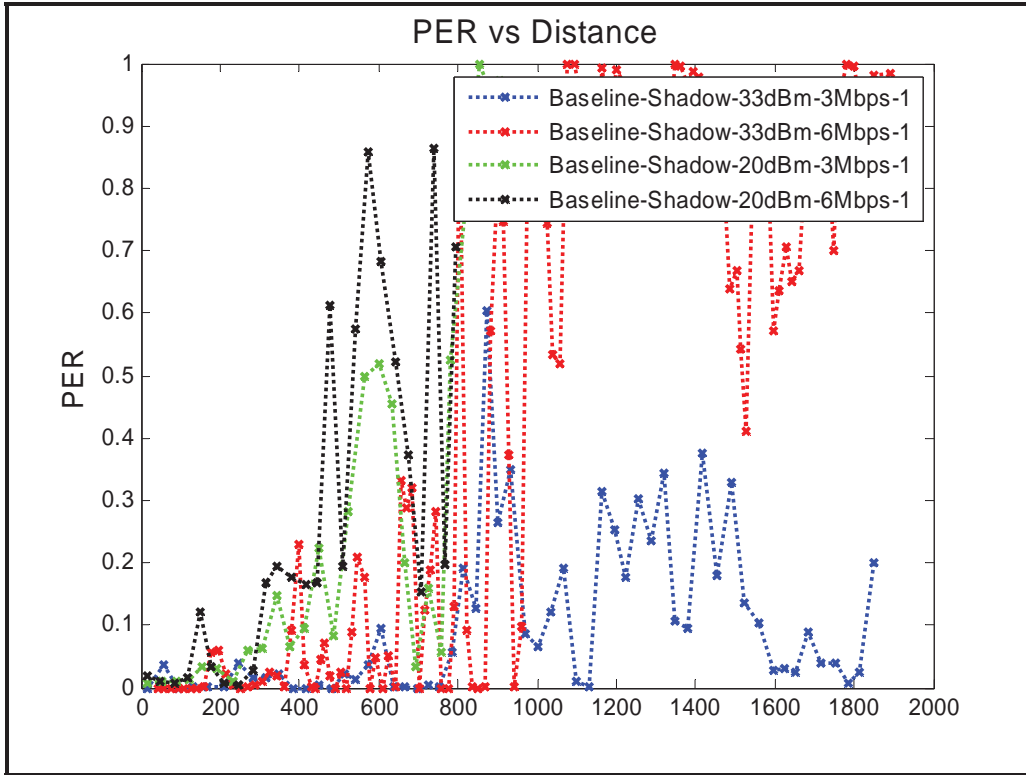


Figure 13: PER versus Distance for 33 dBm and 20 dBm Transmissions at 3 Mbps and 6 Mbps

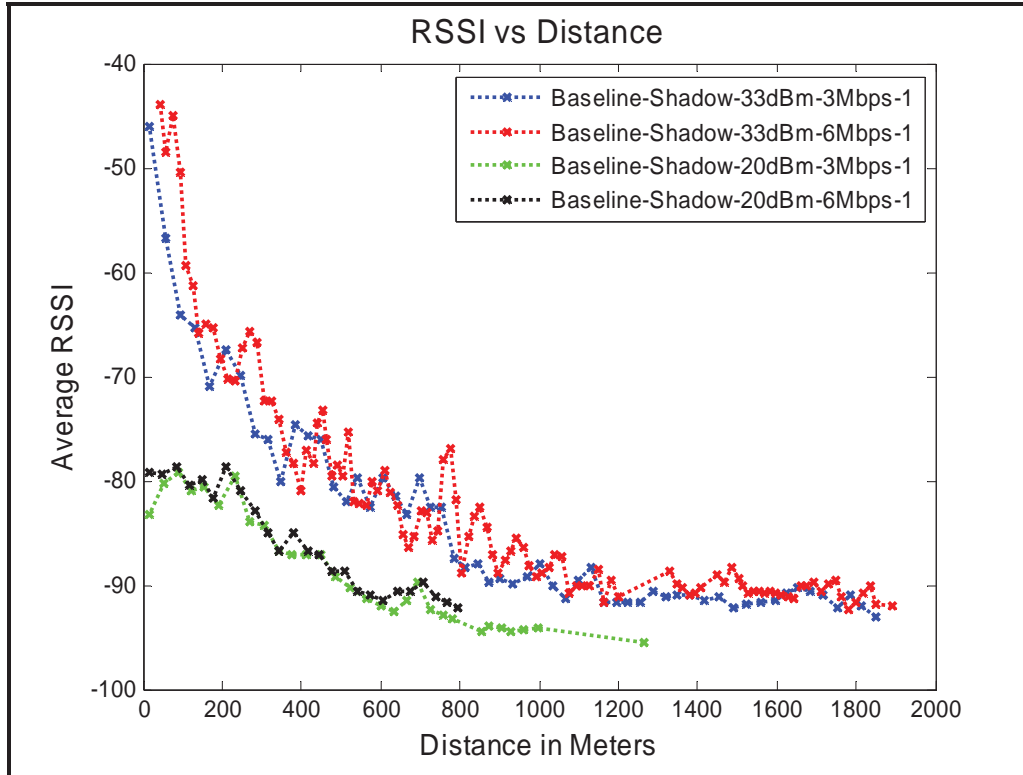


Figure 14: RSSI versus Distance for 33 dBm and 20 dBm Transmissions at 3 Mbps and 6 Mbps

6.2 Baseline Shadowing Scenario Observations

1. Figure 9 shows that at 20 dBm there is effective communication to approximately 900 meters. By comparison, as shown in Figure 11, testing scenarios with the truck indicate the 20 dBm transmissions experience significant PER levels from about 500 meters onward. Similarly, at 5 dBm, there is an effective range of approximately 200 meters without the truck and with the truck PER never falls below 30 percent.
2. The results with the presence of the truck are fairly consistent over the various transmission powers and data rates (i.e., higher power leads to longer range) and lower bit rate correlates with lower PER. In particular, the performance penalty for 6 Mbps versus 3 Mbps is relatively modest at 20 dBm, but is more significant at 33 dBm, as shown in Figure 13.
3. One interesting observation from these shadowing tests concerns performance as the receiver vehicle and truck reach the end of their approach to the transmitter vehicle. Note the increase in PER over the final 100 meters for the 5 dBm curve in Figure 11. Also note the RSSI reductions for both the 5 dBm and 20 dBm curves over that same range in Figure 12. In the 5 dBm case (and also the 10 dBm case, not shown), the RSSI decrease was enough to cause significant packet errors, while in the 20 dBm case, the Signal-to-Noise Ratio (SNR) was sufficient to keep PER low even with the reduced RSSI.

4. The strategy for the baseline shadowing test was to position the truck equidistant from the transmitter and receiver at all times. However, at large V2V distances, the truck contributed minimally as a Non-Line of Sight (NLOS) obstruction.

7 Urban-Straight-Line Scenario Test

The Urban-Straight-Line Scenario test was conducted in downtown San Jose, California, along Santa Clara Street. This scenario was motivated by the safety applications concerned with traffic traveling along a single axis. In this test case, both the transmitter and the receiver were initially parked next to each other. The transmitter drove down Santa Clara Street for about 600 meters and at which point the transmitter pulled over to the side of the street. The receiver then drove toward the transmitter to get an additional set of data points for the same test configuration. This procedure was repeated for the test cases shown in Table 3.

Table 3: Test Cases for the Urban-Straight-Line Scenario Test

TX Power Data Rate	10dBm	20dBm	33dBm
3Mbps	Test 1	Test 3	Test 5
6Mbps	Test 2	Test 4	Test 6

7.1 Location Overview

Santa Clara Street in San Jose is fairly representative of a typical downtown scenario with a moderate-to-high level of traffic and reasonably tall buildings along both sides. Figure 15 and Figure 16 show the propagation environment along the test area. The stretch of Santa Clara Street that could be categorized as an urban setting was about 600 meters long. For this reason, the communication ranges were not measured beyond 600 meters.



Figure 15: Looking East on Santa Clara Street



Figure 16: Looking West on Santa Clara Street

7.2 Data Analysis

Figure 17 and Figure 18 show the PER versus distance and RSSI versus distance curves for the straight-line urban tests. Figure 19 and Figure 20 compare operation at 3 Mbps and 6 Mbps, using 33 dBm and 20 dBm powers as test cases.

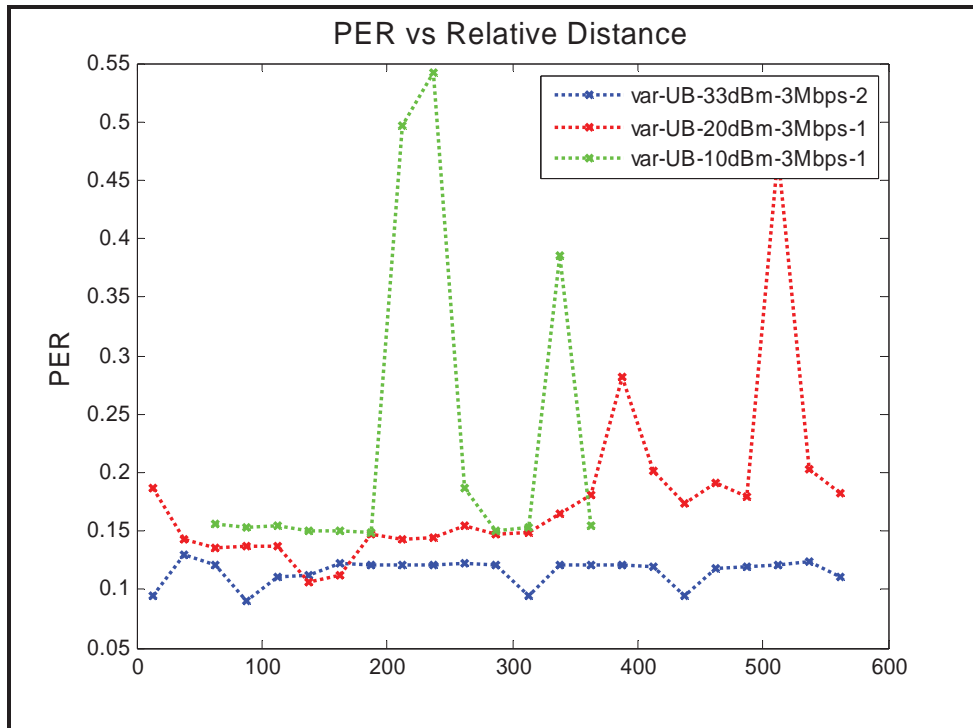


Figure 17: PER versus Distance Curves at Various Power Levels at 3 Mbps for the Urban-Straight-Line Scenario

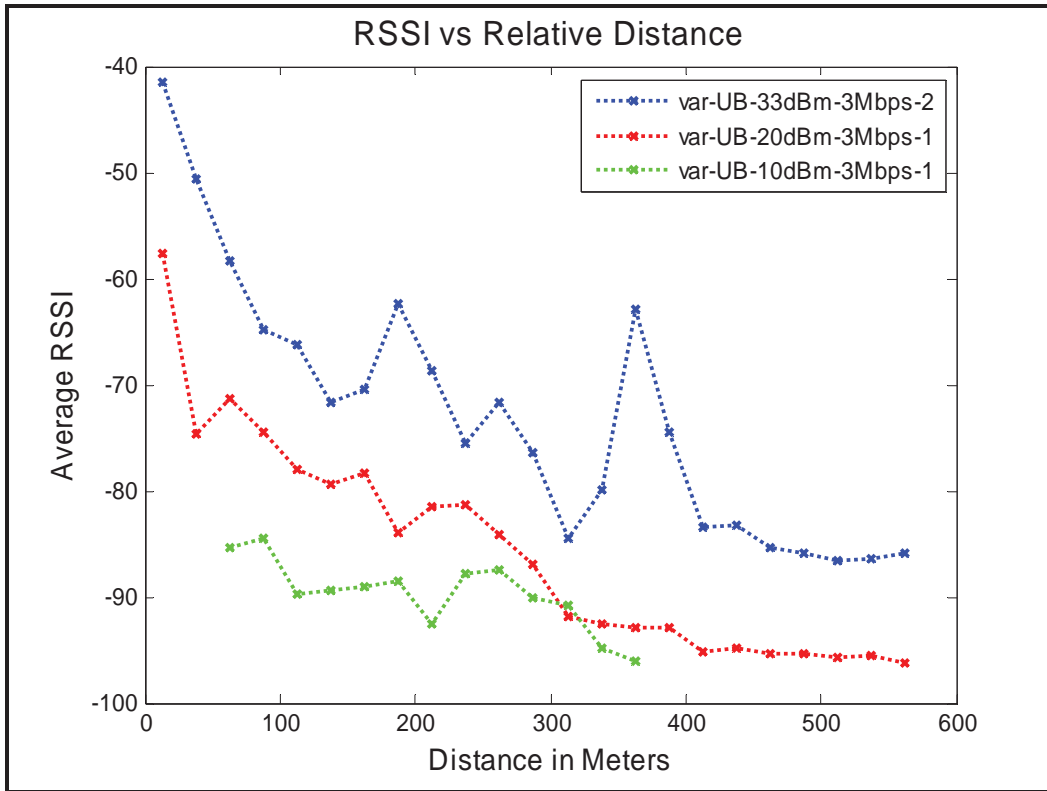


Figure 18: RSSI versus Distance Curves at Various Power Levels at 3 Mbps for the Urban-Straight-Line Scenario

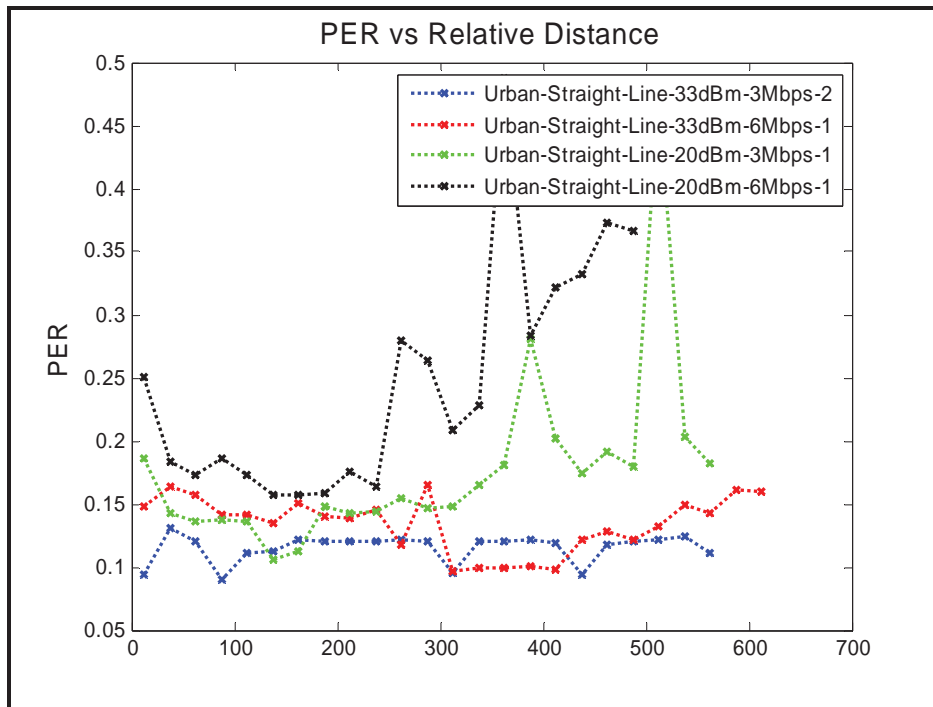


Figure 19: Comparison of PER Curves for 33 dBm and 20 dBm at 3 Mbps and 6 Mbps

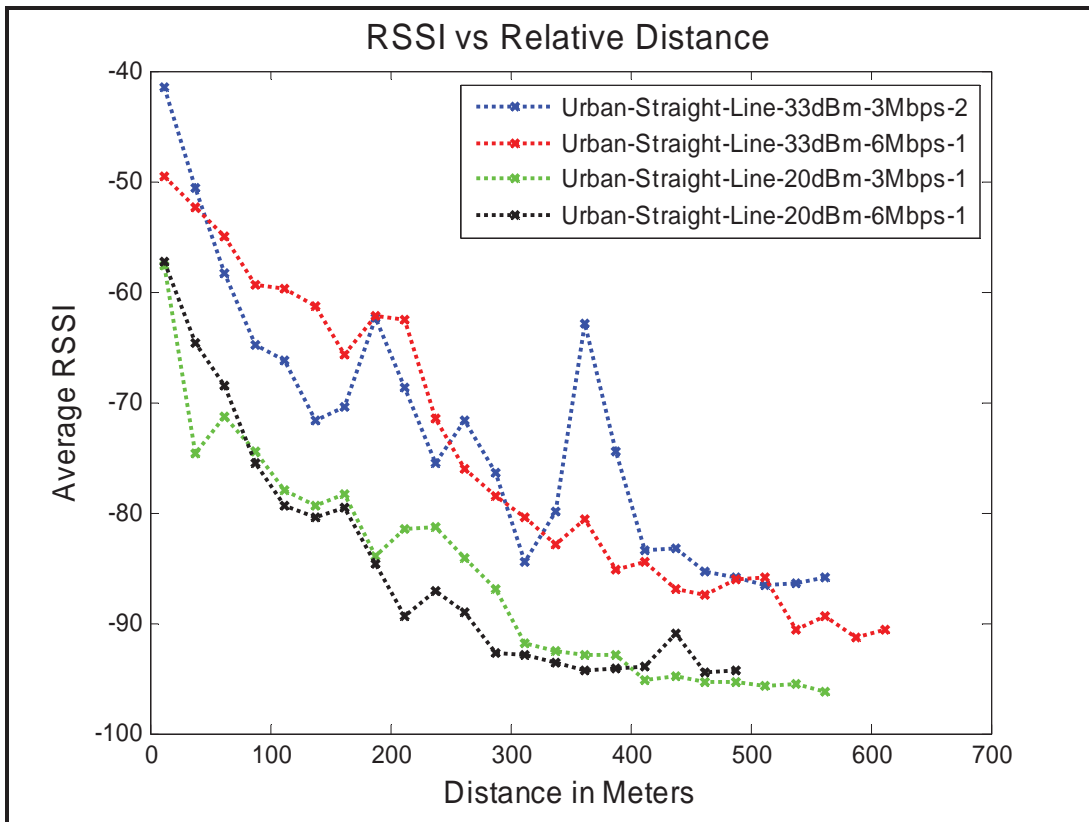


Figure 20: Comparison of RSSI Curves for 33 dBm and 20 dBm at 3 Mbps and 6 Mbps

7.3 Urban-Straight-Line Scenario Observations

1. At 33 dBm and 3 Mbps there is a fairly consistent PER between 10 percent and 15 percent across the entire 0-600 meter range. The non-trivial minimum PER contrasts with the two baseline scenarios, both of which saw PER approach zero as the inter-vehicle distance went to zero. In this case, the persistent 10 percent PER floor might be attributable to multipath due to building and vehicle reflections in the urban environment. The lower transmit powers exhibited a non-zero PER floor as well, and in the 10 dBm case, it was a bit higher, on the order of 15 percent.
2. The 10 dBm power level had a range of about 200 meters. For 20 dBm, communication became unreliable between about 400 and 500 meters. It is unclear whether the longer range associated with 33 dBm is warranted for the applications that would be active in this environment.
3. 6 Mbps transmissions performed somewhat worse than 3 Mbps transmissions at both 33 dBm and 20 dBm, but not dramatically so.

8 Urban-Closed-Intersection Scenario Test

The Urban-Closed-Intersection Scenario test was conducted in downtown San Jose, California, on the corner of Market Street and Santa Clara. This and the other intersection scenarios below were motivated specifically by intersecting geometry safety application(s). This test is categorized as a *closed*-intersection test because of the presence of (reasonably) tall buildings on all four corners of the Market-Santa Clara intersection. The transmitter-to-intersection distance was set at 5 fixed points (0 meters, 25 meters, 50 meters, 100 meters, and 150 meters), while the receiver drove toward the intersection on Santa Clara Street at the speed of traffic in each test. The test cases outlined in Table 4 were repeated three times for each of the transmitter positions.

Table 4: Test Cases for the Urban-Closed-Intersection-Scenario

TX Power Data Rate	10dBm	20dBm	33dBm
3Mbps	Test 1	Test 3	Test 5
6Mbps	Test 2	Test 4	Test 6

8.1 Location Overview

Figure 21 shows the propagation environment along Market Street. The transmitter was parked at fixed locations along this street. The buildings on the right-hand side of the street served as obstructions between the transmitter and receiver (moving down Santa Clara Street). The photo shows the farthest of the five fixed positions, 150 meters from the intersection.



Figure 21: Looking South on Market Street toward the Intersection from 150 Meters

The buildings on the corner of the Market Street and Santa Clara Street intersection served as the primary obstruction between the two vehicles. The receiver approached the intersection heading east along West Santa Clara Street.

8.2 Data Analysis

Figure 22 and Figure 23 show PER and RSSI versus receiver-to-intersection distance curves for a 33 dBm transmission at various transmitter locations (indicated in the legend). Communication performance becomes worse as the transmitter moves away from the intersection.

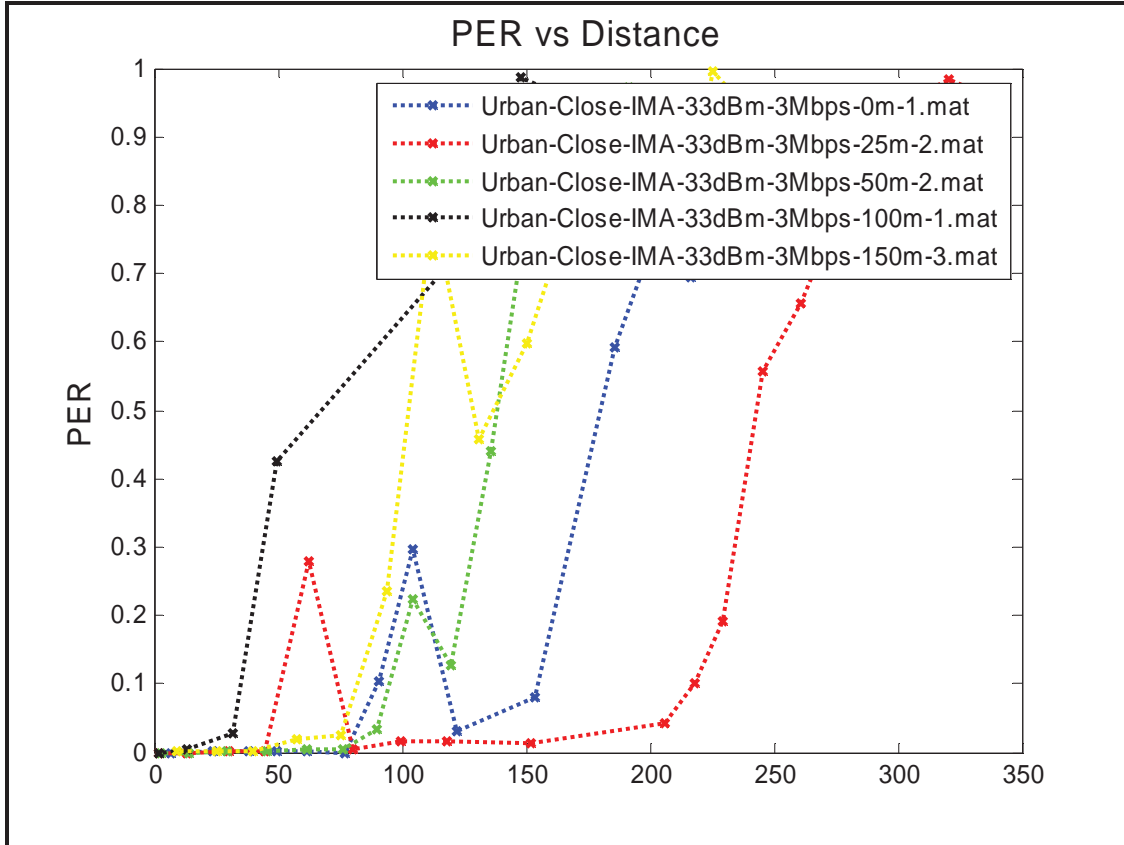


Figure 22: PER versus Distance Curve at 33 dBm and 3 Mbps for all the Different Transmitter Positions

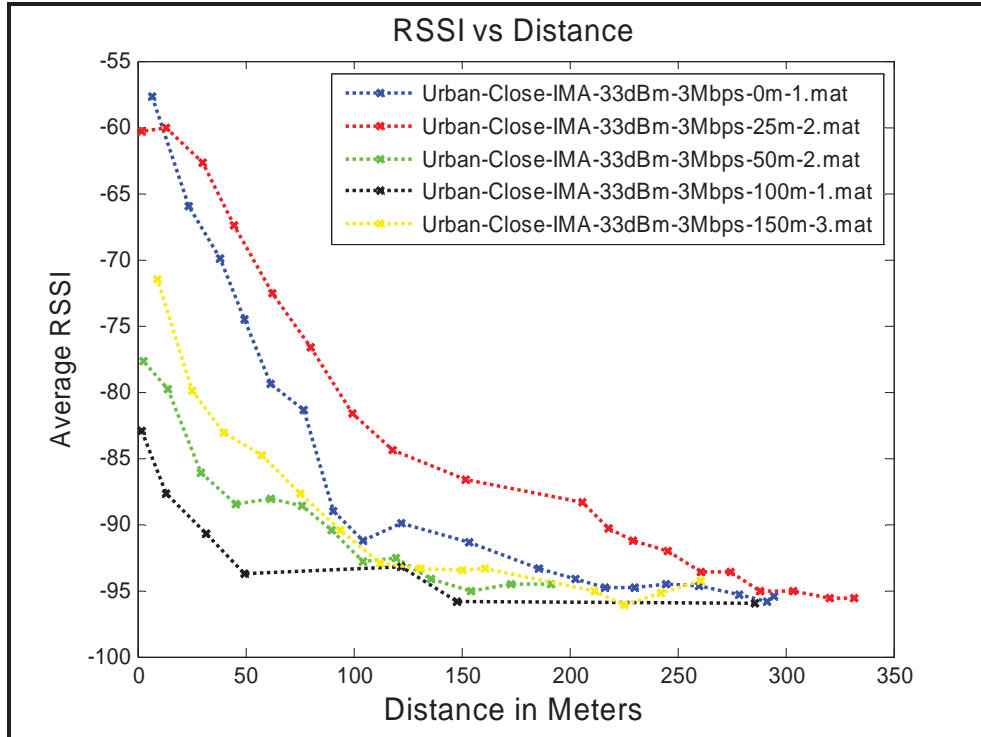


Figure 23: RSSI versus Distance Curve at 33 dBm and 3 Mbps for all the Different Transmitter Positions

Similar trends can be observed for 20 dBm transmissions (Figure 24 and Figure 25). It is clear that 33 dBm transmissions lead to increased reliability in intersection scenarios. The increased reliability of 33 dBm transmissions can be seen directly in Figure 26 and Figure 27, which compare communication performance at 10 dBm, 20 dBm, and 33 dBm.

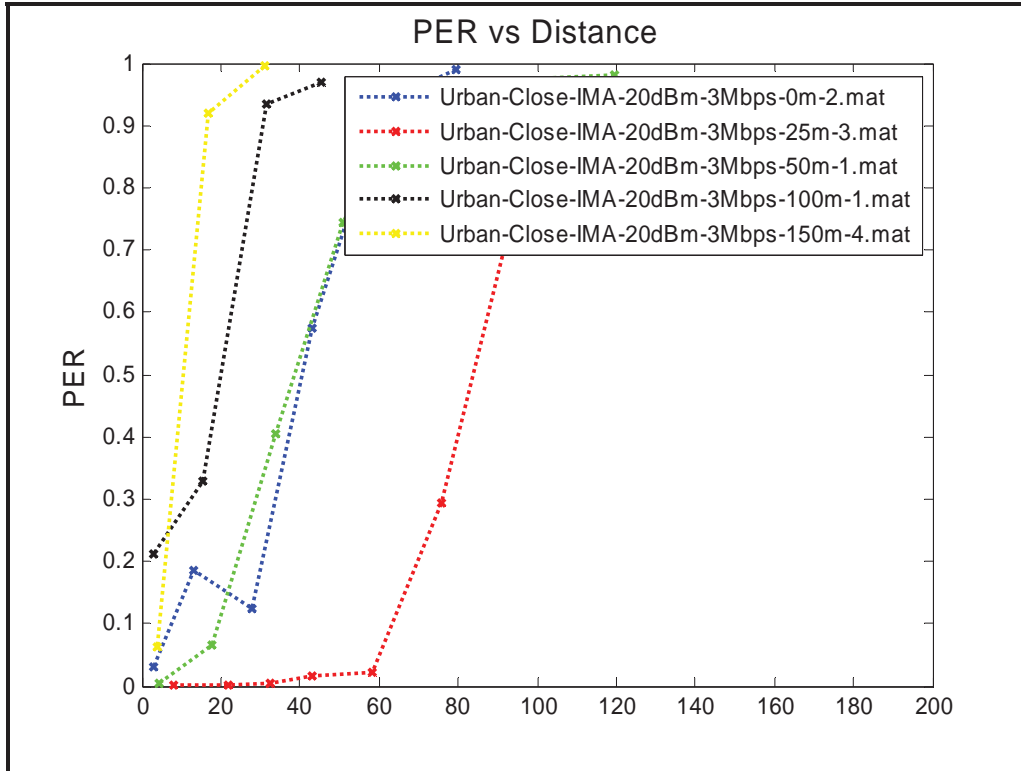


Figure 24: PER versus Distance Curve at 20 dBm and 3 Mbps for all the Different Transmitter Positions

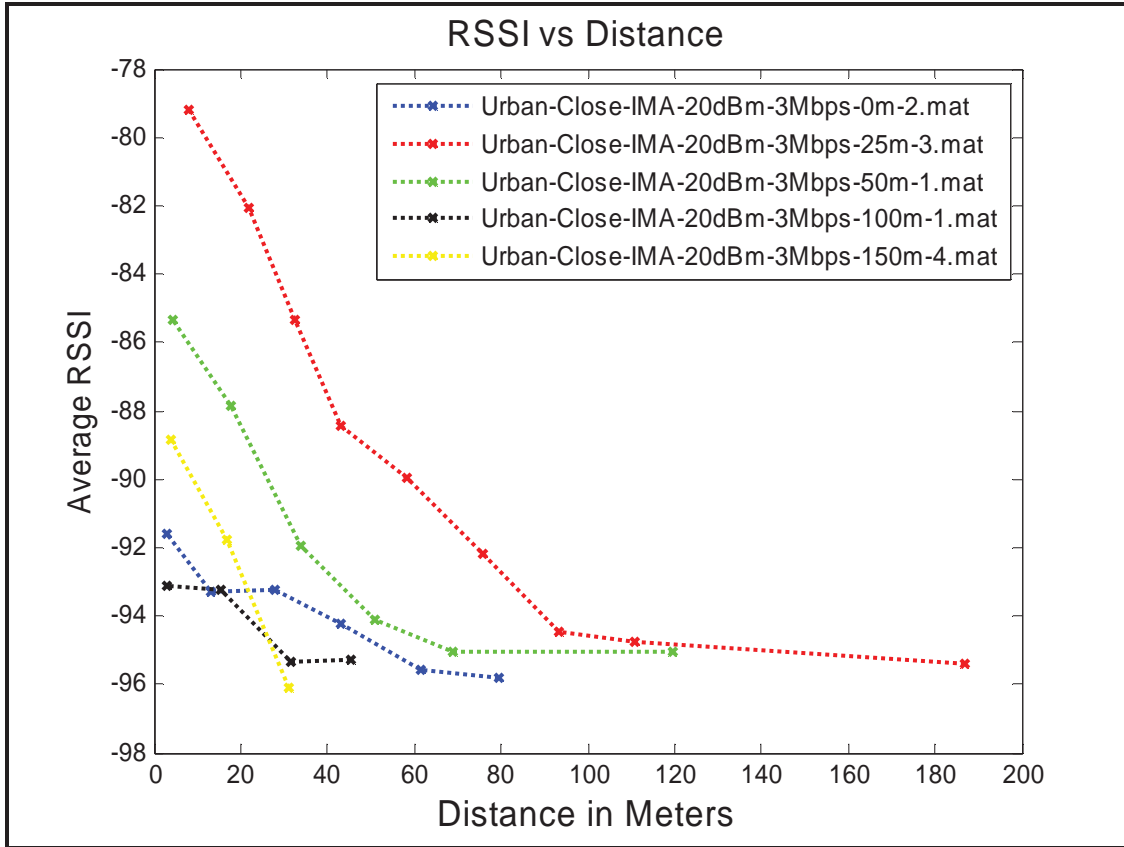


Figure 25: RSSI versus Distance Curve at 20 dBm and 3 Mbps for all the Different Transmitter Positions

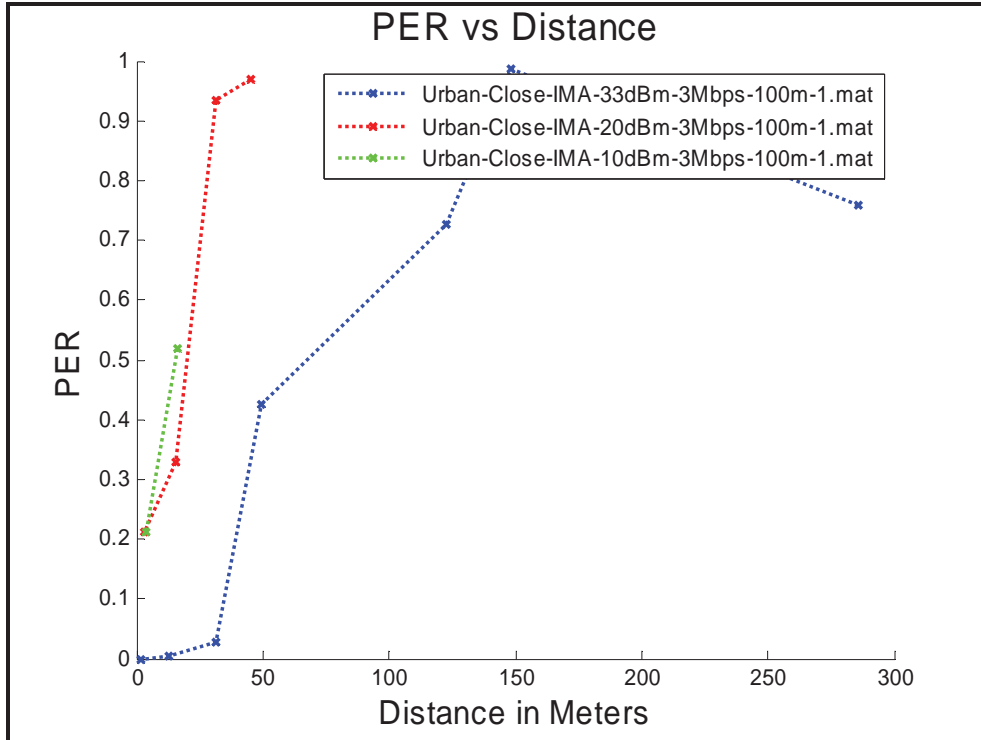


Figure 26: Comparison of PER versus Distance Curves for Various Power Levels when the Transmitter was 100 Meters from the Intersection and Set to Transmit at 3 Mbps

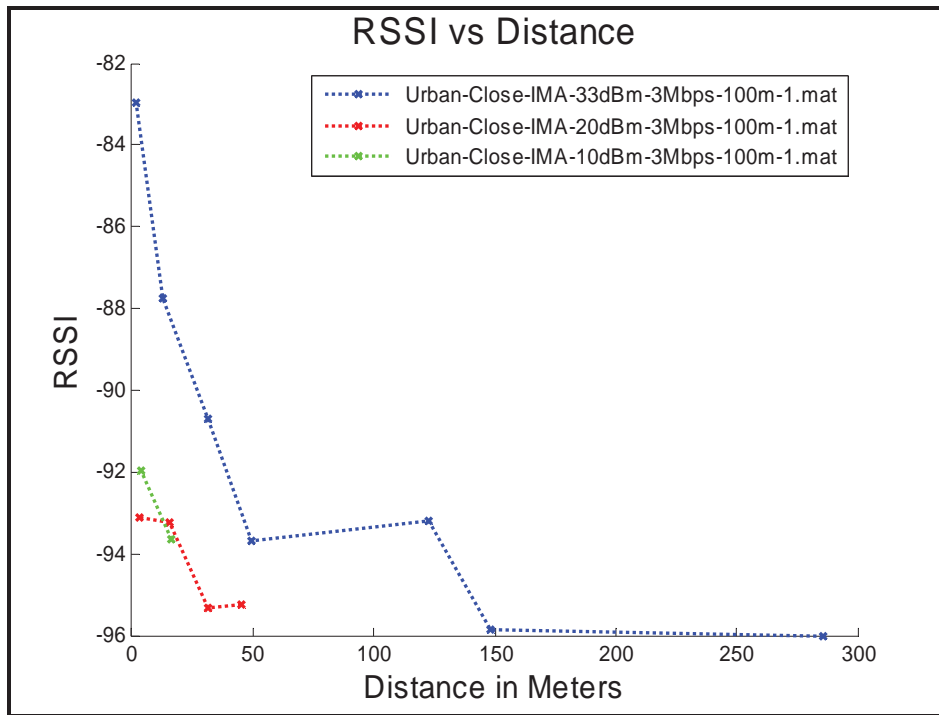


Figure 27: Comparison of RSSI versus Distance Curves for Various Power Levels when the Transmitter was 100 Meters from the Intersection and Set to Transmit at 3 Mbps

Figure 28 and Figure 29 show the effect of different data rates (3 Mbps and 6 Mbps) at different transmit powers (20 dBm and 33 dBm). It is apparent that lower rates offer marginally improved performance.

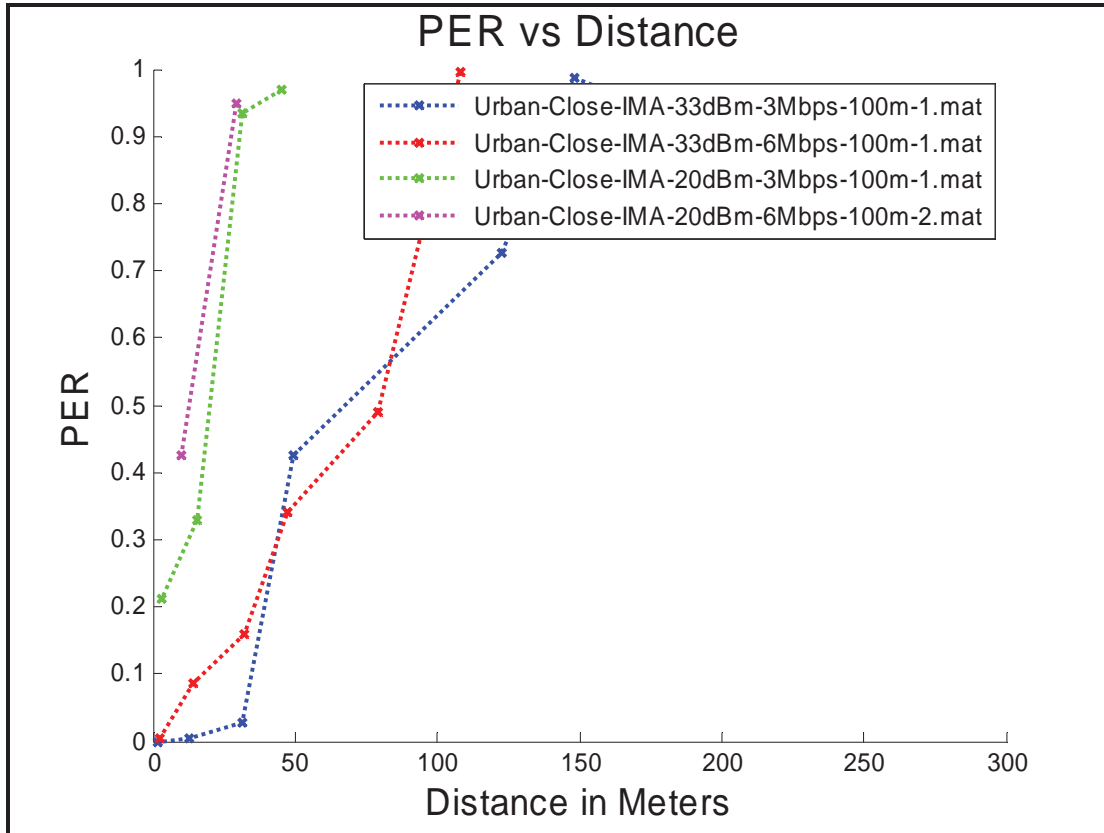


Figure 28: PER Curves in Urban-Closed-Intersection Scenario for 20 dBm and 33 dBm at 3 Mbps and 6 Mbps

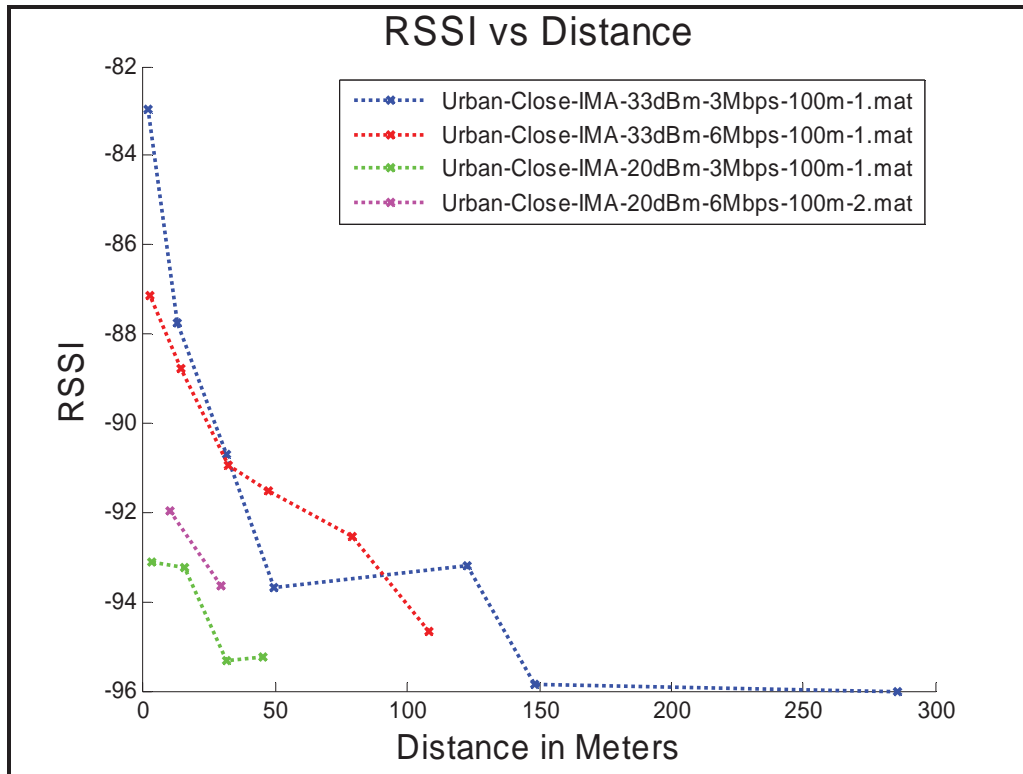


Figure 29: RSSI Curves in Urban-Closed-Intersection Scenario for 20 dBm and 33 dBm at 3 Mbps and 6 Mbps

8.3 Observations for Urban-Closed-Intersection Scenario

The following observations can be drawn with regard to communication performance in an Urban-Closed-Intersection Scenario.

1. Use of lower powers (20 dBm or lower) offered limited communication range around NLOS corners
2. At the highest permissible power level (33 dBm) and when the transmitter was 150 meters from the intersection, the receiver began to receive packets when it also was about 150 meters from the intersection, though the reception did not become dependable until the receiver was about 75 meters from the intersection.
3. By contrast, when a transmitter 150 meters from the intersection used 20 dBm transmission power, the receiver only began to receive packets when it was about 20 meters from the intersection. Reception did not reach a low PER value until the receiver physically reached the intersection.
4. It is interesting to note that the test case where the transmitter was at 100 meters consistently performed worse than the 150 meters case. Similarly, the results when the transmitter was 0 meters from the intersection consistently performed worse than the 25 meter case. These anomalies were consistent for both the 20 dBm and 33 dBm cases. There are a variety of possible explanations for this deviation from expected trends, including reflections from the buildings, building height, and traffic.

9 Urban-3/4-Open-Intersection Scenario Test

The Urban-3/4-Open-Intersection Scenario test was conducted in downtown San Jose, California, on the corner of Santa Clara and 4th Street. The intersection is categorized as 3/4 open because of relatively open spaces on 3 out of the 4 corners. The transmitter-to-intersection distance was set at 4 fixed points (0 meters, 25 meters, 60 meters, and 100 meters), while the receiver drove toward the intersection on Santa Clara Street at the speed of traffic. The test cases outlined in Table 5 were repeated twice for each of the transmitter positions.

Table 5: Test Cases for the Urban-3/4-Open-Intersection Scenario Test

TX Power / Data Rate	10dBm	20dBm	26dBm	33dBm
3Mbps	Test 1	Test 3	Test 5	Test 7
6Mbps	Test 2	Test 4	Test 6	Test 8

9.1 Location Overview

Figure 30 and Figure 31 show the intersection at ground level. Figure 30 shows one of the three “open” corners, the southeast, which is a plaza. Figure 31 shows the building on the southwest corner that constituted the principle NLOS obstruction between the transmitter (south of the intersection) and receiver (approaching from the west). The urban, propagation environment exhibited similarities with the Urban-Straight-Line Scenario test and the Urban-Closed-Intersection Scenario test (i.e., reflections from similar buildings, pavement, and vehicles, though clearly this test had a unique topology).



Figure 30: One Open Corner of the 4th Street and Santa Clara Street Intersection



Figure 31: Closed Corner of the 4th Street and Santa Clara Street Intersection

9.2 Data Analysis

Figure 32 and Figure 33 show PER and RSSI versus distance curves for 33 dBm transmissions at various transmitter locations. It can be seen that as the transmitter moves away from the intersection, communication performance worsens, with the largest degradation occurring between 25 meter and 60 meter transmitter locations.

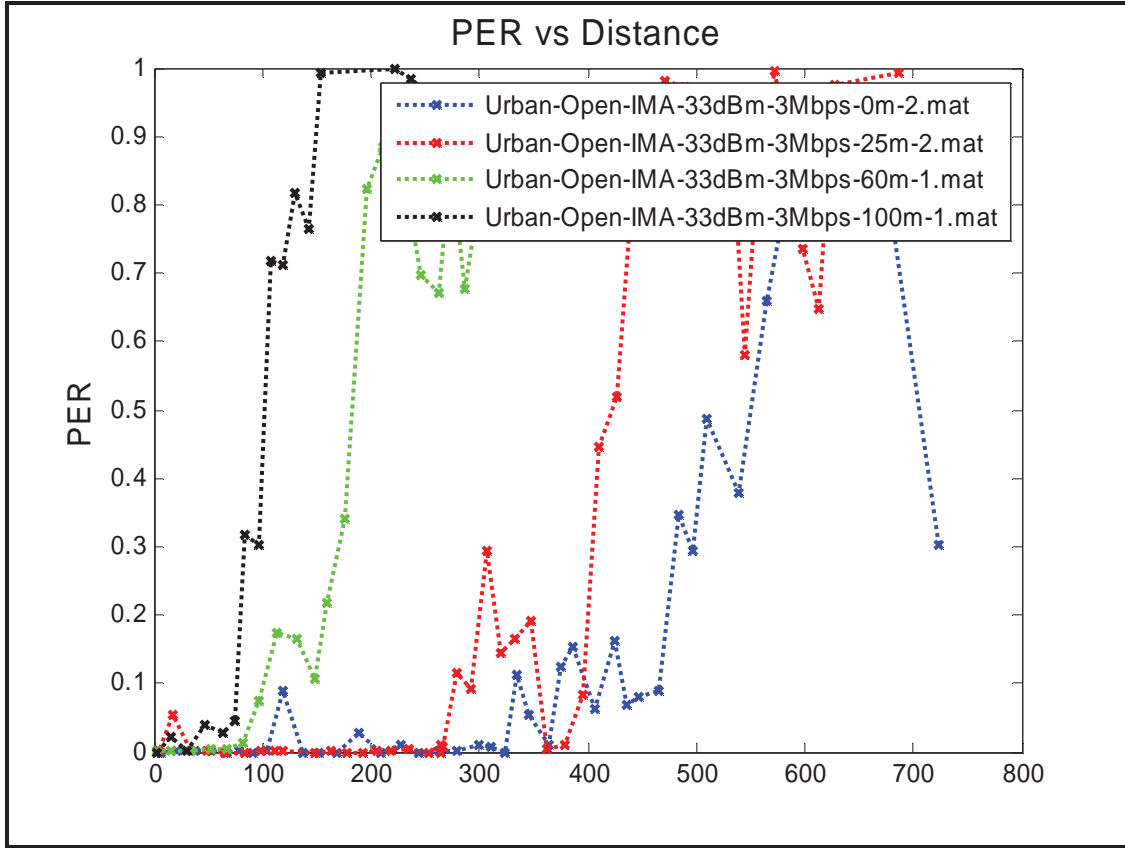


Figure 32: PER versus Distance Curve at 33 dBm and 3 Mbps for all the Different Transmitter Positions

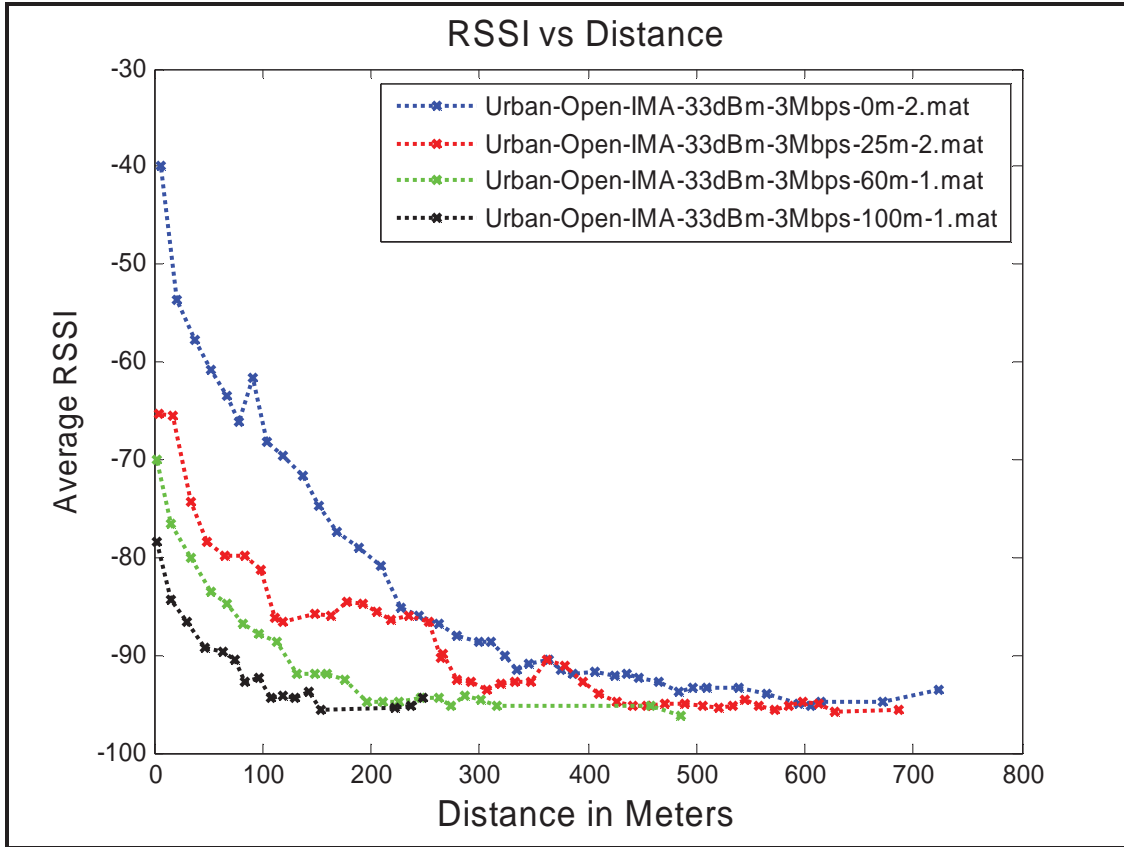


Figure 33: RSSI versus Distance Curve at 33 dBm and 3 Mbps for all the Different Transmitter Positions

Figure 34 and Figure 35 show the relationship between communication performance at 3 different power levels (20 dBm, 26 dBm, and 33 dBm) for the specific case where the transmitter was 100 meters from the intersection.

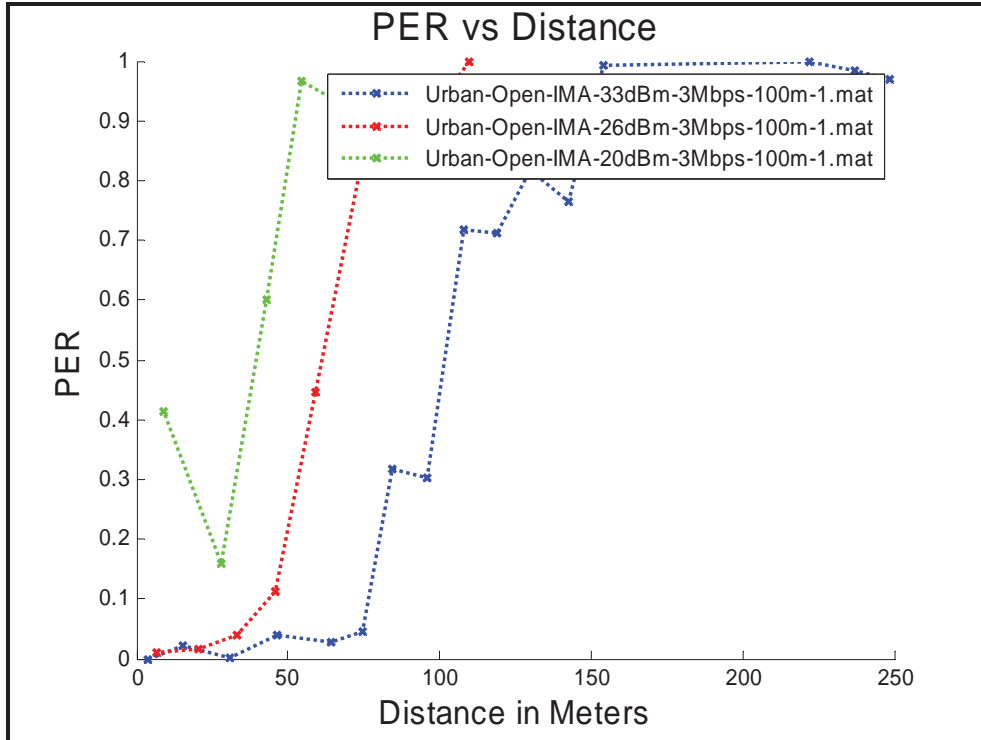


Figure 34: Comparison of PER versus Distance Curves for Various Power Levels when the Transmitter was 100 Meters from the Intersection and Set to Transmit at 3 Mbps

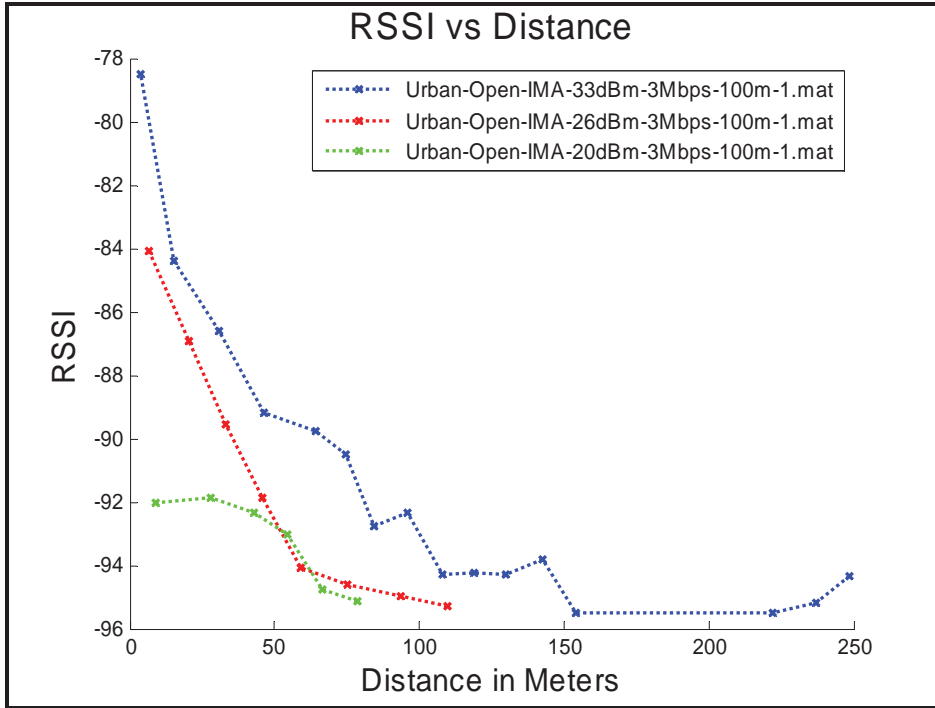


Figure 35: Comparison of RSSI versus Distance Curves for Various Power Levels when the Transmitter was 100 Meters from the Intersection and Set to Transmit at 3 Mbps

Figure 36 and Figure 37 show the effect of different data rates (3 Mbps and 6 Mbps) at different transmit powers (20 dBm and 33 dBm).

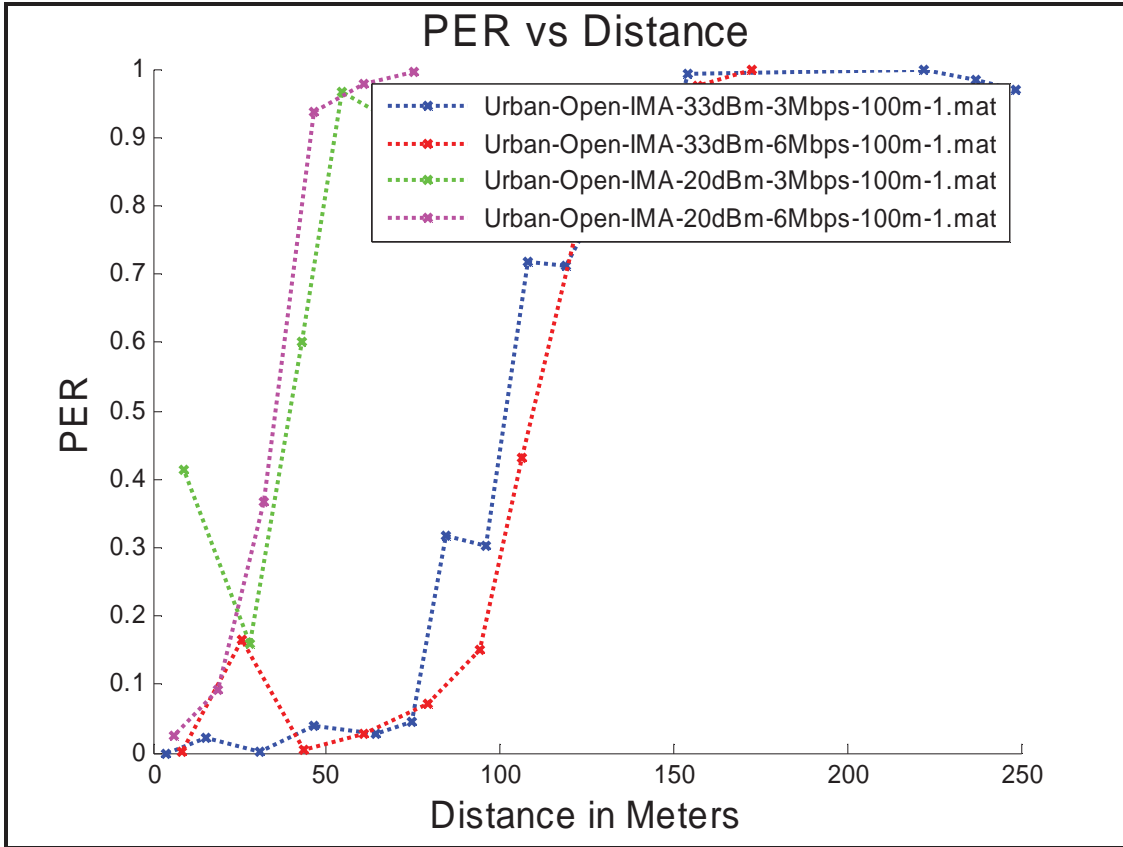


Figure 36: Comparison of PER versus Distance Curves in Urban-Open-Intersection at 33 dBm and 20 dBm for 3 Mbps and 6 Mbps

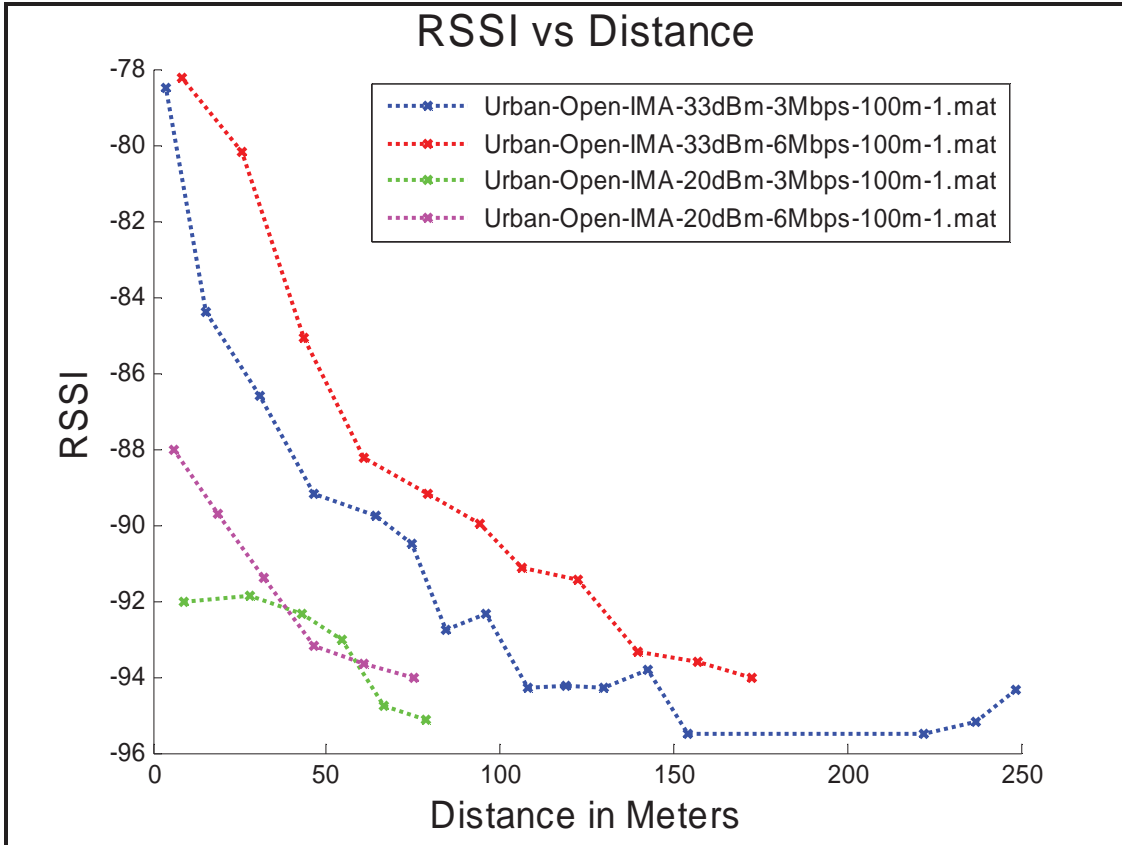


Figure 37: Comparison of RSSI versus Distance Curves in Urban-Open-Intersection at 33 dBm and 20 dBm for 3 Mbps and 6 Mbps

9.3 Observations for Urban-³/₄-Open-Intersection Scenario

The following observations can be drawn with regard to communication performance in a ³/₄-Open-Urban-Intersection Scenario:

1. Use of lower powers (20 dBm or lower) offered limited communication range around NLOS corners. In particular, Figure 36 shows that when the transmitter was 100 meters from the intersection, a 20 dBm transmission could not be heard at all by a receiver more than approximately 50 meters from the intersection, and could not be heard reliably (< 10 percent PER) until the receiver was within a few meters of the intersection.
2. At the highest permissible power level (33 dBm), a transmitter 100 meters from the intersection began to be heard by a receiver about 250 meters from the intersection and reliable communication (PER < 10 percent) began at about 75 meters
3. The lower 3 Mbps bit rate does not offer any appreciable advantage compared to the 6 Mbps bit rate

9.4 Comparison of Urban-Closed-Intersection and Urban-³/₄-Open-Intersection Scenarios

Figure 38 and Figure 39 offer a comparison between the Urban-Closed-Intersection Scenario (3 runs) and Urban-³/₄-Open-Intersection Scenario tests (2 runs) in an urban setting. Only one transmitter location (100 meters) is used for the comparison. It is interesting to note that the Open Intersection case resulted in more reliable communications, extending the range where the receiver experiences 10 percent PER or less from about 40 meters to about 80 meters. This is consistent with a view that the closed intersection’s additional reflection points create a more challenging multi-path environment, but it is contrary to an opposing view that the lack of an obvious reflection point makes the Urban-³/₄-OpenIntersection Scenario test case more difficult.

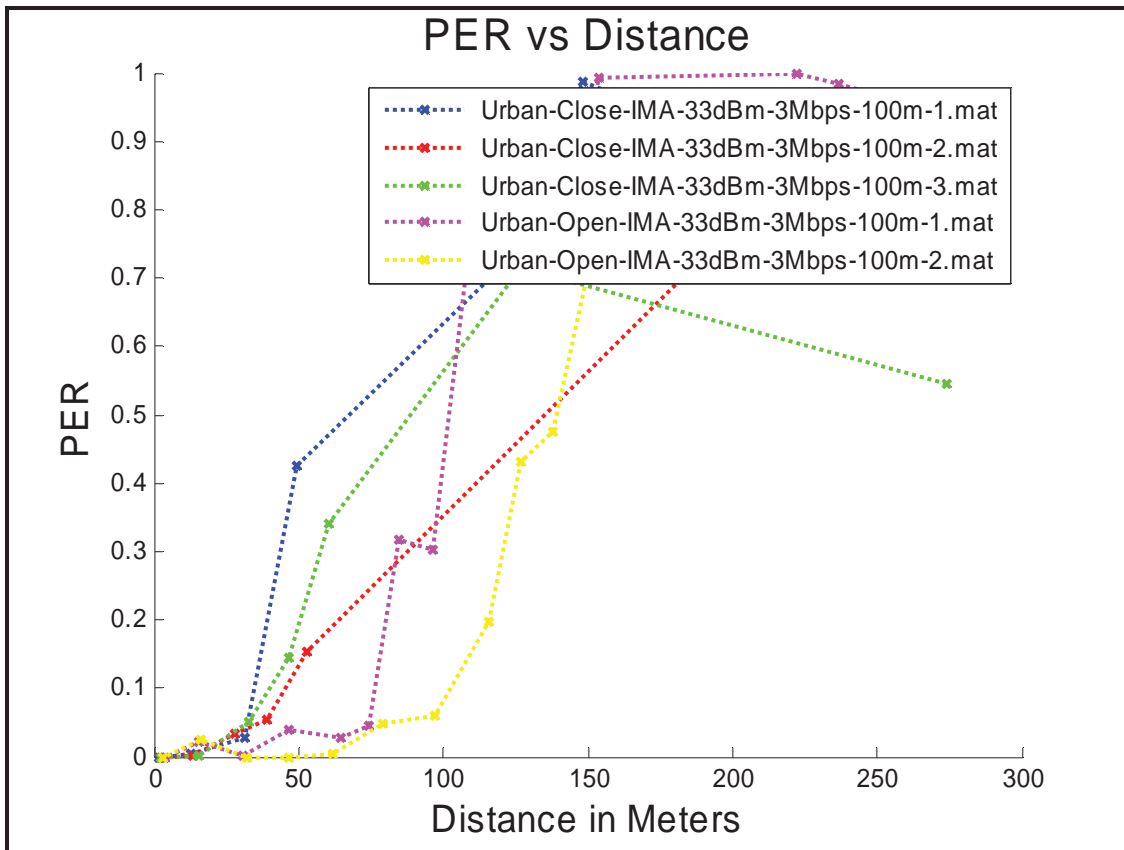


Figure 38: PER Comparison of Urban-Closed-Intersection Scenario and Urban-Open-Intersection Scenario for 33 dBm at 3 Mbps

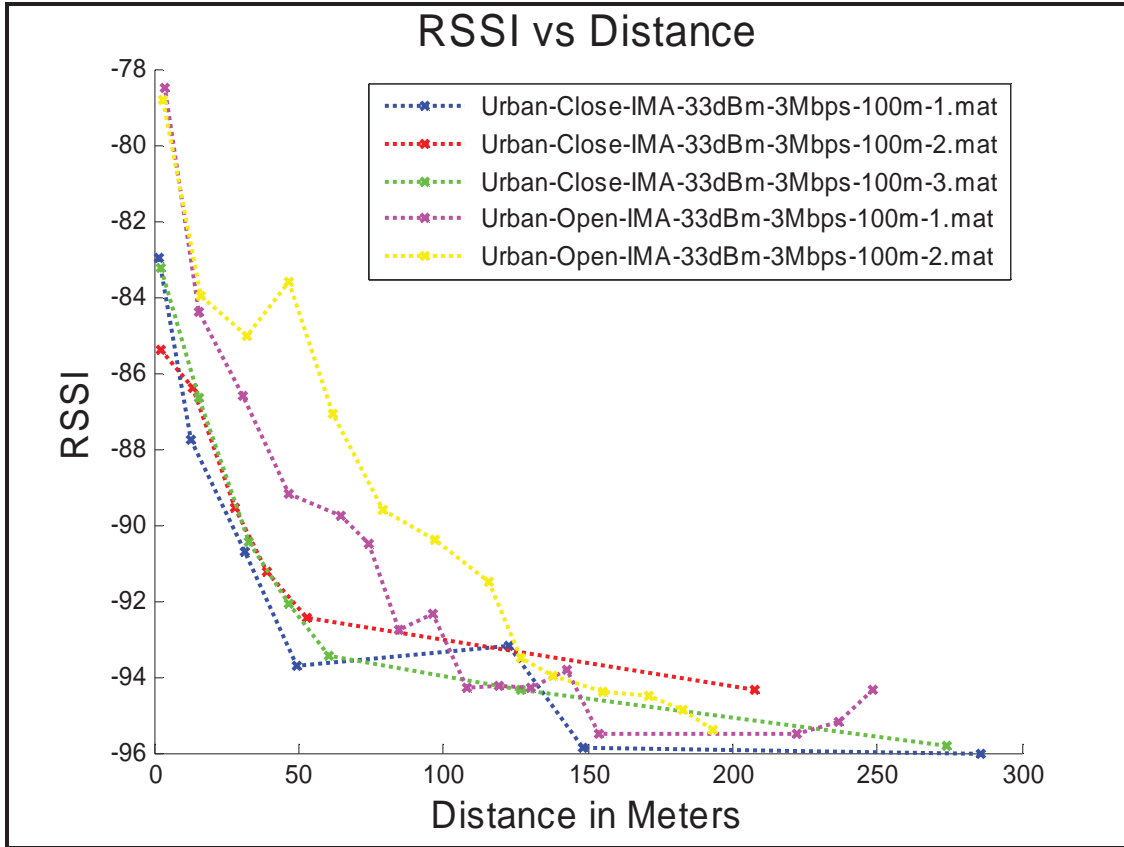


Figure 39: RSSI Comparison of Urban-Closed-Intersection Scenario and Urban-Open-Intersection Scenario for 33 dBm at 3 Mbps

10 Suburban-Closed-Intersection Scenario Test

The Suburban-Closed-Intersection Scenario test was conducted in Palo Alto, California, on the corner of Santa Rita Avenue and Byron Street. The test is categorized as a closed-intersection test because of the presence of homes on all four corners of the intersection. The transmitter-to-intersection distance was set at 3 fixed points (0 meters, 50 meters, and 100 meters), while the receiver drove toward the intersection at a speed of 5 mph. The test cases outlined in Table 6 were repeated for each of the transmitter positions.

Table 6: Test Cases for Suburban-Closed-Intersection Scenario

		TX Power			
		10dBm	20dBm	26dBm	33dBm
Data Rate	3Mbps	Test 1	Test 3	Test 5	Test 7
	6Mbps	Test 2	Test 4	Test 6	Test 8

10.1 Location Overview

Figure 40 and Figure 41 show the propagation environment for the Suburban-Closed-Intersection Scenario. The corner of Santa Rita and Byron is fairly representative of a

typical suburban environment with a lining of trees and single story homes on both sides of the street.

The home on the west corner of the intersection (Figure 40) served as the primary LOS obstruction between the two vehicles.



Figure 40: West Corner of Santa Rita Avenue and Byron Street

Figure 41 gives an idea of the propagation environment as the receiver drove northeast on Santa Rita Avenue toward the intersection².



Figure 41: Propagation Environment along Santa Rita Avenue

² The photo in Figure 41 was not taken on the day of testing; the parked vehicles shown were not present.

10.2 Data Analysis

Figure 42 and Figure 43 show PER and RSSI versus distance curves for a 33 dBm transmission at various transmitter locations. It can be seen that communication performance worsens as the transmitter moves away from the intersection.

Figure 44 and Figure 45 show the relationship between communication performance at two different power levels (20 dBm and 33 dBm).

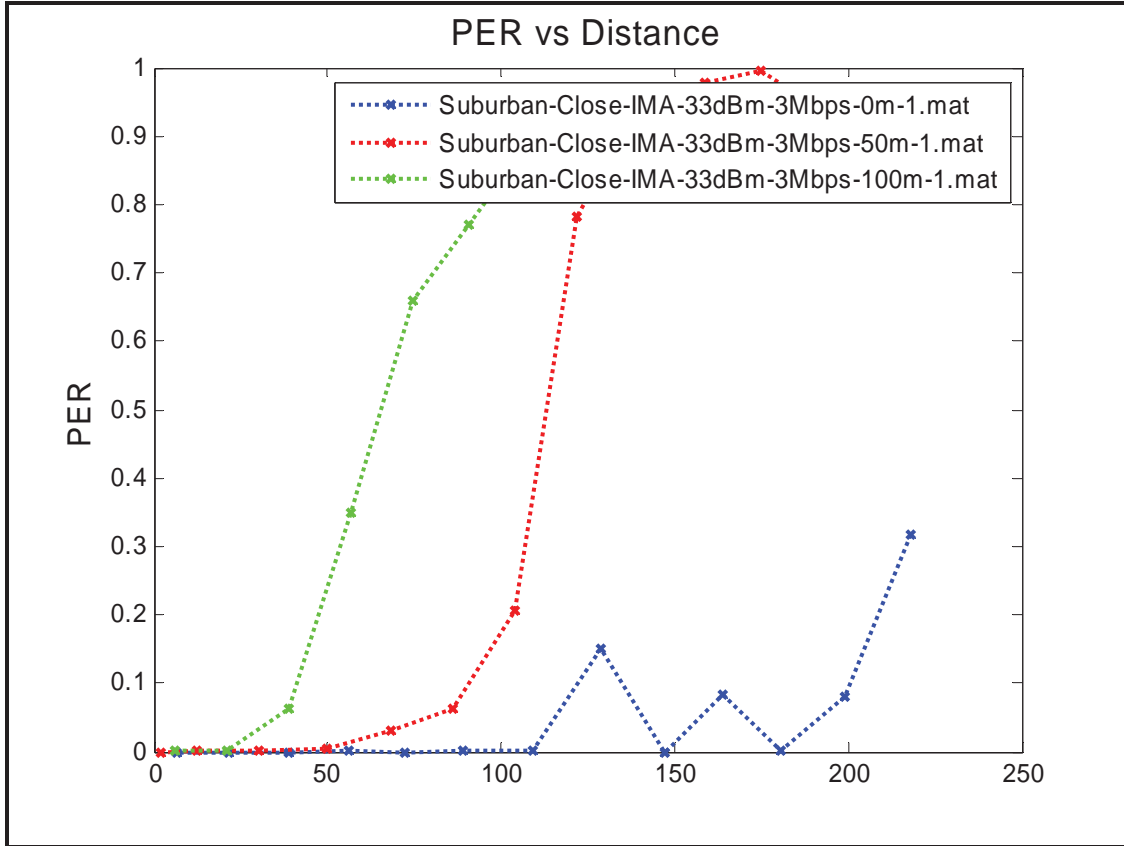


Figure 42: PER versus Distance Curves for Various Transmitter Locations at 33 dBm and 3 Mbps

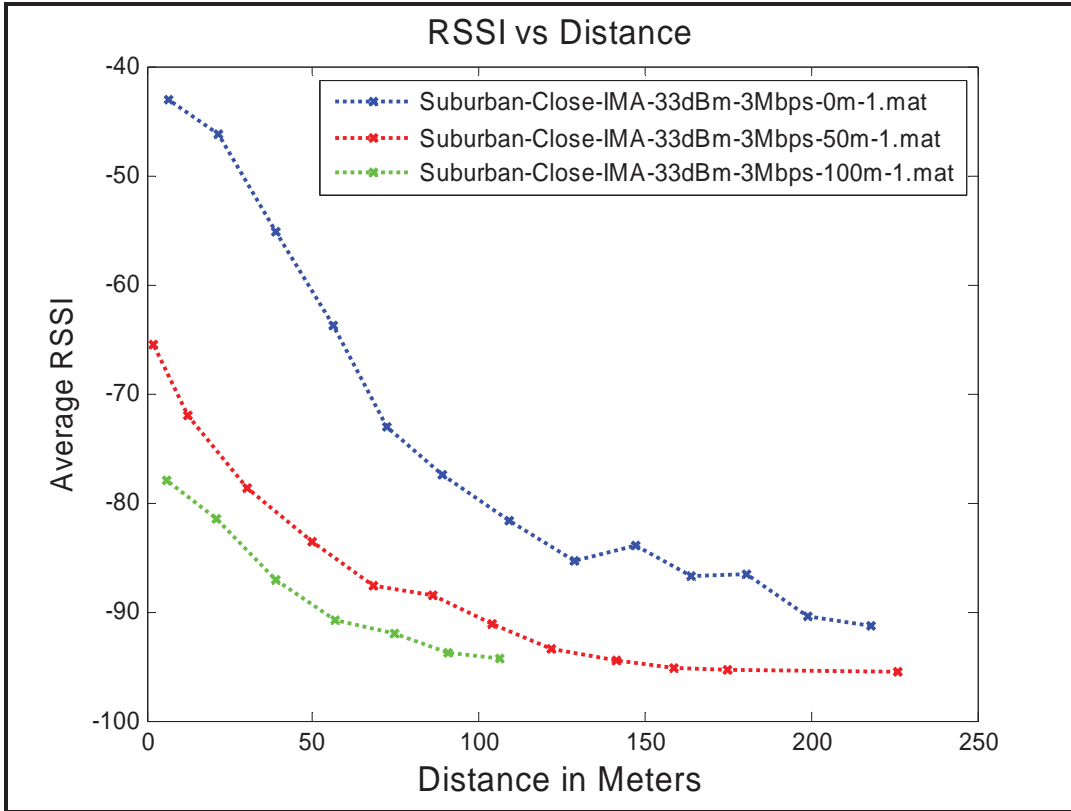


Figure 43: RSSI versus Distance Curves for Various Transmitter Locations at 33 dBm and 3 Mbps

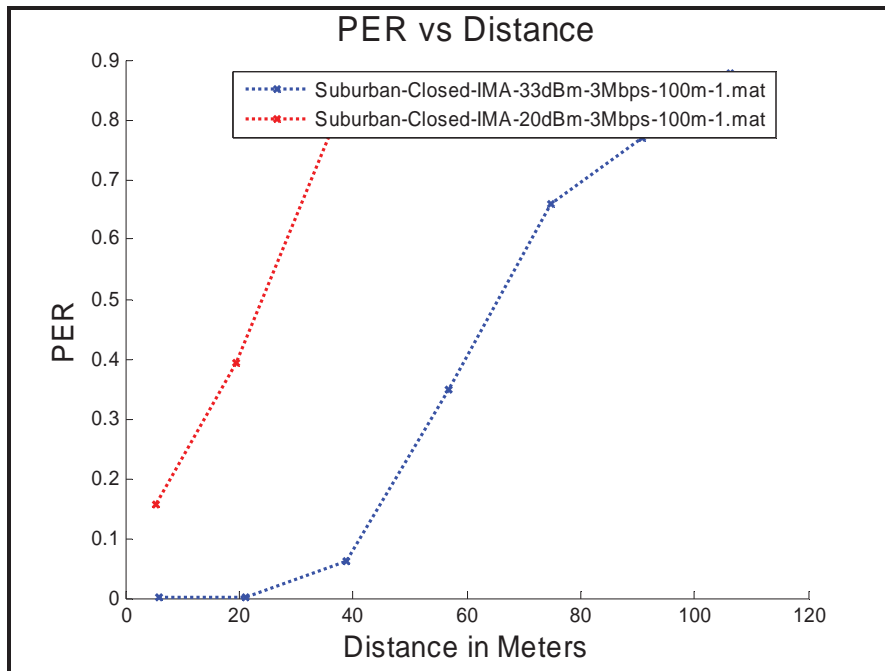


Figure 44: Comparison of PER versus Distance Curves between 20 dBm and 33 dBm when the Transmitter was 100 Meters from the Intersection and Set to Transmit at 3 Mbps

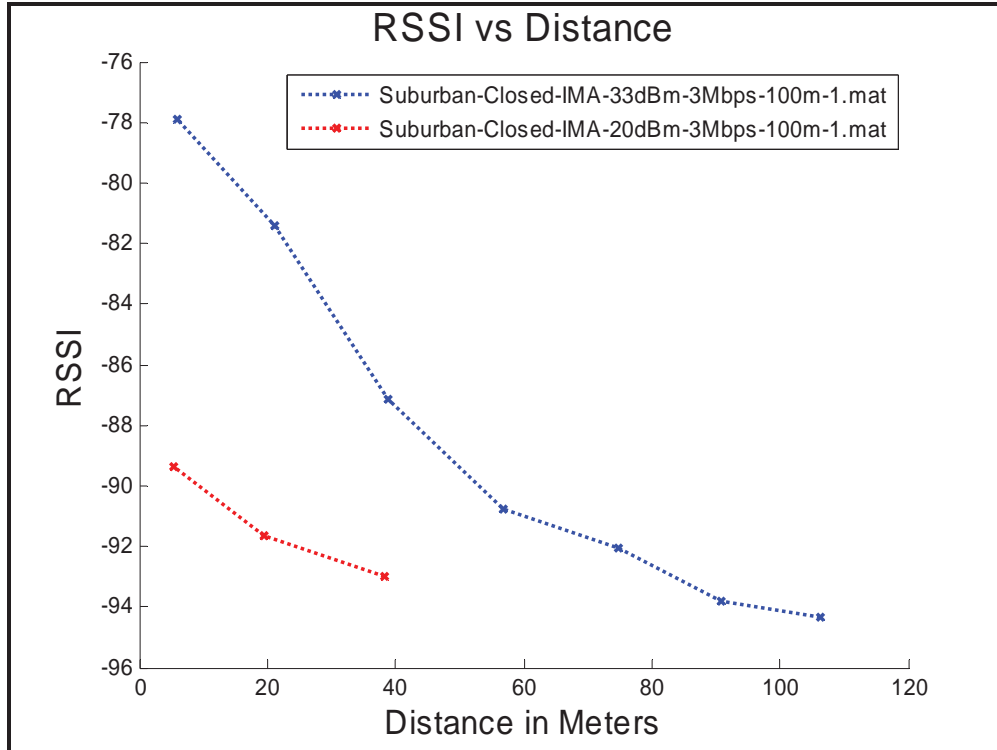


Figure 45: Comparison of RSSI versus Distance Curves between 20 dBm and 33 dBm when the Transmitter as 100 Meters from the Intersection and Set to Transmit at 3 Mbps

Figure 46 and Figure 47 show the effect of different data rates (3 Mbps and 6 Mbps) at different transmit powers (20 dBm and 33 dBm) for the specific case where the transmitter was 50 meters from the intersection.

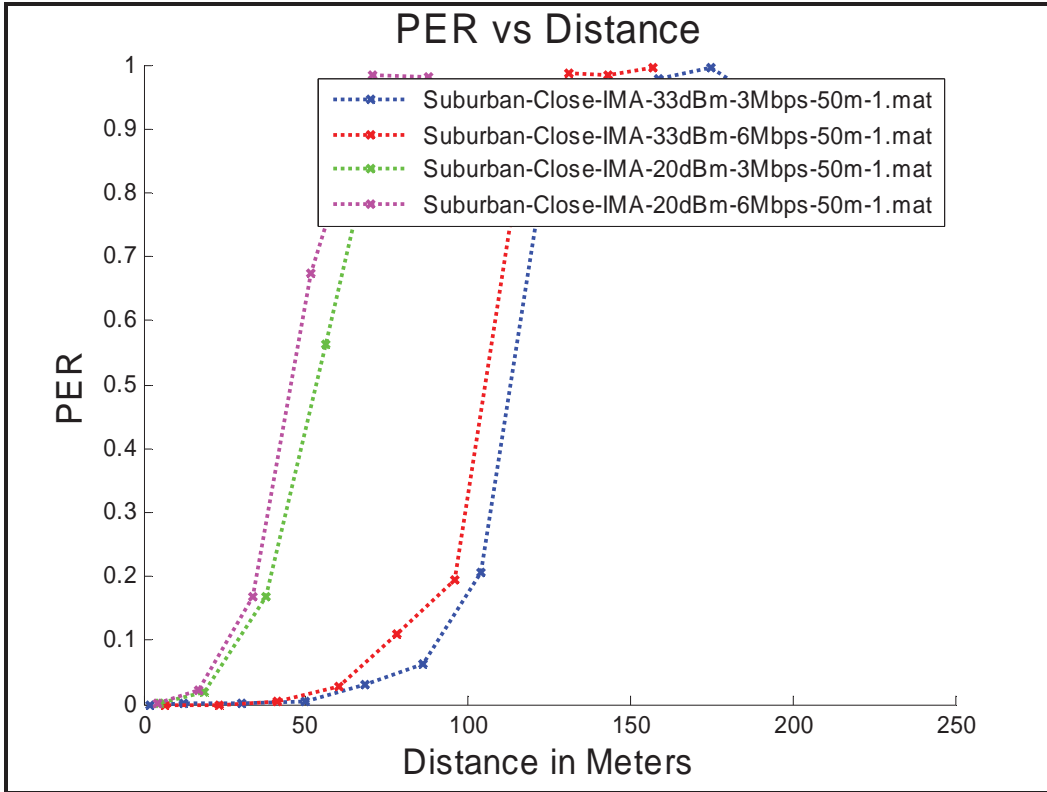


Figure 46: PER Comparison for Suburban-Closed-Intersection Scenario for 33 dBm and 20 dBm at 3 Mbps and 6 Mbps

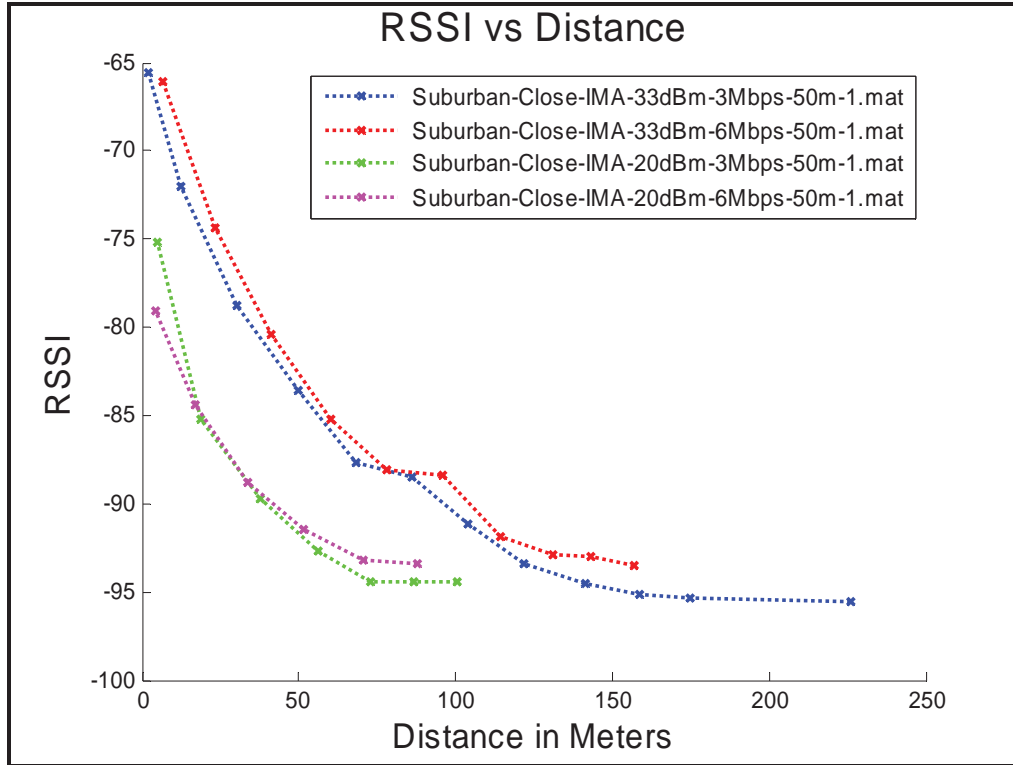


Figure 47: RSSI Comparison for Suburban-Closed-Intersection Scenario for 33 dBm and 20 dBm at 3 Mbps and 6 Mbps

10.3 Observations for Suburban-Closed-Intersection Scenario

The following observations can be drawn with regard to communication performance in a Suburban-Closed-Intersection Scenario:

1. Use of lower powers (20 dBm or lower) offered limited communication range around NLOS corners. In particular, when the transmitter was 100 meters from the intersection, the receiver was not able to achieve a PER lower than 15 percent. When the transmitter was 50 meters from the intersection, the receiver achieved a low PER (< 10 percent) when it was about 25 meters from the intersection. See Figure 44 and Figure 46.
2. By contrast, when the transmitter was set to 33 dBm and was 100 meters from the intersection, the receiver began decoding packets reliably (PER < 10 percent) at about 40 meters from the intersection. When the transmitter was 50 meters from the intersection, reliable reception began at about 80 meters. See Figure 42.
3. The lower 3 Mbps bit rate offers a marginal advantage as compared to the 6 Mbps bit rate

11 Suburban-³/₄-Open-Intersection Scenario Test

The Suburban-³/₄-Open-Intersection Scenario test was conducted in Menlo Park, California, on the corner of Middlefield Road and Willow Road. The intersection is

categorized as $\frac{3}{4}$ open because of relatively open spaces on 3 out of the 4 corners. The transmitter-to-intersection distance was set at 3 fixed points (16 meters, 50 meters, and 80 meters), while the receiver drove toward the intersection at the speed of traffic. The test cases outlined in Table 7 were repeated for each of the transmitter positions.

Table 7: Test Cases for the Suburban-3/4-Open-Intersection Scenario

Data Rate \ TX Power	TX Power			
	10dBm	20dBm	26dBm	33dBm
3Mbps	Test 1	Test 3	Test 5	Test 7
6Mbps	Test 2	Test 4	Test 6	Test 8

11.1 Location Overview

The east corner of this intersection has a one-story office building with trees while the other three corners have lawns or parking with setback buildings. The building on the east corner served as the obstruction between the two vehicles.

11.2 Data Analysis

Figure 48 and Figure 49 show PER and RSSI versus distance curves for 33 dBm transmissions at various transmitter locations. It can be seen that when the transmitter was 16 meters from the intersection, transmitter performance was better than when it moved farther away. Also, there was little difference in performance between the 50 meter and 85 meter transmitter locations.

Figure 50 and Figure 51 show the relationship between communication performance at 3 different power levels (20 dBm, 26 dBm, and 33 dBm).

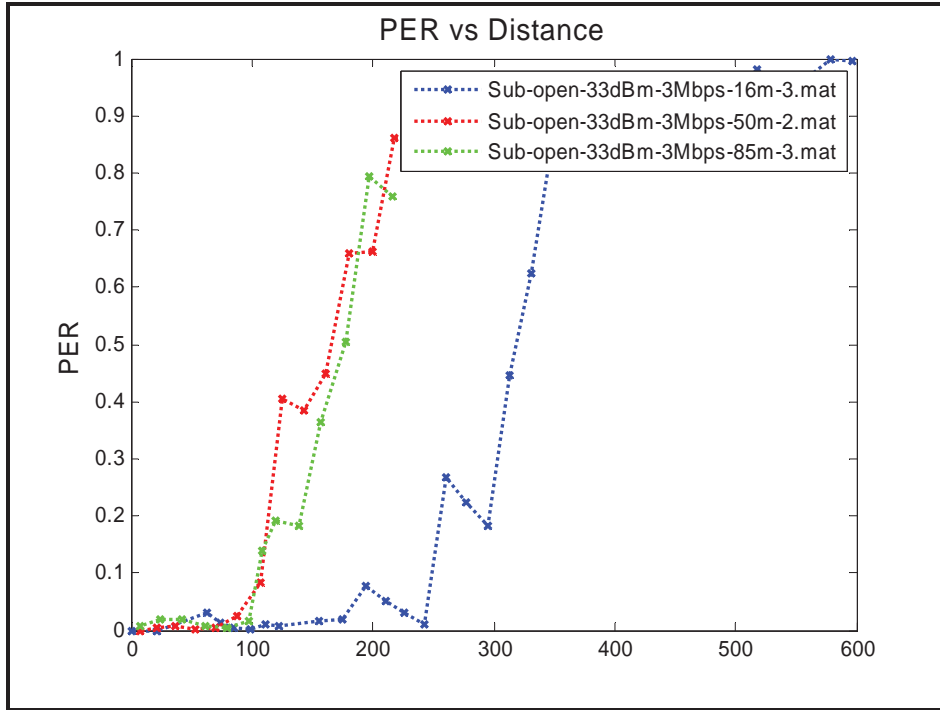


Figure 48: PER versus Distance Curves for Various Transmitter Locations at 33 dBm and 3 Mbps

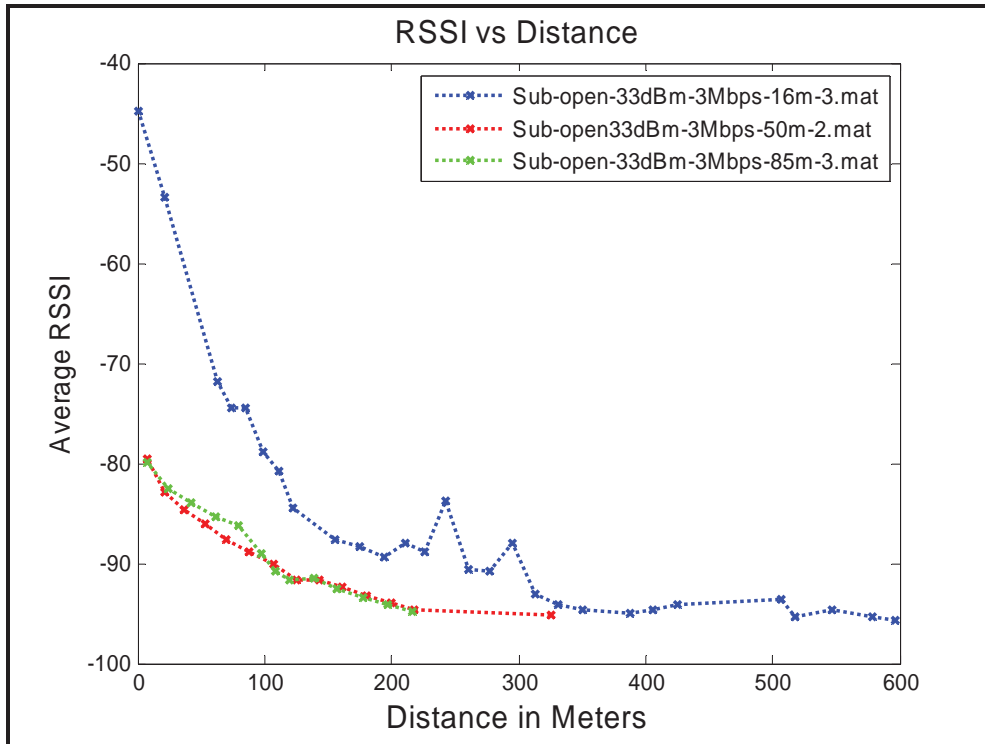


Figure 49: RSSI versus Distance Curves for Various Transmitter Locations at 33 dBm and 3 Mbps

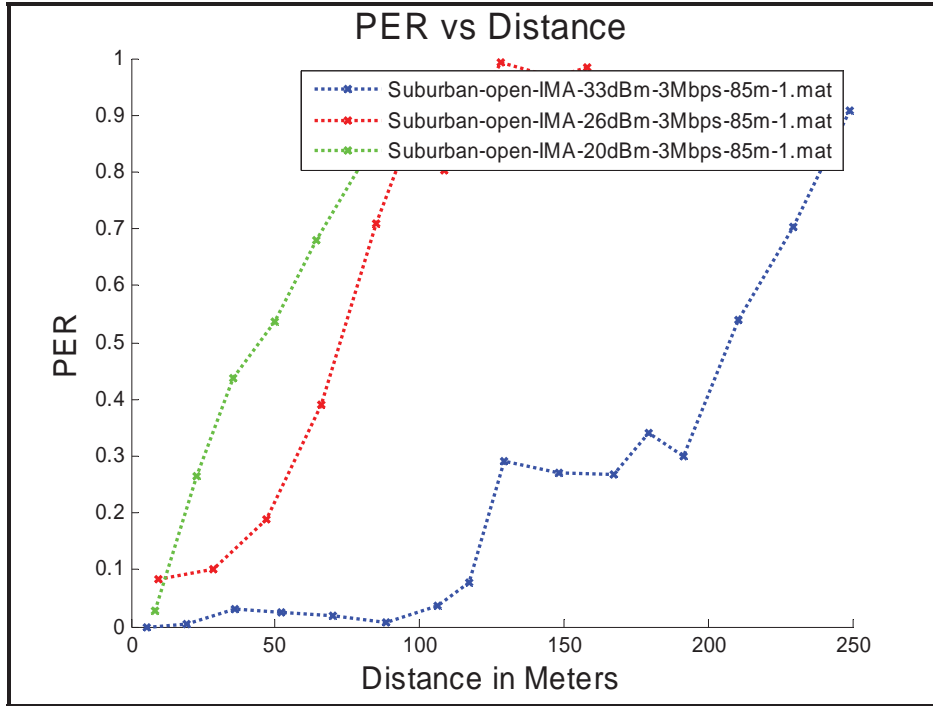


Figure 50: Comparison of PER versus Distance Curves Between 20 dBm, 26 dBm, and 33 dBm when the Transmitter was 85 Meters from the Intersection and Set to Transmit at 3 Mbps

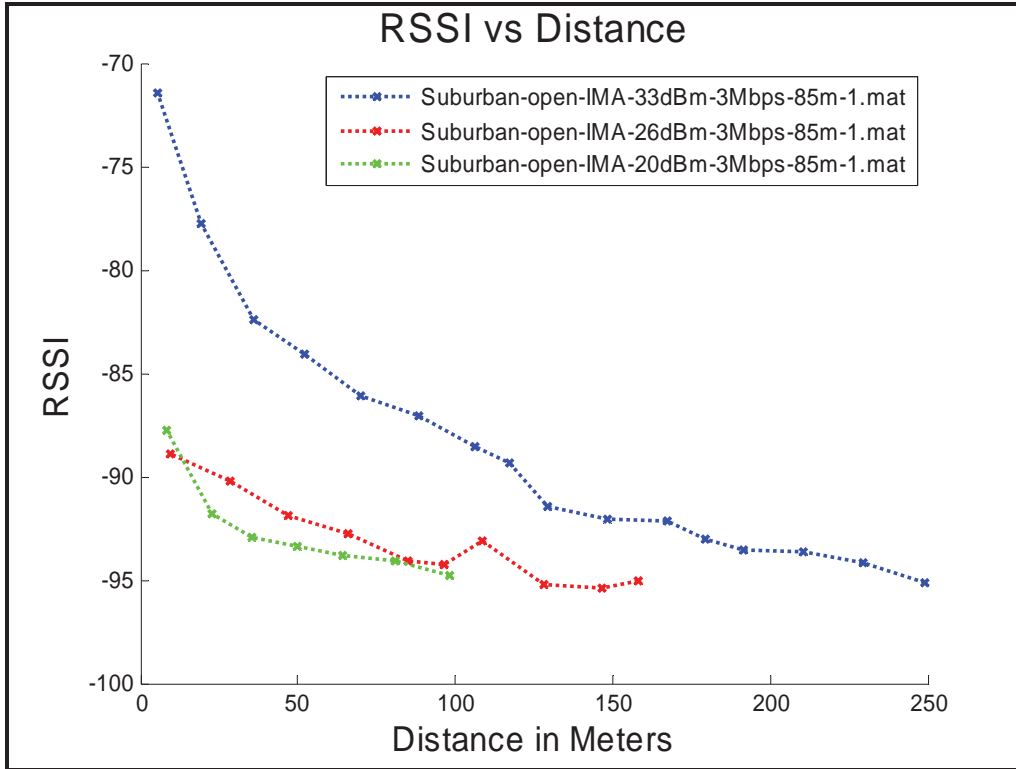


Figure 51: Comparison of RSSI versus Distance Curves between 20 dBm, 26 dBm, and 33 dBm when the Transmitter was 85 Meters from the Intersection and Set to Transmit at 3 Mbps

Figure 52 and Figure 53 show the effect of different data rates (3 Mbps and 6 Mbps) at different transmit powers (20 dBm and 33 dBm) for the specific case where the transmitter was 50 meters from the intersection.

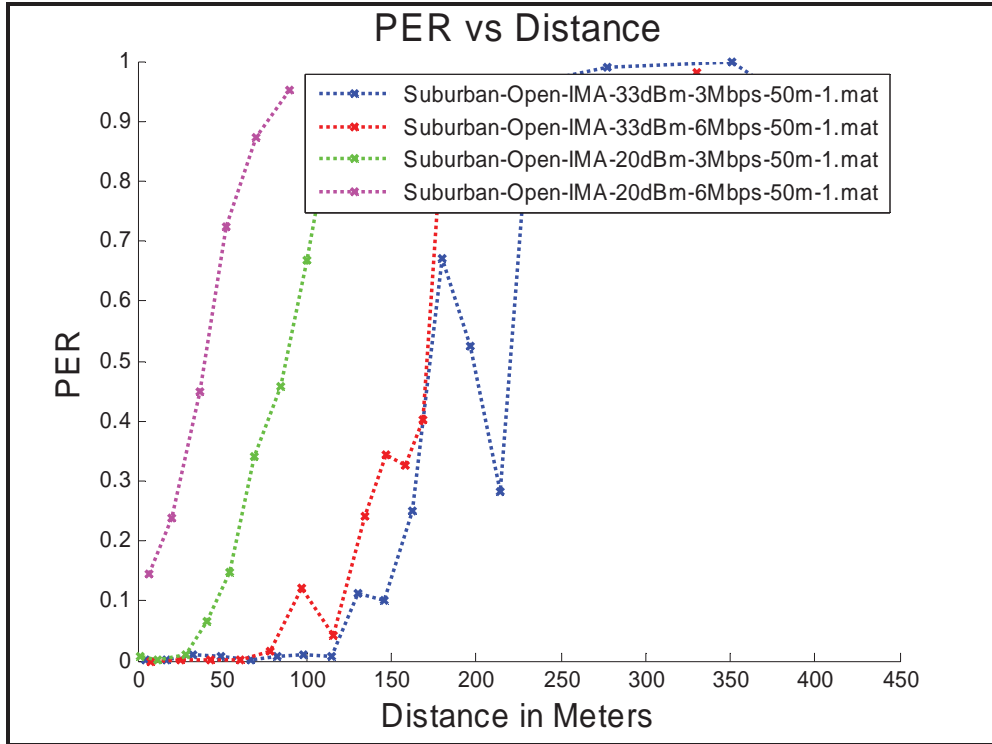


Figure 52: PER Comparison for Suburban-3/4-Open-Intersection Scenario for 33 dBm and 20 dBm at 3 Mbps and 6 Mbps

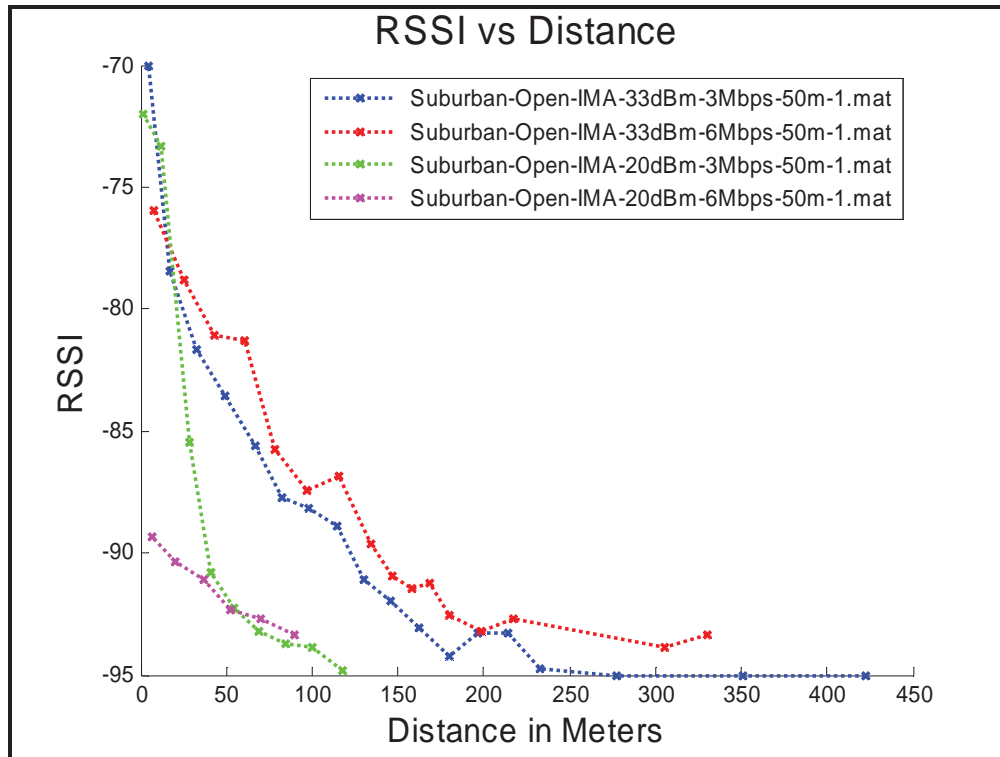


Figure 53: RSSI Comparison for Suburban-3/4-Open-Intersection Scenario for 33 dBm and 20 dBm at 3 Mbps and 6 Mbps

11.3 Observations for Suburban-³/₄-Open-Intersection Scenario

The following observations can be drawn with regard to communication performance in a Suburban -³/₄-Open-Intersection Scenario:

1. Use of lower powers (20 dBm or lower) offers limited communication range around NLOS corners. For example, Figure 50 shows that the signal from a 20 dBm transmitter 85 meters from the intersection could not be decoded reliably until the receiver was within a few meters of the intersection.
2. By contrast, the signal from a 33 dBm transmitter was reliably decoded when the receiver was still more than 100 meters from the intersection
3. For 20 dBm transmissions, the lower 3 Mbps bit rate offers approximately a 50 meter advantage, for a given PER, compared to the 6 Mbps bit rate. For 33 dBm transmissions, the advantage for 3 Mbps is noticeable, but not significant.

11.4 Comparison of Suburban-Closed-Intersection and Suburban-Open-Intersection Scenarios

Figure 54 and Figure 55 offer a comparison between the Closed-Intersection and ³/₄-Open-Intersection Scenario tests in a suburban setting. Only one transmitter location (50 meters) is used for the comparison. It is interesting to note that the Open Intersection case resulted in more reliable communications, extending the range where the receiver experiences 10 percent PER or less from about 80 meters to about 120 meters. This is consistent with a similar comparison in the urban intersection environments (see Section 9.4).

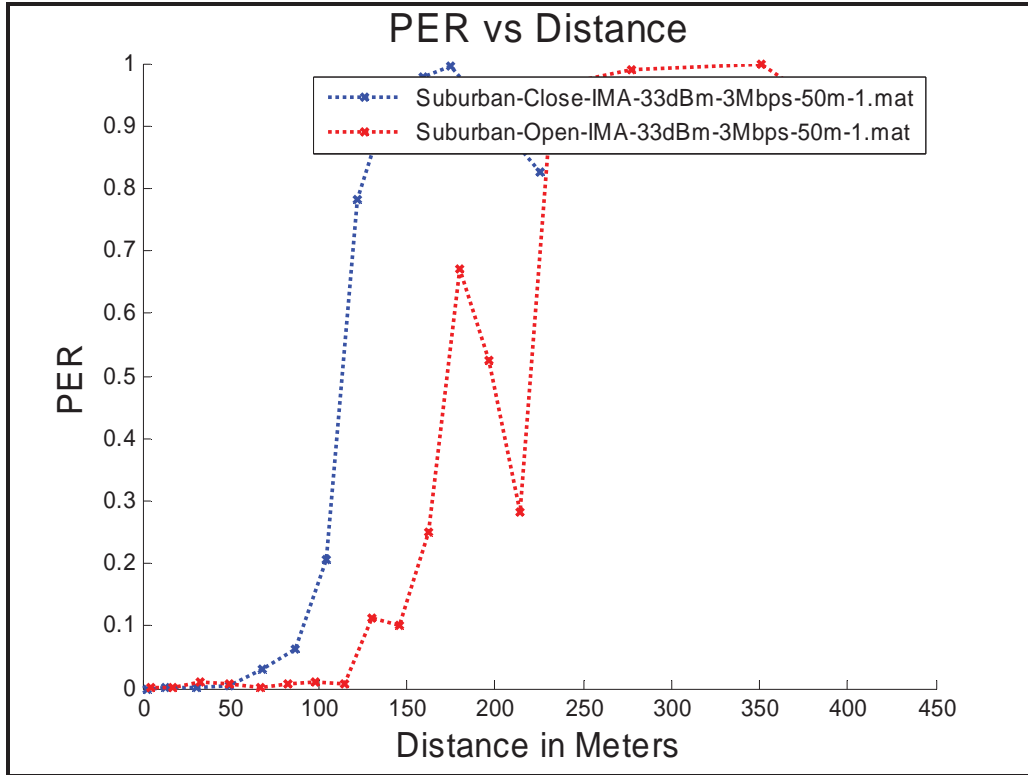


Figure 54: PER Comparison of Suburban-Closed-Intersection and Suburban-Open-Intersection Scenarios for 33 dBm at 3 Mbps

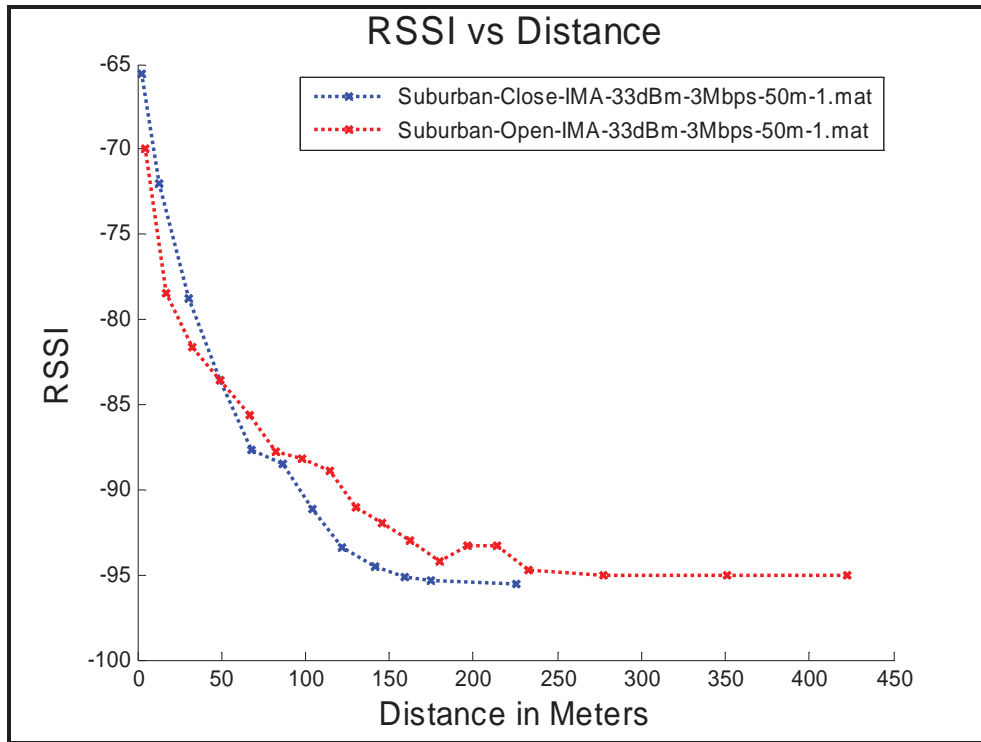


Figure 55: RSSI Comparison of Suburban-Closed-Intersection and Suburban-Open-Intersection Scenarios for 33 dBm at 3 Mbps

12 Rural-Closed-Intersection Scenario Test

The Rural-Closed-Intersection Scenario test was conducted in Morgan Hill, California, on the corner of Miramonte Avenue and Dougherty Avenue. The test is categorized as a Closed Intersection test because of the presence of homes or trees on all four corners of the intersection. The transmitter was placed at 4 fixed points along Dougherty Avenue southeast of the intersection (distances 0 meters, 25 meters, 50 meters, and 100 meters), while the receiver drove northeast toward the intersection on Miramonte Avenue at a speed of 5 mph. The test cases outlined in Table 8 were repeated for each of the transmitter positions.

Table 8: Test Cases for the Rural-Closed-Intersection Scenario

TX Power Data Rate	5dBm	10dBm	20dBm	26dBm	33dBm
3Mbps	Test 1	Test 3	Test 5	Test 7	Test 9
6Mbps	Test 2	Test 4	Test 6	Test 8	Test 10

12.1 Location Overview

The south corner of the intersection, which separated the transmitter and receiver vehicles, included a home, trees, and fence, all of which interrupted LOS communication. The other three corners were occupied by trees and/or buildings, although these were not as close to the corner as in the Closed-Urban-Intersection and Suburban-Intersection Scenarios. By definition, a closed intersection involving man-made obstructions is somewhat unusual in a rural setting.

12.2 Data Analysis

Figure 56 and Figure 57 show PER and RSSI versus distance curves for a 33 dBm transmission at various transmitter locations. It can be seen that as the transmitter moves away from the intersection, communication performance worsens.

Figure 58 and Figure 59 show the relationship between communication performance at 3 different power levels (20 dBm, 26 dBm, and 33 dBm).

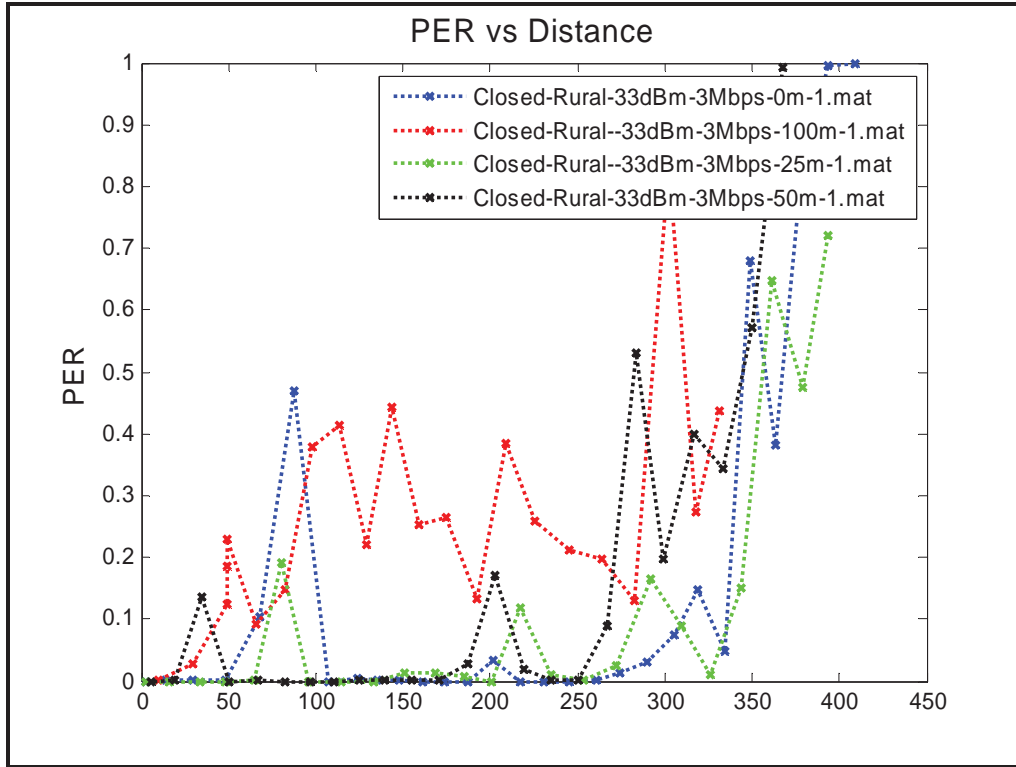


Figure 56: PER versus Distance Curves for Various Transmitter Locations at 33 dBm and 3 Mbps

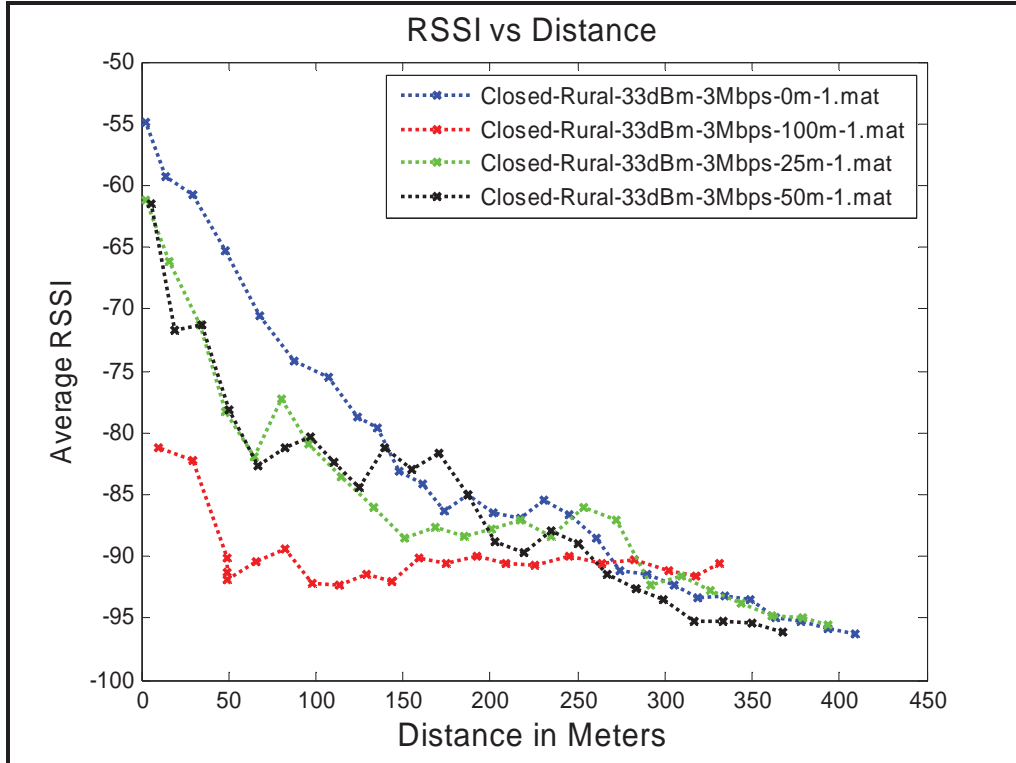


Figure 57: RSSI versus Distance Curves for Various Transmitter Locations at 33 dBm and 3 Mbps

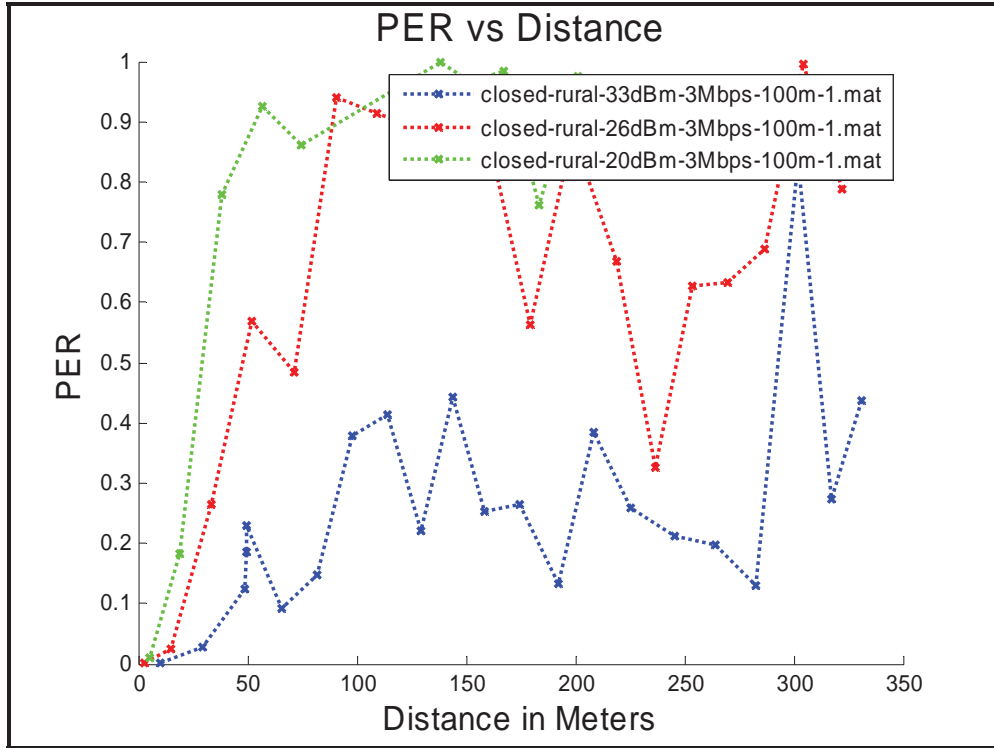


Figure 58: Comparison of PER versus Distance Curves between 20 dBm, 26 dBm, and 33 dBm when the Transmitter was 100 Meters from the Intersection and Set to Transmit at 3 Mbps

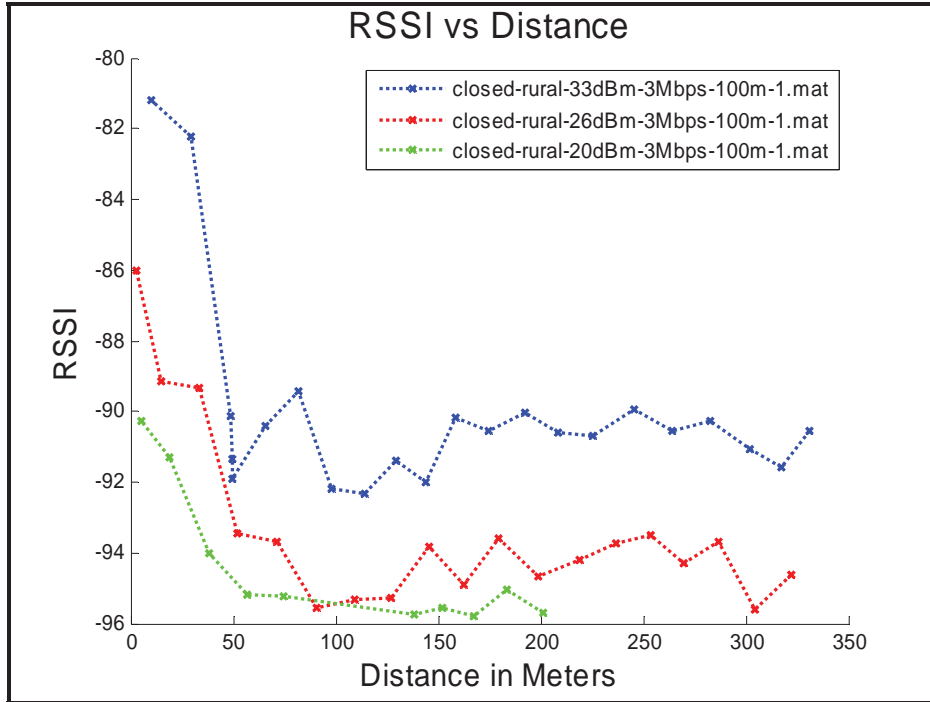


Figure 59: Comparison of RSSI versus Distance Curves between 20 dBm, 26 dBm, and 33 dBm when the Transmitter was 100 Meters from the Intersection and Set to Transmit at 3 Mbps

12.3 Observations for Rural-Closed-Intersection Scenario

The following observations can be drawn with regard to communication performance in a Rural-Closed-Intersection Scenario:

1. Use of lower powers (20 dBm or lower) offers limited communication range around NLOS corners at the rural intersection. Figure 58 shows that for a 20 dBm transmission the PER rises to approximately 80 percent at the 50 meter mark.
2. In the 33 dBm transmission, however, the PER is about 25 percent at 50 meters and remains below 50 percent beyond 250 meters.
3. There seems to be less sensitivity to transmitter-to-intersection distance in this scenario than in the Urban and Suburban closed intersection scenarios. For example, in Figure 56 the performance for transmitter distances of 0 meters, 25 meters, and 50 meters is similar; they all have low PER (ignoring narrow spikes) out to at least 250 meters receiver distance, and they all transition to high PER over about a 150 meter range starting at 250 meters. This contrasts with Figure 22 and Figure 42, in which the transition from low to high PER occurs in non-overlapping distance ranges for the 0 meters, 25 meters (urban only), and 50 meters transmitter-to-intersection cases.

13 Rural-³/₄-Open-Intersection Scenario Test

The Rural-³/₄-Open-Intersection Scenario tests were conducted in Morgan Hill, California, on the corner of Miramonte Avenue and Hale Avenue. The test is categorized as a Rural-³/₄-Open-Intersection Scenario test because of relatively open spaces on 3 out of the 4 corners. The transmitter-to-intersection distance was set at only one location (100 meters), while the receiver drove toward the intersection at the speed of traffic. The test cases outlined in Table 9 were repeated for each of the transmitter positions.

Table 9: Test Cases for the Rural-³/₄-Open-Intersection Scenario

TX Power / Data Rate	20dBm	26dBm	33dBm
3Mbps	Test 1	Test 3	Test 5
6Mbps	Test 2	Test 4	Test 6

13.1 Location Overview

This intersection features a large industrial complex on the west corner, which served as the primary obstruction between the transmitter and receiver. Moving southwest from Hale Avenue, there are about 20 meters of open space before approaching a parking lot lined with trees and a fence and about 30 more meters before approaching a one-story building. Since the building is set back from Hale Avenue by about 50 meters, the transmitter was placed in just one location for this scenario, 100 meters southwest of the intersection on Miramonte. The receiver approached the intersection on Hale, traveling southeast, with the obstruction and transmitter to its right. The other three corners are open. The north corner has a low building set back about 70 meters northeast of Hale and 20 meters northwest of Miramonte. The east and south corners are farm fields.

13.2 Data Analysis

Figure 60 and Figure 61 show the RSSI and PER versus distance curves for the Rural-³/₄-Open Intersection tests.

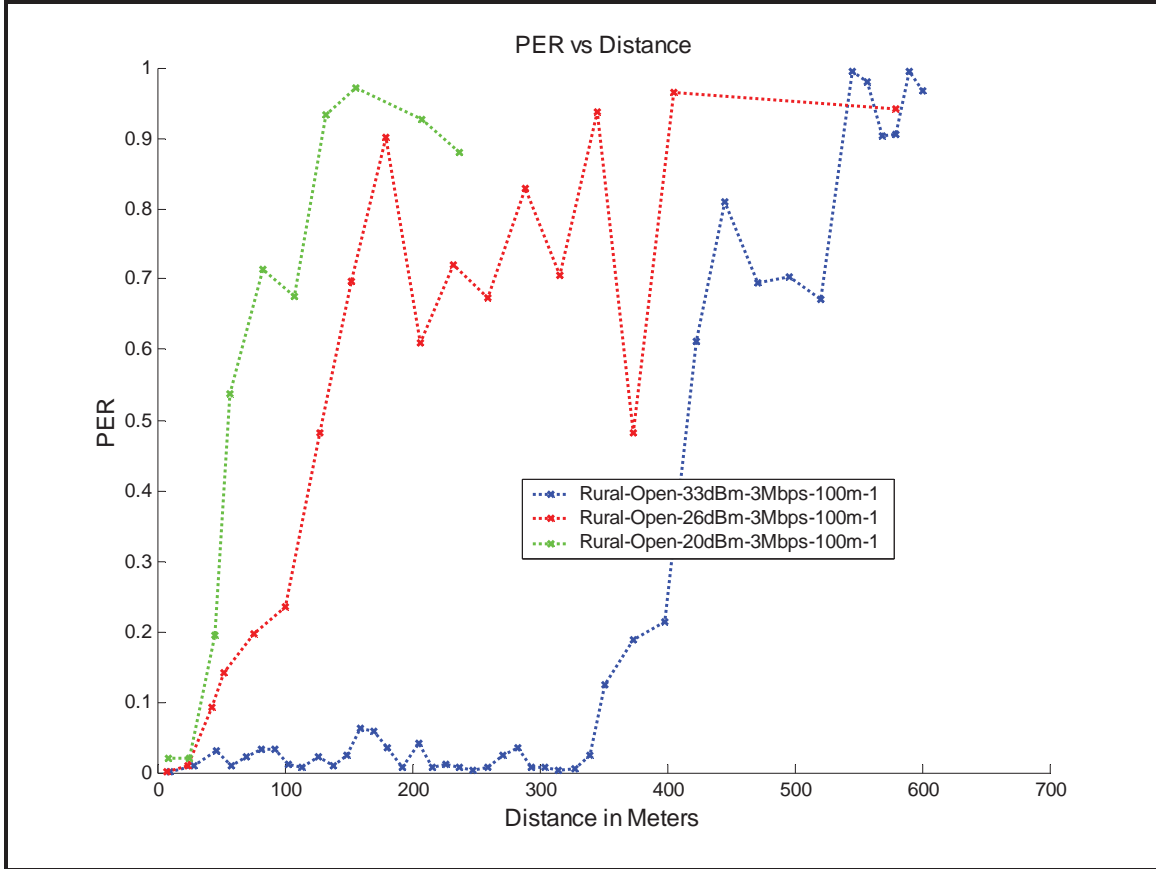


Figure 60: Comparison of PER versus Distance Curves between 33 dBm, 26 dBm, and 20 dBm when the Transmitter was 100 Meters from the Intersection and Set to Transmit at 3 Mbps

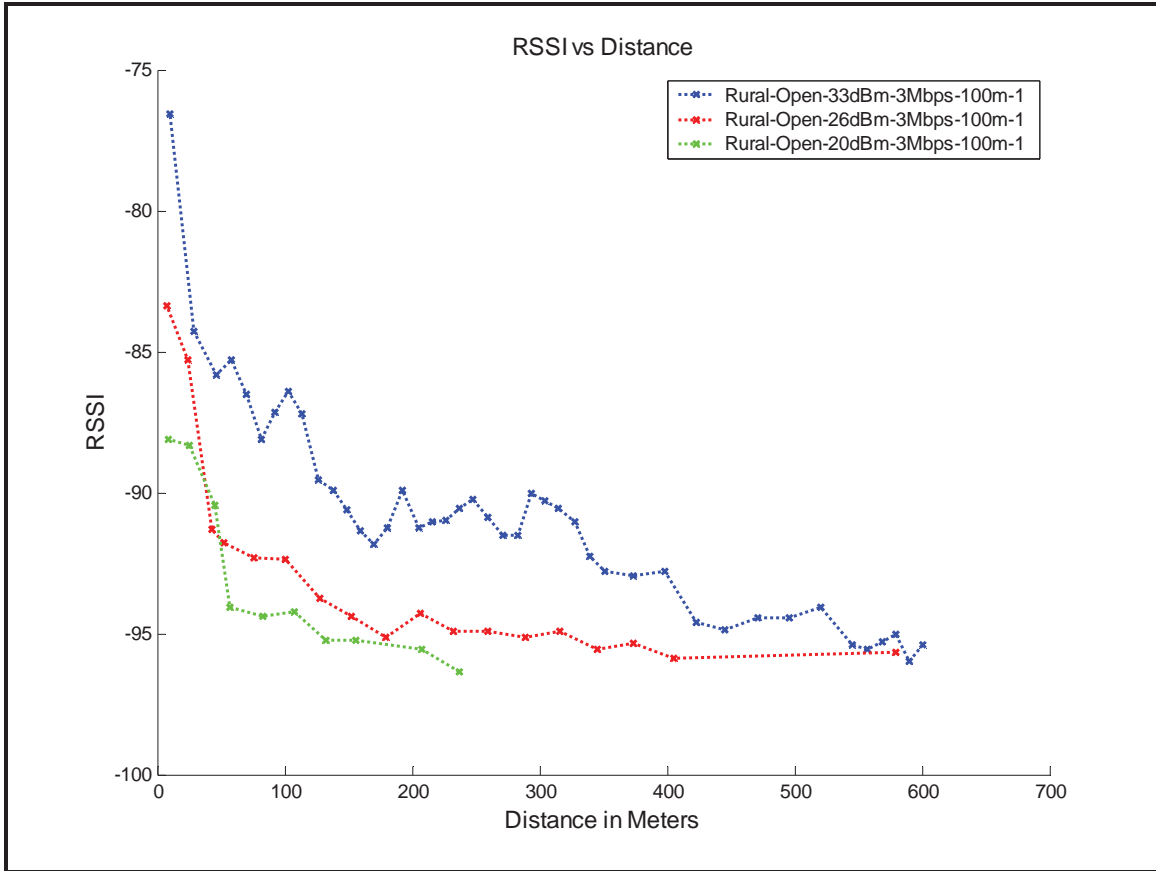


Figure 61: Comparison of RSSI versus Distance Curves between 33 dBm, 26 dBm, and 20 dBm when the Transmitter was 100 Meters from the Intersection and Set to Transmit at 3 Mbps

Figure 62 and Figure 63 show the effect of different data rates (3 Mbps and 6 Mbps) at different transmit powers (20 dBm and 33 dBm). It is clear that the lower rate offers a marginal improvement in performance at 33 dBm, while at 20 dBm there is no clear preference between 3 Mbps and 6 Mbps.

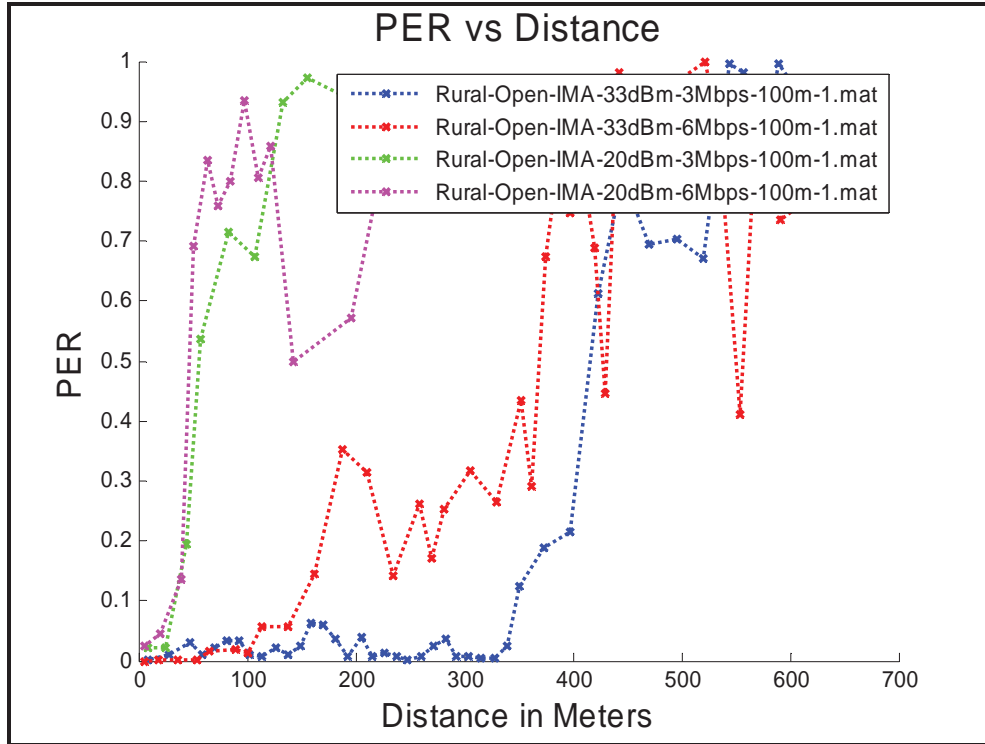


Figure 62: Comparison of PER Curves in Rural-3/4-Open-Intersection for 33 dBm and 20 dBm at 3 Mbps and 6 Mbps

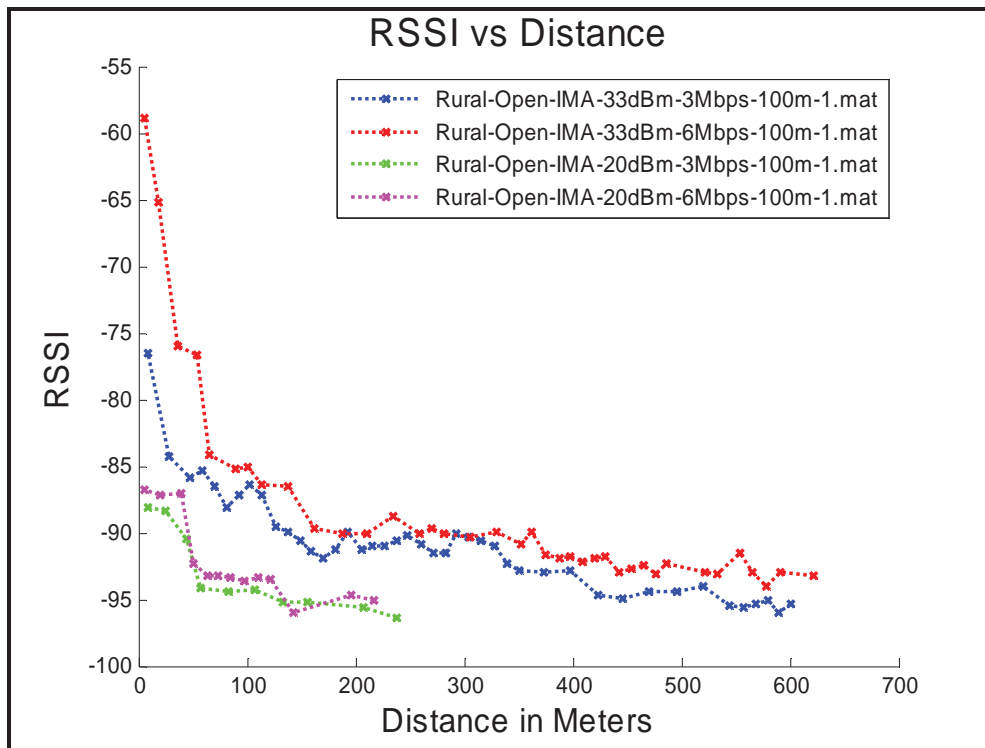


Figure 63: Comparison of RSSI Curves in Rural-3/4-Open-Intersection for 33 dBm and 20 dBm at 3 Mbps and 6 Mbps

13.3 Observations for Rural-³/₄-Open-Intersection Scenario

The following observations can be drawn with regard to communication performance in a Rural-³/₄-Open-Intersection Scenario:

1. Use of lower powers (20 dBm or lower) offers limited communication range around a NLOS corner in this Rural-³/₄-Open Intersection
2. Both 20 dBm and 26 dBm transmissions offer less than 50 meters of reliable communication range (< 10 percent PER)
3. A 33 dBm transmission offers about 300 meters of reliable communication range.
4. Transmission at a lower data rate (3 Mbps) offers a marginal improvement in communication performance

14 Curved-Road Scenario Test

The curved track test was conducted in Cupertino, California, along Stevens Canyon Road at a point where the road goes through an approximate 90 degree turn. The transmitter was placed at one of two fixed locations, 50 meters and 100 meters west of the curve. The receiver drove toward the transmitter southward and then curved to the west. The test was repeated for the test cases shown in Table 10.

Table 10: Test Cases for the Curved-Road Scenario

TX Power Data Rate	5dBm	10dBm	15dBm	20dBm	26dBm	33dBm
3Mbps	Test 1	Test 4	Test 7	Test 10	Test 13	Test 16
6Mbps	Test 2	Test 5	Test 8	Test 11	Test 14	Test 17
12Mbps	Test 3	Test 6	Test 9	Test 12	Test 15	Test 18

14.1 Location Overview

Figure 64 and Figure 65 illustrate the propagation environment in the Curved-Road Scenario test. The curve veers toward the right (west) as vehicles drive south on Stevens Canyon Road. The primary obstruction was the presence of a hill on the bend.



Figure 64: Heading South on Stevens Canyon Road³



Figure 65: Negotiating the Curve

³ Note that the photos in Figure 64 and Figure 65 were taken after the testing was completed, and the trucks shown were not present during the tests.

14.2 Data Analysis

Figure 66 and Figure 67 offer a comparison of PER and RSSI curves in a curved track scenario for a transmission at 33 dBm and 3 Mbps. The curves illustrate the PER/RSSI values when the transmitter is 50 meters and 100 meters from the bend of the curve.

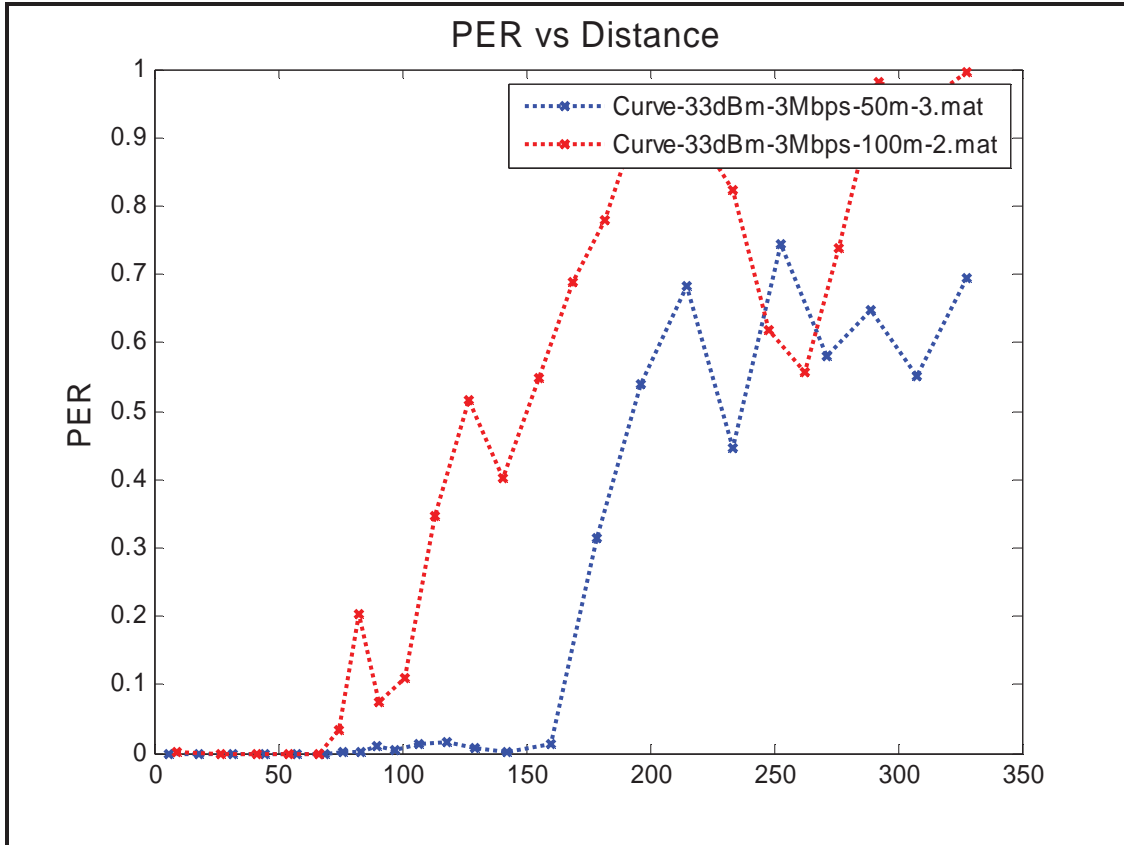


Figure 66: Comparison of PER Curves for Curved-Road Scenario at 50 Meters and 100 Meters for 33 dBm Transmission

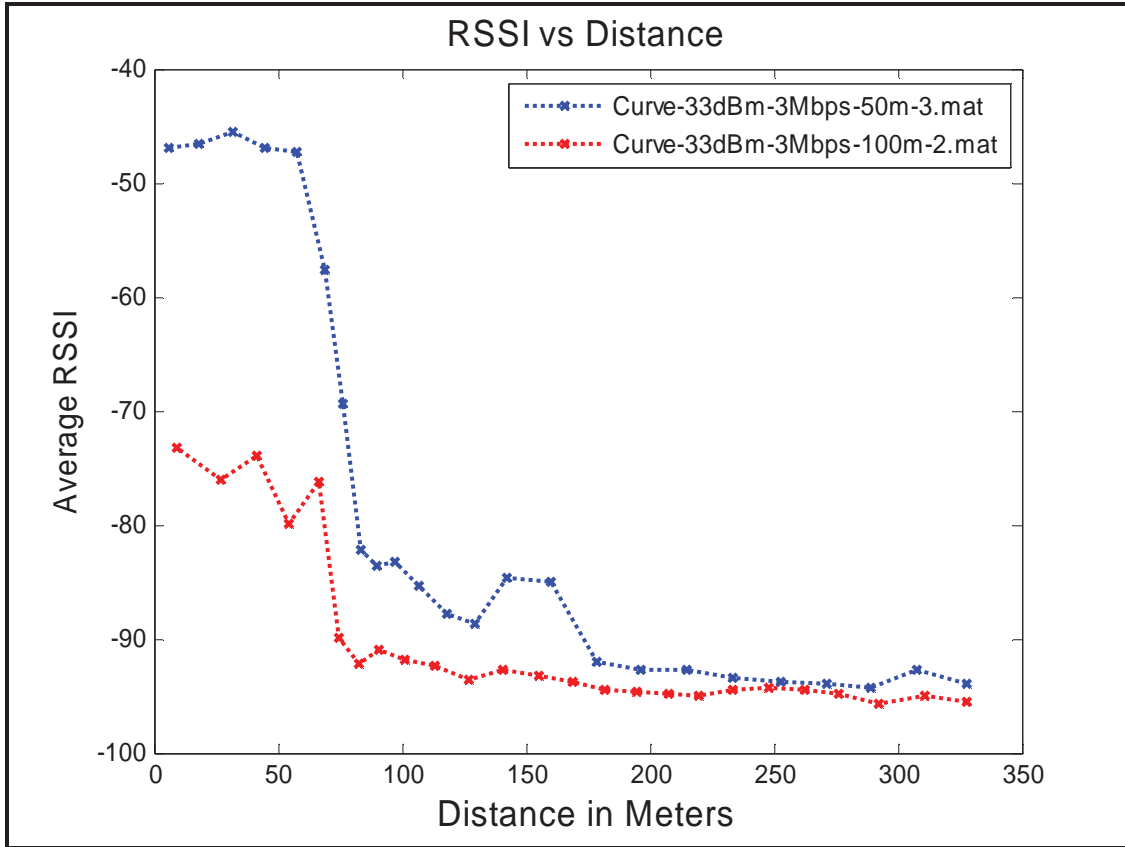


Figure 67: Comparison of RSSI Curves for Curved-Road Scenario at 50 Meters and 100 Meters for 33 dBm Transmission

Figure 68 and Figure 69 show PER and RSSI curves for 3 different power levels (20 dBm, 26 dBm, and 33 dBm) with a transmitter-to-curve distance of 50 meters.

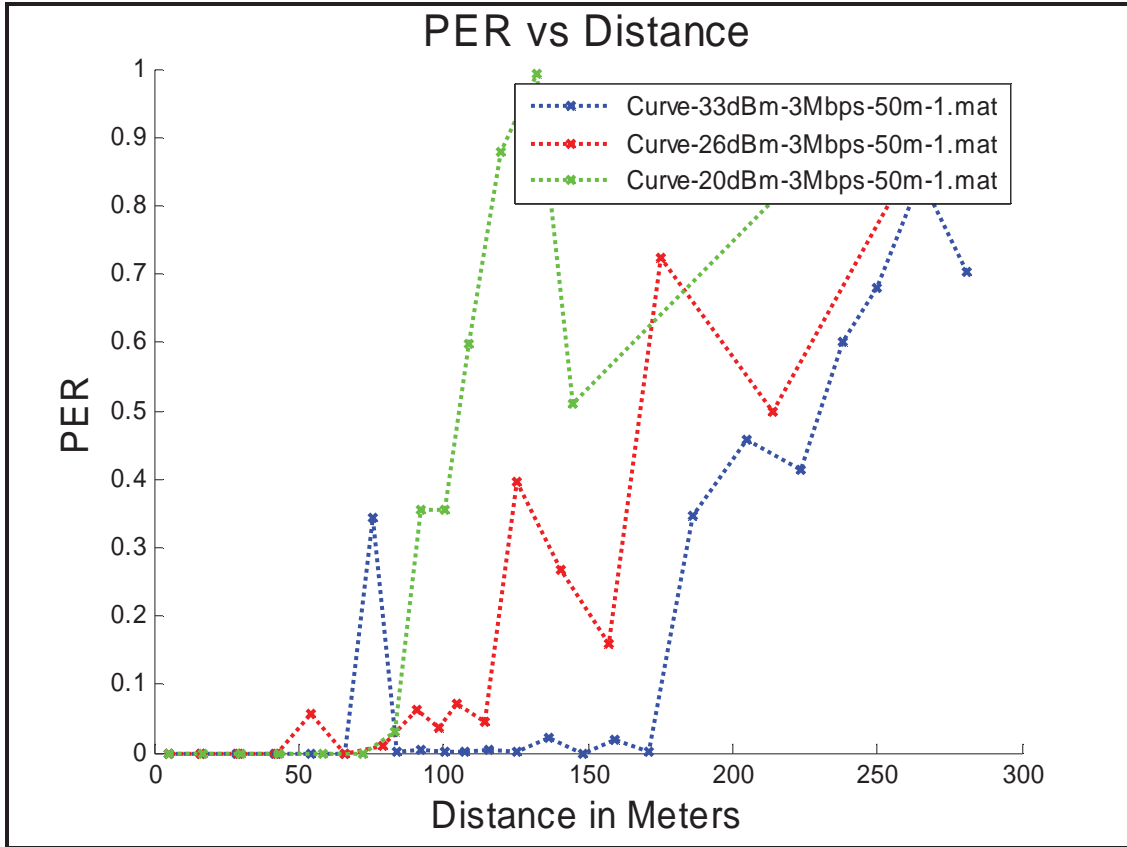


Figure 68: Comparison for PER Curves for a Curved-Road Scenario for 33 dBm, 26 dBm, and 20 dBm Transmissions

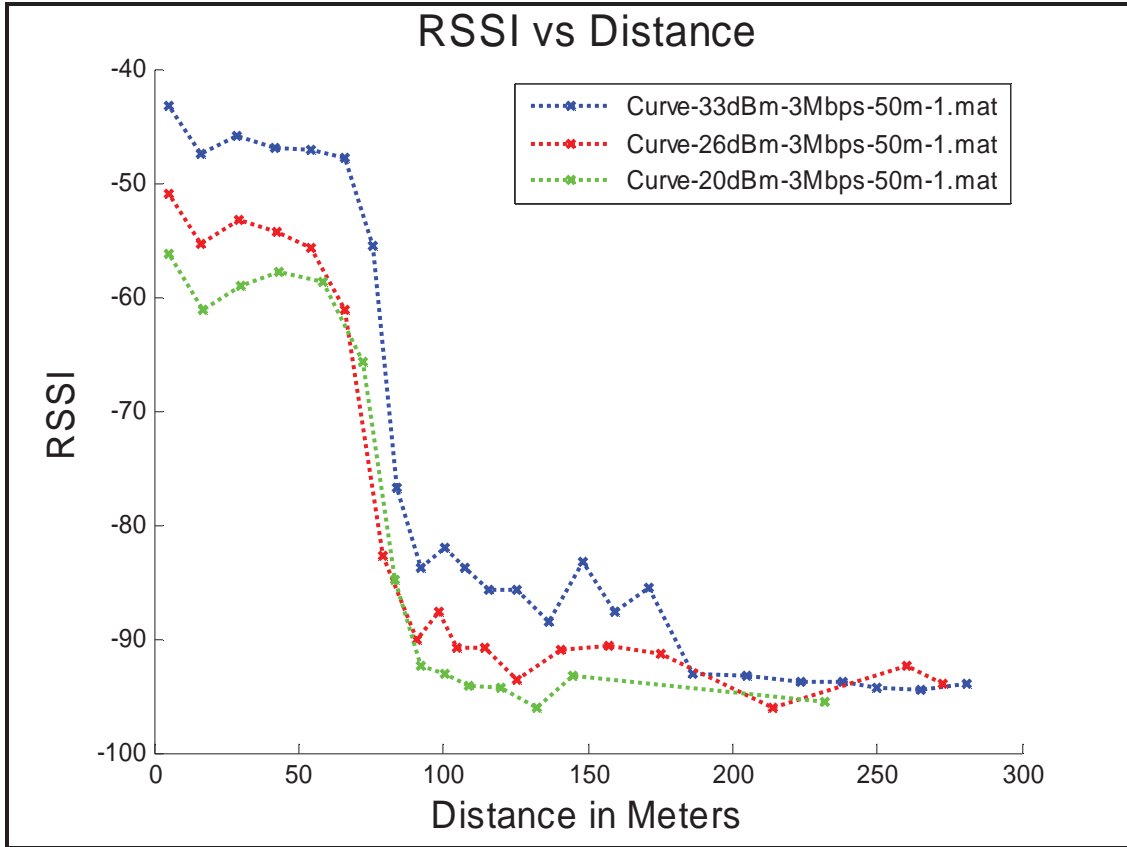


Figure 69: Comparison for RSSI Curves for a Curved-Road Scenario for 33 dBm, 26 dBm, and 20 dBm Transmissions

Figure 70 and Figure 71 show the effect of different data rates (3 Mbps and 6 Mbps) at different transmit powers (20 dBm and 33 dBm). The 3 Mbps rate offers somewhat better performance at 33 dBm. The comparison at 20 dBm shows a slight advantage for 3 Mbps.

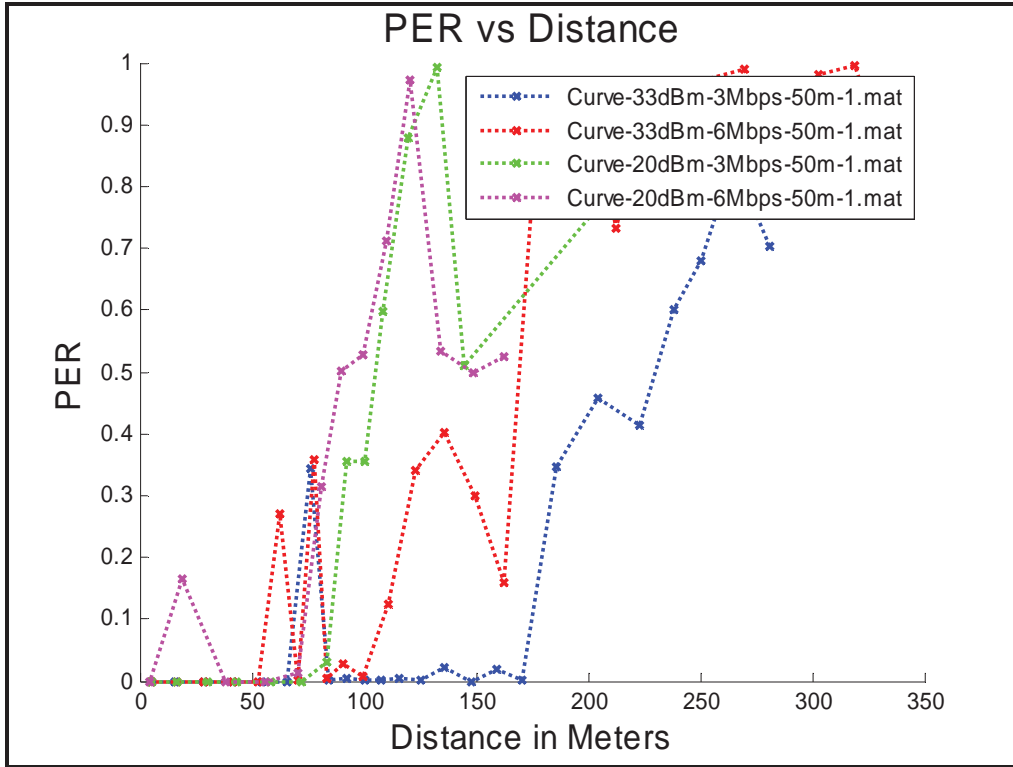


Figure 70: Comparison of PER Curves in a Curved-Road Scenario for 33 dBm and 20 dBm at 3 Mbps and 6 Mbps

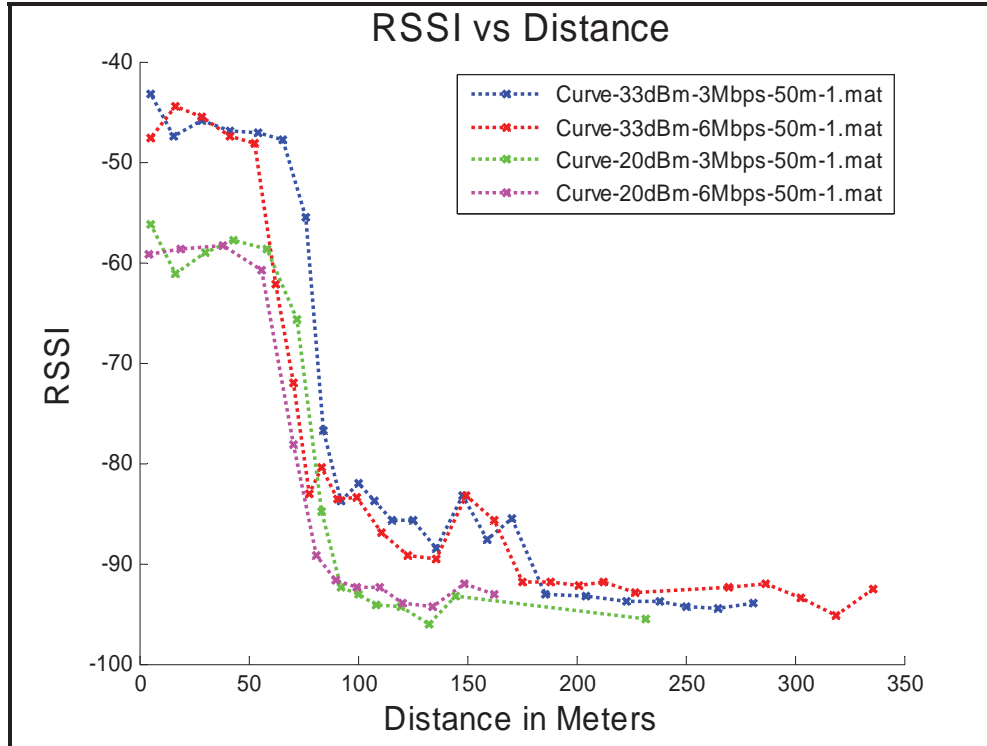


Figure 71: Comparison of RSSI Curves in a Curved-Road Scenario Test for 33 dBm and 20 dBm at 3 Mbps and 6 Mbps

14.3 Observations for Curved-Road Scenario Test

The following observations can be drawn with regard to communication performance in a Curved-Road Scenario:

1. When the transmitter is 100 meters from the bend, a reliable communication link is achieved only when the receiver is 70 meters from the bend or less (Figure 66)
2. Use of lower powers (20 dBm or lower) offers limited communication range around NLOS corners. We can see in Figure 68 that the 20 dBm transmission offers less than 100 meters for reliable communication range, whereas the 26 dBm and 33 dBm transmissions maintain a reliable link well beyond the 100 meter range.
3. The advisability of employing higher powers in a Curved Road test depends on the range requirements of applications that will be active in such a scenario. .

15 Freeway-Line-of-Sight Scenario Test

In this test V2V communication performance was measured along an open freeway without any intentional obstructions or occlusions. The receiver drove at a constant speed of 55 mph while the transmitter varied its speed to obtain a wide range of V2V distances. The test was repeated for all the cases outlined in Table 11.

Table 11: Test Cases for the Freeway-LOS Scenario

Data Rate \ TX Power	TX Power			
	5dBm	10dBm	20dBm	33dBm
3Mbps	Test 1	Test 3	Test 5	Test 7
6Mbps	Test 2	Test 4	Test 6	Test 8

15.1 Location Overview

The V2V Freeway tests were conducted along US-101 in California. US-101 is a 3-4 lane highway with moderate, free-flowing traffic (see Figure 72). There was a 3-foot high median separating traffic in either direction (concrete in some places and steel in others). The freeway was curved and hilly in some sections which might have resulted in temporary loss of LOS and higher PER even though the V2V distance was nominally within communication range.



Figure 72: Heading South on US-101

15.2 Data Analysis

Figure 73 and Figure 74 show the PER and RSSI versus distance curves for the freeway LOS tests. The results were fairly consistent with higher powers offering a longer communication range. The spike above 10 percent PER for the 33 dBm case at about

300 meters corresponded to a curve in the road, which interrupted LOS communication temporarily.

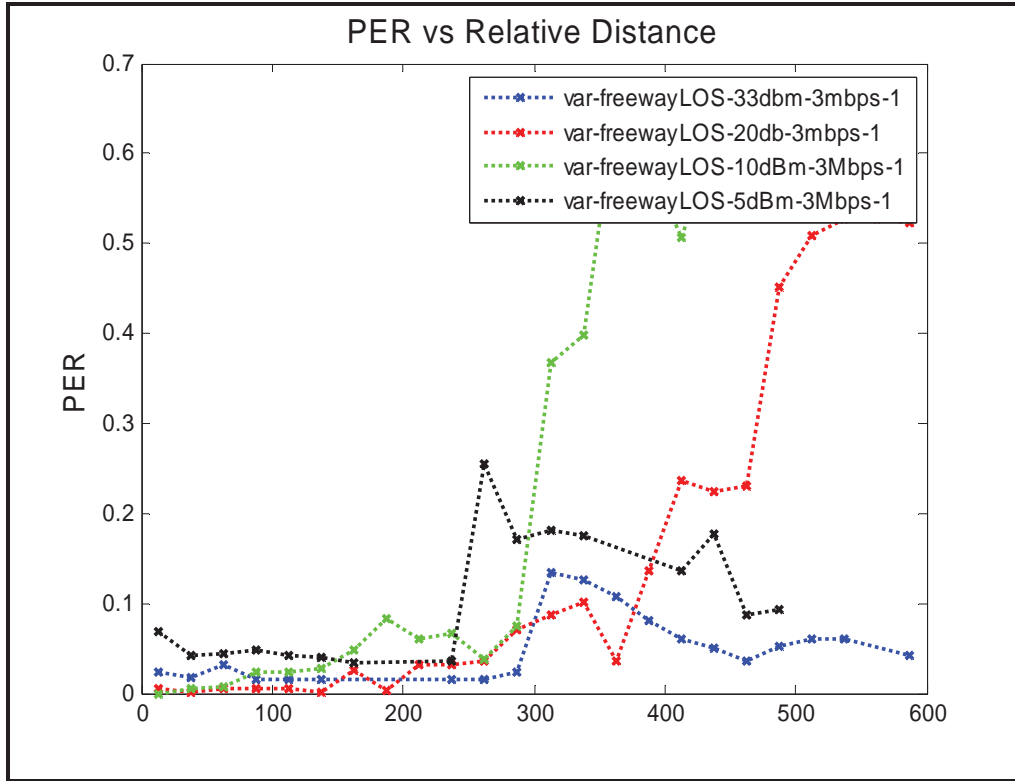


Figure 73: Comparison of PER versus Distance Curves for Various Power Levels in a Freeway-LOS Scenario when Transmitter is Set to 3 Mbps

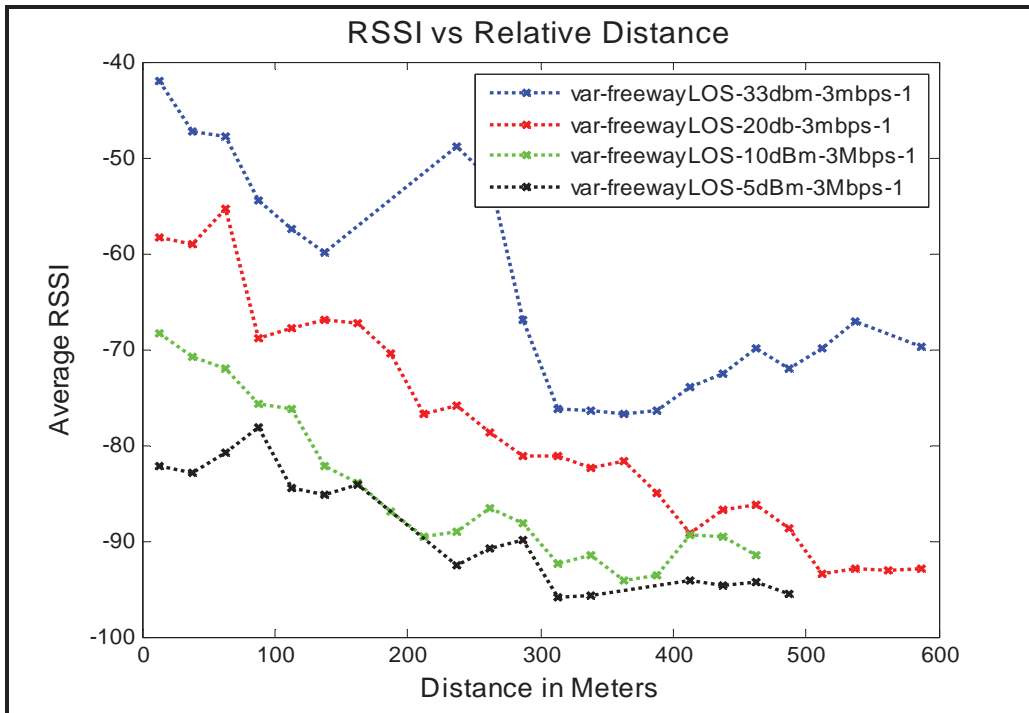


Figure 74: Comparison of RSSI versus Distance Curves for Various Power Levels in a Freeway-LOS Scenario when Transmitter is Set to 3 Mbps

Figure 75 and Figure 76 show the effect of different data rates (3 Mbps and 6 Mbps) at different transmit powers (10 dBm and 20 dBm). In contrast to earlier tests, the 6 Mbps rate appears to have better performance than the 3 Mbps rate at 20 dBm. At 10 dBm the performance is similar at each rate, with a small advantage for 3 Mbps.

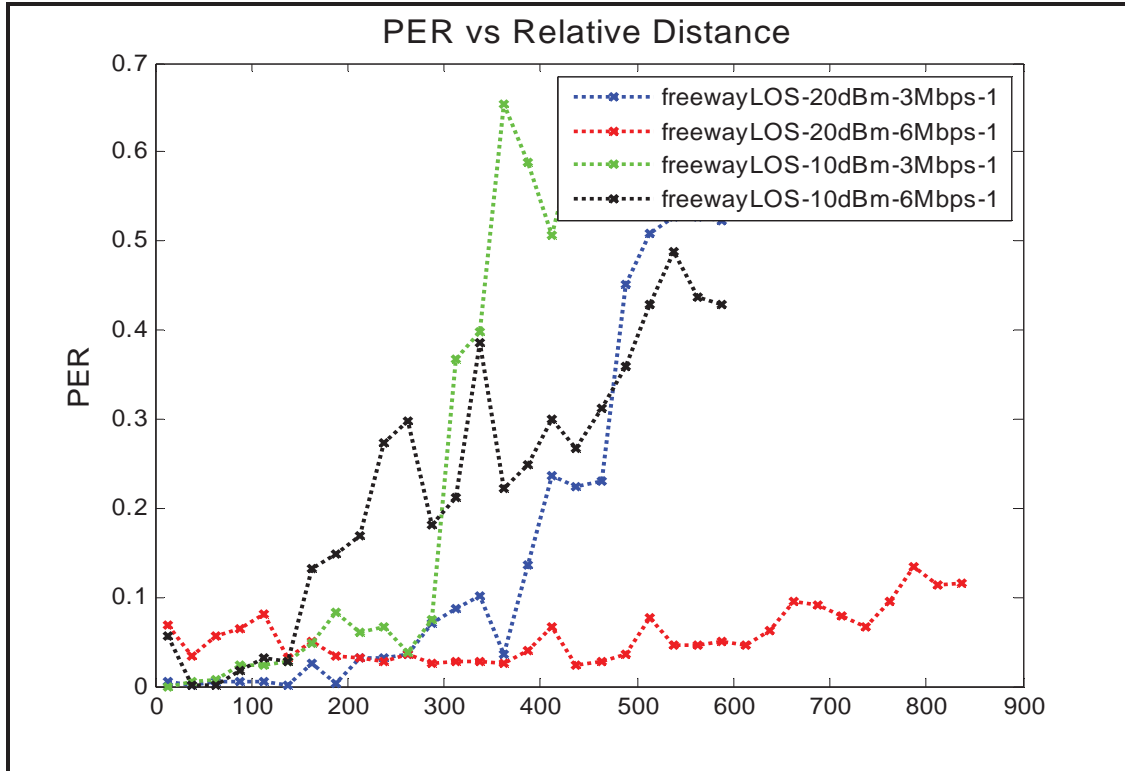


Figure 75: Comparison of PER Curves in a Freeway-LOS Scenario for 20 dBm and 10 dBm at 3 Mbps and 6 Mbps

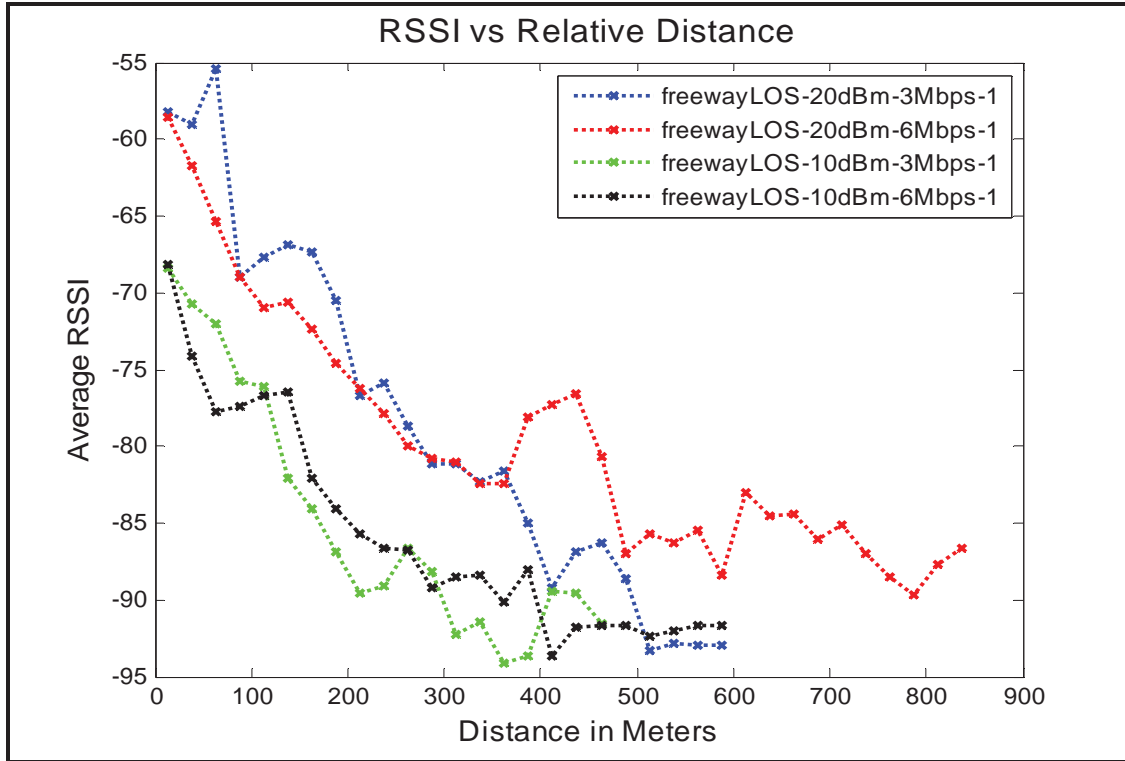


Figure 76: Comparison of RSSI Curves in a Freeway-LOS Scenario for 33 dBm and 20 dBm at 3 Mbps and 6 Mbps

15.3 Observations for Freeway LOS Scenario Testing

The following observations can be drawn with regard to communication performance in a Freeway LOS Scenario:

1. All the power levels (5 dBm-33 dBm) offer reliable communication (PER < 10 percent) up to at least 225 meters
2. 20 dBm transmissions offer reliable communication up to 375 meters
3. 33 dBm transmissions offer reliable communication for the entire 600 meter range tested

16 Rural-Highway, Line-of-Sight Scenario Test

The Rural-Highway LOS Scenario test was conducted in Morgan Hill, California, along Hale Avenue. The receiver maintained a constant speed of 45 mph while the transmitter varied its speed to obtain a wide range of V2V distances. There were no intentional obstacles between the vehicles. The rural highway tests were conducted for the test cases outlined in Table 12.

Table 12: Test Cases for the Rural-Highway-LOS Scenario

TX Power		Data Rate		
		10dBm	20dBm	33dBm
3Mbps		Test 1	Test 3	Test 5
6Mbps		Test 2	Test 4	Test 6

16.1 Location Overview

Hale Avenue is fairly representative of a rural highway with open fields and occasional trees, houses, or farms on either side of the road. The highway was curved along some sections which might have resulted in temporary loss of LOS and higher PER even though the V2V distance was nominally within communication range.

16.2 Data Analysis

Figure 77 and Figure 78 show the PER and RSSI curves for the rural highway LOS tests.

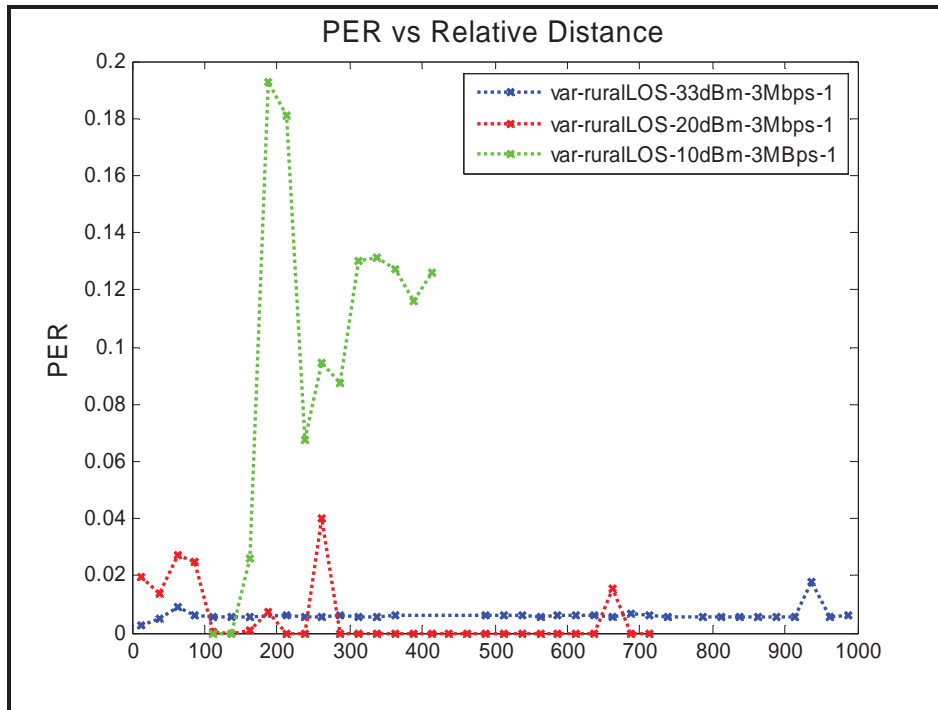


Figure 77: Comparison of PER versus Distance Curves for Various Power Levels in a Rural-Highway-LOS Scenario when Transmitter is Set to 3 Mbps

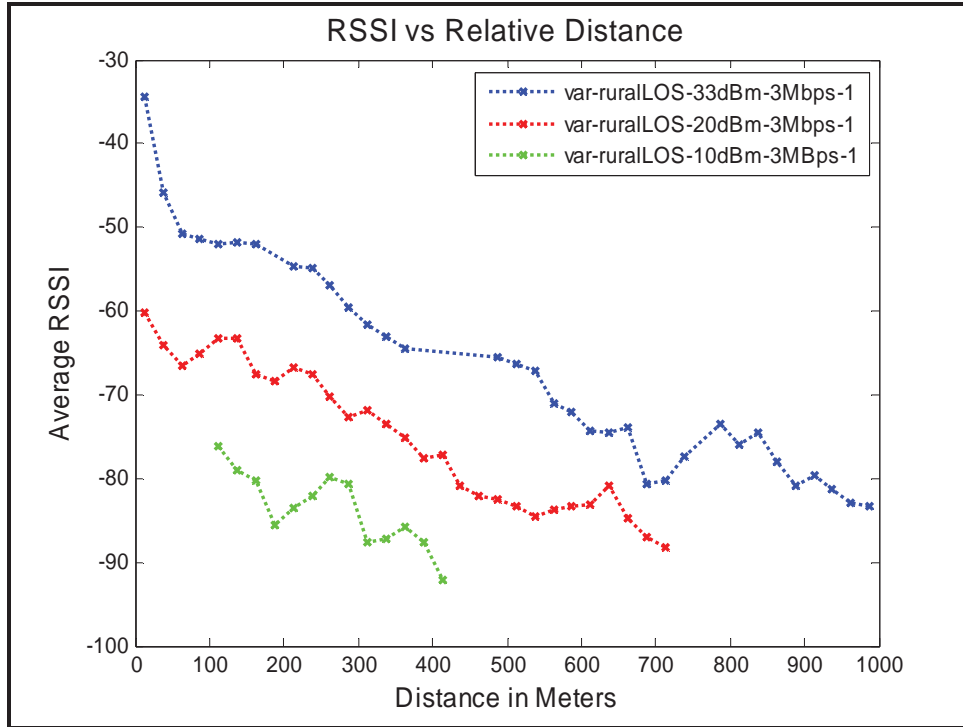


Figure 78: Comparison of RSSI versus Distance Curves for Various Power Levels in a Rural-Highway-LOS Scenario when Transmitter is Set to 3 Mbps

Figure 79 and Figure 80 show the effect of different data rates (3 Mbps and 6 Mbps) at different transmit powers (20 dBm and 33 dBm). The 6 Mbps/33 dBm run was only able to collect data for distances up to about 350 meters. There is a marginal PER advantage for 3 Mbps at 33 dBm over the range tested and a more noticeable range advantage for 3 Mbps at 20 dBm.

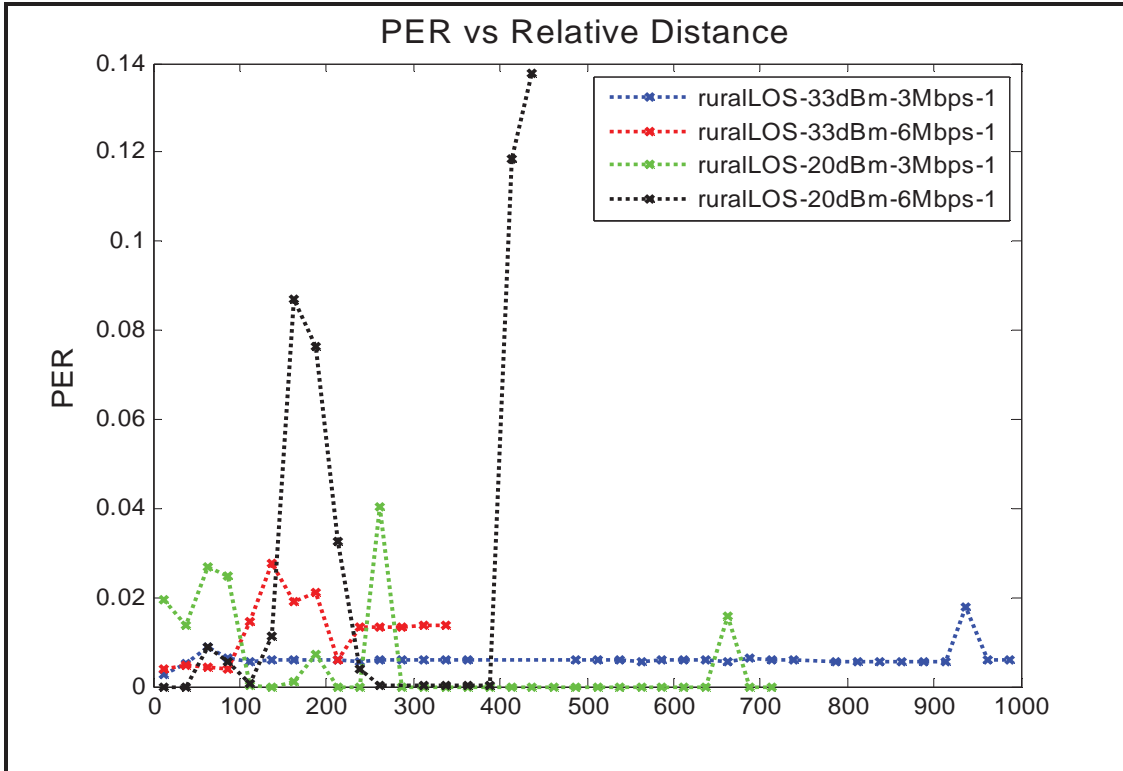


Figure 79: Comparison of PER Curves in a Rural-Highway-LOS Scenario for 33 dBm and 20 dBm at 3 Mbps and 6 Mbps

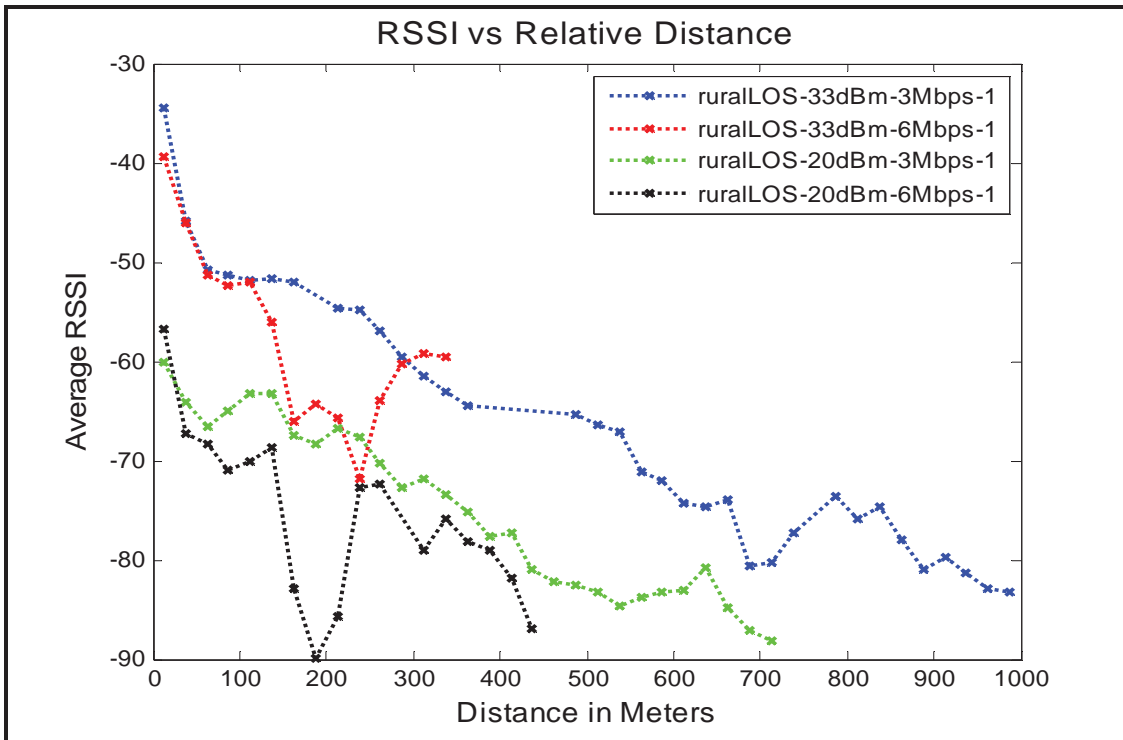


Figure 80: Comparison of RSSI Curves in a Rural-Highway-LOS Scenario for 33 dBm and 20 dBm at 3 Mbps and 6 Mbps

16.3 Observations for Rural-Highway-LOS Scenario Test

The following observations can be drawn for the Rural-Highway-LOS Scenario tests:

1. The two-lane test environment limited flexibility in varying distance between the vehicles. In some of the lower power tests, only a limited range was tested, and the tests were not terminated due to observed loss of communication. In none of the tests were PER values in excess of 20% observed.
2. 33 dBm transmission offers reliable communication ranges (PER < 10 percent) for at least 1000 meters (limit of test)
3. 20 dBm transmission offers reliable communication ranges (PER < 10 percent) for up to 700-800 meters, the actual range could be longer, but the traffic situation made it difficult to extend the V2V distance in the test
4. The 10 dBm transmission was more erratic, possibly due to curves in the highway creating NLOS conditions. The limit of reliable communication was observed to be about 150 meters.

17 Freeway-Shadowing Scenario Test

The Freeway–Shadowing Scenario tests with were conducted along highways US-101 and I-880 between Palo Alto, California, and Oakland, California. The same truck was used in these tests as was used in the Baseline Shadowing tests reported in Section 6. In each test, the transmitter, truck and receiver remained in the same lane. The receiver maintained a safe driving distance behind the truck; while the transmitter varied its speed to achieve a good spread of V2V distances. These tests were conducted for the various test cases outlined in Table 13.

Table 13: Test Cases for the Freeway-Shadowing Scenario Test

TX Power Data Rate	5dBm	10dBm	15dBm	20dBm	26dBm	33dBm
3Mbps	Test 1	Test 4	Test 7	Test 10	Test 13	Test 16
6Mbps	Test 2	Test 5	Test 8	Test 11	Test 14	Test 17
12Mbps	Test 3	Test 6	Test 9	Test 12	Test 15	Test 18

17.1 Location Overview

The propagation environment was identical to that described for the Freeway LOS tests in Section 15, except for the addition of the truck to serve as a NLOS obstruction between the vehicles. Figure 81 shows a typical view of the receiver vehicle behind the truck used in these tests.



Figure 81: Receiver Behind the Truck Along I-880

17.2 Data Analysis

Figure 82 and Figure 83 show the PER and RSSI curves for the freeway shadowing tests. These results are for the following power levels: 5 dBm, 10 dBm, 20 dBm, and 33 dBm. The data rate in each test was 3 Mbps.

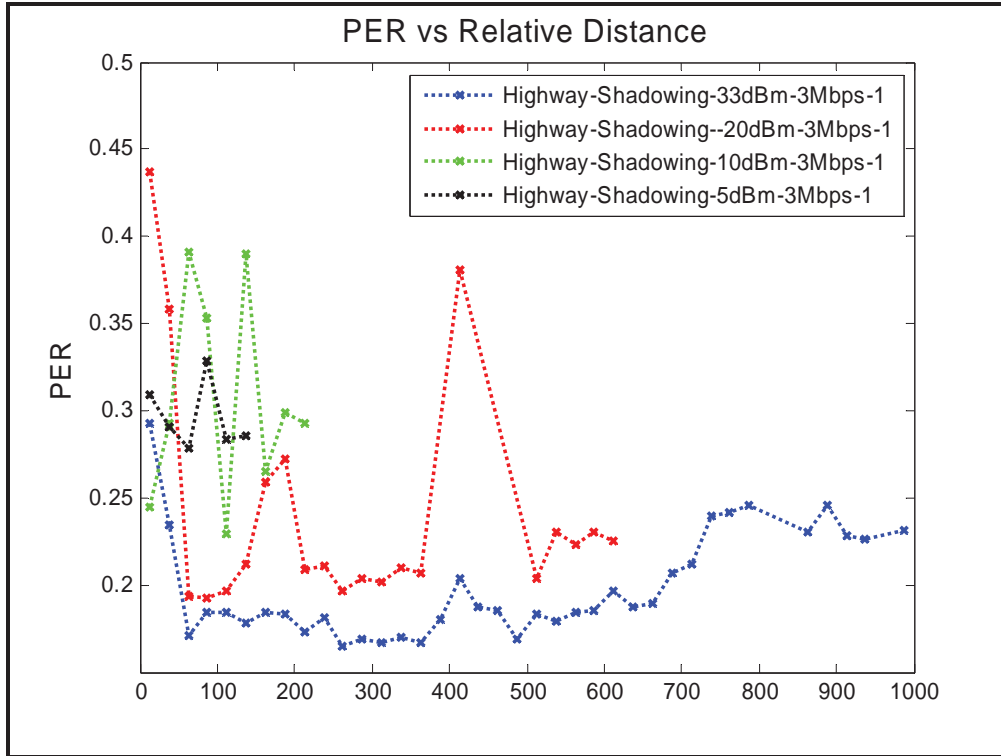


Figure 82: Comparison of PER versus Distance Curves for Various Power Levels in a Freeway-Shadowing Scenario when Transmitter is Set to 3 Mbps

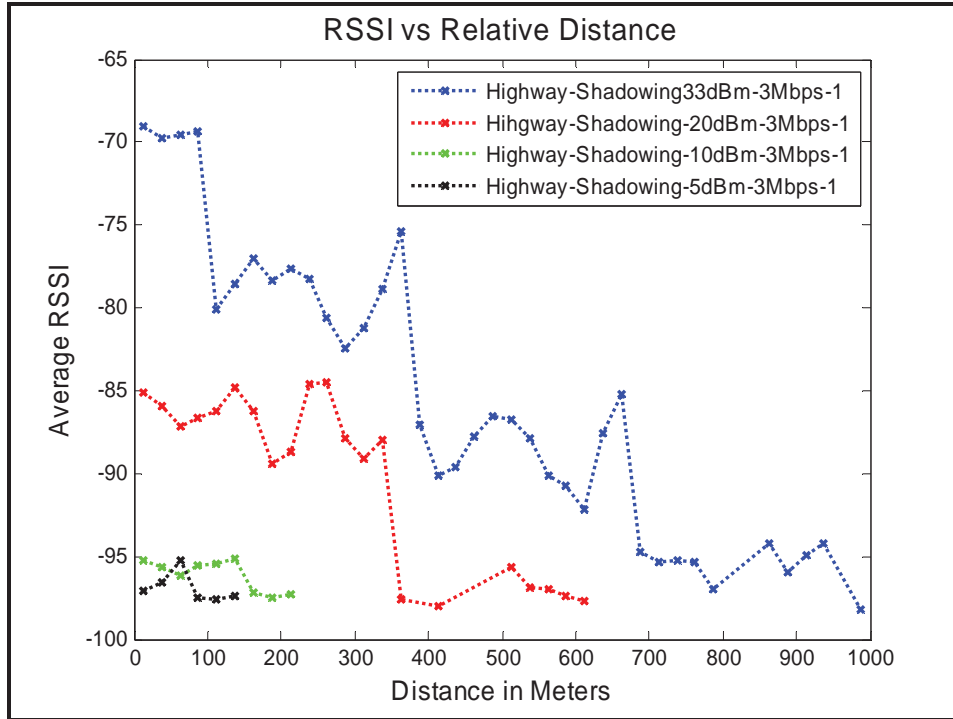


Figure 83: Comparison of RSSI versus Distance Curves for Various Power Levels in a Freeway-Shadowing Scenario when Transmitter is Set to 3 Mbps

Figure 84 and Figure 85 show the effect of different data rates (3 Mbps and 6 Mbps) at different transmit powers (20 dBm and 33 dBm). Performance differences are not significant.

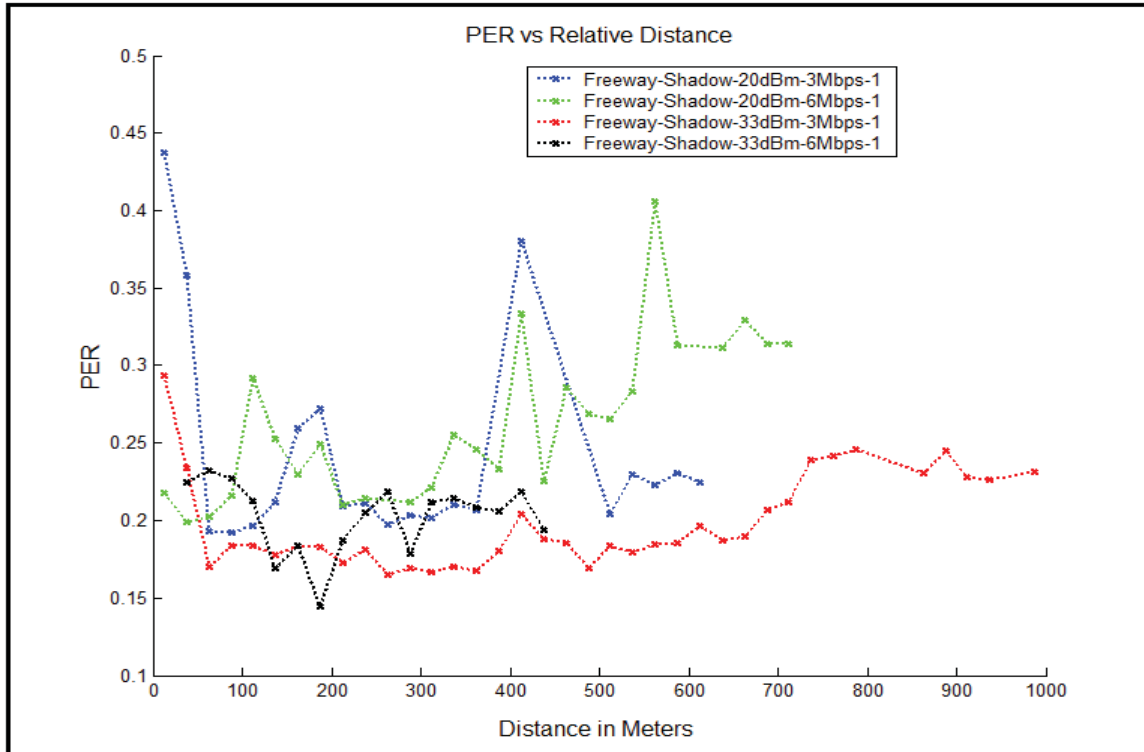


Figure 84: Comparison of PER Curves in a Freeway-Shadowing Scenario Test for 33 dBm and 20 dBm at 3 Mbps and 6 Mbps

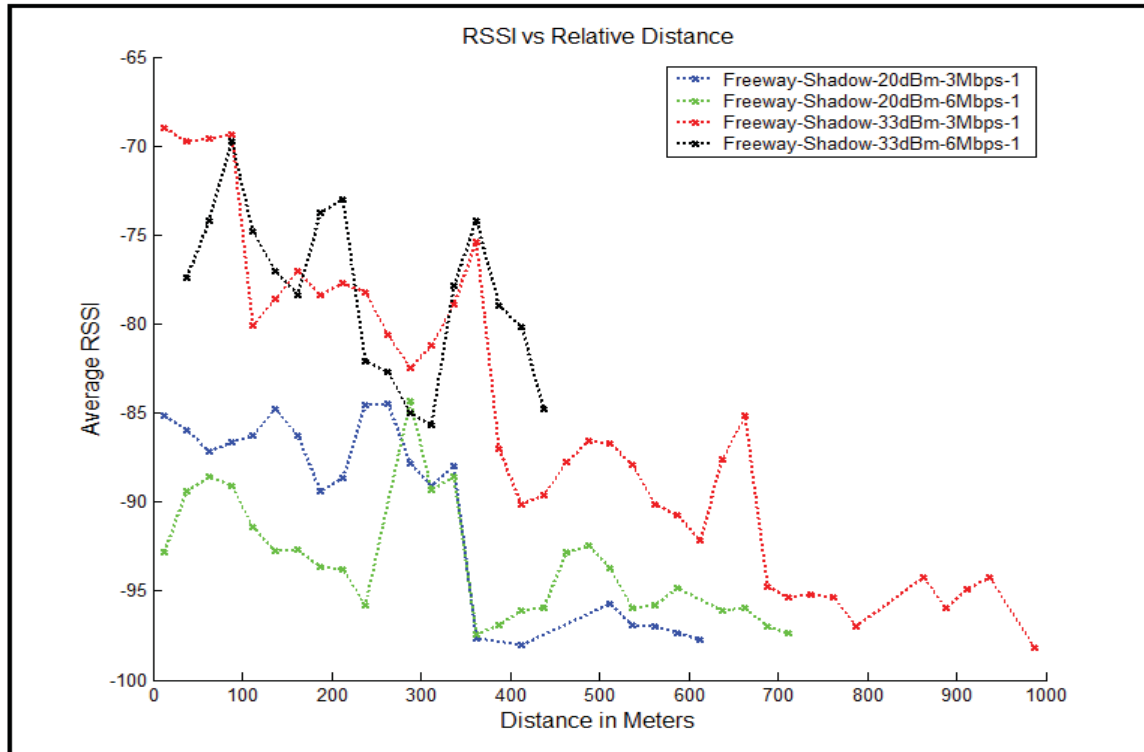


Figure 85: Comparison of RSSI Curves in a Freeway-Shadowing Scenario Test for 33 dBm and 20 dBm at 3 Mbps and 6 Mbps

17.3 Observations for Freeway–Shadowing Scenario Test

1. 33 dBm transmissions offer a PER of about 10 percent for up to 500 meters
2. 20 dBm transmissions offer a PER of about 20 percent for up to 400 meters
3. 5 dBm and 10 dBm transmission cannot support reliable DSRC communications in a Shadowing environment. At these power levels the PER never drops below 20 percent.
4. Regardless of transmit power, when the V2V distance approaches zero the PER increases.. The higher PER at close distances can be attributed to the fact that the truck more completely blocks the receiver from the transmitter. A similar phenomenon was observed in the Baseline Shadowing tests at 5 dBm and 10 dBm (see Section 6).

18 Rural-Highway-Shadowing Scenario Test

The Rural-Highway-Shadowing Scenario test was conducted along Highway 156 in Hollister, California. In this test, the transmitter, truck, and receiver remained in the same lane. The receiver maintained a safe driving distance behind the truck; while the transmitter varied its speed to achieve a good spread of V2V distances. This test was conducted for the various test cases outlined in Table 14.

Table 14: Test Cases for the Rural-Highway-Shadowing Scenario

TX Power Data Rate	10dBm	20dBm	26dBm	33dBm
3Mbps	Test 1	Test 3	Test 5	Test 7
6Mbps	Test 2	Test 4	Test 6	Test 8

18.1 Location Overview

The propagation environment was similar to that of the rural highway environment described in Section 16 except for the addition of the truck to serve as a NLOS obstruction between the vehicles. The road is fairly representative of a rural highway with open fields and occasional trees, houses, or farms on either side of the road. Figure 86 shows the propagation environment on Highway 156. Note that in comparison with the Freeway Shadowing environment discussed in Section 17, the rural highway generally had lower vehicle density, and thus less vehicle-related multipath.



Figure 86: Driving Down Highway 156

18.2 Data Analysis

Figure 87 shows the PER measured in the Rural-Highway-Shadowing Scenario tests at 3 Mbps for various transmission power levels.

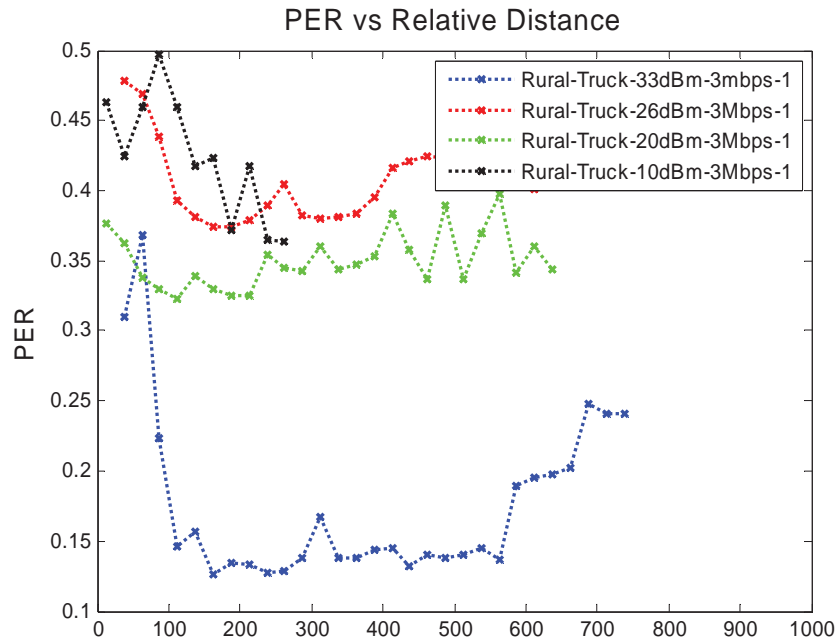


Figure 87: Comparison of PER versus Distance Curves for Various Power Levels in a Rural Highway Shadowing Scenario when Transmitter is Set to 3 Mbps

Figure 88 and Figure 89 show the effect of different data rates (3 Mbps and 6 Mbps) for a 33 dBm transmission. There appears to be little difference in performance.

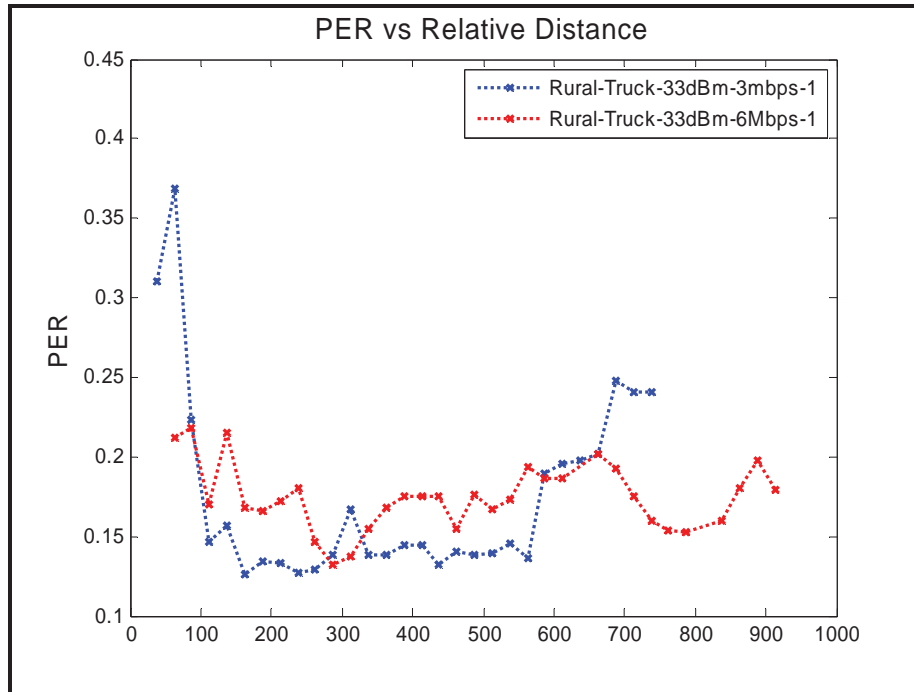


Figure 88: Comparison of PER versus Distance Curves for a Rural-Highway-Shadowing Scenario when Transmitting at 33 dBm and Different Data Rates

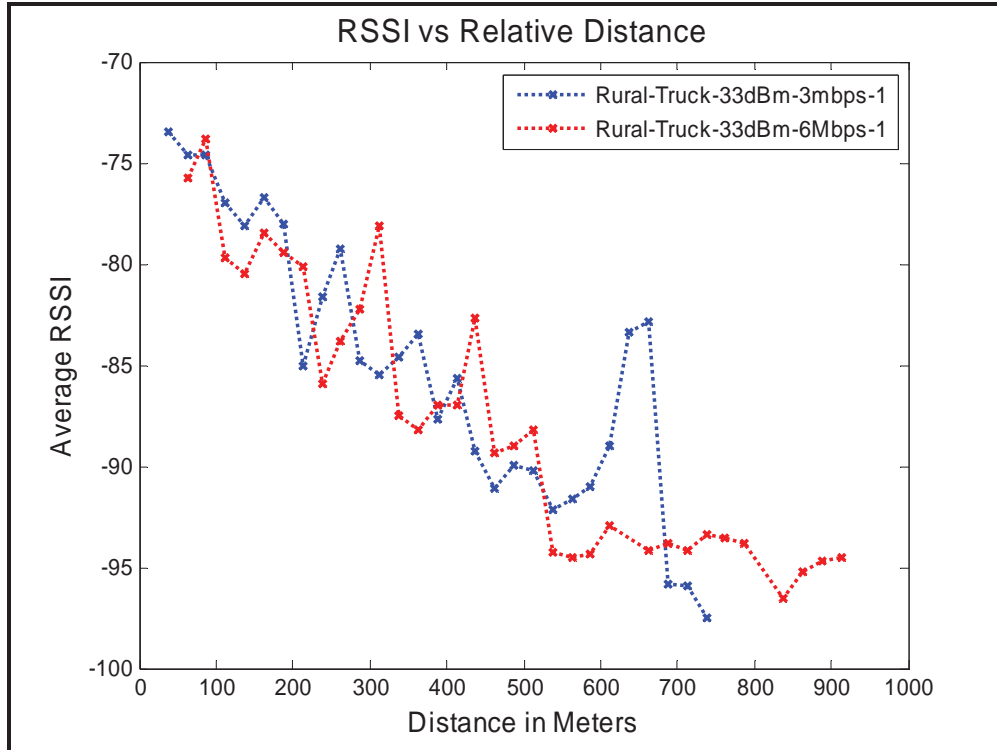


Figure 89: Comparison of RSSI versus Distance Curves for a Rural-Highway-Shadowing Scenario when Transmitting at 33 dBm and Different Data Rates

18.3 Observations for Rural-Highway-Shadowing Scenario

1. 33 dBm transmissions offer a PER of about 15 percent or less between 100 and 600 meters
2. Transmissions at or below 20 dBm maintain a PER above 30 percent at all distances
3. Regardless of transmit power, when the V2V distance approaches zero the PER increases or remains high. This phenomenon was also observed in other shadowing scenarios.

19 Arterial–Road-Shadowing Scenario-Test

The Arterial-Road-Shadowing Scenario tests were conducted along El Camino Real in the vicinity of Mountain View in Palo Alto, California. In these tests, the transmitter, truck, and receiver remained in the same lane. The receiver maintained a safe driving distance behind the truck while the transmitter varied its speed achieve a good spread of V2V distances. This test was conducted for the various cases shown in Table 15.

Table 15: Test Cases for the Arterial-Road-Shadowing Scenario Test

Data Rate \ TX Power	TX Power					
	5dBm	10dBm	15dBm	20dBm	26dBm	33dBm
3Mbps	Test 1	Test 4	Test 7	Test 10	Test 13	Test 16
6Mbps	Test 2	Test 5	Test 8	Test 11	Test 14	Test 17
12Mbps	Test 3	Test 6	Test 9	Test 12	Test 15	Test 18

19.1 Location Overview

El Camino Real is a fairly busy arterial with a moderate- to high-level of traffic any time of day. The road is lined with trees, strip malls, and apartment complexes along the sides. In some places there are trees in a narrow median. There are several major intersections per mile, in addition to smaller intersections. The road is 6- to 8-lanes wide in most places. Figure 90 shows a typical view along El Camino.



Figure 90: Driving North Along El Camino Real

19.2 Data Analysis

Figure 91 and Figure 92 show PER and RSSI versus distance at 3 Mbps and for three transmit power levels: 10 dBm, 20 dBm, and 33 dBm.

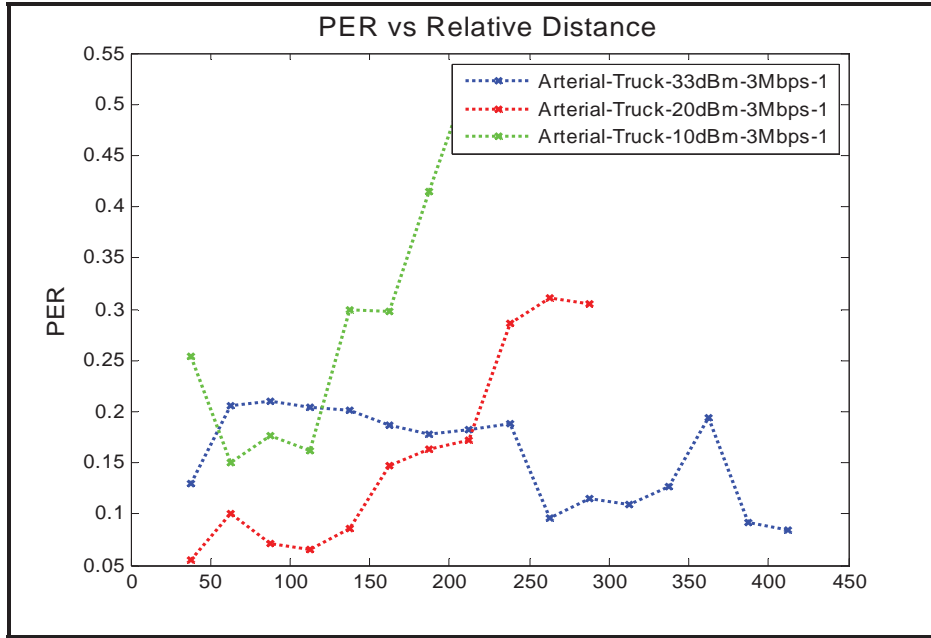


Figure 91: Comparison of PER versus Distance Curves for Various Power Levels in an Arterial-Road-Shadowing Scenario when Transmitter is Set to 3 Mbps

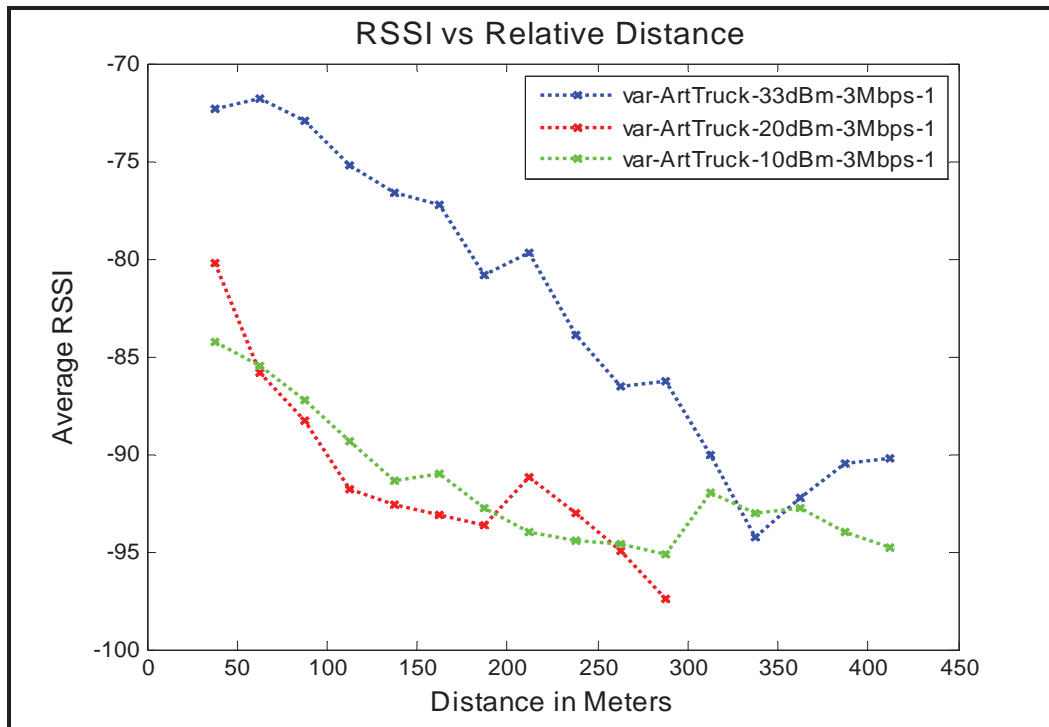


Figure 92: Comparison of RSSI versus Distance Curves for Various Power Levels in an Arterial-Road-Shadowing Scenario when Transmitter is Set to 3 Mbps

19.3 Observations for Arterial-Road-Shadowing Scenario

The following observations can be drawn with regard to communication performance in Arterial Shadowing environments:

1. This appears to be a relatively challenging communication setting, with even 33 dBm transmission unable to achieve a consistently low PER at any distance. Similar results were observed in other shadowing tests.
2. The effective transmission range increases with transmit power as expected, with low-power (10 dBm) performance falling off quickly after about 100 meters, nominal-power (20 dBm) performance remaining relatively good until about 150 to 200 meters, and high-power (33 dBm) performance consistently between 10 and 20 percent PER over the 450 meter distance range tested

20 Expressway-Shadowing Scenario Test

The Expressway-Shadowing Scenario tests were conducted along Central Expressway between Palo Alto and Santa Clara, California. As in the other shadowing tests, the transmitter, truck, and receiver remained on the same lane. The receiver maintained a safe driving distance behind the truck while the transmitter varied its speed to achieve a good spread of V2V distances. This test was conducted for the various test cases outlined in Table 16. Higher powers were not included in the tests due to time constraints with the rented truck.

Table 16: Test Cases for the Expressway-Shadowing Scenario Test

TX Power / Data Rate	5dBm	10dBm	15dBm
3Mbps	Test 1	Test 3	Test 5
6Mbps	Test 2	Test 4	Test 6

20.1 Location Overview

The Central Expressway allows for higher traffic speed (40-50 mph) than the El Camino arterial discussed in Section 19 but lower speed than a freeway or highway. The road is 4- to 6-lanes wide in most places. In some places it has a median and in others it does not. Intersections are less frequent than on El Camino. It runs through suburban sections of towns and has a propagation environment similar to the locations where the suburban tests were conducted. Figure 93 shows a typical view along the Central Expressway.



Figure 93: Driving East on Central Expressway

20.2 Data Analysis

Figure 94 and Figure 95 show PER and RSSI curves for the 5 dBm, 10dBm, and 15 dBm test cases.

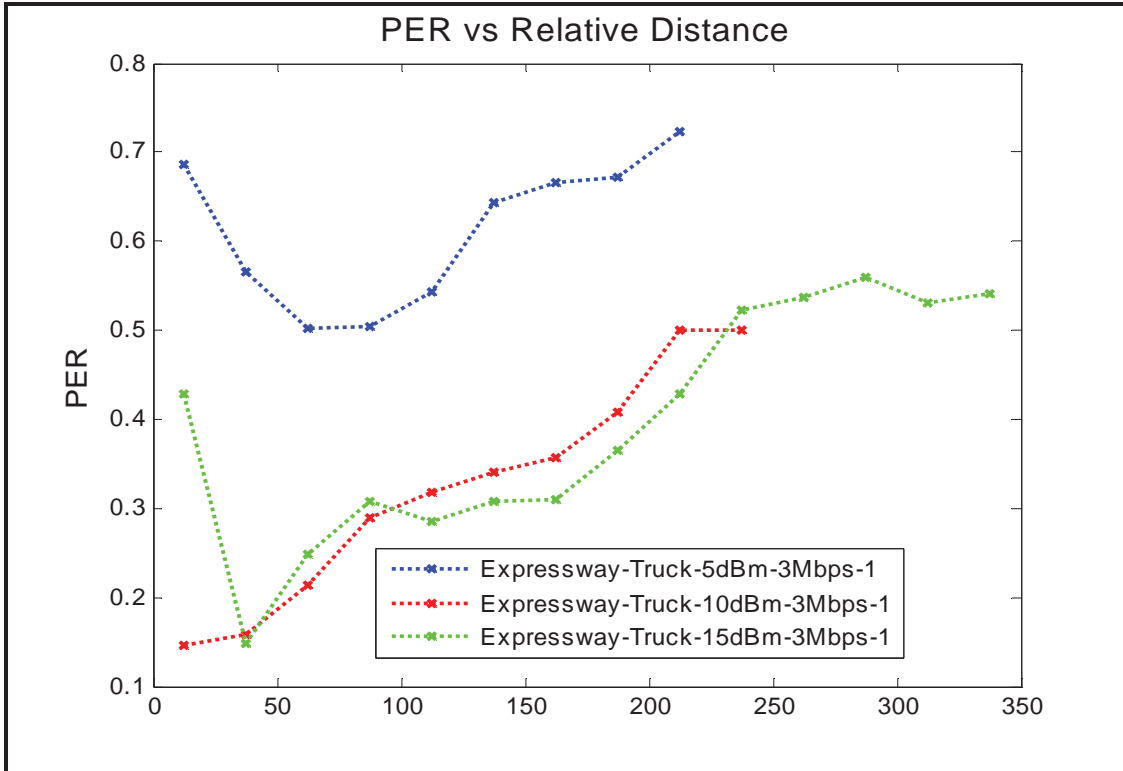


Figure 94: Comparison of PER versus Distance Curves for Various Power Levels in an Expressway-Shadowing Scenario when Transmitter is Set to 3 Mbps

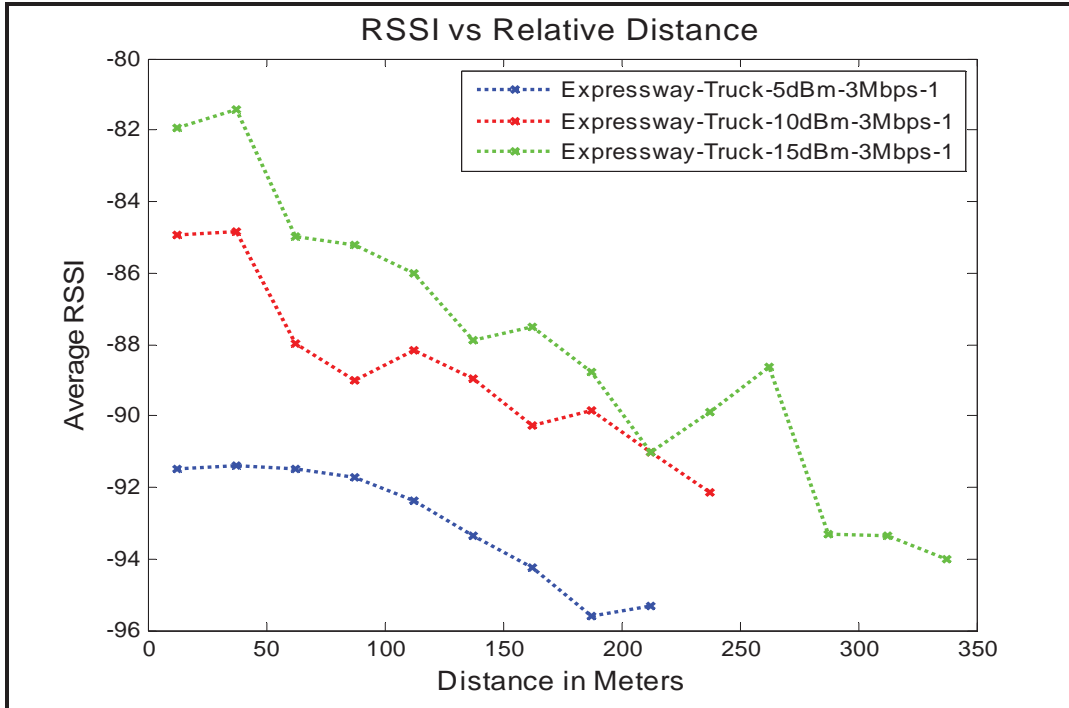


Figure 95: Comparison of RSSI versus Distance Curves for Various Power Levels in an Expressway-Shadowing Scenario when Transmitter is Set to 3 Mbps

20.3 Observations for Expressway–Shadowing Scenario

The following observations can be drawn with regard to communication performance in the Expressway Shadowing tests:

1. Time constraints limited the tests only to lower power levels
2. Use of lower powers (< 20 dBm) offers limited communication range in these NLOS conditions. All three power levels (5 dBm, 10 dBm and 15 dBm) had PERs of greater than 20 percent for V2V separation of greater than 20 meters.

21 Power Test Conclusions

Power tests were conducted in 16 environments. These scenarios were motivated by the VSC-A safety applications. The primary performance metrics were related to lower-layer behavior: PER and RSSI. As such, they give some indication of application layer performance but not a definitive answer. In scenarios where the indications flowing from these tests are not sufficiently precise, additional application-level testing may be warranted.

As expected, higher power consistently (though not universally) translated to better performance (e.g., lower PER at a given distance and/or larger achievable communication range). In the case of the intersection scenarios, there is reason to believe that the additional range provided by higher powers (i.e., above 20 dBm) may sufficiently improve application performance to be warranted. For example, in the Urban–Closed-

Intersection Scenario, Figure 26 shows that a 33 dBm transmission 100 meters from the intersection can be received reliably within about 35 meters of the intersection on the perpendicular street; whereas a 20 dBm transmission cannot be received with less than 20 percent PER even when the receiver is at the stop line of the intersection.

The scenarios that utilized a truck to create shadowing between the transmitter and receiver indicated a similar potential application advantage to using high-power transmission. For example, Figure 87 shows that in the Rural-Highway-Shadowing Scenario test when the transmit power was 33 dBm, a receiver was able to maintain fairly reliable connectivity (PER < 15 percent) up to distances on the order of 500 meters. On the other hand, for lower-transmit powers, the receiver could not achieve a PER less than about 30 percent at any distance.

The tests for which the transmitter and receiver were able to maintain Line-of-Sight indicate that higher powers may not be necessary for good application performance. For example, Figure 73 shows that in a Freeway-LOS test the link range was on the order of 250 to 300 meters even at 5 or 10 dBm.

While PER is an important performance metric, there are others that may be of interest as well. For example, statistics of the inter-message delay at a receiver (assuming a given message broadcast rate) can provide information related to application-level latencies. The power test data logs have been subjected to a limited amount of burst error analysis and are available for additional analysis.

The VSC-A team made use of an external power amplifier to produce high-power transmissions. If high power capability is desired in deployed DSRC safety systems, it would be advantageous for the power amplifier function to be built in.

22 Observations of Reduced Range in Some Baseline LOS Tests

The team noticed that after a certain point on the afternoon of the first day of testing, the ranges observed were lower than expected. For example, tests at 26 dBm and 33 dBm achieved lower range than 20 dBm tests conducted earlier in the day. A repetition of the 20 dBm test case showed a reduced range as well. The team was unable to identify a change in the environment that would explain the reduced range. Potential explanations include an equipment malfunction⁴, movement of ships in the channel, and a fog that appeared off the bay; but the cause could have been something else as well. The 20 dBm and 33 dBm LOS tests were repeated on the second day of tests, and the range achieved was consistent with observations from the morning of the first day and were higher than on the afternoon of the first day. The 26 dBm LOS test was not repeated on the second day due to time constraints. The PER plots in Figure 9 use runs that correspond to expected ranges, with the exception of the 26 dBm plot. The observed inconsistency can be seen in Figure 96, which shows the RSSI for seven 20 dBm baseline LOS tests. Six of the tests occurred either early on day 1 or on day 2. These exhibit the expected range, and the RSSI plots of these six runs are highly correlated. The seventh plot (labeled

⁴ Note that the equipment was checked for consistency of transmit output power level, and no inconsistencies were observed.

LOS-20 dBm-3 Mbps-Day1-3 p.m.) is from a run late on the first day and exhibits the reduced range observed at that time. Similarly, Figure 97 illustrates the reduced range observed on the first day for the 33 dBm Baseline LOS tests. This figure shows the results of five tests. The two plots labeled “Day 1” have reduced range compared to the three plots labeled “Day 2.”

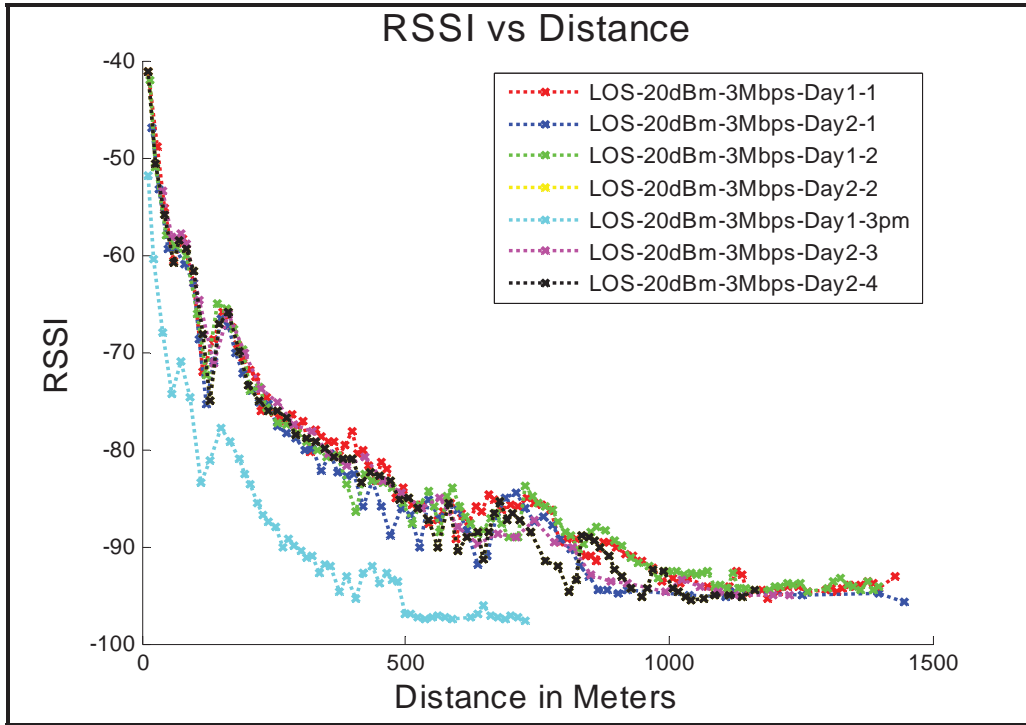


Figure 96: RSSI versus Distance at 20 dBm and 3 Mbps for the Baseline-LOS-Scenario Test

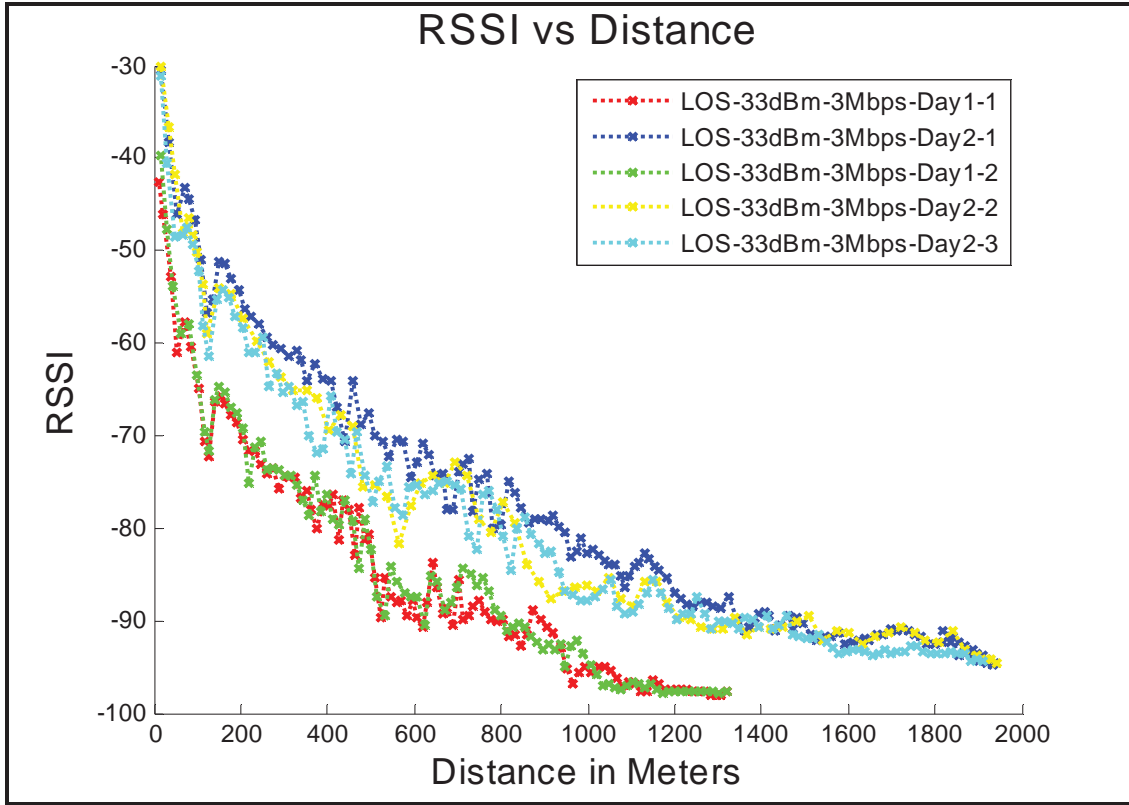


Figure 97: RSSI versus Distance for 33 dBm and 3 Mbps in Baseline LOS

VSC-A Final Report: Appendix D-2

Multi-Channel Operations

List of Acronyms

BSM	Basic Safety Message
CAMP	Crash Avoidance Metrics Partnership
CCI	Cross-Channel Interference
DSRC	Dedicated Short Range Communications
FCC	Federal Communications Commission
I-V or I2V	Infrastructure-to-Vehicle
MAC	Medium Access Control
NHTSA	National Highway Traffic Safety Administration
OEM	Original Equipment Manufacturers
RSE	Road Side Equipment
SPaT	Signal Phase and Timing
USDOT	United States Department of Transportation
UTC	Universal Coordinated Time
V2V or V-V	Vehicle-To-Vehicle
WAVE	Wireless Access in Vehicular Environments
WG	Working Group
WSM	WAVE Short Message

Table of Contents

List of Acronyms.....	D-2-ii
1 Introduction.....	D-2-1
2 Background.....	D-2-1
2.1 The Trial-Use 1609.4 Standard	D-2-1
2.2 FCC Designation of DSRC Channel 172	D-2-4
3 Phase I Alternative Approaches	D-2-4
3.1 Phase I Constraints	D-2-4
3.2 Phase I Taxonomy of Scenarios Studied	D-2-5
3.3 Channel Usage Map and Time Usage Map for Default Approach	D-2-6
3.4 An Alternative Approach that uses Channel 172 for an Always-On Safety Channel.....	D-2-7
3.5 Cross-Channel Interference Effect	D-2-9
3.6 Other Phase I Scenarios.....	D-2-10
3.7 Phase I Conclusion	D-2-10
4 Phase II Alternative Approaches	D-2-11
4.1 Capability/Channel 172 Approach	D-2-13
4.2 Intention/CCH Approach	D-2-14
5 Summary of Research Results	D-2-16
6 Proposal for the Header Bits in the Next Version of IEEE 1609.3...D-2-17	
7 Conclusion	D-2-18
8 References	D-2-20

List of Figures

Figure 1: Time Division in the Trial-Use 1609.4 Standard	D-2-2
Figure 2: Taxonomy of Phase I Multi-Channel Scenarios.....	D-2-5
Figure 3: Channel Usage Map – Scenarios 1B+1D	D-2-6
Figure 4: Time Usage Maps – Scenarios 1B+1D	D-2-7
Figure 5: Channel Usage Map – Scenarios 2B+2C	D-2-7
Figure 6: Time Usage Maps – Scenarios 2B+2C	D-2-8
Figure 7: Default Vehicle in the Neighborhood	D-2-12
Figure 8: No Default Vehicles in the Neighborhood.....	D-2-13

List of Tables

Table 1: FCC Allocation of DSRC Spectrum.....	D-2-2
Table 2: Summary of Multi-Channel Approaches.....	D-2-16
Table 3: VSC-A Proposal to IEEE 1609 for Header Bits.....	D-2-18

1 Introduction

This appendix reports on research results obtained under the VSC-A Project: Channel 172 Usage / Multi-Channel Operations. The goal of this research is to determine the potential best ways to use the Dedicated Short Range Communication (DSRC) spectrum in the U.S. for vehicle-to-vehicle (V2V) safety communication. A complete answer would require consideration of both technical and non-technical factors; the latter include business, market penetration, and regulatory issues. The research conducted under the VSC-A Project only explored the technical dimensions of the question, while recognizing the existence of the non-technical factors. Two documents informed the organization of the work: the Trial-Use IEEE 1609.4 Standard on Multi-Channel Operation [2] and the U.S. Federal Communications Commission (FCC) designation of DSRC Channel 172 “exclusively for V2V safety communications for accident avoidance and mitigation, and safety of life and property applications [4].” These are discussed as part of the background material in the next section. The research was conducted in two phases, and there is a section devoted to each below. The most promising approaches are summarized in Section 5. Section 6 reports on a proposal that the VSC-A team made to the IEEE 1609 Working Group (WG) regarding additional header bits to support multi-channel operation. The final section of the appendix provides a brief conclusion.

2 Background

V2V safety is enabled by the frequent exchange of vehicle state information in the form of Basic Safety Messages (BSMs), which are defined in the SAE J2735 Message Set Dictionary Standard [3]. This work was motivated by the existence of two nascent, potentially competing concepts of how to use the DSRC spectrum for BSM exchange between neighboring vehicles. The first flows from the IEEE 1609.4 Multi-Channel Operation Trial-Use Standard, which provides a means for all interested devices to rendezvous on one channel in a certain interval of time for the exchange of critical data. Under this concept, BSMs would be among the critical data exchanged on that channel in that interval. The other concept is related to an FCC designation of a different DSRC channel for use in safety communication. The two documents are not explicitly in conflict, but to many people they imply inconsistent safety communication models.

2.1 The Trial-Use 1609.4 Standard

The FCC has allocated 75 MHz of spectrum in the 5.9 GHz band for DSRC. This is divided into seven non-overlapping 10 MHz channels, plus a 5 MHz guard band, as shown in Table 1.

The Trial-Use 1609.4 Standard defines a time division mechanism for a device to operate on both the control channel (CCH) and one or more service channels (SCHs). The mechanism assumes each device is synchronized to Coordinated Universal Time (UTC). Time is divided into sync intervals which are further sub-divided into a CCH interval and a SCH interval. There are guard intervals at the start of each CCH and SCH interval as well. See Figure 1. The nominal sync interval is 100 ms, which corresponds to the

default BSM interval for V2V safety communications. The default division within a sync interval is 50 ms for the CCH interval and 50 ms for the SCH interval.

Table 1: FCC Allocation of DSRC Spectrum

Channel No.	Frequency Range (MHz)	Channel Use	Notes
170	5850-5855	Reserved	Guard band
172	5855-5865	Service Channel	Special FCC designation for V2V safety and other safety
174	5865-5875	Service Channel	
176	5875-5885	Service Channel	
178	5885-5895	Control Channel	
180	5895-5905	Service Channel	
182	5905-5915	Service Channel	
184	5915-5925	Service Channel	Special FCC designation for longer distance public safety

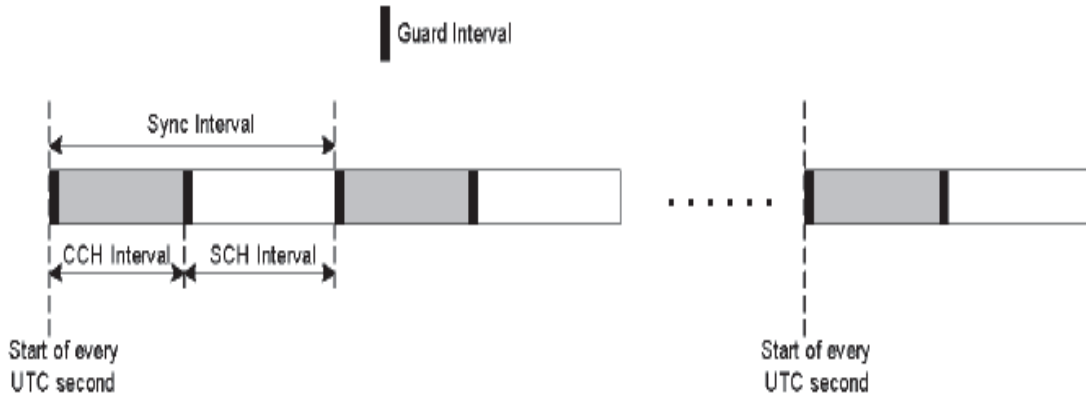


Figure 1: Time Division in the Trial-Use 1609.4 Standard

The combination of the CCH spectrum and the CCH time interval constitute a “rendezvous” capability. Without need of any other coordination, devices know that certain types of information exchanges will occur in this band and interval. These include the broadcast of service advertisements and other control packets.

V2V safety applications can use this rendezvous capability as well. According to this approach, vehicles interested in V2V safety send and receive BSMs on the CCH during the CCH interval. This V2V safety communication model is not required by IEEE 1609.4, or any other standard, but is taken as the default approach for the purposes of this research. The goal of the research is to investigate alternative approaches for V2V safety communication and compare them with each other and with the default approach.

The default approach has several advantages and disadvantages. One of the main advantages is that it allows a single-radio vehicle to participate in V2V safety by exchanging BSMs with its neighbors and also to avail itself of DSRC services that are offered during SCH intervals (e.g., by Road Side Equipment (RSE)). This capability is especially attractive as part of an initial DSRC deployment strategy to boost market penetration. One of the main disadvantages is that safety messages are effectively limited to the CCH interval, and thus channel congestion is a significant concern. At high channel loads, the probability that two or more packets “collide” due to overlapping transmissions can become significant.

Determining channel capacity via analysis is quite complex due to the Medium Access Control (MAC) protocol used in DSRC. However, a back-of-the-envelope calculation shows why 1609.4 time division causes a concern for V2V safety. If a DSRC channel supports 6 Mbps, this is equivalent to 2000 messages/second⁵ for 3000 bit messages (the approximate size of an average BSM). At 10 messages/second/vehicle, this is equivalent to 200 vehicles in a given transmission region. With BSMs confined to the CCH interval, the capacity is cut to about 45 percent due to the guard interval and the need to complete packet transmissions before the start of the SCH interval. In this simple example, that is equivalent to 90 vehicles in a region. It is not difficult to construct realistic traffic scenarios in which a capacity of 90 vehicles in a transmission region represents a significant constraint.

While Trial-Use 1609.4 allows single-radio devices to access both the CCH and the SCHs, it also allows for multi-radio devices. It is worth considering what the addition of a second optional radio can do for a system that wishes to participate in V2V safety and also access other DSRC services. Two models have been discussed by the VSC-A team and are described below.

In the first model, Radio #1 remains tuned to the CCH all the time, and Radio #2 is available for tuning to a SCH at any time. In the second model, Radio #1 performs just as a single-radio system would, tuning to the CCH in the CCH interval and perhaps tuning to a SCH in the SCH interval to access services. In this model, Radio #2 can tune to any channel at any time.

In the first dual-radio model, Radio #1 is not very useful during the SCH interval since the CCH is not expected to carry critical information outside of the CCH interval. Therefore, the second model provides an advantage over the first in that the vehicle can access two SCHs at one time, and thus more services.

⁵ We use 100% channel utilization in this simple example, but in reality the inefficiencies of the MAC protocol reduce maximum effective utilization well below that level.

With regard to the narrower question of safety communication performance, however, neither dual-radio model improves significantly on the single-radio system. BSM broadcasts are still limited to the CCH during the CCH interval, because dual-radio and single-radio systems will, in general, co-exist. The CCH interval constitutes the primary limitation on safety communication performance. It is possible for a dual-radio system to tune both radios to the CCH during the CCH interval and, therefore, have two chances to receive each BSM from another vehicle. However, dual receivers will do little to overcome collision-based packet loss.

The conclusion, then, is that under the default approach single-radio and dual-radio systems will have similar safety communication performance. Furthermore, among the dual-radio models, the model in which both radios are available to tune to an SCH during the SCH interval has advantages over the model in which one radio remains tuned to the CCH all the time.

2.2 FCC Designation of DSRC Channel 172

The FCC has designated DSRC Channel 172 “exclusively for V2V safety communication for accident avoidance and mitigation, and safety of life and property applications” [4]. This designation limits what can be sent on channel 172, but does not require that any particular safety communication be carried out on that channel. In that sense, it is not in conflict with the default approach described above in which BSMs are sent on the CCH. One goal of this subtask is to explore alternative safety communication approaches that make more use of Channel 172.

The FCC language quoted above is quite general and is subject to some interpretation. Since it is clear that the designation includes the exchange of BSMs between vehicles, it is not critical to analyze the various interpretations to which the language can be subjected, but these do have some implications for the assessment of approaches that will be considered below.

3 Phase I Alternative Approaches

The default approach described in the previous section has advantages and disadvantages. The goal of the research under this subtask is to investigate alternatives and assess their merits relative to each other and to the default approach.

3.1 Phase I Constraints

The team carried out its research in two phases. In the first phase the approaches were subject to the following constraints:

- No additional over-the-air (OTA) protocol information is available beyond what is available in the Trial-Use 1609 standards and the IEEE 802.11 header
- Each vehicle attempts to hear all V2V safety messages, i.e. there are commonly understood times and channels during which all vehicles will be listening for safety messages. Of course, the unreliability of the IEEE 802.11 protocol does not ensure that any given broadcast will be correctly received.

- A single-radio is sufficient to fully participate in safety communication; a second radio is optional

3.2 Phase I Taxonomy of Scenarios Studied

The team developed a set of eleven approaches, including the default approach, and classified each according to how many radios are used, which channel is used for safety communication, and other factors. Figure 2 shows this classification. The two-character codes are used as shorthand labels for each approach.

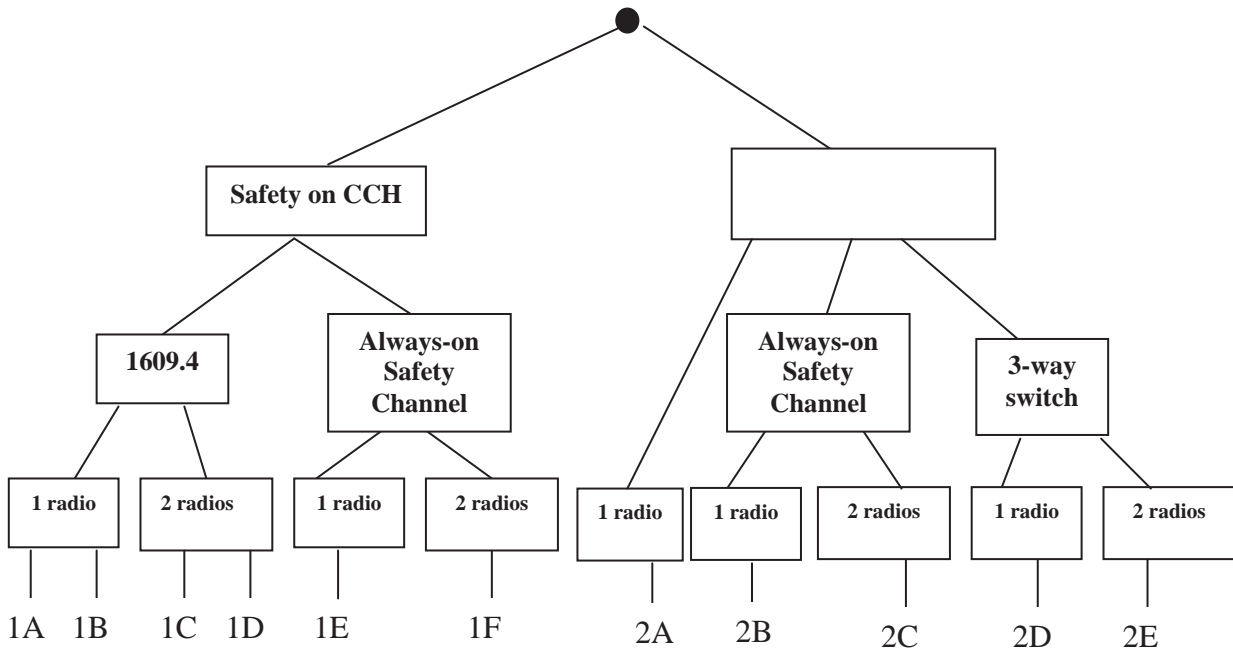


Figure 2: Taxonomy of Phase I Multi-Channel Scenarios

Note that some scenarios separate safety and control messages by using Channel 172 as the safety channel, while others continue to use the CCH for the safety channel. Also, some of the scenarios consider an “always-on” safety channel, meaning that a sender can expect a safety message to be heard no matter when it is sent, while others use time division.

Scenario 1B represents the single-radio default approach described in Section 2.1. It sends and receives BSMs on the CCH during the CCH interval, and it may switch to a SCH to take advantage of a general DSRC service during the SCH interval. Though BSMs are exchanged on the CCH, a default approach implementation might use Channel 172 for some other type of safety exchange, referred to here as a “session-oriented safety service.” Such a service, which would be advertised in a control message on the CCH, is beyond the scope of the VSC-A Project.

The two dual-radio models consistent with the default approach, discussed in Section 2.1 above, are labeled 1C and 1D, respectively, in Figure 2. Scenario 1C keeps one radio tuned to the CCH all the time and was shown to be less attractive than Scenario 1D,

which can access services on two SCHs simultaneously during the SCH interval. So, Scenarios 1B and 1D can co-exist and interoperate and are, thus, considered a single deployment approach.

3.3 Channel Usage Map and Time Usage Map for Default Approach

The team used a graphical tool to concisely represent the scenarios under consideration. The tool consists of two drawings, a Channel Usage Map and a Time Usage Map. The Channel Usage Map uses colors and shading to indicate how each of the seven DSRC channels is used in that scenario. The Time Usage Map shows how each radio segregates its functions in time. The Channel Usage Map and Time Usage Map for the combination of Scenarios 1B and 1D are shown in Figure 3 and Figure 4.

The Channel Usage Map shows a blend of red and blue in the CCH, which supports both safety and control data exchanges. Channel 172 is colored red because it supports session-oriented safety services. The other SCHs are green indicating they support general DSRC services.

The Time Usage Map for Radio #1 alternates between the CCH during the CCH interval and an SCH during the SCH interval. Since the SCH could be Channel 172, a more accurate shading would be a blend of green and red in those boxes, but since session-oriented safety is beyond the scope of the VSC-A Project, that level of detail in these diagrams has been omitted. Optional Radio #2 is shown switching to an SCH during the SCH interval just like Radio #1 and, therefore, Figure 4 shows graphically the capability of Scenario 1D to support two SCH accesses simultaneously. During the CCH interval, Radio #2 could do a variety of things, including tuning to the CCH or to an SCH. If it is tuned to the CCH, it is largely redundant with Radio #1, and, in particular, it must be careful not to add to channel congestion by transmitting. If it tunes to an SCH, it will communicate with other devices that have dual-radios and/or are not participating in V2V safety. Since single-radio vehicles will not be able to participate in these exchanges, they are labeled “non-critical” exchanges. And since they take place on an SCH during the CCH interval, they are labeled “off-interval” exchanges. Scenario 1B is represented in these figures with the omission of optional Radio #2 in Figure 4.

Ch 172	Ch 174	Ch 176	Ch 178	Ch 180	Ch 182	Ch 184
Session-oriented Safety messages	General DSRC messages	General DSRC messages	Control messages and Safety messages	General DSRC messages	General DSRC messages	General DSRC messages

Figure 3: Channel Usage Map – Scenarios 1B+1D

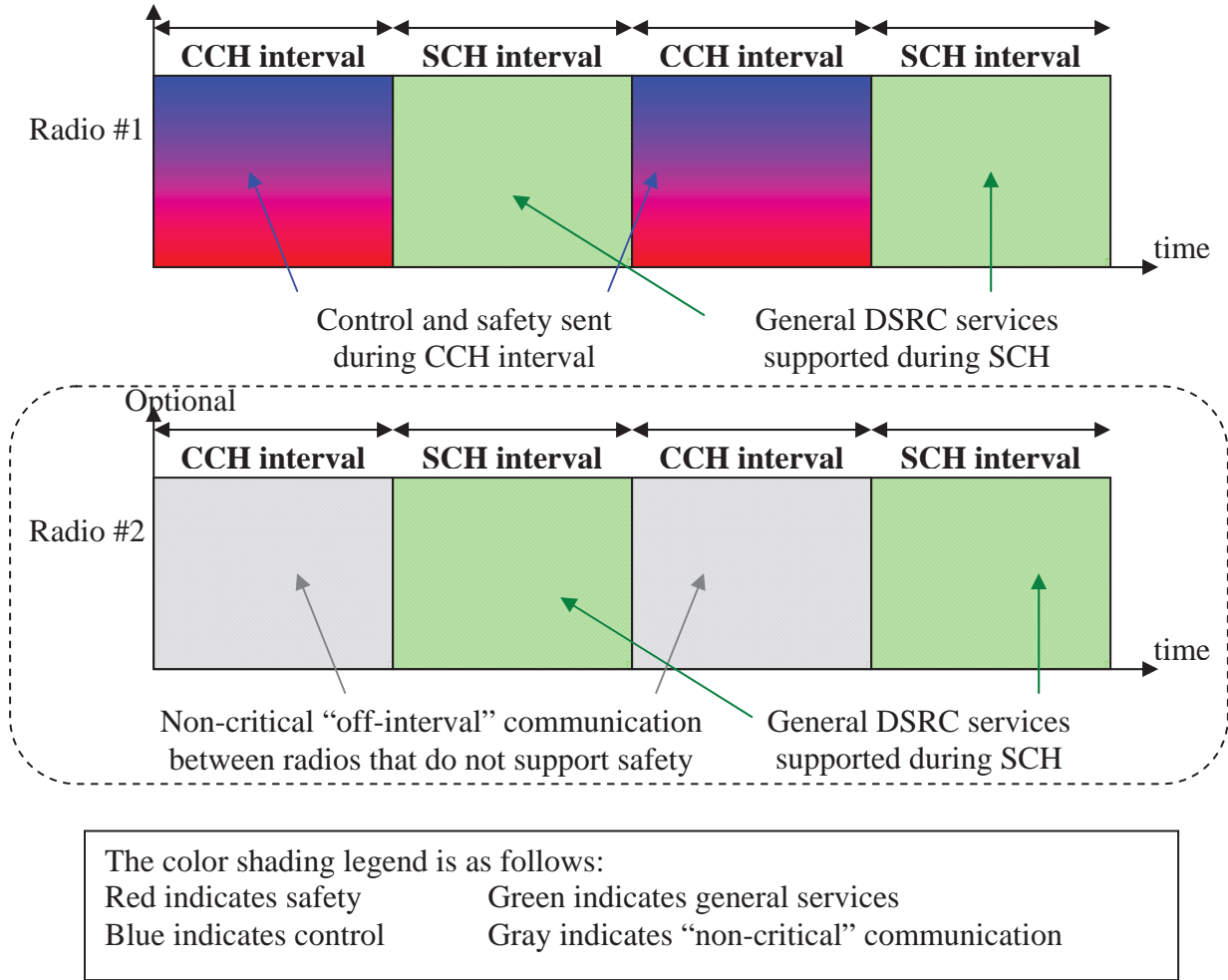


Figure 4: Time Usage Maps – Scenarios 1B+1D

3.4 An Alternative Approach that uses Channel 172 for an Always-On Safety Channel

Compared to the default approach, the most attractive Phase I alternative is represented by the combination of Scenarios 2B and 2C in Figure 2. The Channel and Time Usage Maps for these scenarios are illustrated in Figure 5 and Figure 6.

Ch 172	Ch 174	Ch 176	Ch 178	Ch 180	Ch 182	Ch 184
Safety messages	General DSRC messages	General DSRC messages	Control messages	General DSRC messages	General DSRC messages	General DSRC messages

Figure 5: Channel Usage Map – Scenarios 2B+2C

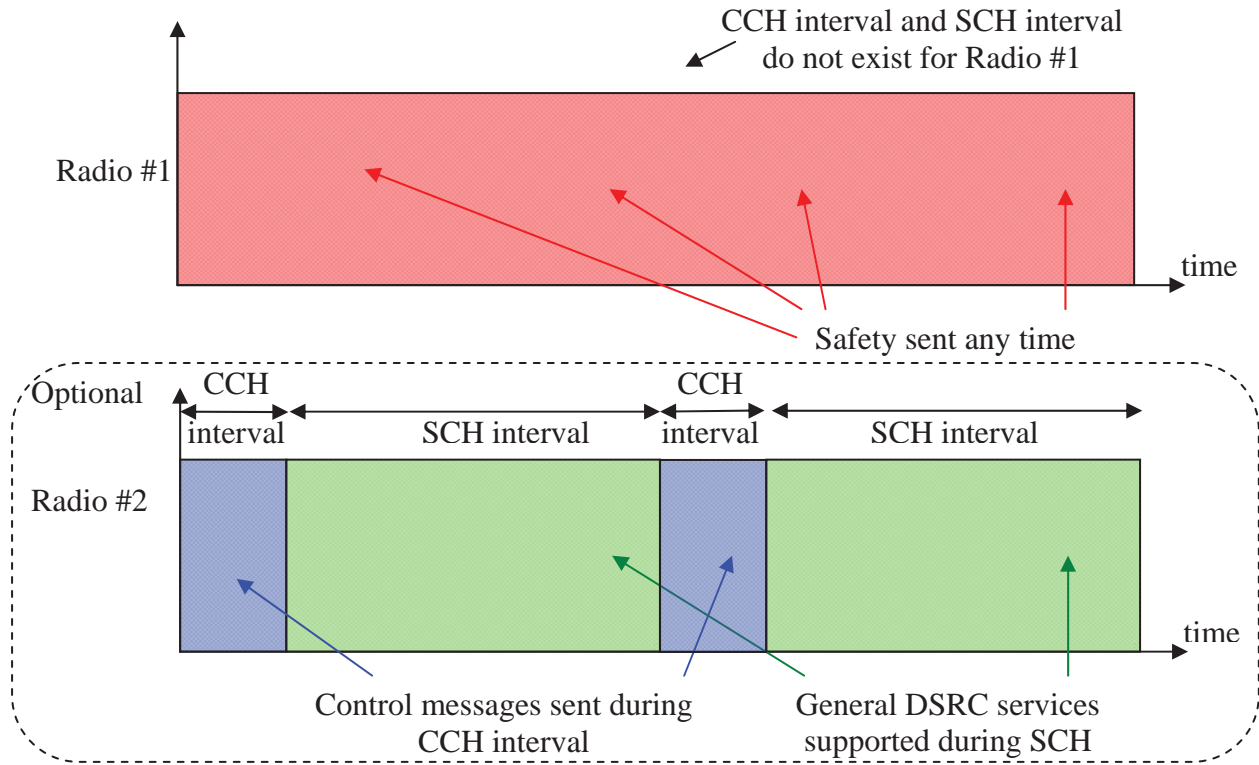


Figure 6: Time Usage Maps – Scenarios 2B+2C

In Scenarios 2B and 2C, safety communication is moved entirely to Channel 172. So, in Figure 5, the CCH is no longer a red/blue blend as in Figure 3, but rather it is solid blue. Channel 172 is now labeled simply “safety messages,” since it supports all safety communication not just that of a session-oriented nature. Scenario 2B has a single-radio, Radio #1, which tunes to Channel 172 at all times. It does not concern itself with the CCH or SCH interval. Scenario 2C includes an optional Radio #2, which monitors the CCH during the CCH interval, and could switch to an SCH to access a service if it wished during the SCH interval. Radio #2 follows more traditional 1609.4 channel switching but does not participate in safety communication since that is all handled by Radio #1. Scenarios 2B and 2C can co-exist and interoperate and are considered a single deployment approach. Note that with BSMs removed from the CCH, the team observed that the optimal division between the CCH interval and SCH interval might now favor the SCH interval. This observation is illustrated in Figure 6, though the particular division shown should not be interpreted as optimal.

The biggest advantage of the 2B+2C approach, compared to the default approach, is that BSM communication takes place on an always-on safety channel, which has more than twice the capacity of the CCH interval.

The biggest disadvantage of the 2B+2C approach is that a single-radio implementation that wants to support V2V safety can do nothing else outside of Channel 172. It does not monitor the CCH for control messages, and it cannot switch to another SCH to access general DSRC services. One consequence of this is that the question of what falls within

the FCC designation for Channel 172 becomes very important because single-radio vehicles will not hear anything transmitted outside of Channel 172. For example, in some prototype efforts for intersection collision avoidance applications using infrastructure-to-vehicle (I2V) communication, Signal Phase and Timing (SPaT) messages and intersection geographic description messages have been sent on other channels. These would need to be moved to Channel 172 if a single-radio vehicle is to be able to support those I2V safety applications.

3.5 Cross-Channel Interference Effect

Another point of comparison among multi-channel approaches is their susceptibility to cross-channel interference (CCI). CCI is the energy in a target channel that results from a transmission in another channel. There are standards that limit this energy, but it cannot be eliminated entirely. CCI, like other forms of noise, can reduce the reception probability for a packet. In this section, the effect that CCI can have on reception probability of a BSM under various multi-channel approaches is discussed.

Field tests were performed with prototype DSRC radios to study how CCI affects packet reception probability [5]. Two important factors are:

- The spectral distance between the channel on which the BSM is transmitted and the channel on which the interfering signal is transmitted. The effect is much more prevalent when the interferer is in the adjacent channel (e.g., Channel 174 in the case of a BSM transmission on Channel 172), than when the interferer is two or more channels away.
- The ratio of the BSM transmitter-to-receiver distance to the interferer-to-receiver distance. When that ratio is at least 10:1, the CCI affect on packet reception was found to be much more significant.

As an example and considering a receiver on Channel 172 using the 2B+2C approach, if an interfering transmitter is 10 meters away and using Channel 174 at the same time that a vehicle 100 or more meters away is sending a BSM on Channel 172, the probability of correctly receiving the BSM is expected to be significantly reduced. On the other hand, if the interfering transmission is not on Channel 174, or if the ratio of distances becomes less than 10:1, the probability of correctly receiving the BSM is expected to be similar to the case where there is no CCI. The ratio threshold of 10:1 should be considered a rough rule of thumb for a continuously varying effect, not a given.

The time division inherent in IEEE 1609.4 might be expected to make CCH receptions immune to a CCI effect. However, IEEE 1609.4 does not prohibit SCH transmissions during the CCH interval. Indeed, the version of the IEEE 1609.4 Standard published in 2010 defines explicit protocol enhancements to announce a service that will be available on a SCH during the CCH interval. If such a service is offered on either of the channels adjacent to the CCH, Channel 176 or Channel 180, there could be a significant CCI effect on BSM receptions on the CCH.

To some extent, all of the approaches considered, including the default approach, are subject to some degree of CCI. Without specifying detailed use cases, it is difficult to compare the impact that CCI has on BSM receptions in different multi-channel

approaches. While CCI is not a prominent factor in the research reported in this document, it should be considered in more definitive assessment.

3.6 Other Phase I Scenarios

The other scenarios investigated as Part of Phase I were found to be less attractive than the 2B+2C combination. These are described briefly below for completeness.

Scenario 1A: This was included as an incremental approach leading to Scenario 1B and need not be discussed further.

Scenarios 1E and 1F: These expanded safety communication on the CCH to occupy the entire sync period with no concern for CCH or SCH intervals. Scenario 1E uses a single radio, Radio #1, which is tuned to the CCH all the time. Scenario 1F adds an optional Radio #2, which is capable of switching to any of the channels to access DSRC services. This pair of scenarios has some similarities to the 2B+2C combination, namely an always-on safety channel that a single-radio system never leaves, and the consequent inability of a single-radio system to access general DSRC services like the default approach can. Compared to 2B+2C, the combination of 1E+1F has an advantage in that the single-radio in 1E can hear control messages in addition to safety messages. In the future, there may be control messages of importance to such a radio. A disadvantage of this is that safety messages compete for channel access with control messages, and thus suffer higher collision rates than in the 2B+2C Approach where the safety channel is not shared with control. Another difference for the 1E+1F combination is that it does not use Channel 172.

Scenario 2A: This is a single-radio approach in which the radio alternates between the CCH during the CCH interval and Channel 172 during the SCH interval. It exchanges all BSMs on the latter channel. An advantage is that the single-radio has access to both safety and control messages. However, it has a big disadvantage compared to the 2B+2C approach because it does not use Channel 172 in an always-on manner. By perpetuating the time division on Channel 172, it suffers the same congestion weakness as the default approach. On the other hand, the single-radio implementing Scenario 2A cannot access both safety and general DSRC services as it can in Scenario 1B.

Scenarios 2D and 2E: This is the final pair of scenarios. They not create an always-on safety channel and instead add a third time division to each sync period. In addition to a CCH Interval and an SCH Interval, the 2D+2E combination creates a Safety Interval. During the Safety Interval, all devices wishing to participate in V2V safety tune to Channel 172 and exchange BSMs. This approach not only perpetuates the channel capacity problems of the default approach, it actually magnifies them with the third time division. Any capacity allocated to one interval is explicitly unavailable for the other two types of communication. This approach was not investigated further by the team.

3.7 Phase I Conclusion

The conclusion of the Phase I part of the research is that among the scenarios considered the 2B+2C combination offers the best alternative to the default approach. Each of these approaches has advantages and disadvantages, some of which are documented in Table 2

below. Single-radio versions of both approaches were implemented in the VSC-A test bed prototype.

More specifically, the VSC-A team recognized that the single-radio, 1609.4 channel switching approach, Scenario 1B, has the aforementioned advantages of supporting both safety and general services with one radio, which is good for DSRC market penetration. The team also recognized that the dual-radio Scenario 2C represents an attractive model at higher penetration levels where congestion will likely be a concern because it supports safety with the capacity of an always-on safety channel in addition to supporting general services as well.

For a scenario whereby initial deployments would follow channel switching as in Scenario 1B and later deployments would utilize an always-on Channel 172 as in Scenario 2C, the Section 3.1 constraints create a dilemma in which there is no clear migration strategy which would allow early deployment radios to communicate with later deployment radios.

This migration dilemma led the team to initiate Phase II of the study.

4 Phase II Alternative Approaches

In Phase II of the multi-channel operation research, the constraint against introducing new OTA protocol information is relaxed. The goal of this phase is to identify one or more approaches that allow co-existence between implementations that can only send and receive BSMs according to the default approach (i.e., on the CCH during the CCH interval) and implementations that can utilize an always-on safety channel. Such a co-existence approach would facilitate a migration from the former type of implementation to the latter over time.

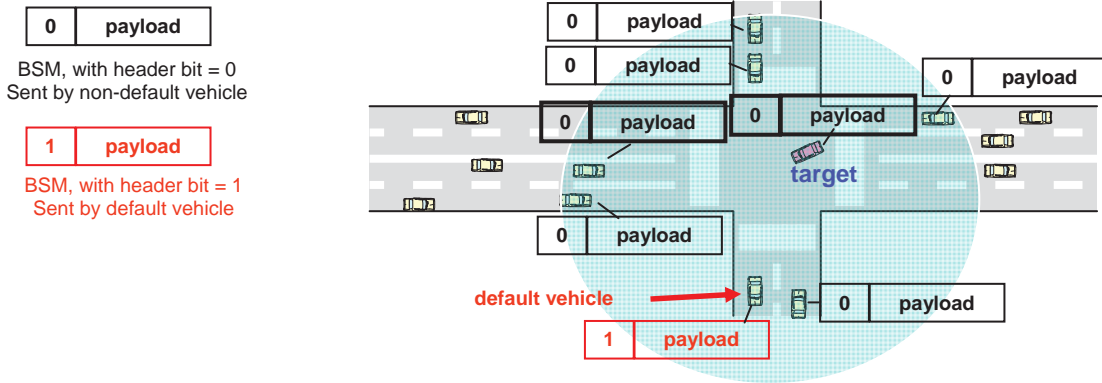
In each co-existence approach identified in this phase, there is a single always-on channel. For simplicity, a vehicle that cannot take advantage of this always-on channel and is constrained to exchange BSMs on the CCH during the CCH interval is referred to as a “default vehicle.” A vehicle that can take advantage of the always-on channel is referred to as a “non-default vehicle.” The co-existence approaches studied in Phase II require two things:

- A non-default vehicle must be capable of exchanging BSMs with a default vehicle on the CCH during the CCH interval (i.e., of adapting its communication to accommodate the default vehicle)
- A non-default vehicle must be capable of determining when it has one or more default vehicles within its transmission range

The technical innovation that enables an approach to meet the second requirement is the addition of an OTA bit (or bits) in the safety message, the state of which identifies the sender’s type (default or non-default). The concept behind the Phase II research is illustrated in Figure 7 and Figure 8.

In Figure 7, each vehicle includes a header bit in its BSM broadcast. Default vehicles set the bit to 1, and non-default vehicles set the bit to 0 (the polarity could just as easily be reversed). The figure shows the transmission region of a given target vehicle in the

intersection and shows one default vehicle within that region. The target vehicle detects the presence of its default vehicle neighbor via the header bit. When it knows it has a default vehicle neighbor, it sends its BSMs on the CCH during the CCH interval so that the default vehicle can hear them.



If at least one vehicle in a neighborhood sends packets with bit = 1, the target vehicle (center) sends BSMs during the CCH interval on the CCH.

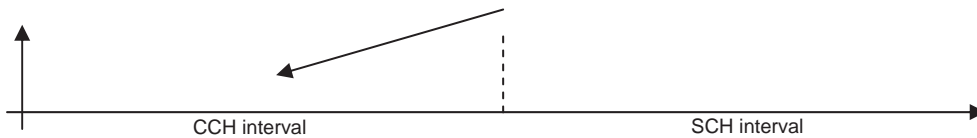
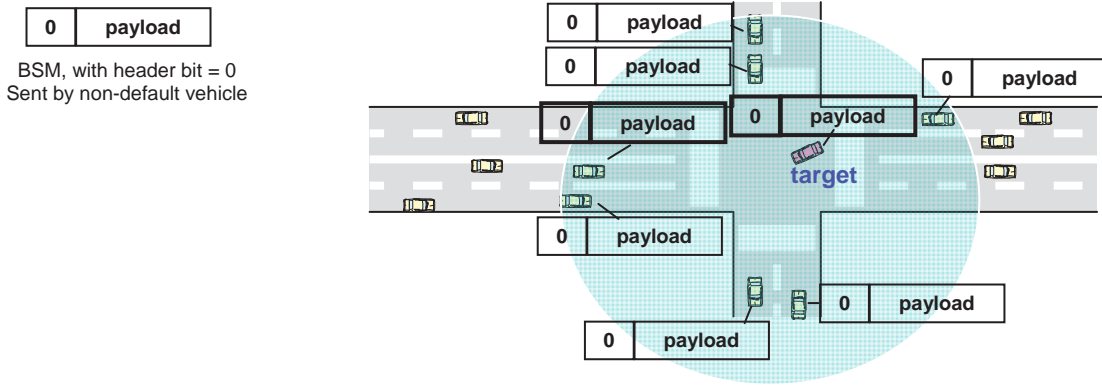


Figure 7: Default Vehicle in the Neighborhood

Figure 8 shows the same intersection scenario, but this time the transmission region around the target vehicle has only non-default vehicles. When the target vehicle determines that all of its neighbors are non-default vehicles, it transmits its BSMs on the always-on safety channel at any time.

Every non-default vehicle must monitor the CCH during every CCH interval to detect the presence of a default neighbor. However, it need only adjust its BSM transmissions when a default neighbor is present. A default vehicle must set the header bit correctly, but does not need to monitor the header bits in received BSMs. Its BSM transmission and reception behavior does not change as a function of the types of vehicles in its neighborhood.



If all vehicles in a neighborhood send packets with bit = 0, the target vehicle (center) is free to send BSMs at anytime in the safety channel.

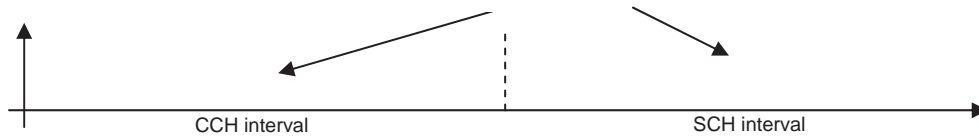


Figure 8: No Default Vehicles in the Neighborhood

These figures illustrate the basic paradigm of the co-existence approaches investigated in Phase II of the research. Specific approaches are documented below. There are a number of implementation issues associated with these types of approaches (e.g., if a non-default vehicle has detected a neighboring default vehicle but then misses an expected BSM from that vehicle, how does it manage the transition back to the no-default-vehicle-neighbors state?) These are beyond the scope of the research conducted in this project.

The team investigated a number of co-existence approaches. Of these, two were judged to be feasible and preferable to the others. The next two subsections present details of each of these approaches.

4.1 Capability/Channel 172 Approach

In this approach, the always-on safety channel is Channel 172. The approach uses one new header bit to communicate vehicle type. This bit is referred to as a “capability bit,” because it conveys the capability of the vehicle in terms of whether it has one radio or more than one radio. This approach is characterized by the following behaviors:

Single-Radio Vehicle:

- A single-radio vehicle sends and receives BSMs on the CCH during the CCH interval. This radio is available to switch to a SCH during the SCH interval if desired. In other words, it follows the default approach.
- It sets the header bit in its outgoing BSMs to indicate it is a single-radio vehicle

Multiple-Radio Vehicle:

- A multi-radio vehicle keeps one radio tuned to Channel 172 all the time. The vehicle sends and receives BSMs on Channel 172 at any time, without regard to time division within the sync period.
- A second radio is tuned to the CCH during the CCH interval to listen for BSMs and control messages. This radio may switch to an SCH during the SCH interval. In other words, it follows the default approach.
- If the header bit of a BSM received on the CCH indicates its sender is a single-radio vehicle, the multi-radio vehicle also begins sending its BSMs on the CCH during the CCH interval. It sends each BSM twice, once with each radio. When it sends a BSM on the CCH, it sets the header bit to indicate it is a multi-radio vehicle.
- If the multi-radio vehicle determines that it has no single-radio neighbors, it ceases sending its BSMs on the CCH during the CCH interval to avoid unnecessary loading on the CCH

Performance:

In this approach, multi-radio vehicles are able to communicate with each other on the always-on safety channel (Channel 172). So, the performance of a link between two such vehicles is that associated with an undivided channel (and of course dependent on vehicle density, transmit power, distance, and the multi-path environment, among other factors). For example, the performance between multi-radio vehicles under the Capability/Channel 172 approach should be similar to that between vehicles in the 2B+2C approach of Phase I.

By comparison, a single-radio vehicle communicates with other vehicles on the CCH during the limited CCH interval. The performance of communication to or from a single-radio vehicle should be similar to that between two vehicles in the default approach.

4.2 Intention/CCH Approach

In this approach the always-on safety channel is the CCH (i.e., the CCH is used by both default vehicles and non-default vehicles). Some BSMs are limited to the CCH interval and some are sent at any time on the CCH. BSMs are not sent on Channel 172. Like the Capability/Channel 172 approach, the Intention/CCH approach uses one new header bit to communicate vehicle type. This bit is referred to as an “intention bit,” because it conveys the sender’s intention to switch away from the CCH during the SCH interval. In this approach the team distinguished between three types of vehicles:

- A single-radio vehicle that intends to switch away from the CCH in the next SCH interval (call this a “switching” vehicle)
- A single-radio vehicle that intends to remain tuned to the CCH in the next SCH interval (call this a “non-switching” vehicle)
- A multi-radio vehicle

This approach is characterized by the following behaviors:

Single-Radio Switching Vehicle:

- A single-radio switching vehicle sends and receives BSMs on the CCH during the CCH interval
- It sets the header bit to indicate it intends to switch away from the CCH during the next SCH interval

Single-radio Non-switching Vehicle:

- A single-radio non-switching vehicle keeps its radio tuned to the CCH throughout the current sync period
- It sets the header bit to indicate it does not intend to switch away from the CCH during the next SCH interval
- If it detects a switching vehicle among its neighbors, it sends its BSM during the CCH interval. Otherwise it chooses any time during the sync period to send its BSM.

Multiple-Radio Vehicle:

- The behavior of the first radio of a multi-radio vehicle is identical to that of a single-radio, non-switching vehicle above
- The second radio can be used as desired, for example, to access a service on an SCH during the SCH interval. It is similar to the second radio in the Phase I Scenario 1D. It has essentially no impact on safety communication.

Performance:

Note that in the Intention/CCH approach the classification of a single-radio vehicle can be dynamic. It may be a switching vehicle in one sync period and a non-switching vehicle in another. This raises a minor timing issue with regard to setting the Intention Bit. For example, if a non-switching vehicle sends a BSM early in a sync period and then receives a service advertisement and decides to leave the CCH to access the service on the next SCH interval, it cannot indicate this change in state until it sends its next BSM in the following sync period. This can lead to additional latency before the single-radio vehicle hears BSMs from some of its neighbors.

From a congestion perspective, the performance of the Intention/CCH approach should be considered for two cases: i) within a neighborhood consisting only of non-switching vehicles, and ii) within a neighborhood with at least one switching vehicle.

Where all vehicles are non-switching, the communication performance is that of an always-on channel. In other words, it is similar to the performance of the 2B+2C approach from the Phase I study, and similar to the performance of the Capability/Channel 172 approach in a neighborhood consisting only of multi-radio vehicles. In the Intention/CCH case, there could be a slight degradation due to the fact that the safety channel is also the CCH, and thus carries control messages in addition to BSMs.

Where there is at least one switching vehicle, all the BSMs are constrained to be sent during the CCH interval. These BSM transmissions are, thus, subject to the higher

channel load associated with that constraint. The communication performance between any pair of vehicles in that neighborhood is affected and will be similar to the performance of the default approach. Note that this is true even between non-switching vehicles. The fact that performance between non-switching vehicles is constrained in the neighborhood of a switching vehicle contrasts with the performance of the Capability/Channel 172 approach in the neighborhood of a single-radio vehicle. In the Capability/Channel 172 case, communication between multi-radio vehicles is not constrained by the CCH interval, and the performance between those vehicles is much better than the default approach. This point of comparison can be interpreted as an advantage for the Capability/Channel 172 approach over the Intention/CCH approach. On the other hand, the Intention/CCH approach has the following advantage over the Capability/Channel 172 approach: all single-radio vehicles create a region of constrained performance in the Capability/Channel 172 approach, whereas only those single-radio vehicles that are currently switching create such a region in the Intention/CCH approach. Thus, an assessment of the Intention/CCH approach requires estimating how frequently a vehicle will switch away from the CCH.

Note that the VSC-A team considers the Capability/Channel 172 approach and the Intention/CCH approach to be mutually exclusive. No attempt has been made to consider interoperation between the two.

5 Summary of Research Results

This research assessed the default approach (Section 2.1) and developed three potential alternatives: the “all safety on Channel 172 approach” (Section 3.4), the Capability/Channel 172 approach (Section 4.1), and the Intention/CCH approach (Section 4.2). The major advantages and disadvantages of each of these four approaches are summarized in Table 2.

Table 2: Summary of Multi-Channel Approaches

Approach	Safety Band(s)	Advantages	Disadvantages
Default	CCH during CCH interval	Single-radio vehicle supports safety and non-safety services	Congestion due to CCH interval capacity limit
All Safety on Channel 172	Channel 172	Always-on safety channel for all BSMs Possible optimization of CCH/SCH interval ratio	Single-radio vehicle cannot support both safety and non-safety

Approach	Safety Band(s)	Advantages	Disadvantages
Capability/ Channel 172	Channel 172, and CCH during CCH interval	Safety and non-safety for single-radio vehicles Multi-radio vehicles have access to always-on safety channel	Requires new header bit Uses 1.5 channels for safety
Intention/CCH	CCH, during both intervals	Safety and non-safety for single-radio vehicles Non-switching vehicles have access to always-on safety channel; only a switching vehicle triggers CCH interval limitation (dynamic)	Requires new header bit Presence of switching vehicle limits performance for all neighbors, even between non-switching vehicles

6 Proposal for the Header Bits in the Next Version of IEEE 1609.3

In the event that the default approach for V2V safety communication is chosen for initial deployment, it is possible that the automotive industry will eventually adopt an alternative to this approach. A vehicle deployed after such a decision could be designed to conform to the new approach. A vehicle deployed before such a decision may or may not be able to conform. The VSC-A team recognized that it would be advisable to “future proof” the standards now, to the extent possible, to maximize the chance that a vehicle deployed prior to an eventual multi-channel decision would be able to conform to it.

The IEEE 1609.3 Standard [1] defines the Wireless Access in Vehicular Environments (WAVE) Short Message (WSM), which is the Network Layer packet in which BSMs will be carried. As reported above, two of the alternative approaches researched require the addition of a new header bit. A logical place to allocate such bits is in the WSM header. The IEEE 1609.3 Standard is currently being revised with an expected publication date in 2010. At the October 2009 IEEE 1609 meeting, the VSC-A team proposed [6] that 2 bits be allocated in the WSM header to allow the sender to advertise its multi-channel capability and intention. This proposal was accepted by the IEEE 1609 WG, subject to editing, for inclusion in the draft 1609.3 Standard. One modification is that instead of using WSM header bits, the requested bits will be placed in a new WSM sub-layer header, which will only appear in a WSM that carries a safety message. The WSM sub layer is defined in IEEE 1609.3 draft.

The capability bit and intention bit concepts were developed with the idea that one or the other, but not both, would be provided in the packet header. But the October 2009

VSC-A proposal covered both cases, and the most efficient way to do that was with a pair of bits that collectively provide the information necessary for either the Capability/Channel 172 approach or the Intention/CCH approach. Neither of these bits can be identified precisely as a capability bit or an intention bit. The specific 2-bit proposal from VSC-A is shown in Table 3.

Table 3: VSC-A Proposal to IEEE 1609 for Header Bits

Bit Values	Meaning
00	Sender requires others' safety messages to be sent on the CCH during the CCH interval.
01	Sender requires others' safety messages to be sent on the CCH, but has no time interval constraint.
10	Sender is capable of receiving others' safety messages on a designated Safety Channel that is distinct from the CCH (in the U.S. this is Channel 172).
11	Sender is not capable of processing received safety messages (all other categories above implicitly assume sender can process safety messages).

Bit Values 00 and 01 provide the information necessary to enable the Intention/CCH approach. Under this approach, the 10 value would not normally be used, and vehicles deployed after a decision to follow this approach would not send value 10. A non-switching vehicle receiving the 10 value would treat the sender as a switching vehicle, and they could exchange BSMs on the CCH during the CCH interval.

Bit Values 00 and 10 provide the information necessary to enable the capability/Channel 172 approach. Under this approach, the 01 value would not normally be used. A multi radio vehicle receiving the 01 value would treat the sender as a single-radio vehicle, and they could exchange BSMs on the CCH during the CCH interval.

Bit Value 11 is useful so that a transmit-only safety device (e.g., an aftermarket device using the BSM to provide limited location and speed information) does not trigger an unnecessary transmission behavior in a more capable vehicle.

7 Conclusion

The VSC-A team assessed the default approach for safety communication under IEEE 1609 and researched alternatives. The research was conducted in two phases. Phase I identified one alternative in which all safety communication is carried out on DSRC Channel 172. Phase II identified two additional alternatives, each of which employ a new header bit and provide a migration path, should it be needed, between deployments that

conform to the default approach and deployments that can take advantage of an always-on safety channel. One of these approaches uses both channel 172, as an always-on safety channel, and the CCH, during the CCH interval. The other approach expands use of the CCH to an always-on mode for vehicles that can keep one radio tuned to that channel. Table 2 summarizes the advantages and disadvantages of the default approach and the three alternative approaches. The VSC-A team worked with the IEEE 1609 WG to define two header bits in the 1609 packet to support the two Phase II alternative approaches.

8 References

- [1] IEEE Vehicular Technology Society, “*IEEE Trial-Use Standard for Wireless Access in Vehicular Environments – Networking Services*,” IEEE Std. P1609.3TM-2007, April 2007.
- [2] IEEE Vehicular Technology Society, “*IEEE Trial-Use Standard for Wireless Access in Vehicular Environments – Multi-channel Operation*,” IEEE Std. P1609.4TM-2006, November 2006.
- [3] SAE InternationalTM, “*SAE J2735 Dedicated Short Range Communications (DSRC) Message Set Dictionary*,” DSRC Committee, November 2009.
- [4] Federal Communications Commission, “*Amendment of the Commission’s Rules Regarding Dedicated Short-Range Communication Services in the 5.850-f.925 GHz band (5.9 GHz band)*,” FCC Memorandum Opinion and Order, FCC 06-110, adopted July 20, 2006, released July 26, 2006, WG Docket no. 01-90.
- [5] Rai, V., Bai, F., Kenney, J., and Laberteaux, K., “*Cross-Channel Interference Test Results: A report from the VSC-A Project*,” IEEE 802.11 11-07-2311-00-000p, July 2007.
- [6] CAMP VSC2 Consortium, “*Proposal to define WSMP bits to support Multi-Channel Operation for Safety*,” IEEE 1609 WG, Oct. 20, 2009.

VSC-A Final Report: Appendix E-1

**Relative Positioning Software Performance
Analysis**

List of Acronyms

CAMP	Crash Avoidance Metrics Partnership
CICAS-V	Cooperative Intersection Collision Avoidance System for Violations
DSRC	Dedicated Short Range Communications
GPS	Global Positioning System
GUI	Graphical User Interface
HV	Host Vehicle
ITS	Intelligent Transportation Systems
LOS	Line-of-Sight
NHTSA	National Highway Traffic Safety Administration
OTA	Over-the-Air
RMS	Root Mean Square
RTK	Real-Time Kinematic
RV	Remote Vehicle
SDH	Sensor Data Handler
SP	Single Point
SW	Software
USDOT	United States Department of Transportation
VSC2	Vehicle Safety Communications 2 (consortium)
VSC-A	Vehicle Safety Communications – Applications
V2I	Vehicle-to-Infrastructure
V2V	Vehicle-to-Vehicle
WAAS	Wide Area Augmentation System
WAVE	Wireless Access in Vehicular Environments
WGS84	World Geodetic System 84
WMH	Wireless Message Handler
WRM	WAVE Radio Module

Table of Contents

List of Acronyms.....	E-1-ii
1 Background and Objectives	E-1-1
1.1 Absolute and Relative Positioning Accuracy	E-1-1
1.2 VSC-A RTK Software-Based Relative Positioning vs. Alternative Methods	E-1-3
1.3 Impact of GPS Outages	E-1-4
2 Test Setup, Scenarios and Objectives	E-1-4
2.1 Test Objectives	E-1-4
2.2 Test Setup	E-1-5
2.3 Collected Data	E-1-5
2.4 Test Scenarios.....	E-1-6
3 Analysis Summary.....	E-1-6
3.1 Analysis Methodology	E-1-6
3.2 Data Decoding and Processing.....	E-1-7
3.3 Generating the Truth Solution.....	E-1-8
4 Results.....	E-1-9
4.1 Scenario 1: Impact of Differences in Satellite Visibility	E-1-9
4.2 Scenario 2: Impact of Positioning Mode on Relative Positioning	E-1-14
4.3 Scenario 3: Impact of Using Other Positioning Mode Combinations.....	E-1-16
4.4 Impact of Short Complete GPS Interruptions	E-1-18
5 Conclusions	E-1-20
6 References	E-1-21

List of Figures

Figure 1: Typical Accuracy Bounds Depending on Positioning Mode	E-1-2
Figure 2: Between Vehicle Distance.....	E-1-3
Figure 3: VSC-A Test Bed – Positioning Components	E-1-4
Figure 4: Vehicle Hardware Setup.....	E-1-5
Figure 5: Global to Local Coordinate Transformation	E-1-7
Figure 6: Post-Mission L1 Forward-Backward Solution Discrepancy.....	E-1-8
Figure 7: SP Relative Positioning Method Dependency on Satellite Visibility	E-1-9
Figure 8: Visibility Difference Analysis Set 1 (WAAS)	E-1-10
Figure 9: Visibility Difference Analysis Set 2 (GPS).....	E-1-11
Figure 10: Visibility Difference Analysis Set 3.....	E-1-12
Figure 11: Visibility Difference Analysis Set 4.....	E-1-13
Figure 12: Visibility Difference Analysis Set 5.....	E-1-13
Figure 13: SP Relative Positioning Method Dependency on Positioning Mode	E-1-14
Figure 14: Positioning Mode Impact Analysis Set 1	E-1-15
Figure 15: Positioning Mode Impact Analysis Set 2	E-1-16
Figure 16: Positioning Mode Impact Analysis Set 3	E-1-17
Figure 17: Positioning Mode Impact Analysis Set 4	E-1-18
Figure 18: Impact of GPS Interruptions on Relative Positioning Set 1	E-1-19
Figure 19: Impact of GPS Interruptions on Relative Positioning Set 2.....	E-1-20

1 Background and Objectives

Relative positioning is a critical system component of the Vehicle Safety Communications – Applications (VSC-A) test bed. Based on preliminary studies, team experience, and industry expert input, the test bed is designed to use Global Positioning System (GPS) Real-Time Kinematic (RTK) positioning for relative positioning of vehicles. The objective of this report was to investigate certain performance characteristics of the VSC-A RTK software (SW). This SW is a commercial, off-the-shelf SW product from a leading GPS system. This report summarizes a series of evaluation tests conducted by the VSC-A team and an analysis of its accuracy and solution availability characteristics. The performance of VSC-A RTK SW is also compared against that of alternative methods of relative positioning.

This section outlines the background information relating to vehicle positioning modes, absolute versus relative positioning accuracy, and basic information about the RTK method. Objectives of this report are discussed in this section.

1.1 Absolute and Relative Positioning Accuracy

Positioning accuracy can be split into two components as absolute accuracy and relative accuracy. Absolute accuracy is expressed with respect to a global frame (typically World Geodetic System 84 (WGS84) when GPS is used) and becomes a critical requirement when the vehicle position needs to be determined with respect to, for instance, individual lanes on a roadway. Achievable absolute accuracy of a positioning system is dependent on the technologies used in positioning. Three vehicle positioning technologies were used in the work given in this report and these are identified as Positioning Modes. For the purpose of this report, the three Vehicle Positioning Modes used were:

1. GPS: Standalone GPS without any augmentation or correction sources
2. WAAS: Wide Area Augmentation System (WAAS) enabled GPS
3. RTK: Positioning conducted using GPS RTK relative to a fixed base (vehicle-to-infrastructure (V2I) case) or a moving vehicle (moving base, vehicle-to-vehicle (V2V) case). Essentially this involves estimating a precise baseline between two entities using raw GPS. More information on this mode can be found in Misra and Enge (2006) [1].

Expected accuracy of these modes differ, and a general comparison is given in Figure 1. Figure 1 shows a vehicle (A) traveling in the left-most lane of a three-lane road, and its actual position is indicated as A_{ACTUAL} . Centered at the actual position of vehicle A are three error ellipses corresponding to typical accuracies achievable with using GPS, WAAS, and RTK Positioning Modes. Using GPS L1 only, typical values for these modes are 5, 2, and better than 1 m correspondingly [1]. Hence, for the scenario shown, the actual position estimate coming out of a GPS receiver could be anywhere within the error ellipse for a given mode. For instance, a receiver in GPS mode could report A_{GPS} as the vehicle location instead of reporting A_{ACTUAL} due to positioning mode dependent errors.

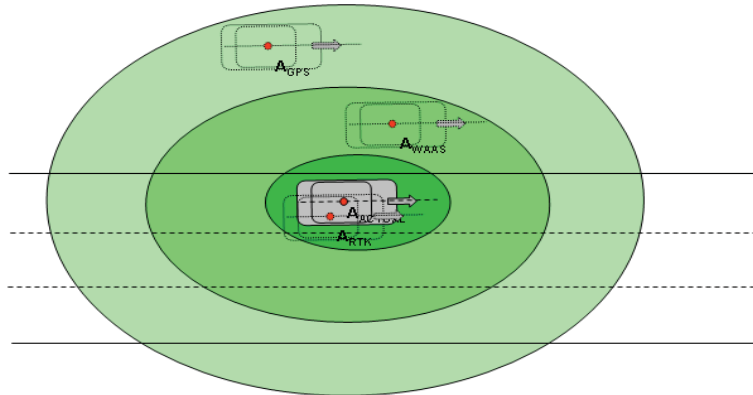


Figure 1: Typical Accuracy Bounds Depending on Positioning Mode

Relative positioning accuracy refers to the accuracy of a relative solution, for instance, the along and across distances between two vehicles. Extending the Figure 1 illustration to two vehicles, if two vehicles are traveling in adjacent lanes as shown in Figure 2, there is a high likelihood of both vehicles experiencing almost the same absolute error given the following assumptions are true:

1. Using the same Positioning Mode (i.e., GPS, WAAS, or RTK)
2. Sky visibility is identical
3. Receiver/antenna characteristics including positioning algorithms are identical

Given that the above are true, both vehicles A and B in Figure 2 most likely will have almost identical 2D absolute errors. The illustration shows errors in excess of 3 m as shown by the error vector between the actual position of vehicle A (A) and the WAAS augmented reported position of it (A_{WAAS}). If individual vehicle GPS receiver reported positions (A_{WAAS} and B_{WAAS}) are used to derive the relative position of one vehicle with respect to the other, the relative errors that are almost negligible due to the fact that common errors cancel each other.

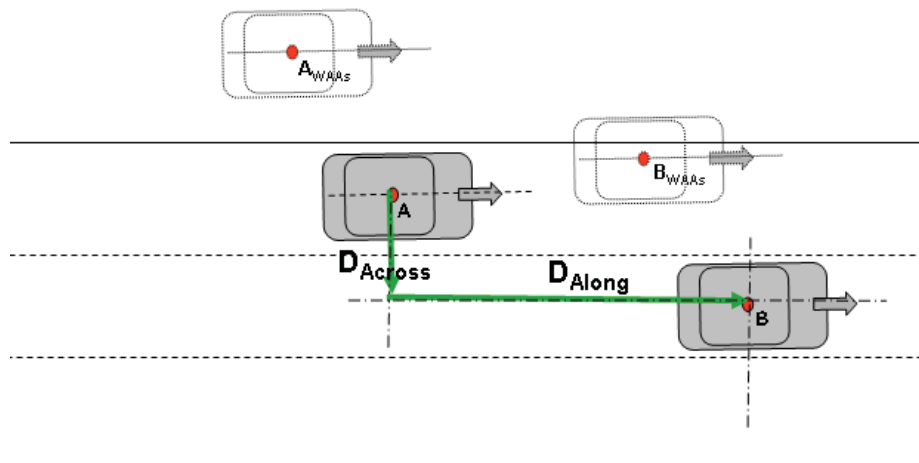


Figure 2: Between Vehicle Distance

It is noted that if the positioning mode of one of the vehicles change, for instance vehicle A changed from WAAS to GPS, the absolute positioning error associated with vehicle A may change as the probable positioning mode dependent error increases. Thus a relative position derived using reported position A may abruptly change as indicated later in the analysis.

It is important to note that in the RTK method, the GPS raw measurements are the key variables shared between vehicles and that these do not change due to positioning modes of individual vehicles. The errors/biases in GPS raw measurements made by vehicles in a particular region (i.e., typically within a radius of several tens of km under normal ionospheric activity) are almost identical and, therefore, are nearly eliminated in relative positioning. It is noted that in RTK mode, the accuracy concept should be applied in the relative sense only. For instance, the RTK method error becomes an error in a vector, whereas it is a function of accuracies of two receivers if the relative positioning is done using the positions reported by them.

The primary objective of the tests given in this report is to investigate the relative positioning accuracy of the VSC-A system. The emphasis was to verify that the system performance meets the VSC-A specification of *Which Lane* or better relative positioning accuracy and is *Which Road* level absolute positioning accuracy. It is noted that the tests described in this report specifically looked for situations where assumptions given in this section are violated in normal day-to-day driving.

1.2 VSC-A RTK Software-Based Relative Positioning vs. Alternative Methods

The VSC-A system design provides Over-the-Air (OTA) data for implementing two basic relative positioning approaches. These two approaches are evaluated as alternatives in this report.

Firstly, since vehicle position and other kinematic information with respect to a global frame is shared using OTA messaging (i.e., latitude, longitude, and heading), straightforward latitude longitude differencing can be used to determine the relative position of a vehicle with respect to any other. This method is identified as the Single Point (SP) method of relative positioning in the rest of the report.

The second approach involves using the well-established GPS RTK techniques using the VSC-A RTK SW. This method is identified as the RTK or VSC-A RTK SW method of relative positioning in the rest of the report. More information on RTK can be found in [1].

1.3 Impact of GPS Outages

GPS is a line-of-sight (LOS) system and, therefore, sky visibility obstructions can deteriorate the performance of GPS. In extreme cases, reduced signal availability may totally disable the functionality of a GPS device. More information on performance characteristics of GPS can be found in [1] and other literature.

The analysis presented in this report particularly looks at the availability of the VSC-A RTK SW solution and its accuracy in short GPS outages (i.e., under a few seconds). Also investigated is the time taken for VSC-A RTK SW to start generating solutions after a short complete GPS outage. It is noted that the current implementation of VSC-A relative positioning system is designed specifically for open sky operation and that VSC-A future enhancements are expected to add-in the no-GPS positioning capability in latter stages of the project.

2 Test Setup, Scenarios and Objectives

2.1 Test Objectives

The objective of these tests was to confirm that the VSC-A relative positioning method and the selected SW is capable of providing *Which Lane* level relative positioning capability under operating conditions defined for the VSC-A implementations. Only the positioning system components were used for these tests as shown in Figure 3.

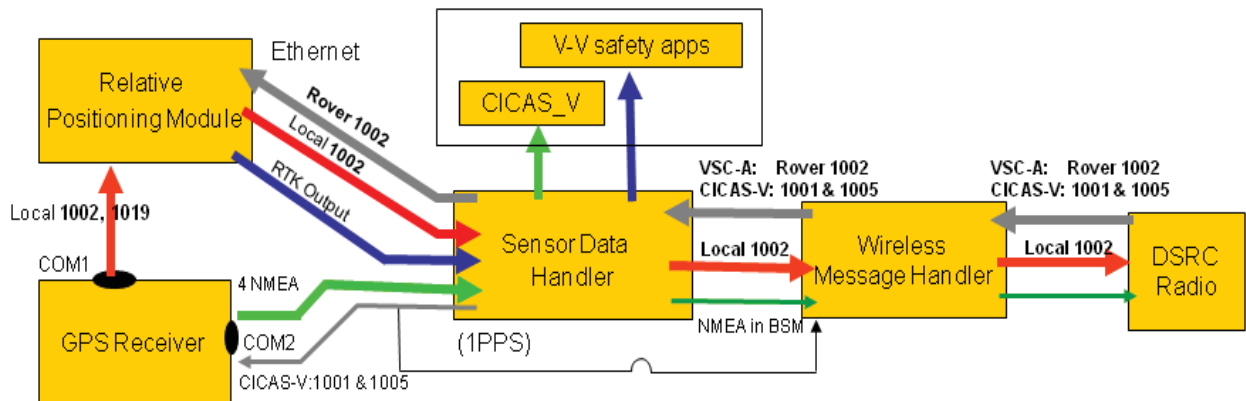


Figure 3: VSC-A Test Bed – Positioning Components

This report investigates the following characteristics of relative positioning in detail:

1. Achievable relative positioning accuracy using VSC-A RTK SW
2. Assessment of accuracy benefits compared to the alternative method
3. Relative position solution availability with GPS outages

2.2 Test Setup

The test setup was a scaled down version of the full VSC-A test bed as shown in Figure 3. No applications were run in the test setup. Instead, the relative positioning system output was logged and post-mission analysis was conducted. Functions of the VSC-A test bed components Dedicated Short Range Communications (DSRC) Radio, Wireless Message Handler (WMH), and Sensor Data Handler (SDH) were handled using a Wireless Access in Vehicular Environments (WAVE) Radio Module (WRM) and a PC in the test setup. The Relative Positioning Module (VSC-A RTK SW or its non-Graphical User Interface (GUI) version) and the GPS receiver (NovAtel[®] OEMV[®]-1) in the test setup were identical to that of the full VSC-A implementation. The generic test setup with the Cooperative Intersection Collision Avoidance System for Violations (CICAS-V) system as an add-on is shown in Figure 4.

All tests included two or more vehicles with the same basic setup that included an OEMV-1 GPS receiver, test PC, and the WRM. A single vehicle with CICAS-V capability was included in the tests, and this vehicle was configured such that a CICAS-V-enabled GPS receiver is used in the test setup. Several vehicles were equipped with alternative GPS receivers, and these were used only in data logging mode. Standard data logging tools that come with these receivers were used for logging, and analysis was conducted only in the post-mission mode.

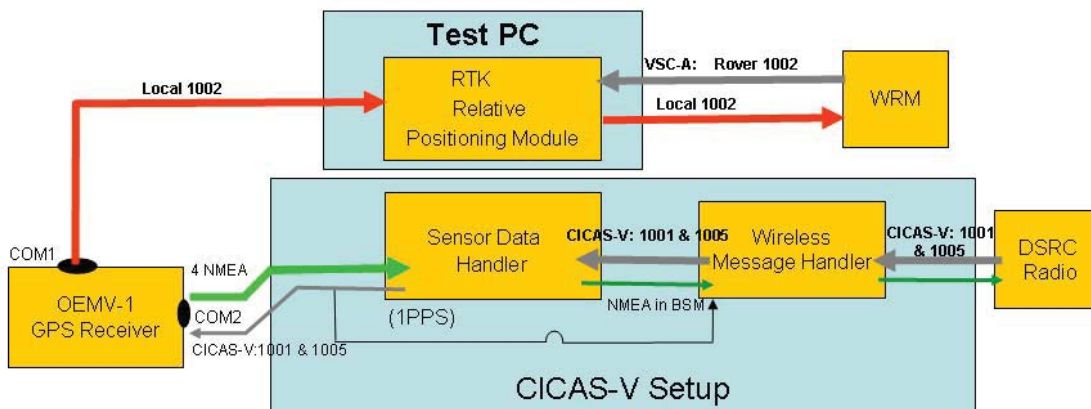


Figure 4: Vehicle Hardware Setup

2.3 Collected Data

The following data was collected from each vehicle:

- VSC-A RTK SW real-time relative position solutions for each vehicle
- Raw GPS data from host vehicle (HV) (RTCMV3.0 and device-specific binary)
- Raw GPS data as received from other vehicles (RTCMV3.0)
- HV position, speed, and heading (device-specific binary)

2.4 Test Scenarios

Test scenarios were designed such that a range of vehicle operating conditions and GPS visibility conditions were covered. The following variables were used to define the scenarios:

- Sky visibility: Open sky, short complete interruptions (i.e., overpasses), and tree cover
- Vehicle speed: slow speed (< 40 mph) and high speed (> 55 mph)
- Roadway: freeway and urban streets
- Local GPS measurement noise: mainly addressed by looking at high and low density traffic

3 Analysis Summary

The analysis is primarily focused on assessing the relative positioning accuracy benefits of the VSC-A relative positioning SW. The SP method and RTK method of relative positioning are compared in the analysis. The impact of short GPS outages on the RTK solution is also investigated.

3.1 Analysis Methodology

Between-vehicle across distance (D_{Across}) was used as the primary analysis variable. The selection was based on the fact that this is one of the most critical relative distance measures for VSC-A SW applications. The ease of measuring this variable for validation was also a factor in the analysis variable selection. The following two methods were used to validate D_{Across} in the tests.

1. Using a post-mission truth solution generated using raw GPS data gathered during the tests. A post-mission precise positioning version of VSC-A RTK SW was used to generate the truth solution as discussed below.
2. The tests were designed and executed such that the D_{Across} measure is always a multiple of lane width except for turns and situations where it is unsafe to do so. For instance, vehicles were always driven in the same lane or adjacent lane formations such that D_{Across} is either approximately zero or approximately a single lane width.

3.2 Data Decoding and Processing

For each scenario analysis, a vehicle was picked as the HV and the others were considered remote vehicles (RVs). Analysis is always done using a local coordinate frame, and the HV position is considered the origin of the local coordinate frame. It is noted that any given vehicle in a test can be considered the host and the others as remotes. The data decoding and processing involved the following steps:

1. Decode RTK output records from Host logs
2. Decode HV heading information
3. Time match (1) and (2) and estimate D_{Across} and D_{Along} using the coordinate transformation shown in Figure 5. It is noted that regardless of the relative positioning method used, GPS-based relative observations will always generate D_{East} and D_{North} with respect to the global coordinate frame. The same coordinate transformation routine will be implemented in the SDH in the full VSC-A implementation.
4. Decode vehicle position records (Latitude and Longitude) from Host and Remote logs
5. Derive D_{East} and D_{North} by first time matching host and remote position record (4) and then converting remote position into local coordinates with respect to the host position at the same time epoch. Note that these coordinate transformation functions are also identical to that implemented in the full VSC-A implementation.
6. Generate reference D_{Across} and D_{Along} using values using post-mission RTK SW
7. Plot D_{Across} and D_{Along} generated using RTK method (3) and SP method (5) along with reference data from (6), if generated

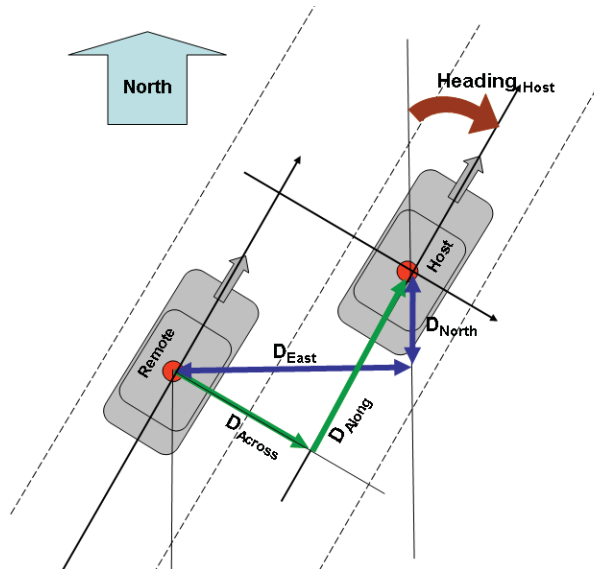


Figure 5: Global to Local Coordinate Transformation

3.3 Generating the Truth Solution

Two methods were used to validate the real-time between vehicle distances generated by the RTK and the same values estimated by the SP method discussed below:

1. Formation of vehicles during the test scenarios: Vehicles were driven in the same lane and in adjacent lanes during all possible times. Lane changes were kept to sharp changes that are short rather than a slow deviation from a lane to the next. Hence, the across distances between vehicles are expected to be either close to zero (same lane) or a multiple of a lane width (adjacent lane) for most of the test durations.
2. Post-mission truth trajectory using post-processing SW: Raw GPS data gathered from all test vehicles were individually post-processed using a SW tool to generate a reference vehicle trajectory solution D_{Across} and D_{Along} .

It is noted that reference solutions for the majority of tests were generated using only L1 GPS. This method does not guarantee a cm-level solution due to the convergence time required for such a solution to converge to cm-level. The accuracy of the reference solution can be indirectly estimated by using the forward-backward solution comparison method in the post-processing tool. In general, forward and backward L1 reference vehicle position solutions were found to agree within 0.4 m whereas the corresponding L1L2 solutions agree within a few cm. An example of the forward-backward solution discrepancy plot is shown in Figure 6. For these tests, only L1 reference solutions were available and may not be presented in the analysis.

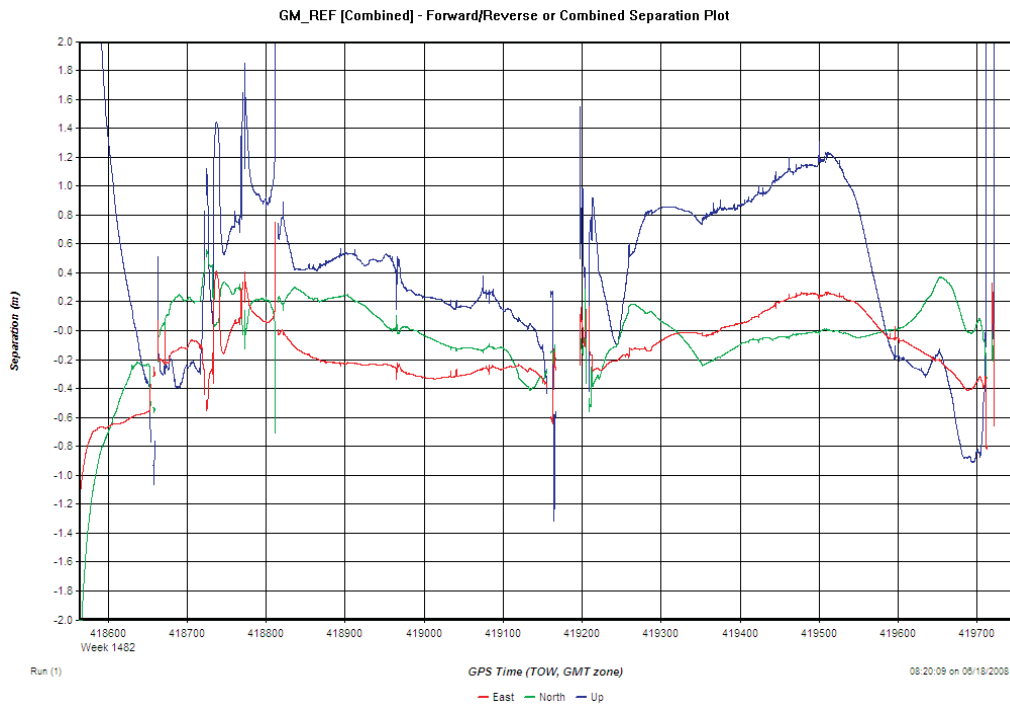


Figure 6: Post-Mission L1 Forward-Backward Solution Discrepancy

4 Results

An analysis summary is presented below under several scenarios.

4.1 Scenario 1: Impact of Differences in Satellite Visibility

This scenario looks at the impact of sky visibility differences between V2V (i.e., one vehicle using a GPS satellite or more that is not available to the other) and its impact on relative positioning using SP and RTK methods. As observed during these field tests, such difference may occur often depending on the sky visibility obstructions around the vehicles. A typical example is a situation where a vehicle is driven next to (i.e., adjacent lane) a semi-like vehicle that obstructs a part of the sky view of the vehicle and other vehicles in the same area may not have such obstructions.

An illustration of how this impacts the SP method is given in Figure 7. At time = 0, vehicles A and B are in adjacent lanes and both are operating in WAAS positioning mode. Given that certain conditions discussed in background are true, vehicle receivers output their locations as A_{WAAS} and B_{WAAS} . As shown in Figure 7, the reported positions (i.e., A_{WAAS} and B_{WAAS}) are offset by a common error vector from the actual positions of the vehicles A and B. However, at time = 5 sec, vehicle B may see additional GPS satellites that are not seen by vehicle A, and its error vector may change. This could result in a change of reported vehicle position B_{WAAS} . This error vector change is a function of many variables including quality of the additional/lost satellite(s) measurement(s) and the way each receiver translates the GPS measurements into position solutions. From a VSC-A point of view, if the SP method is used to estimate D_{ACROSS} in this sequence of events, D_{ACROSS} could potentially change from a single lane width to more than (as depicted in Figure 7) or less than a lane width with no actual vehicle orientation change.

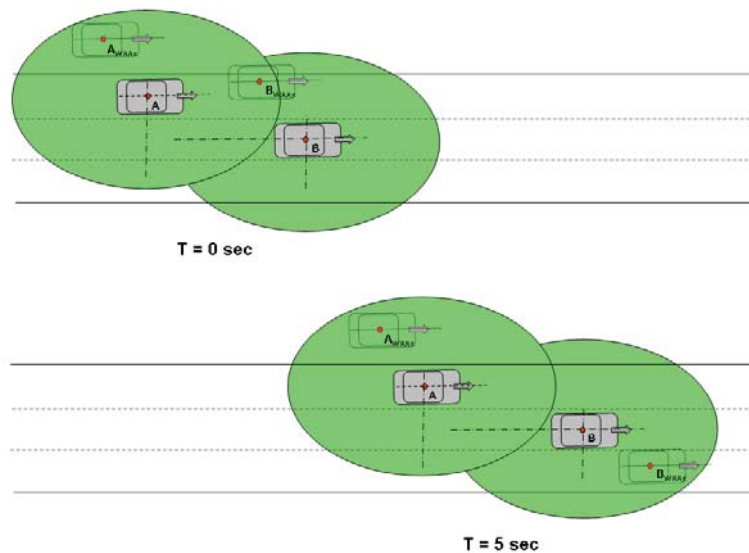


Figure 7: SP Relative Positioning Method Dependency on Satellite Visibility

It is noted that the sky visibility changes only affects the number of observations available to a given vehicle. If a certain subset of satellites is seen by both vehicles in

consideration, measurements from those satellites are not affected by the local obstruction. Therefore, this scenario is not expected to impact a relative positioning method that uses actual GPS measurements such as the RTK method. More information on the technical basis for this hypothesis can be found in the Background section (section 1) of this report and the references.

In order to verify the above hypothesis, D_{Across} estimated using SP method and RTK method of relative positioning was compared in situations in which GPS satellite count seen from each test vehicle were different. Figure 8 to Figure 12 show segments of data highlighting such time intervals. A description of the vehicle orientation and other parameters are given with each figure.

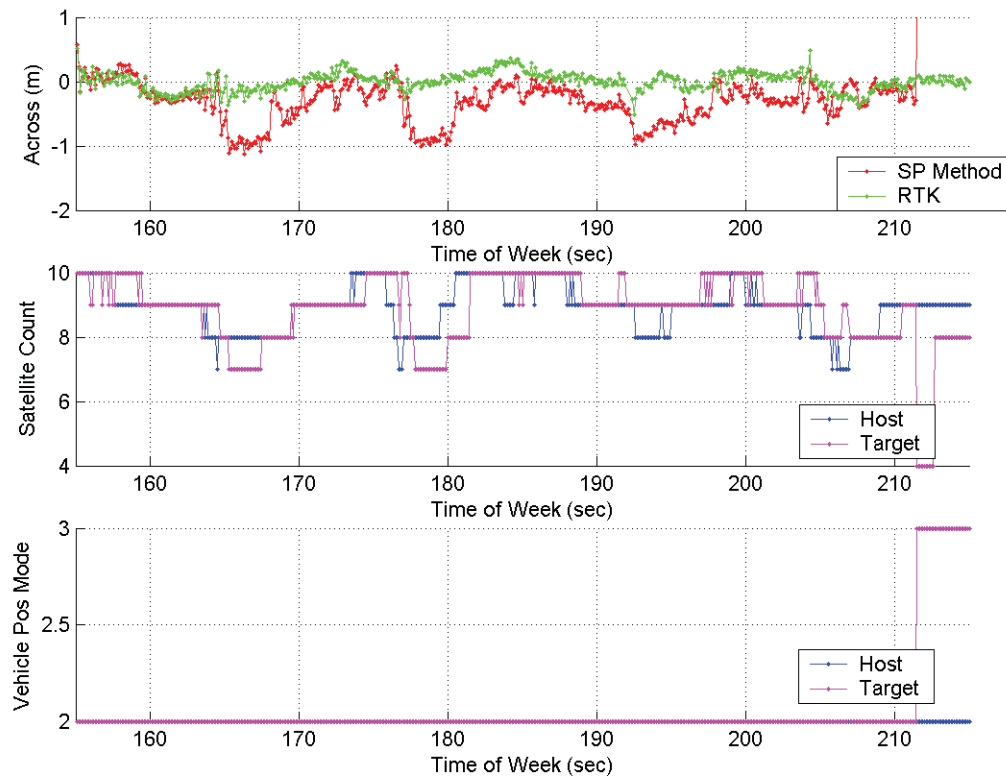


Figure 8: Visibility Difference Analysis Set 1 (WAAS)

Figure 8 shows a 60-second time window in which the host and the target (i.e., remote) vehicles were driven in the same lane on a straight-road segment. D_{Across} observed using RTK and WAAS methods is shown in the top plot of Figure 8. The plot in the middle shows the total number of satellites seen by each vehicle. The bottom plot shows the positioning modes of individual vehicles which indicates mode 2 (WAAS) for both vehicles for the majority of the duration shown.

As expected, the D_{Across} estimated by the RTK method shows values around zero for the whole duration, and the maximum deviation was found to be within ± 0.5 m from 0 m, the best estimate of the reference D_{Across} for the same lane formation. However, for the SP method based estimate, clear deviations of up to 1 m are seen. These deviations are directly related to the differences in total number of satellites seen by vehicles. For

instance, the deviation around 180 seconds is highly correlated with the target vehicle satellite count dropping one below that of the host. However, it is noted that every satellite count differences does not necessary result in a bias in SP method D_{Across} estimate as indicated by data shown around time 158 seconds and 210 seconds. The target vehicle positioning mode changes after 210 seconds to the run, and the impact of this is discussed in a later scenario. Importantly, D_{Across} observed by the RTK method remains unchanged throughout the whole time interval, including after the target vehicle positioning mode change.

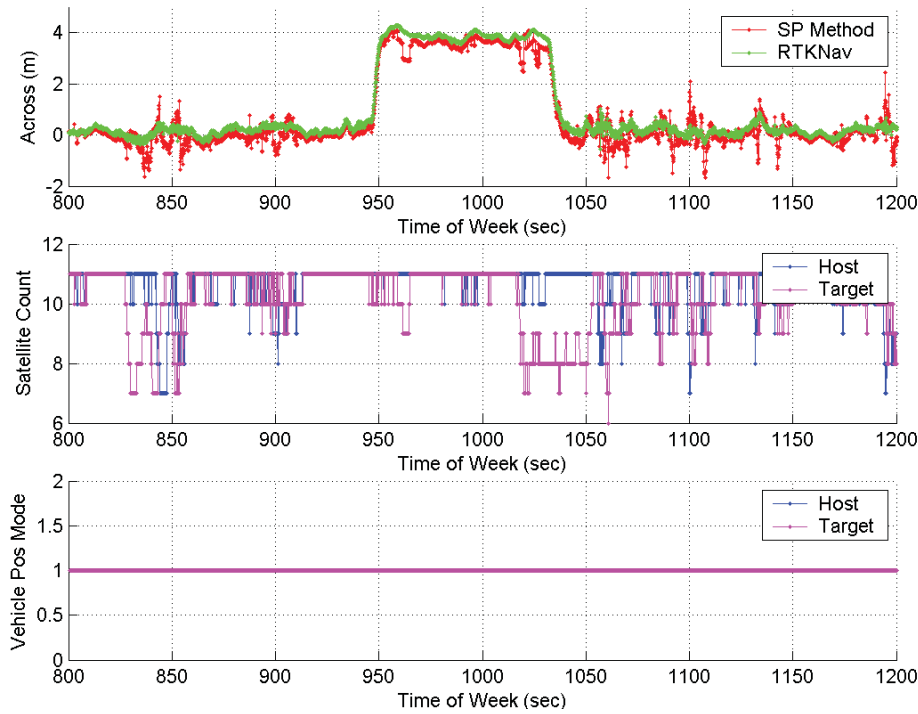


Figure 9: Visibility Difference Analysis Set 2 (GPS)

Figure 9 shows a dataset in which one of the vehicles changed lanes and came back to the original lane during the time period shown. As seen in the top plot, both the target and the HV remained in the same lane until time 950 seconds based on the near zero D_{Across} . The target vehicle subsequently changed lanes to the adjacent lane, as indicated by a D_{Across} close to a single lane width. After around 70 seconds, the target vehicle comes back to the same lane formation with the HV.

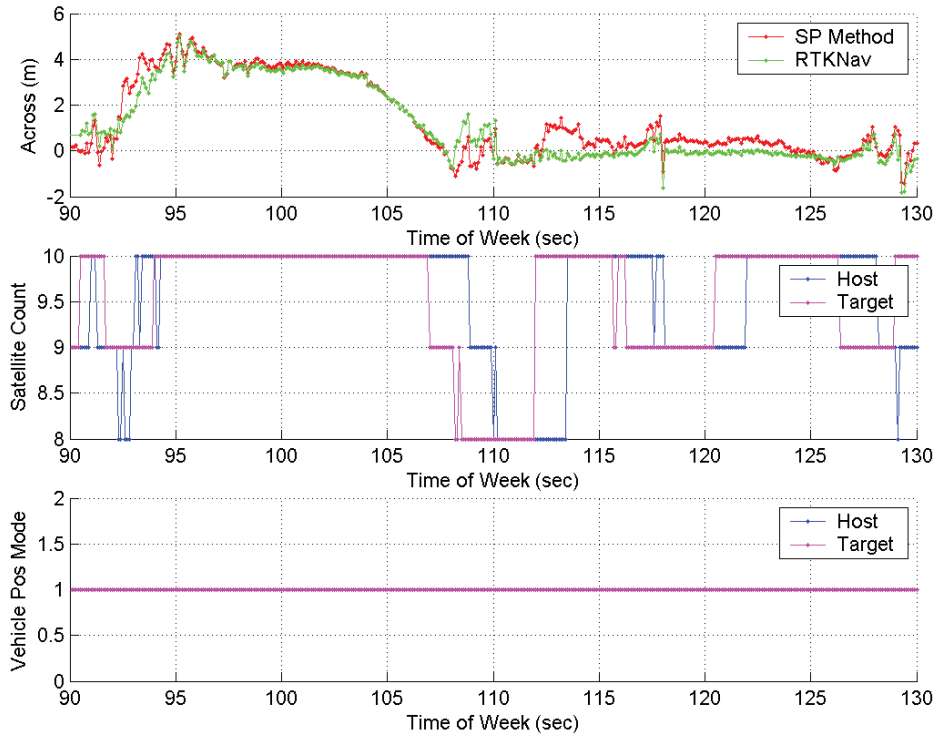


Figure 10: Visibility Difference Analysis Set 3

Figure 10 shows the time duration where the target vehicle performs a lane change maneuver similar to the one in Figure 9. Errors in excess of 1 m are seen when using the SP mode of relative positioning. Around 112 seconds, a deviation in SP D_{Across} is observed due to the HV seeing two satellites less than the target vehicle. However, it is noted that the visibility difference around 120 seconds, where the HV once again sees two satellites less than the target vehicle, does not introduce any significant changes to the SP method D_{Across} .

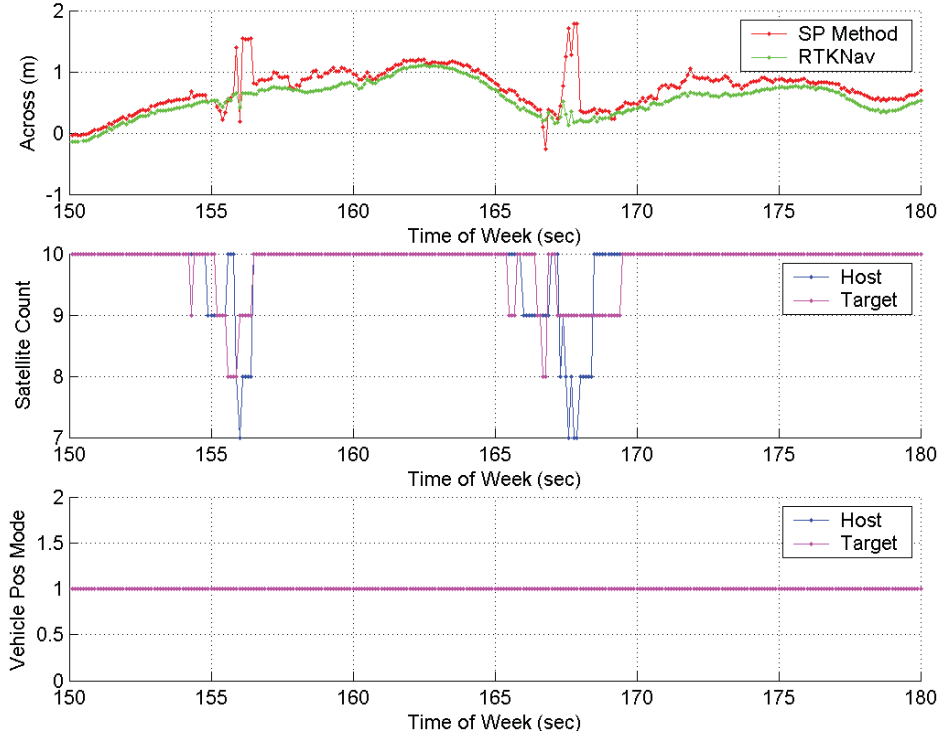


Figure 11: Visibility Difference Analysis Set 4

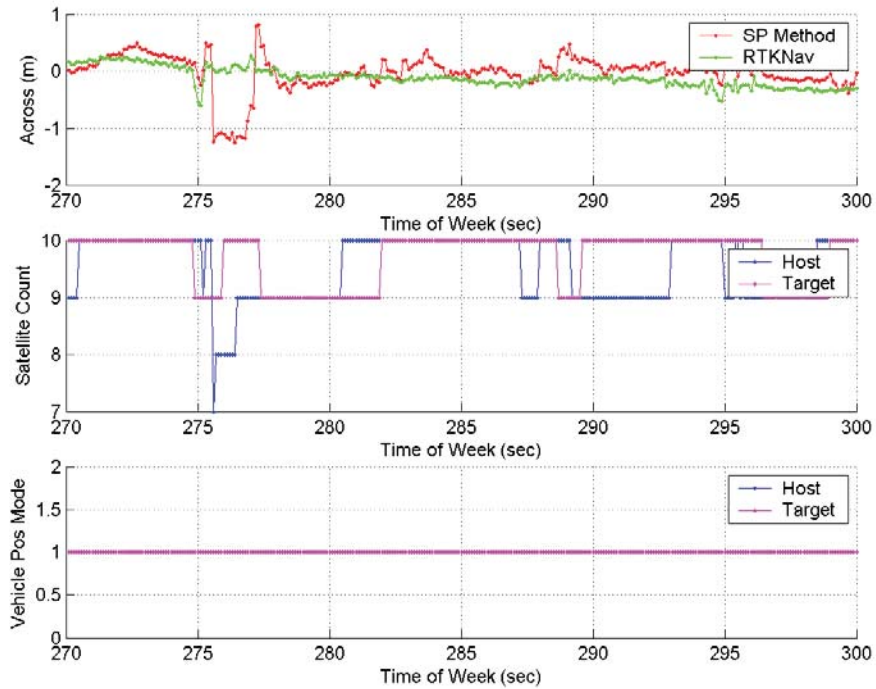


Figure 12: Visibility Difference Analysis Set 5

Figure 11 and Figure 12 also show two other data segments in which the SP method reported D_{Across} becomes erroneous due to satellite visibility changes.

4.2 Scenario 2: Impact of Positioning Mode on Relative Positioning

As outlined in the Background section, error characteristics of different positioning modes are significantly different. These differences cause problems when receivers change modes or vehicles operating in different modes use SP method for relative positioning. The root of these issues is the variations of vehicle position reported by receivers when positioning modes switch. In the case of vehicles operating in difference modes, positioning mode dependent errors may not cancel out in the SP mode. This scenario investigates the impact of vehicle positioning mode on the relative positioning when using RTK and SP methods.

This scenario is considered especially important for the deployment of VSC-A and CICAS-V-like applications as positioning mode changes are inevitable under these conditions. For instance as illustrated in Figure 13, a CICAS-V enabled vehicle is most likely to operate in WAAS mode when local RTK data is not available from a CICAS-V intersection. As the vehicle enters a CICAS-V coverage area (i.e., at $t = 5$ seconds in Figure 13), the vehicle positioning mode will change from WAAS to RTK and this in turn tightens the absolute accuracy of the vehicle position. As a result, the reported vehicle position may have an instantaneous change that could be as high as 2 m (i.e., WAAS has a root mean square (RMS) accuracy bound of ~ 2 m, and RTK typically has an accuracy bound better than 0.5 m). If multiple vehicles are considered that are traveling very close to each other, such mode transition may not take place at the same time. In Figure 13 illustration, only vehicle B has switched to the RTK mode and vehicle A remains in WAAS mode at $t = 5$ seconds. Hence, using the SP mode of relative position under these conditions is expected to create relative positioning issues. It is noted however that RTK method is not vulnerable to this mode of failure as GPS measurements used in RTK method are vehicle position mode independent.

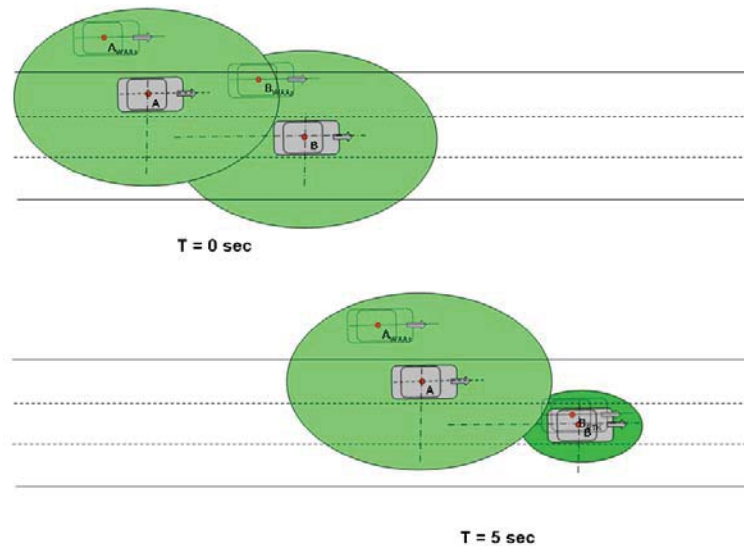


Figure 13: SP Relative Positioning Method Dependency on Positioning Mode

Figure 14 shows a segment of data from a driving scenario where the host and the target vehicles were in the same lane and were driving toward a CICAS-V intersection in a straight road. Both vehicles were configured to operate using WAAS and only one of them was configured to work with CICAS-V data (RTK mode) when available. From time 715 seconds onward, the vehicles were stopped for a traffic light in the same lane.

The target vehicle switched to RTK mode around 650 seconds as shown in the bottom plot of Figure 14. It is noted that the number of satellites used in the target vehicle drops to 5 at the same time as shown in the middle plot of Figure 14. This is a characteristic of the RTK engine which starts precise positioning by using the best 4 satellites and later adds additional satellites to the solution. Although not presented in this report, the absolute position accuracy of the target vehicle increases to better than 0.5 meters after the mode switch to RTK whereas that of the host remains the same.

The top plot shows the D_{Across} estimated by the SP and RTK modes, and the mode switch introduces a bias of ~ 1 meter due to the mode transition. It is noted that this is solely due to the error in Host vehicle position that is in WAAS mode. As expected, the RTK D_{Across} remains within ± 0.5 meters of the expected D_{Across} of 0 meters as the vehicles are in the same lane formation.

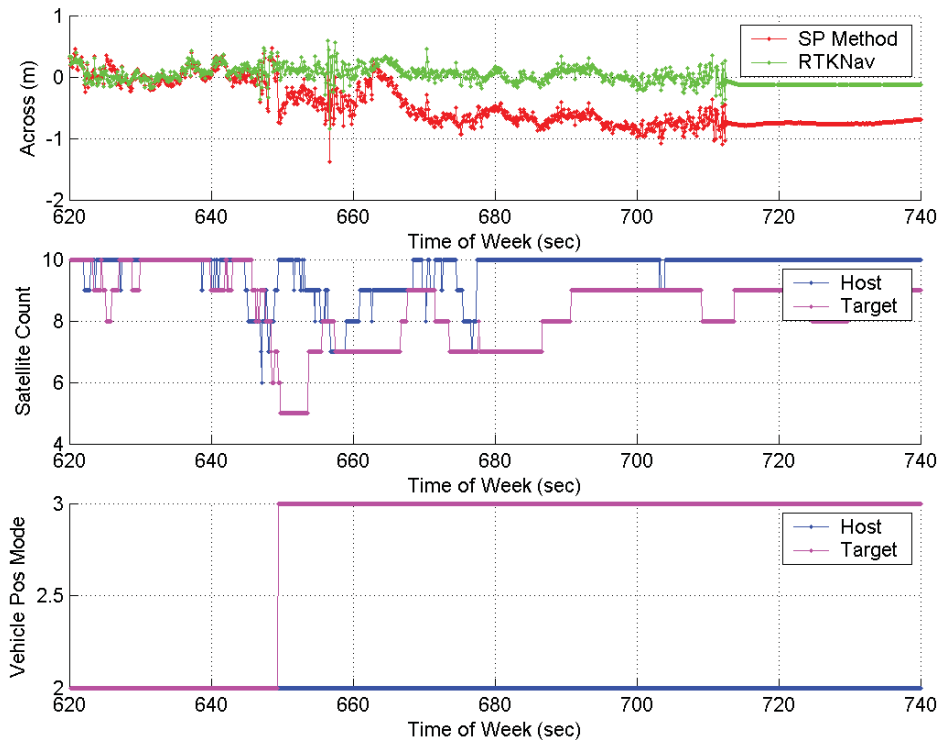


Figure 14: Positioning Mode Impact Analysis Set 1

Figure 15 shows a driving scenario where the host and target vehicles were driven in the same lane while driving through a CICAS-V intersection coverage area. The vehicles perform three lane changes at 1525, 1560, and 1580 seconds. Each of these lane changes was performed such that the target vehicle changes to the adjacent lane first followed by the host performing the same lane change. The vehicles were in the same lane formation

outside of the three lane changing maneuvers. As shown in the bottom plot of Figure 15, the target vehicle enters RTK mode around 1500 seconds and leaves the CICAS-V coverage area around 1585 seconds, thus transitioning back to WAAS mode.

As seen in the top plot of Figure 15, the HV RTK D_{Across} estimate correctly reflects the orientation of the target vehicle which shows D_{Across} values of the order of a lane width when the lane changes take place and close to 0 values when the vehicles are in the same lane formation. However, the SP method shows a D_{Across} error of approximately 2 meters for the whole duration the target vehicle is in RTK mode. As pointed out in the preceding discussion, this happens due to the presence of ~ 2 meters of absolute positioning error in the HV position as it operates in WAAS mode. This error is corrected by the RTK processing using the local data in the target vehicle. When both vehicles are in WAAS mode, this absolute error is almost removed in relative processing as they are similar in both vehicle positions. It is noted, however, that in WAAS mode, both vehicles are ~ 2 meters off from the true location of the vehicle which is not acceptable for CICAS-V operations.

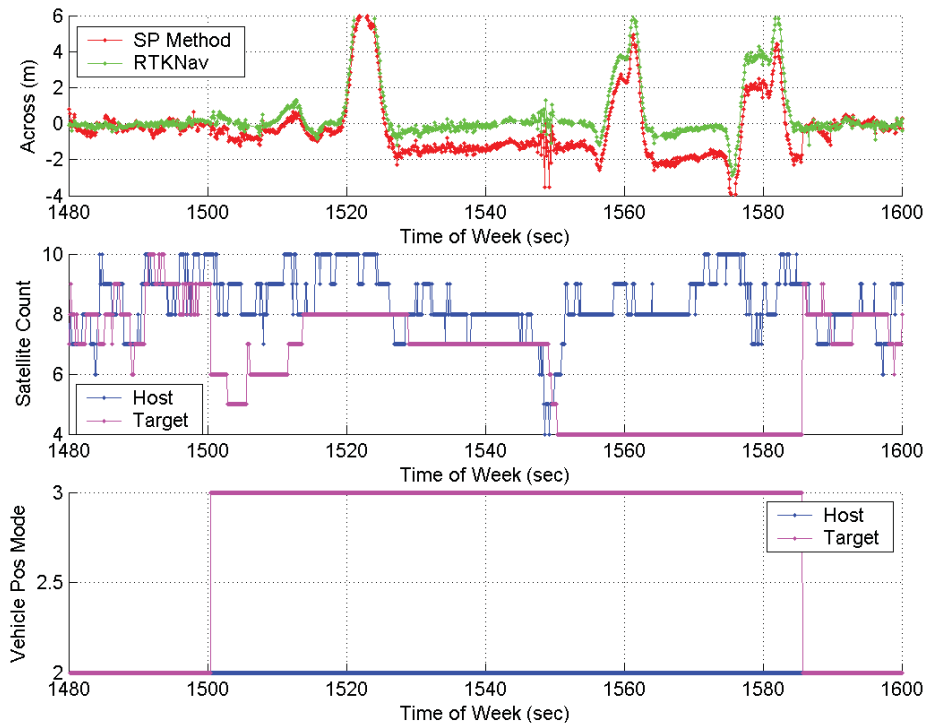


Figure 15: Positioning Mode Impact Analysis Set 2

4.3 Scenario 3: Impact of Using Other Positioning Mode Combinations

This section illustrates the impact of vehicles using positioning mode combinations other than WAAS/RTK on relative positioning. One of the vehicles in these tests was set to operate in standalone GPS mode at all times. Although VSC-A/CICAS-V systems are likely to operate in WAAS mode by default, there could be many instances where some

vehicles could operate in GPS mode due to unavailability of WAAS data (for instance, due to local visibility restrictions).

Figure 16 illustrates a driving scenario in which the target vehicle starts in the same lane as the host, performs a lane change around 230 seconds, drives in adjacent lane for around 20 seconds before changing back to the same lane formation around 250 seconds into the run. As shown in the top plot of Figure 16, the RTK D_{Across} estimate reflects these changes as expected and within the ± 0.5 meter error bound of reference D_{Across} for same lane and adjacent lane formations. However, the D_{Across} estimate from the SP method shows an error of 2 meters around 260 seconds that remains for the rest of the time duration shown. It is noted that the vehicles were brought to a stop in a same lane formation at the end of the run (i.e., after 280 seconds). In addition, the SP method D_{Across} shows errors in the order of 1 meter due to satellite visibility differences around 215 and 225 seconds prior to the transition of target vehicle to RTK mode.

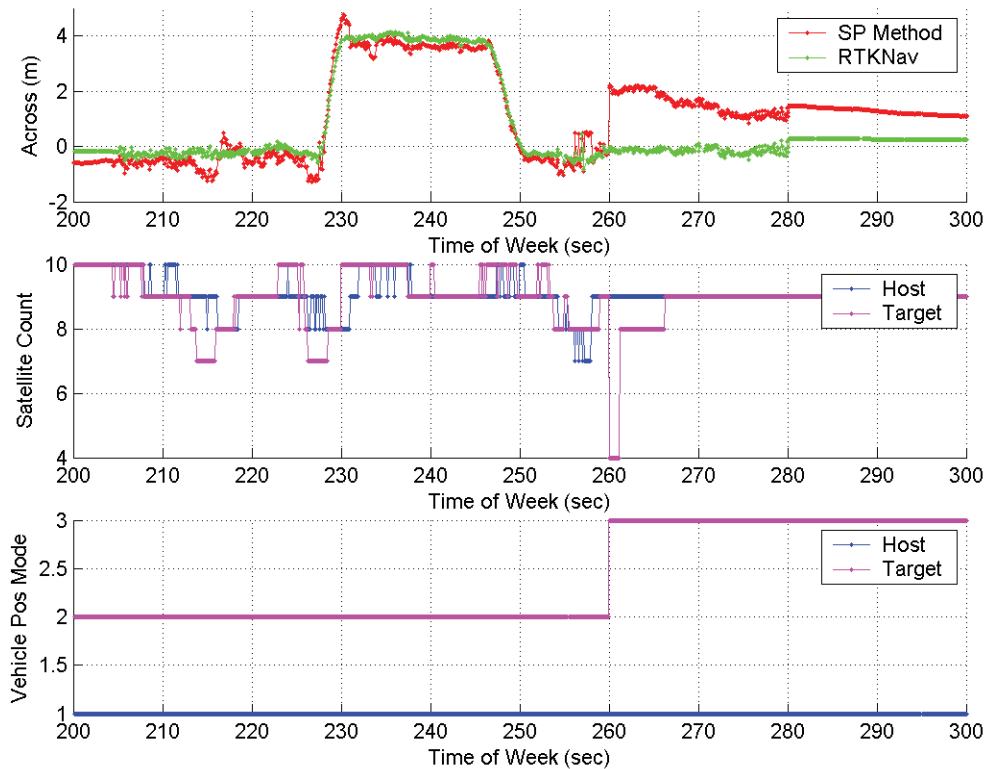


Figure 16: Positioning Mode Impact Analysis Set 3

Figure 17 illustrates a similar scenario to that shown in Figure 16 with two lane change maneuvers by the target vehicle and an instance where the satellite availability in both the target and host drops to 5 or less (i.e., at 1600 seconds). It is noted that the SP mode D_{Across} error in this case vary from almost zero to more than 2 meters when the target vehicle is in the RTK mode. Also the satellite visibility differences compound the SP mode D_{Across} estimate error, causing it to reach errors as high as ~5 meters at around 1600 seconds.

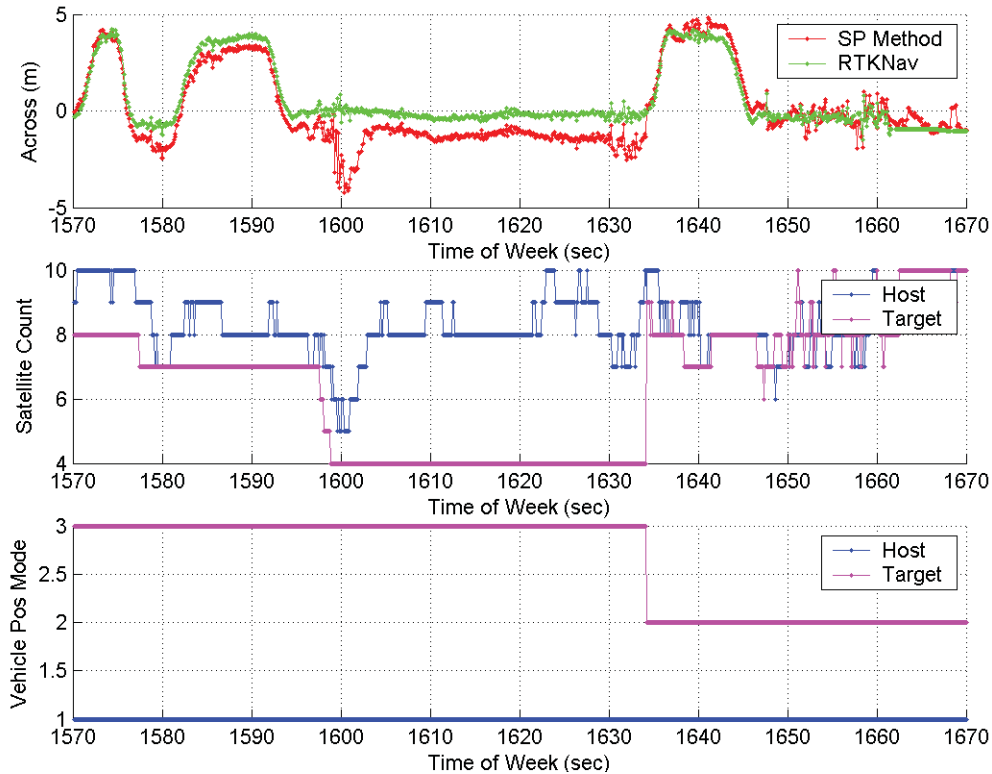


Figure 17: Positioning Mode Impact Analysis Set 4

4.4 Impact of Short Complete GPS Interruptions

The current implementation of the VSC-A test bed is designed for open-sky GPS conditions. However, this implementation is expected to perform under conditions that are commonly encountered but are not necessarily open sky. An example would be a situation where an overpass obstructs the view of the sky for a short duration on a freeway that is otherwise mostly open sky. Under these conditions, the VSC-A positioning system is expected not to provide misleading information to applications. Also the relative positioning system is expected to recover within a certain amount of time after normal GPS reception becomes available. This section shows some data excerpts that illustrate the behavior of the RTK and SP relative position solutions under short but complete GPS outages.

Figure 18 shows a data plot for a 30 second time duration within which the test vehicles were driven under two overpasses. As seen in the plot in the middle, two complete outages (i.e., satellite count dropping to zero) of approximately 3 seconds each were experienced by both vehicles. It is also noted that both vehicles were operating in GPS mode as shown by Vehicle Pos Mode 1 in the bottom plot. The VSC-A RTK SW stops outputting data as soon as common satellite visibility drops below 4. More importantly, VSC-A RTK SW starts outputting accurate estimates with 4-5 seconds of seeing more than 4 common satellites after the outage. This was considered typical under such conditions.

Since the GPS receivers continue to produce predicted vehicle position data during the outage, the SP method continues to generate estimates during the outage. As seen in the top plot of Figure 18, these estimates can be erroneous and highly unreliable. However, in contrast to the VSC-A RTK method, the SP method starts outputting position estimates near immediately within seeing 4 or more satellites.

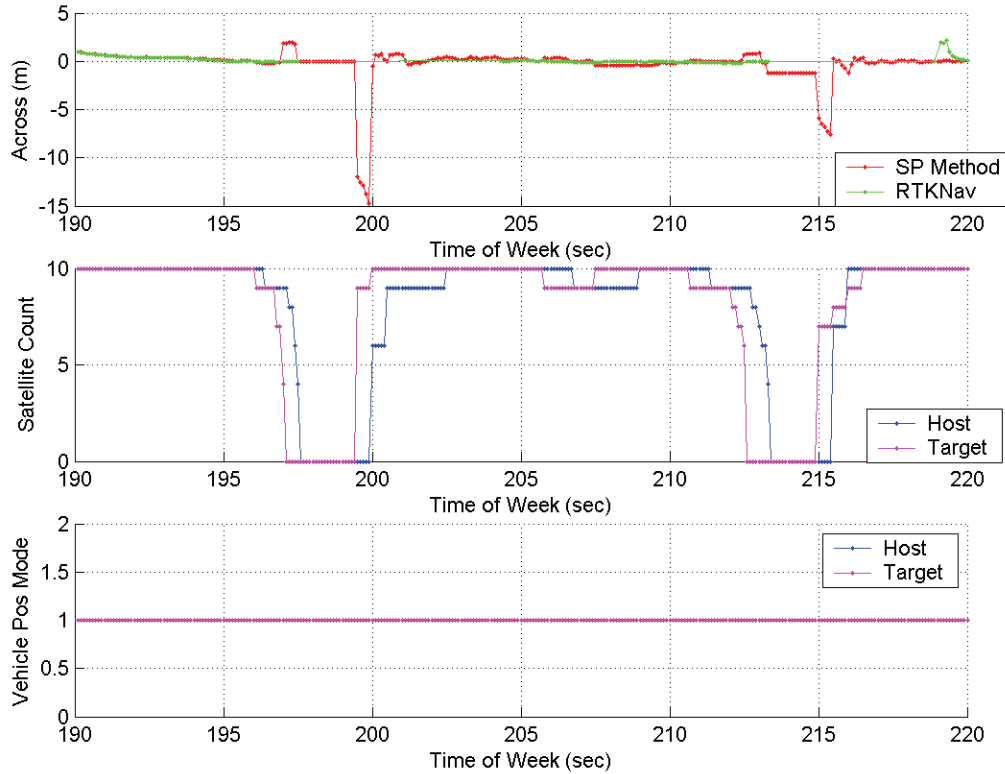


Figure 18: Impact of GPS Interruptions on Relative Positioning Set 1

Figure 19 shows another data duration that shows similar SP and VSC-A RTK SW relative positioning performance during and after GPS outages. The VSC-A RTK SW stops sending estimates as soon as the common satellite count drops below 4, and it resumes reliable output within 5 seconds of getting measurements from 4 or more satellites. Whereas the SP method continues providing a solution during the outage which should be considered unreliable, however, starts providing a solution near immediately after getting measurements from 4 or more satellites.

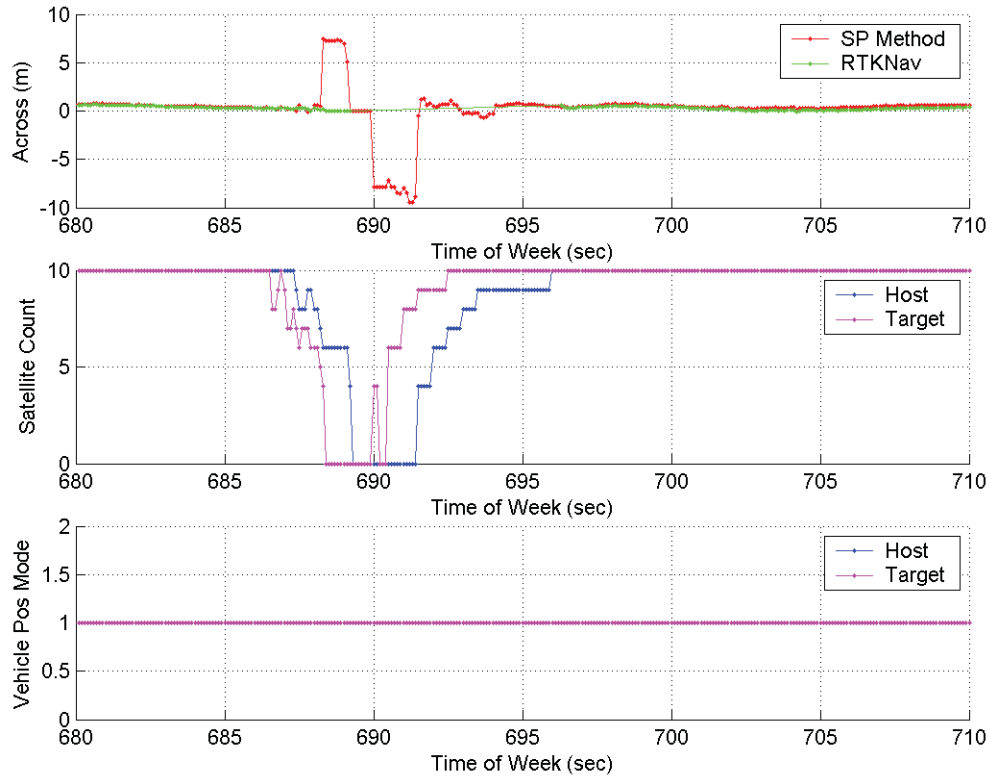


Figure 19: Impact of GPS Interruptions on Relative Positioning Set 2

5 Conclusions

Please refer to the main body of the final report for the positioning conclusions and recommendations.

6 References

- [1] Misra, P. and Enge, P., “*Global Positioning System: Signals, Measurements, and Performance*,” Second Edition, Ganga-Jamuna Press, 2006.

VSC-A Final Report: Appendix E-2
GPS Service Availability Study Literature Review

Prepared by
PLAN Group
University of Calgary

List of Acronyms

CAMP	Crash Avoidance Metrics Partnership
CEP	Circular Error Probable
CODE	Center for Orbit Determination in Europe
CORS	Continuously Operating Reference Station
DD	Double-Differenced (measurement)
DGPS	Differential Global Positioning System
DOD	Department of Defense
DOP	Dilution of Precision
DRMS	Distance Root Mean Squared
EKF	Extended Kalman Filter
EU	European Union
FAA	Federal Aviation Administration
FDMA	Frequency Division Multiple Access
FKP	Flächen Korrektur Parameter
GAO	U.S. Government Accountability Office
GDOP	Geometric Dilution of Precision
GIM	Global Ionosphere Map
GLONASS	Global Navigation Satellite System
GNSS	Global Navigation Satellite System
GPS	Global Positioning System
HDOP	Horizontal Dilution of Precision
HW	Hardware
I2V or I-V	Infrastructure-to-Vehicle
IGS	International GNSS Service
IMU	Inertial Measurement Unit
INS	Inertial Navigation System
ITS	Intelligent Transportation Systems
JPO	Joint Program Office
LKF	Linearized Kalman Filter
MEMS	Micro-Electro-Mechanical System

MRSE	Mean Radial Spherical Error
NHC	Non-Holonomic Constraints
NHTSA	National Highway Traffic Safety Administration
PDOP	3d Position Dilution of Precision
PF	Particle Filter
PPM	Parts Per Million
PRN	Pseudo-Random Noise
RITA	Research and Innovative Technology Administration
RMS	Root Mean Squared
RTK	Real Time Kinematic
SEP	Spherical Error Probable
SP	Single Point
SPKF	Sigma Point Kalman Filter
TDOP	Time Dilution of Precision
UERE	User Equivalent Range Error
UKF	Unscented Kalman Filter
USAF	United States Air Force
URE	User Range Error
USDOT	United States Department of Transportation
UTC	Coordinated Universal Time
V2I	Vehicle-to-Infrastructure
VDOP	Vertical Dilution of Precision
VRS	Virtual Reference Station
VSC2	Vehicle Safety Communications 2
VSC-A	Vehicle Safety Communications – Applications
V-V or V2V	Vehicle-to-Vehicle
WASS	Wide Area Augmentation System
ZUPTs	Zero Velocity Updates

Table of Contents

List of Acronyms.....	E-2-ii
1 Introduction.....	E-2-1
2 GPS Overview	E-2-1
2.1 Constellation Overview	E-2-1
2.2 GPS Signal Structure.....	E-2-1
2.3 GPS Modernization	E-2-2
3 Outline of GPS Error Sources and Characteristics	E-2-3
3.1 Spatially Correlated Errors	E-2-3
3.1.1 Ionosphere Errors	E-2-3
3.1.2 Troposphere Errors	E-2-5
3.1.3 Orbit Errors	E-2-6
3.1.4 Clock and Timing Errors.....	E-2-6
3.2 Uncorrelated Errors	E-2-7
3.2.1 Noise and Multipath.....	E-2-7
3.2.2 Differences in Receiver Technology.....	E-2-10
3.3 Measurement Errors in V2V Navigation.....	E-2-12
4 Parameters that Impact GPS Performance.....	E-2-13
4.1 Definitions of Performance Measures	E-2-13
4.2 Factors that Affect Dilution of Precision	E-2-15
4.2.1 Availability of Satellites and Constellation Size.....	E-2-15
4.2.2 Time of Day	E-2-16
4.2.3 Geographic Location.....	E-2-16
4.2.4 Elevation Mask Angle and Obstructions.....	E-2-20
5 Reference Stations and Reference Station Networks	E-2-22
5.1 Differential GPS	E-2-22
5.2 WAAS	E-2-23
5.3 Local Base Stations	E-2-24
5.4 Network-based RTK.....	E-2-25
6 Review of Integration of GNSS with Inertial Navigation	E-2-29
6.1 Introduction and Motivation.....	E-2-29
6.2 Methodology	E-2-30
6.2.1 Inertial Navigation Basics	E-2-30

6.2.2	Equations of Motion and Error Equations	E-2-31
6.2.3	Integration of GNSS and INS	E-2-33
6.3	Review of Published Results.....	E-2-36
7	Impact of Future GNSS and GPS Modernization	E-2-45
7.1	Impact of New GPS Signals.....	E-2-45
7.2	Potential Use of Galileo, GLONASS, and COMPASS.....	E-2-45
7.2.1	Additional GNSS Constellations	E-2-47
8	References	E-2-52

List of Figures

Figure 1: L1 Ionosphere Error for January 1, 2004, at 0:00 Coordinated Universal Time (UTC) Derived from a Global Ionosphere Map from the CODE.....	E-2-5
Figure 2: DD Code Residuals – Combined Effect of Noise and Multipath for L1 C/A Code for a High Quality L1 Receiver	E-2-8
Figure 3: DD L1 Phase Residuals – Combined Effect of Noise and Multipath for L1 Carrier Phase for a High Quality L1 Receiver	E-2-9
Figure 4: DD Code Residuals – Combined Effect of Noise and Multipath for L1 C/A Code for a High Sensitivity “Low Cost” Receiver	E-2-9
Figure 5: DD L1 Phase Residuals – Combined Effect of Noise and Multipath for L1 Phase for a High Sensitivity “Low Cost” Receiver	E-2-10
Figure 6: Zero Baseline L1 Double Difference Phase Errors for u-blox LEA-4T for June 31, 2006 (from Schleppe 2006)	E-2-11
Figure 7: Zero Baseline L1 Double Difference Phase Errors for NovAtel OEM4 – April 20, 2006 (from Schleppe 2006)	E-2-12
Figure 8: Median HDOP (50 Percentile Value) over the United States Computed with the Current 31-Satellite GPS Constellation Simulated on June 21, 2009, Using a 15-Degree Elevation Mask.....	E-2-17
Figure 9: Median HDOP (50 Percentile Value) over the United States Computed with the “as Designed” 24-Satellite GPS Constellation Simulated on June 21, 2009, Using a 15-Degree Elevation Mask.	E-2-18
Figure 10: 95 Percentile HDOP (95 Percent of the Time the Values are Less than This) over the United States Computed with the Current 31-Satellite GPS Constellation Simulated on June 21, 2009, Using a 15-Degree Elevation Mask	E-2-19
Figure 11: 95 Percentile HDOP (95 Percent of the Time the Values Are Less than This) over the United States Computed the “As-Designed” 24-Satellite Constellation Simulated on June 21, 2009, Using a 15-Degree Elevation Mask	E-2-20
Figure 12: 95 th Percentile HDOP Value for a 24-Satellite GPS Constellation and a 10-Degree Elevation Mask	E-2-21
Figure 13: 95 th Percentile HDOP Value for a 24-Satellite GPS Constellation and a 20-Degree Elevation Mask	E-2-22
Figure 14: Example of the Measurement Error of One Satellite Across a Region (red line) (This error is measured at two locations indicated by the green and blue reference stations.)	E-2-26
Figure 15: The Estimated Residual Dispersive (Ionosphere) Error for a Single Reference Station User (Left) and a Network Reference Station User (Right)	E-2-27
Figure 16: The Estimated Residual Non-Dispersive (Troposphere/Geometry) Error for a Single Reference Station User (Left) and a Network Reference Station User (Right)	E-2-27
Figure 17: Concept of GNSS/INS Integration	E-2-34
Figure 18: 95 th Percentile HDOP Using a 24-Satellite GPS Constellation and a 20-Degree Elevation Mask	E-2-48

Figure 19: 95 th Percentile HDOP Using a 24-Satellite GPS constellation in Conjunction with a 30-Satellite Galileo Constellation and a 20-Degree Elevation Mask.....	E-2-49
Figure 20: 95 th Percentile HDOP Using GPS, Galileo, and GLONASS with a 20-Degree Elevation Mask	E-2-50
Figure 21: 95 th Percentile HDOP Using GPS, Galileo, GLONASS, and Compass with a 20-Degree Elevation Mask.....	E-2-51

List of Tables

Table 1: Combined Code and Carrier Phase Noise and Multipath RMS Error Shown in Raquet (1998)	E-2-7
Table 2: GPS Errors in Single Point and Differential Mode Assume a Baseline Length of the Order of 10s of Kilometers and a Baseline Length of 10s of Seconds (after Misra and Enge 2001)	E-2-13
Table 3: Key Characteristics of GNSS and INS	E-2-29
Table 4: General IMU Classifications (from Petovello 2003b).....	E-2-31
Table 5: Summary of Results with Navigation-Grade IMUs	E-2-39
Table 6: Summary of Results with Tactical-Grade IMUs	E-2-40
Table 7: Summary of Results with Automotive-Grade IMUs	E-2-42
Table 8: Summary of Results with Reduced IMUs	E-2-44
Table 9: Comparison of GPS and Galileo Ambiguity Resolution over a 1 KM Baseline (from Cao, et al. 2008b).....	E-2-47

1 Introduction

This is the first of two reports as part of the Vehicle-to-Vehicle (V2V) and Vehicle-to-Infrastructure (V2I) testing and analysis project. This report contains the literature review only. The other report contains the results, analysis, and conclusions from the study.

2 GPS Overview

The Global Positioning System (GPS) is an all-weather satellite navigation system operated by the United States Air Force (USAF). The system consists of three segments: the Control Segment, consisting of ground-based tracking and control stations; the User Segment, which includes all user receivers; and the Space Segment, which consists of a constellation of satellites in medium Earth orbit that transmit synchronized ranging signals, and information about the satellite orbit, to users on or near the surface of the Earth. Users must track at least four satellites, decode the navigation message transmitted by each in order to determine the satellite positions, and then use this information and the four or more range observations to compute four unknowns, which are the user's three coordinates (latitude, longitude, and altitude) and the user-receiver clock offset. The system is well described in a number of textbooks. Two popular texts are Misra and Enge (Misra and Enge 2001) and Leick (2004). A more detailed treatment is given in the two volume GPS Blue Books (Parkinson and Spilker, Jr. 1996).

2.1 Constellation Overview

The system design calls for 24 satellites in near circular 12-hour orbits distributed in 6 orbital planes inclined at 55 degrees to the equator. The 24 satellites in the guaranteed constellation were originally described as 21 satellites plus 3 active spares; however, since at least 1995, the guaranteed minimal constellation is 24 operational satellites (DOD 1995). The constellation is designed to ensure at least four satellites are in view at all times at all locations on Earth. As of June 2009, there were 31 operational GPS satellites. Updates on constellation status, as well as almanac files describing the satellite orbits and notices to users, can be found at the United States Coast Guard Navigation Centre webpage. Although GPS has reliably provided continuous and consistent service for many years, there are concerns that it will not be possible to maintain the same level of service in the future. The U.S. Government Accountability Office (GAO) (2009) suggests that there is a small chance that the number of active GPS satellites could decrease below 24 over the next five years if efforts are not made by the USAF to correct management projects in its satellite procurements programs.

2.2 GPS Signal Structure

The GPS signal structure is complex and will not be reviewed in detail here. Instead, only the material relevant to this report is provided. For more details on the signal structure, refer to Ward (1996), Spilker (1996b), and Misra and Enge (2001).

The GPS signal is comprised of two frequencies, namely L1 (1575.42 MHz) and L2 (1227.60 MHz). Modulated on these carriers are the:

- Pseudo-Random Noise (PRN) codes used for ranging measurements
- Navigation data to communicate the satellite's position, time, health, etc., to users in real-time (50 bps modulation)

Currently, only two types of PRN codes are used, namely the Coarse/Acquisition code (C/A-code) on L1, and the Precise code (P-code) on L1 and L2. Exploiting the characteristics of the signal structure, the following three types of measurements can be obtained from most GPS receivers.

- Pseudorange (code) measurements - These are derived from the PRN codes and are, therefore, classified according to code and frequency as L1-C/A, L1-P, and L2-P
- Carrier phase (phase) measurements - By measuring the phase of the incoming carrier (L1 and/or L2), the range to a satellite can be measured; however, it is biased by an ambiguous number of cycles. This is due to the fact that it is only possible to measure a phase between 0 and 360 degrees and its subsequent change over time, and it is not possible to determine a pseudorange directly from a phase measurement.
- Doppler measurements - The derivative of the carrier phase measurement is the Doppler shift caused by the relative receiver-satellite motion

In terms of code measurements, the P-code theoretically provides better overall performance. Unfortunately, the P-code signal is currently encrypted in an attempt to limit its use to the military community (including the entire L2 signal). However, codeless and semi-codeless tracking techniques have been developed which allow the civil community access to these signals. Unfortunately, these techniques decrease the signal-to-noise ratio by 14 dB or more and, therefore, produce considerably noisier measurements than would otherwise be expected. These techniques are described as "unauthorized use" by the USAF and are generally limited to land surveying and scientific applications while consumer and civil aviation and maritime users use L1 C/A exclusively. Almost all currently commercially available dual frequency receivers use codeless or semi-codeless techniques and, therefore, are more expensive than a dual frequency receiver that is to track a second frequency directly such as L2C.

2.3 GPS Modernization

The GPS L1 and L2 signal structure was designed in the 1970's and has been used operationally for over 30 years. In parallel with ongoing replacement of satellites, several major initiatives are underway to modernize the GPS signal for both civil and military users. Only those aspects of GPS modernization relevant to civil users are discussed here. The first modernization is the addition of a civil code to the L2 signal. L2C (for L2 Civil) is, at the time of this writing, available on five recently deployed GPS satellites. The addition of this new ranging code allows for direct acquisition of L2 and allows civil use of L2 without the requirement for codeless techniques which will result in less expensive dual frequency GPS being available in the near future.

A third frequency, L5 1176.45 MHz, is planned; and one L5 capable satellite has been deployed. The fully modernized GPS, or GPS III, will consist of at least 24 satellites each broadcasting civil signals on three frequencies. The implications of this for users are discussed in Section 7 below as well as the other global navigation satellites systems that are being developed and deployed by the European Union, Russia, and China.

3 Outline of GPS Error Sources and Characteristics

The precision, accuracy and reliability of GPS positioning and navigation is dependent on the level of errors present in the observations. The properties of observation errors change over time and geographic region. This section describes the error sources relevant to single point (SP) and differential code and carrier phase positioning.

The error sources effecting GPS observables can be roughly divided into two categories based on whether or not the errors are correlated with the antenna location (i.e., spatially correlated). Errors that are spatially correlated can be reduced or eliminated by differencing between receivers that are located close to one another. Between receiver observation difference works because both receivers are affected by similar levels of systematic errors. If observations are affected by similar (spatially correlated) systematic errors, then the common part of these errors will be cancelled out in the difference leaving a smaller residual error. In the process, the position estimation changes from estimating the absolute position of one receiver to estimating the relative position or baseline between the two receivers. In the case that the coordinates of one receiver are already precisely known, then the coordinates of the other receiver can be determined. This is the basis for differential GPS, which is discussed in Section 3.3 below.

3.1 Spatially Correlated Errors

The GPS errors that can be reduced or eliminated by differencing between receivers include the ionosphere, troposphere, and satellite clock. The two atmospheric errors (troposphere and ionosphere) can be reduced by differencing between receivers. The shorter the distance between the receivers, the greater the reduction of correlated errors due to the signal traveling through more or less the same path in the atmosphere to reach the two receivers. The remaining errors after differencing are called differential errors and are usually expressed in relative terms (such as parts per million (PPM)) with respect to the baseline length. One PPM is equivalent to 1 mm of error over 1 km. In the case of the satellite clock error, it is cancelled completely using between-receiver differencing. Each error is discussed below.

3.1.1 Ionosphere Errors

The ionosphere is a region of the atmosphere which contains weakly ionized plasma (Klobuchar et al 1995). The ion content (free electrons) in this region has various effects on electromagnetic signals, such as GPS.

The ion content of the ionosphere is distributed from 60 to more than 1000 km above the surface of the Earth (Klobuchar et al 1995; Leva et al 1996). However the peak density is located around 300 to 450 km. The effect of the ionosphere on radio-navigation signals is

a function of the integration of the electron density along the signal's path. The effect of the ionosphere is a function of the frequency of the signal for L-band signals. Carrier phase measurements are advanced by the ionosphere by the same amount that the code is delayed. This property is commonly used to estimate or mitigate the ionospheric effect.

The ionosphere's variability is due to the number of free electrons, which is a function of solar radiation. As a result, there is a daily variation of the ionosphere such that it is relatively calm at night and is most active around 14:00 local time.

There are also regional effects due to the sun. These effects can be seen in Figure 1, which shows the estimated global ionospheric error on January 1, 2004, at 0:00 UTC. This is derived from a Global Ionosphere Map (GIM) produced by the Center for Orbit Determination in Europe (CODE). There is a significant ionosphere gradient at low geomagnetic latitudes which is amplified at approximately 14:00 local time. During ionospheric storms, there can also be significant ionospheric gradients at the poles.

Ionospheric storms can also cause localized pockets of charged particles. When the Global Navigation Satellite System (GNSS) signals pass through these pockets, they can change rapidly. These rapid changes can cause significant measurement biases and, in some cases, cause the receivers to lose tracking lock of the signals. This effect is called scintillation and only occurs under the most severe circumstances in high latitudes and in equatorial regions.

The ionosphere error is, at times, the largest error source for absolute GNSS positioning. It can vary from less than 5 meters to more than 150 meters during extreme conditions (Wells 1999) although is typically 2 to 10 meters (Wells 1999).

The ionosphere is also the largest error source for differential GPS ranging from less than 1 part per million (ppm) of the inter-antenna distance during low ionospheric periods at mid latitudes to greater than 10 ppm at low geomagnetic latitudes during midday.

For vehicle-to-vehicle (V2V) relative positioning, with distances less than 1 km, the magnitude of the residual differential ionosphere error typically ranges from 1 mm to 1 cm depending on the level of ionospheric activity.

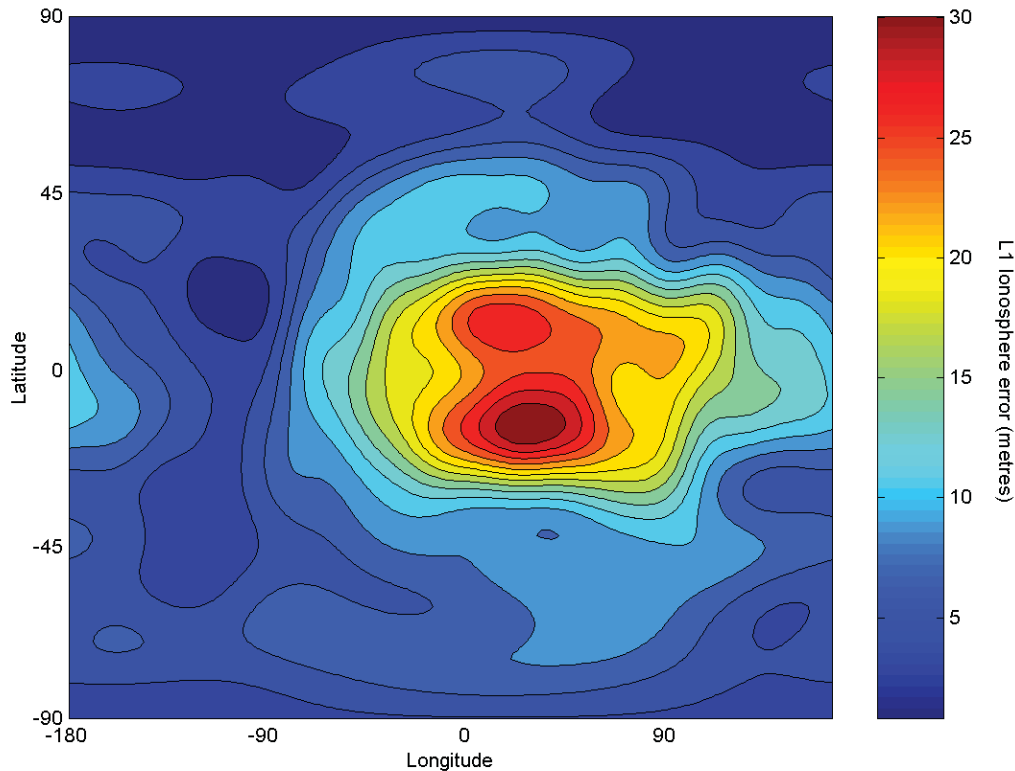


Figure 1: L1 Ionosphere Error for January 1, 2004, at 0:00 Coordinated Universal Time (UTC) Derived from a Global Ionosphere Map from the CODE

3.1.2 Troposphere Errors

The troposphere is a region of the atmosphere that spans from the Earth's surface from 12 to 14 km above the surface (Spilker, Jr. 1996b). The composition of the gases in this region has an impact on GPS signals. As the signal travels through these tropospheric gases, the signal refracts and slows the transmission speed of the signal, which both lengthens the measurement's path causing a delay in the time at which the signal is received by the user. The magnitude of the delay is relative to the atmospheric profile along the signal path.

The tropospheric delay is divided into two components, the dry and wet delays. The dry (or hydrostatic) part is due to the non-water content, and the wet delay is caused by the water content in the atmosphere. The hydrostatic part comprises approximately 90 percent of the delay but can be predicted with an accuracy of about 1 percent at the zenith using meteorological data. In contrast, the wet term makes up the remaining 10 percent of the error and can only be predicted with about 10–20 percent accuracy (de Jong, et al. 2002). The wet delay varies by 10 to 20 percent in a few hours (Spilker, Jr. 1996b).

Many models have been developed to reduce the effect of the troposphere on GPS measurements. Shrestha (2003) and Zhang (1999) give an overview of many common troposphere models.

The hydrostatic error is typically around 2.3 meters at the zenith and up to 10 times higher at low elevations; however, this effect is reduced to a few millimeters using any of the troposphere models (Zhang 1999; Shrestha 2003). The wet delay can be less than a few centimeters up to 35 centimeters depending on the amount of water vapor in the atmosphere. The differential residual troposphere error (after modeling) is on the order of 0.1 to 0.4 ppm of the inter-antenna distance (Alves 2005). This residual error over distances of less than 1 km (V2V navigation applications) is less than the magnitude of the measurement noise and is, therefore, negligible.

3.1.3 Orbit Errors

The orbit error is due to inaccuracies in the satellite position reported by the broadcast ephemeris. The effect of a satellite position error on the differential position is the projection of this error onto the direction of the observation vector (Parkinson 1996).

The magnitude of the absolute errors are about 3.5 m (50th percentile) (Ryan, 2002) and vary slowly with time (Olynik 2002). Orbit errors are also correlated as a function of the inter-antenna distance. Raquet (1998) shows that orbit error is usually less than 0.1 ppm of the inter-antenna distance. In terms of V2V navigation, the effect of orbit errors is less than 1 mm and is negligible.

3.1.4 Clock and Timing Errors

SP GPS positioning assumes that transmitting satellites are time synchronized to a time system called GPS Time. GPS Time is a realization of Coordinated Universal Time (UTC), and it is based on an average of the atomic clocks operated by the control and space segments of GPS. The time system is steered such that it follows UTC with the exception that it does not contain leap seconds. The GPS time scale is expressed in weeks and seconds from 0h UTC January 6, 1980. In reality, all of the satellite clocks differ from GPS time. This difference is called the satellite clock error, or offset. To mitigate this effect, each GPS satellite is monitored by the control segment; and a clock correction model is broadcast as part of the navigation message. The clock correction consists of a polynomial model representing the clock offset, drift, and rate of drift. After this correction is applied, a small residual satellite clock error term remains. 1 ns of satellite clock error corresponds to 30 cm of ranging error.

Separate from the satellite clock error, is a receiver clock error or offset. This arises from the fact the receiver clock is usually a low-cost crystal oscillator. The approach usually taken to remove this effect is to estimate it along with the unknown position of the receiver. Estimating the receiver clock offset will completely remove the effect of receiver clock biases provided that all of the measurements on the receiver are taken at precisely the same time. The satellite clock error contributes to 1-3 m of position error in SP mode (Kaplan 1996; Parkinson and Spilker 1996).

In differential mode, there is a small error created by the differences in measurement times of the two receivers. To minimize this effect, receivers steer their internal clocks to GPS time using the internal position and timing computations.

The estimated clock offset is correlated with the estimated position solution (since all 4 parameters, 3-D position, and receiver clock offset, are estimated together). The clock estimate is most highly correlated with the height component of the position estimation. This makes sense intuitively since if the receiver clock offset is estimated incorrectly and satellites are more or less uniformly distributed around but above the user, the average effect of the clock offset estimation error will be to either raise or lower the estimated position. This is the reason that GPS estimates height more poorly than the horizontal position components. The addition of a clock constraint (using a high quality clock) will improve the vertical solution and conversely the application of a height constraint will improve the clock offset estimation.

Another method for removing the effect of the clock is through differencing measurements from different satellites. The effect of receiver clock biases can be removed by differencing the measurements of two satellites that were observed at the same receiver and the effect of satellite clock biases can be removed by differencing the measurements of the same satellite that was observed at two different receivers. Differencing these two differences removes both the satellite and receiver clocks. This combination of measurements is called a double-differenced (DD) measurement.

3.2 Uncorrelated Errors

The uncorrelated errors, namely noise and multipath, are not a function of distance between antennae. These errors are described in more detail in this section.

3.2.1 Noise and Multipath

Multipath error is caused by the interference of a reflected signal mixing with the direct satellite signal. The level of multipath is a function of the receiver tracking technology, the antenna type, and the antenna environment.

The noise term consists of receiver measurement noise and the sum of all other unmodeled and second order effects. This is also a function of the receiver technology used. Raquet (1998) shows the code and carrier phase noise and multipath root mean squared (RMS) errors (Table 1) from sample data using a Trimble 4000 SSi receiver.

Table 1: Combined Code and Carrier Phase Noise and Multipath RMS Error Shown in Raquet (1998)

Measurement Type	RMS Error
L1 CA code	0.4 m
L2 P code	1.0 m
L1 phase	4.3 mm
L2 phase	6.2 mm

Figure 2, Figure 3, Figure 4, and Figure 5 show the combined effects of noise and multipath for L1 C/A code, and L1 carrier phase, respectively, for a high quality L1

receiver and a high sensitivity “low cost” receiver. The data was obtained in an open-road-kinematic-vehicular environment from the Final Field Study. The misclosure is the remaining error after the effect of receiver and satellite positions have been removed. See Petovello (2003a) for a detailed explanation of how the noise and multipath is calculated using GPS data.

Noise is not a spatially correlated effect; therefore, the magnitude of the errors will be the same regardless of the antenna separation. Multipath is generally considered not to be spatially correlated; however, there is some spatial correlation over extremely short (1 to 10 centimeter) inter-antenna distances (Ray 2000).

Multipath and noise are the largest error sources for short inter-antenna baselines since all of the other GPS error sources are spatially correlated and are thus removed during processing.

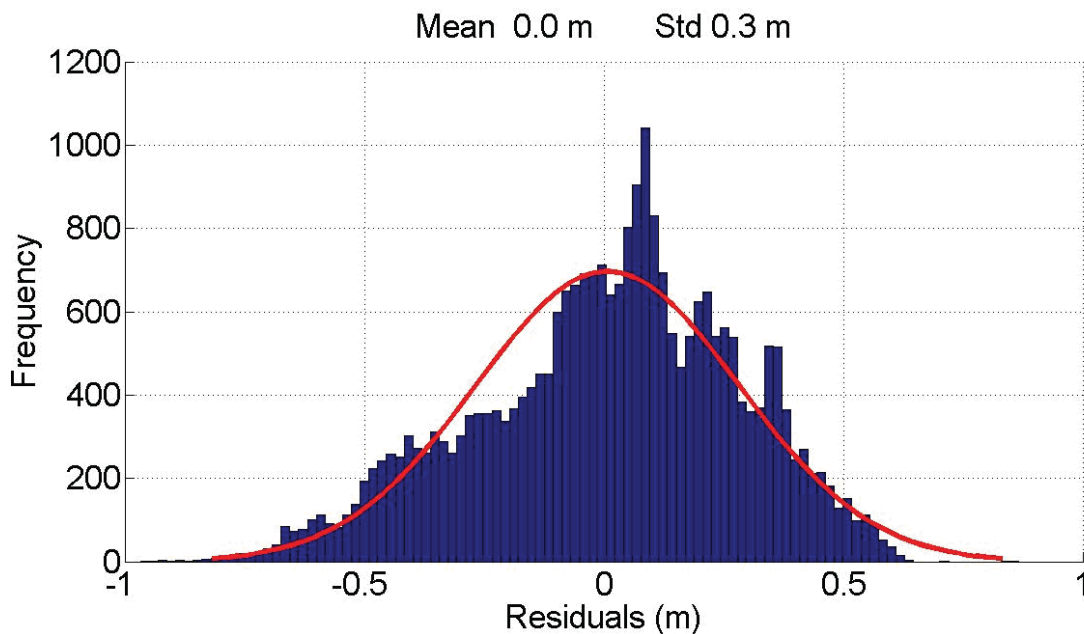


Figure 2: DD Code Residuals – Combined Effect of Noise and Multipath for L1 C/A Code for a High Quality L1 Receiver

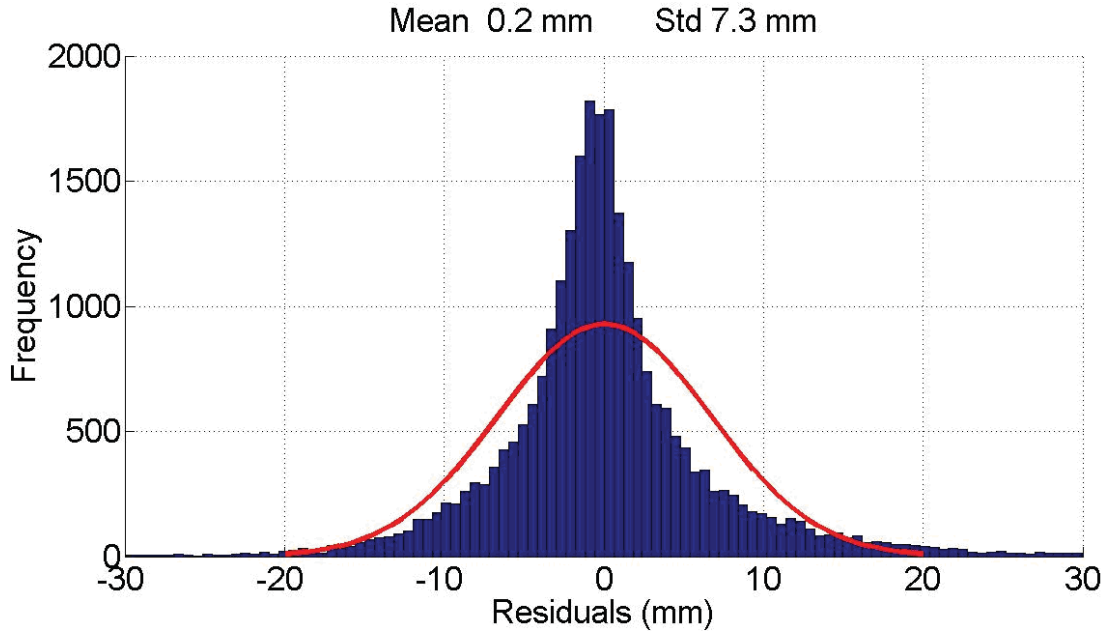


Figure 3: DD L1 Phase Residuals – Combined Effect of Noise and Multipath for L1 Carrier Phase for a High Quality L1 Receiver

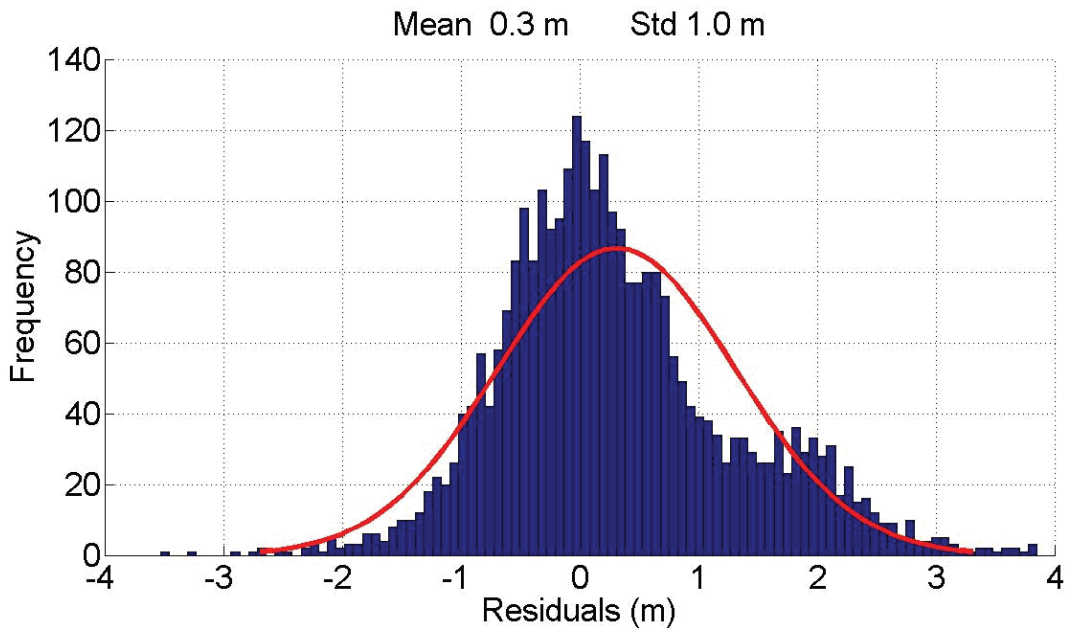


Figure 4: DD Code Residuals – Combined Effect of Noise and Multipath for L1 C/A Code for a High Sensitivity “Low Cost” Receiver

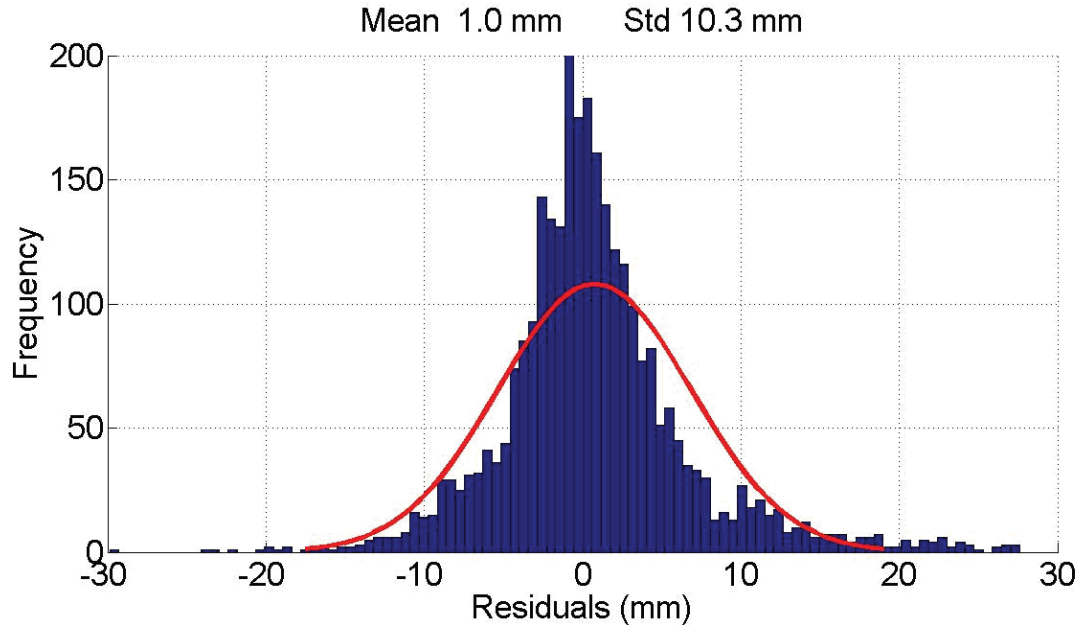


Figure 5: DD L1 Phase Residuals – Combined Effect of Noise and Multipath for L1 Phase for a High Sensitivity “Low Cost” Receiver

3.2.2 Differences in Receiver Technology

Receivers have an array of tuning parameters that can be adjusted depending on the intended use of the receiver. High sensitivity receivers are specially tuned to have high sensitivity so that they can maximize the number of satellites tracked. This can be especially advantageous in environments where there are obstructions between the receiver and satellite antennas, such as under foliage or in urban canyons. The disadvantage of high sensitivity receivers is that they are more susceptible to multipath and measurement noise.

Figure 6 and Figure 7 show the L1 phase double difference measurement noise for two u-blox LEA-4T receivers and for two NovAtel OEM4 receivers, respectively. The RMS of the two solutions (with outliers removed) is 6.6 mm for the u-blox LEA-4T receiver pairs and 4.8 mm for the NovAtel receiver pairs. These are consistent with the results shown in Table 1. The u-blox receivers have 38 percent more receiver noise as a consequence of the higher sensitivity. See MacGougan (2003) for more information about the properties and capabilities of high sensitivity receivers relative to surveying quality receivers.

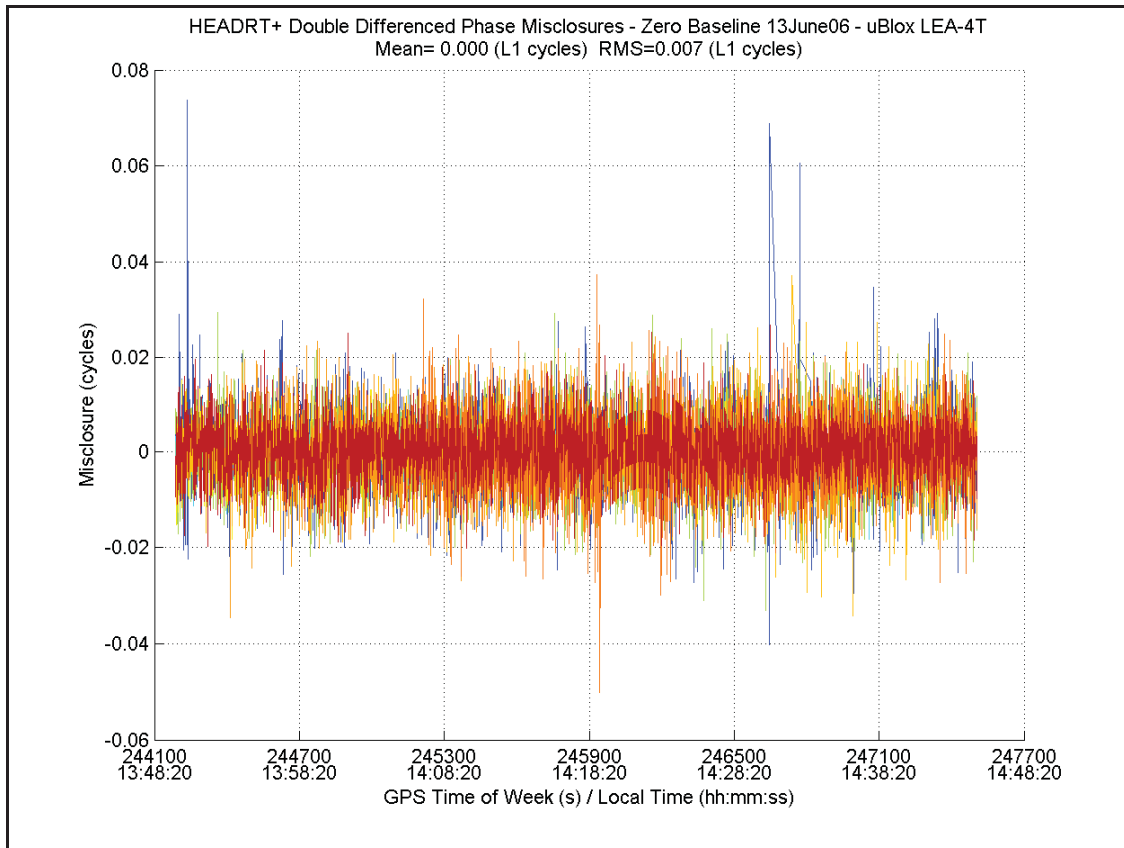


Figure 6: Zero Baseline L1 Double Difference Phase Errors for u-blox LEA-4T for June 31, 2006 (from Schleppe 2006)

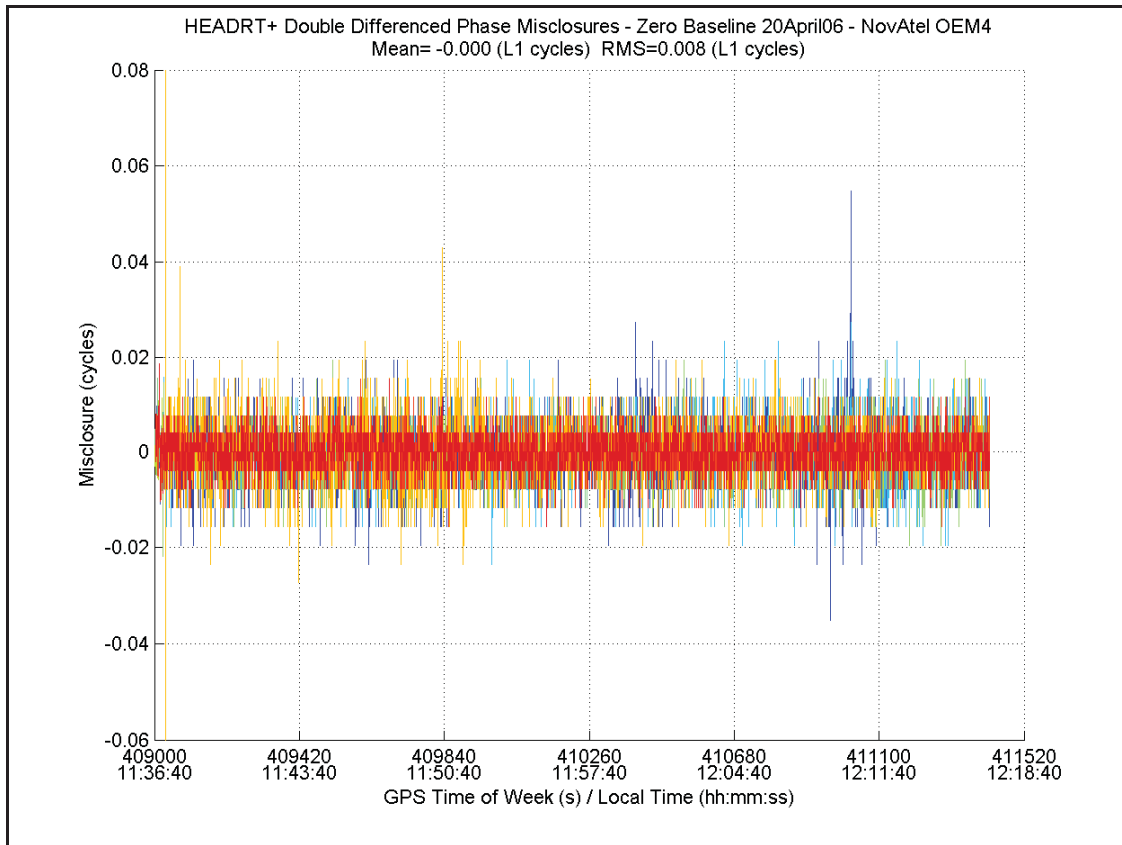


Figure 7: Zero Baseline L1 Double Difference Phase Errors for NovAtel OEM4 – April 20, 2006 (from Schleppe 2006)

3.3 Measurement Errors in V2V Navigation

Spatially correlated errors can be reduced or removed by differencing the measurements of the same satellite that is observed at two different receivers, provided the time between the observations (latency) to be differenced is short. Approximate error levels before and after between-receiver differencing are given in Table 2.

The effect of the errors discussed in this section can be applied to short distance (< 1 km) V2V-relative navigation. When the same satellite is used in the positioning calculation for each vehicle, then the differential errors shown in Table 2 are expected. Namely, decimeter level errors for correlated error sources. Multipath is the largest error source on the order of 0.5 to 1 m.

For all satellites that are not common between the two receivers, the correlated error sources (ionosphere, troposphere, satellite clock, and orbit error) will not be reduced and will, therefore, have the full effect. When one receiver tracks a satellite that the other vehicle's receiver cannot, this satellite is most likely a low elevation satellite; because low elevation satellites typically have the lowest signal strength. In addition, low elevation satellites have the greatest impact on horizontal position error. Consequently, using uncommon-view satellites in V2V applications decreases horizontal position accuracy.

Table 2: GPS Errors in Single Point and Differential Mode Assume a Baseline Length of the Order of 10s of Kilometers and a Baseline Length of 10s of Seconds (after Misra and Enge 2001)

Error Source	Error Size	Residual Differential Error
Satellite Clock	2 m	0 m
Orbit	2 m	0.1 m
Ionospheric Delay	2 – 10 m	Broadcast model 1-5 m Differential Error 0.2 m
Tropospheric Delay	2.3-2.5 m (zenith)	Models 0.1-1 m Differential Error 0.2 m
Multipath	in a “clean” environment Code 0.5 – 1 m Carrier 0.5 – 1 cm	Uncorrelated Mitigated by antenna and receiver design
Receiver Noise	Code 0.25-0.5 m Carrier 1-2 mm	Uncorrelated

4 Parameters that Impact GPS Performance

The purpose of this section is to document parameters that affect GPS performance other than the errors discussed in Section 3 above. In general, GPS performance is a function of the level of errors in the observations and the geometry of the satellites contributing to the position solution. First, these and other performance measures will be defined and then factors that affect the geometry of the satellites will be discussed in detail.

4.1 Definitions of Performance Measures

There is a wide range of performance measures used to assess GPS positioning. In general, they include system measures such as availability and reliability, solution quality indicators such as accuracy or precision, and time and statistical performance metrics such as “time to first fix.” Each of these will be defined below.

Availability can have two meanings. The first is “is a position solution (meeting some performance measure) available or not.” However, availability can also be used to indicate “the number of satellites available;” in other words, “tracked by the receiver” or “used in the solution.” In this report a detailed description of what is being used will be described when the meaning of availability is ambiguous.

Reliability also has two meanings. The first is simply “can the system be trusted.” The second is a more specific meaning in the field of high-precision positioning where reliability indicates the ability of a system to control gross errors or blunders through the detection and elimination of outlier observations. Reliability will not be discussed in this report.

Accuracy, broadly defined, is the closeness of an estimate or a group of estimates to the true value, while precision represents the closeness of a group of estimates to the mean value of the group. Several very specific measures of accuracy have been developed and are used to assess navigation systems including GPS. The most common include Circular Error Probable (CEP), Spherical Error Probable (SEP), Distance Root Mean Squared (DRMS), and Mean Radial Spherical Error (MRSE) (de Jong, et al. 2002). All of these are based on the probable density function of the position solution which can be represented by a 3x3 covariance matrix of the estimated position solution coordinates. Shown here expressed in east, north, height coordinates (E,N,h) but equally valid in any other coordinate system.

$$C_{\hat{x}} = \begin{bmatrix} \sigma_E^2 & \sigma_{EN} & \sigma_{Eh} \\ \sigma_{EN} & \sigma_N^2 & \sigma_{Nh} \\ \sigma_{Eh} & \sigma_{Nh} & \sigma_h^2 \end{bmatrix}$$

CEP is a 2-dimensional error defined as the radius of a circle containing 50 percent of the probability density of the 2-D solution. In other words, 50 percent of the time the true solution will be within a circle of radius CEP centered at the estimated solution. SEP is the 3-dimensional equivalent to this. CEP and SEP are difficult to determine theoretically and are generally obtained by assessing a large time series of solutions obtained at known points.

A more theoretical measure is DRMS, which is derived from the covariance matrix of the horizontal coordinates ([x,y] or [E,N] or [latitude, longitude]). It is the geometric mean of the estimated standard deviations of the horizontal coordinates and is obtained by taking the square-root of the diagonal elements of the covariance matrix.

$$DRMS = \sqrt{\sigma_E^2 + \sigma_N^2}.$$

MRSE is the 3-D analogue of DRMS and is defined as

$$DRMS = \sqrt{\sigma_E^2 + \sigma_N^2 + \sigma_h^2}.$$

All of these accuracy measures depend on the probability distribution of the position estimate which in turn depends on two things: The accuracy of the measurements, and the geometry of the satellites. The accuracy of the measurements depends on all of the error sources described in Section 3. The level of measurement error can be expressed by a single number called either User Equivalent Range Error (UERE) or just User Range Error (URE). If the assumption is made that all of the ranges used in a solution have the same UERE, then this value can be factored out of the error estimate. What remains is a dimensionless term that represents the satellite geometry which is called the Dilution of Precision (DOP). The definition of DOP depends also on what is being estimated leading to the definition of HDOP (horizontal) VDOP (vertical), PDOP (3d position), TDOP (time), and GDOP (Geometric, or the DOP associated with estimating 3d position and

receiver clock offset). Specifically HDOP and PDOP are related to DRMS and MRSE through UERE as follows:

$$HDOP = \frac{1}{UERE} DRMS = \frac{1}{UERE} \sqrt{\sigma_E^2 + \sigma_N^2}$$

and

$$PDOP = \frac{1}{UERE} MRSE = \frac{1}{UERE} \sqrt{\sigma_E^2 + \sigma_N^2 + \sigma_h^2}.$$

The advantage of using DOP to assess GPS performance is that it allows the satellite availability and geometry to be assessed independently of the ranging measurement accuracy. The DOP can then simply be multiplied by the ranging accuracy to obtain a positioning accuracy; so, for example, if a standalone or SP GPS has a ranging accuracy of 5 meters, code differential 1 meter, and fixed ambiguity carrier phase 2 cm, then in horizontal accuracy in a scenario where HDOP = 1.2 (a typical value, for example) can be assessed as 6 m, 1.2 m, and 2.4 cm without having to repeat an evaluation for each type of measurement.

4.2 Factors that Affect Dilution of Precision

Spilker, Jr., (1996a) presents an excellent overview of the design of the GPS constellation and factors that affect DOP. Many others have used DOP to assess proposed new constellations or changes to the GPS constellation. The main factors that affect DOP in open sky conditions are constellation size, time of day, and geographic location. DOP is clearly dependent on the number and location of satellites in view and will be further affected when the view of the sky is obstructed.

4.2.1 Availability of Satellites and Constellation Size

The GPS constellation, as designed, consists of 24 satellites in 6 orbital planes, with 4 satellites unequally spaced in each plane. According to Spilker, Jr., (1996a) this design was chosen to ensure continuous worldwide availability of at least 5 satellites and also to minimize the effect of a single satellite failure. The 24 satellite constellation represents a minimum level of service guaranteed by the United States government. In practice, the number of available satellites has been greater than 24 for at least the past decade. In 2000 there were 27 active satellites, and there are presently 31 active satellites. Clearly, increasing the constellation size improves performance (shown as better or smaller values of HDOP). Figure 8 and Figure 9 show the 50 percentile values of HDOP over the United States over the period of 1 day that can be obtained using the current 31 satellites and the “as-designed” 24 satellite constellation. These were computed by computing the locations of all satellites using the GPS almanac file for the week of June 21-27, 2009, and a second almanac file containing the parameters for the “as-designed” 24 satellite constellation as published in Spilker, Jr., (1996a). Looking at these figures, there appears to be very little difference, and this is true. The median HDOPs obtainable with a 24

satellite constellation and with a 31 satellite constellation are on the order of 1 to 1.5 with a slight improvement in the case of the 31 satellite constellation.

4.2.2 Time of Day

Because GPS satellites have an orbital period of 12 sidereal hours, the GPS ground tracks repeat (in theory) exactly once every sidereal day. In the time it takes the satellite to make two orbits, the Earth has rotated exactly once. Thus, the configuration of the constellation with respect to the Earth repeats once every sidereal day (approximately 23h56m). Based on this, the performance of the constellation can be evaluated by simulating a single day of operation. During a day the performance does vary. A useful way of presenting performance over a day is to evaluate a higher percentile value, for example, when HDOP is better (smaller) than a particular value 95 percent of the time. Figure 10 and Figure 11 show the 95th percentile value of HDOP over the United States for the same 2 simulations (31 and 24 satellite constellations). Clearly in this case, the 24 satellite constellation performs poorly compared to 31 satellites. What Figure 11 indicates is that with a 24 satellite constellation, on the particular day of simulation, 5 percent of the time the HDOP was greater than 10 over much of the eastern United States when using a 15 degree elevation mask. Contrast this with Figure 10 where the HDOP only exceeds 3 5 percent of the time and then only over a limited region around the Great Lakes. This indicates the importance of the additional satellites that currently form part of the GPS constellation and their role not in maintaining average performance but in insuring continuous reliable operation of the system.

4.2.3 Geographic Location

The above simulations were limited to the United States; however, numerous studies have shown that GPS coverage varies slightly with latitude and when averaged over a day but does not vary greatly with longitude. Both Spilker, Jr., (1996a) and O'Keefe, et al., (2002) show that GPS coverage, in terms of availability is best at low and high latitudes and is slightly degraded at mid-latitudes. DOP corresponds generally to availability and is generally better in the equatorial and high latitude regions; however, at high latitude locations, the HDOP is generally improved while the VDOP is degraded. This occurs because the 55-degree inclination of the orbits means that north of latitude of 55 degrees, satellites will no longer pass overhead. At the pole, the maximum elevation of a GPS satellite would be 44.7 degrees (Spilker, Jr., 1996a) making vertical position estimation difficult.

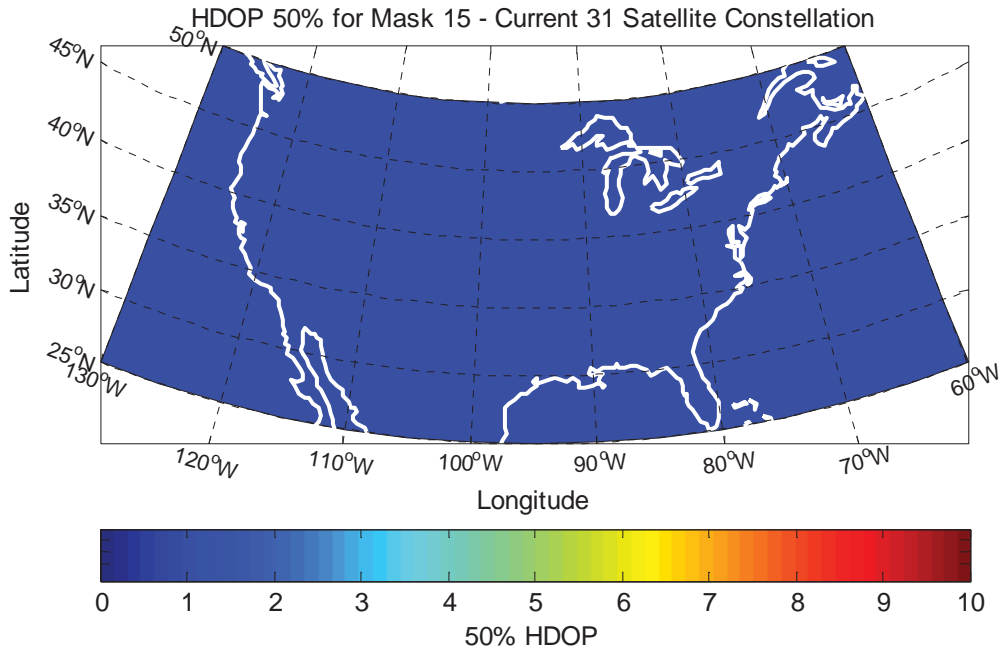


Figure 8: Median HDOP (50 Percentile Value) over the United States Computed with the Current 31-Satellite GPS Constellation Simulated on June 21, 2009, Using a 15-Degree Elevation Mask

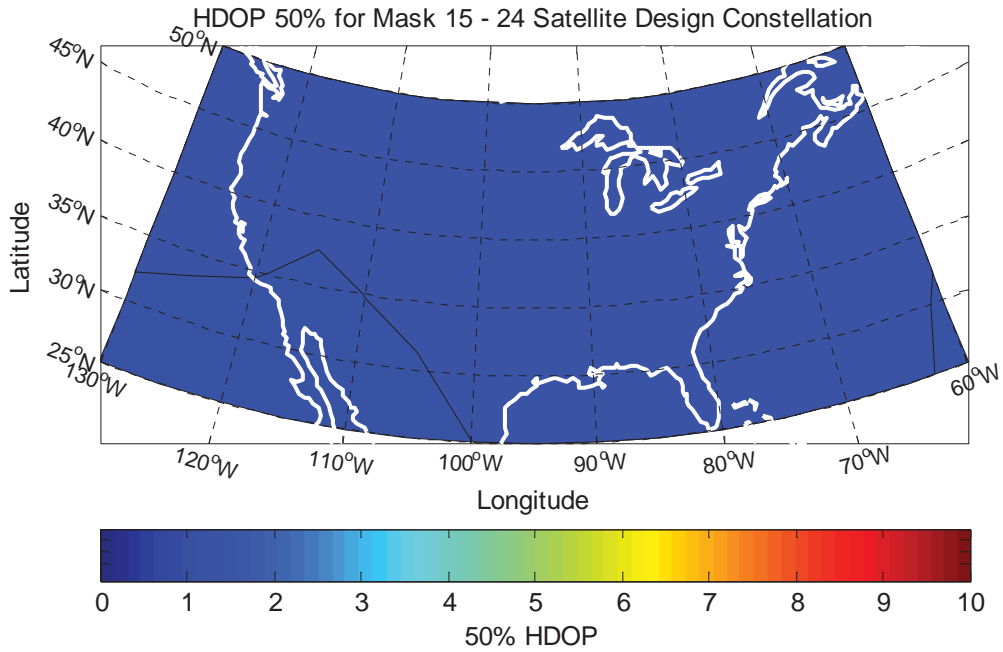


Figure 9: Median HDOP (50 Percentile Value) over the United States Computed with the “as Designed” 24-Satellite GPS Constellation Simulated on June 21, 2009, Using a 15-Degree Elevation Mask

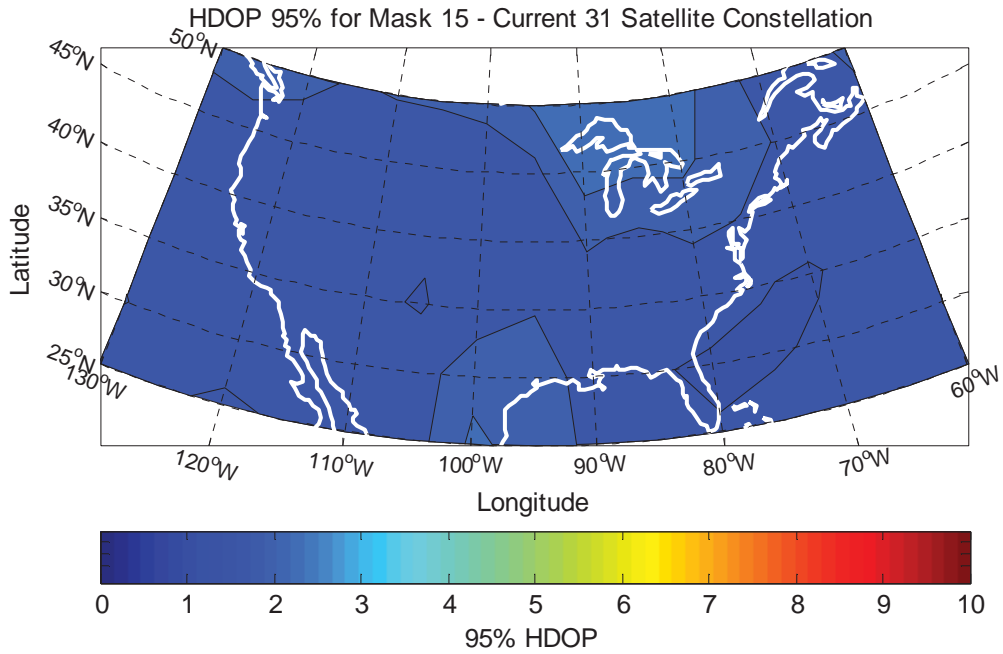


Figure 10: 95 Percentile HDOP (95 Percent of the Time the Values are Less than This) over the United States Computed with the Current 31-Satellite GPS Constellation Simulated on June 21, 2009, Using a 15-Degree Elevation Mask

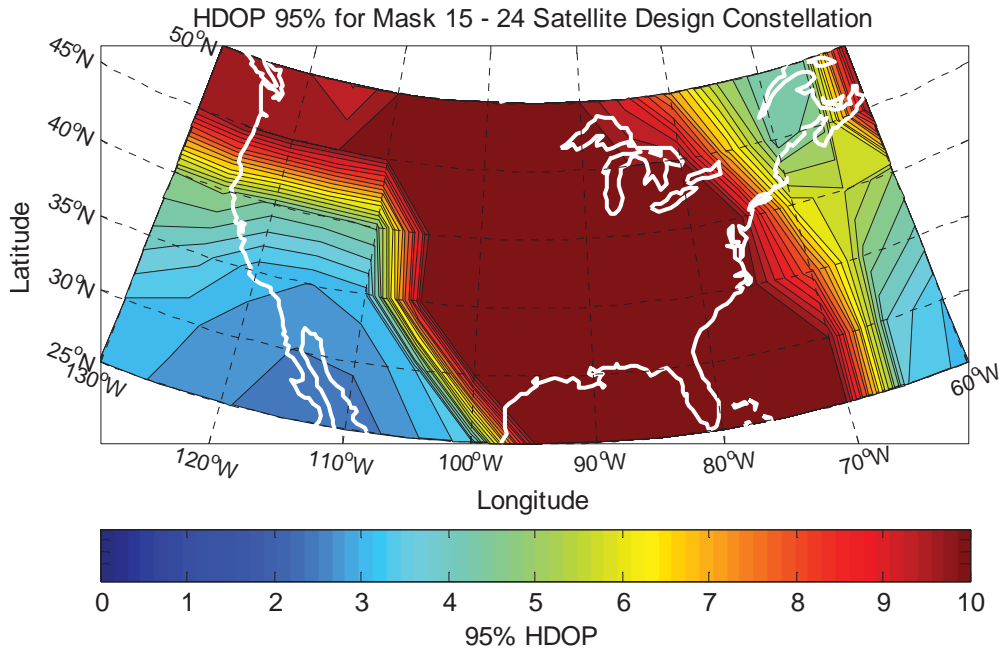


Figure 11: 95 Percentile HDOP (95 Percent of the Time the Values Are Less than This) over the United States Computed the “As-Designed” 24-Satellite Constellation Simulated on June 21, 2009, Using a 15-Degree Elevation Mask

4.2.4 Elevation Mask Angle and Obstructions

Figure 12 shows the 95th percentile value of HDOP for a 27-satellite GPS constellation with a 10 degree elevation mask. In contrast, Figure 13 shows the same when a 20-degree elevation mask is used. The degradation in the high-mid latitudes is evident in this case. In general as the elevation mask is increased, performance is decreased as satellites are excluded from the solution. Generally elevation mask values of 10 to 15 degrees are used in order to include as many satellites as possible while excluding extremely low elevation satellites that generally exhibit more multipath and ionospheric error.

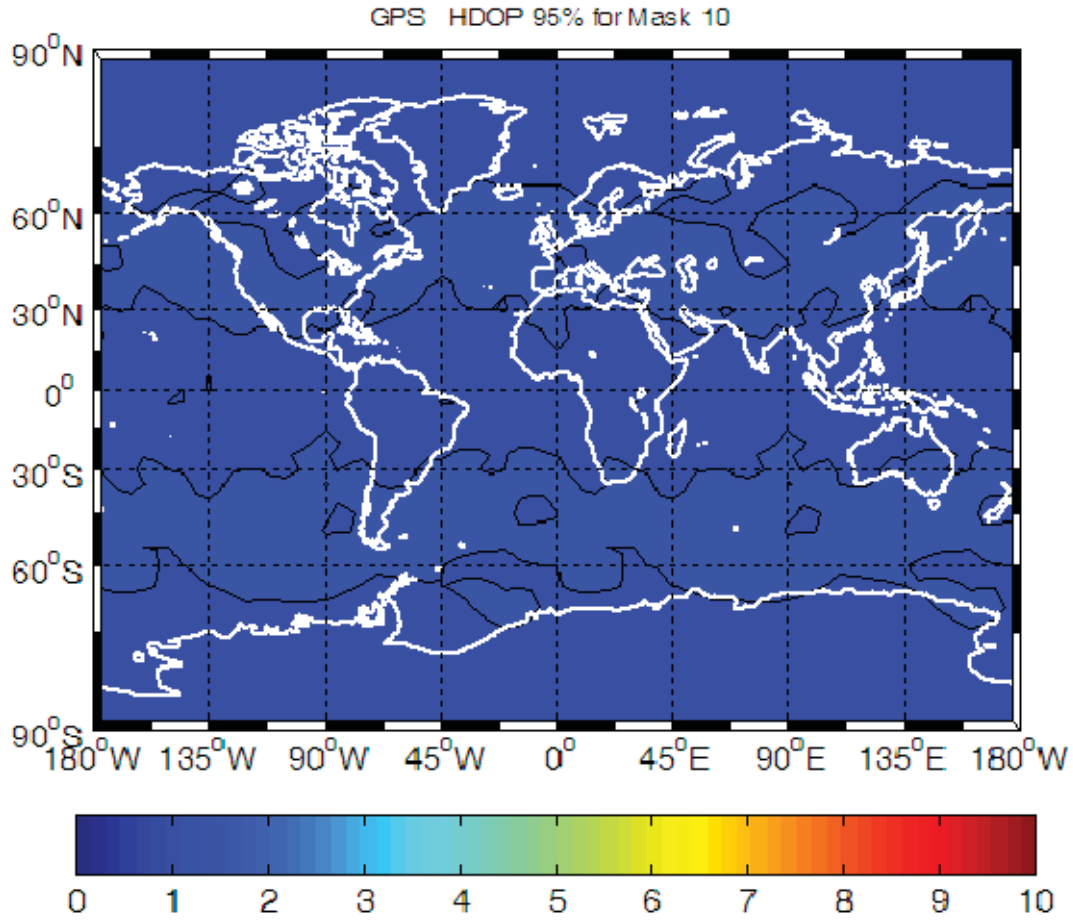


Figure 12: 95th Percentile HDOP Value for a 24-Satellite GPS Constellation and a 10-Degree Elevation Mask

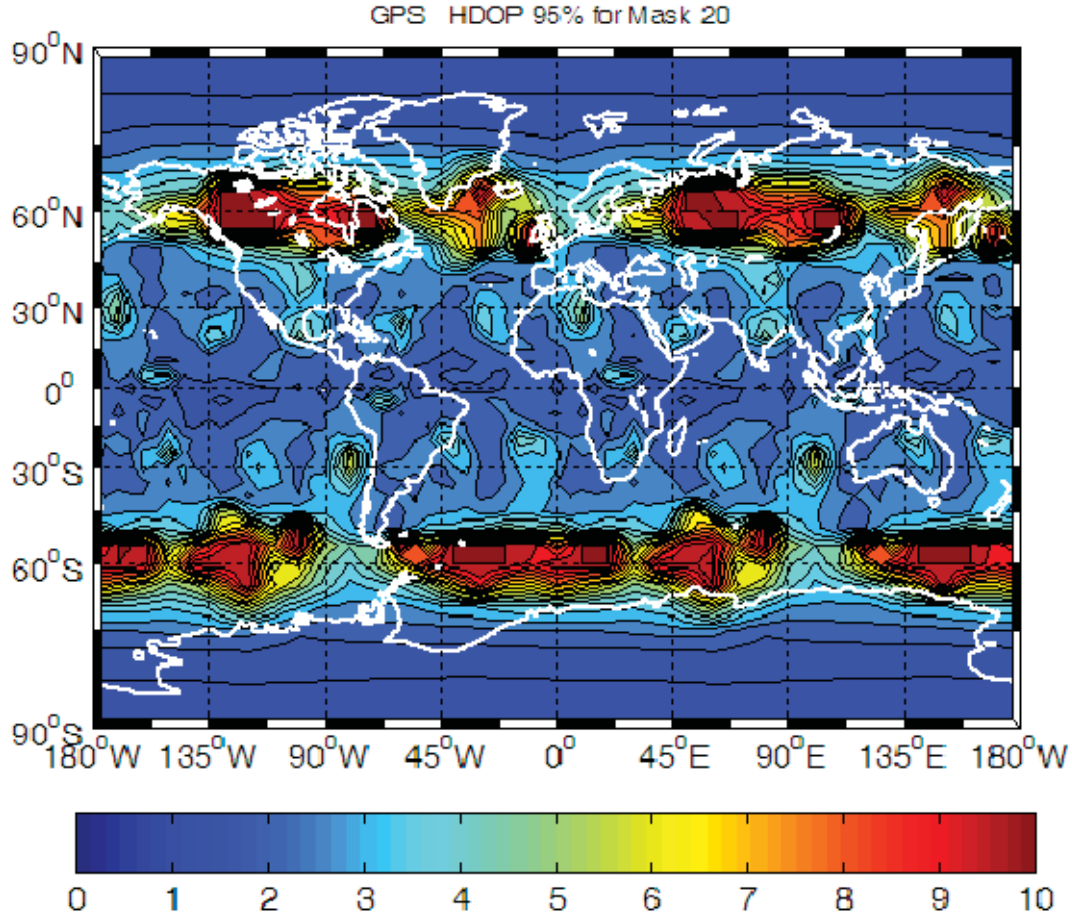


Figure 13: 95th Percentile HDOP Value for a 24-Satellite GPS Constellation and a 20-Degree Elevation Mask

5 Reference Stations and Reference Station Networks

This section describes the impact of reference stations and reference station networks on GNSS accuracy and reliability. Single reference station differential GPS (DGPS), Wide Area Augmentation System (WAAS), precise carrier phase positioning (RTK), and network-based RTK are discussed in the context of vehicle navigation.

5.1 Differential GPS

Combining the GPS error sources summarized in Table 2 a single, stand-alone GPS receiver is expected to achieve approximately 9 meters of position accuracy assuming low levels of atmospheric errors and a large number of GPS satellites well distributed throughout the sky. The global average position domain accuracy for GPS is less than 9 meters (95 percent) in the horizontal direction and 15 meters (95 percent) in the vertical (DOD 2008). The worst site position domain accuracy is 17 meters (95 percent) and 37 meters in horizontal and vertical, respectively (DOD 2008). The United States Department of Defense (DoD) is committed to maintaining these minimum levels of accuracy. These accuracies may be worse than what is commonly achievable under the

current constellation and receiver technology because these accuracies are the minimum commitment with a 24-satellite constellation.

The most significant error sources shown in Table 2 can be reduced or completely removed by using a nearby reference station to estimate the regional error sources. DGPS is the use of mainly code measurements for positioning using a reference station. DGPS position accuracy can be reduced to less than one meter (one sigma) if the reference station is 50 km from the user's antenna (Parkinson and Spilker, Jr., 1996) provided the base and user GPS devices are of sufficient quality. This accuracy decreases steadily as the distance between the reference station and the user increases.

5.2 WAAS

The WAAS is a GPS correction estimation and distribution system. The Federal Aviation Administration (FAA) administers the program, which has been available in initial operational capability mode for aviation use since July 10, 2003 (FAA 2007). GPS measurement errors are monitored for WAAS corrections using a reference station network distributed throughout the Continental U.S. with additional stations in Alaska, Canada, and Mexico. The correction messages for WAAS are distributed through geostationary satellites.

WAAS has many services including integrity monitoring and error modeling. The geostationary satellites are themselves additional ranging satellites which provide further satellite availability along with the other data services.

The integrity messages notify users within 6 to 8 seconds if a satellite's ranging data becomes unstable or unusable (FAA 2007). This is a critical feature for many applications because it allows for protection levels of GPS service. If the GPS ranging errors exceed the protection levels, then the integrity messages alert the applications that there may be a problem.

The WAAS network measures and monitors the clock, orbit, and ionosphere errors throughout the network and provides corrections for these error sources. The clock corrections are transmitted at a high rate and a slow rate for different applications. Yousuf (2005) shows that the RMS WAAS clock corrections are 31 to 44 percent better than the broadcast clock model, and the RMS error of the satellite positions is 13 to 35 percent better than the broadcast positions. This study did show significant outliers in the WAAS corrections due to satellites entering the view of the network. These outliers could exceed 50 meters in error for some cases.

Yousuf (2005) concludes that the accuracy of the WAAS ionosphere correction is 2 to 3 meters during low ionosphere periods; however, it can be much larger during ionosphere storms. The ionosphere errors after applying the WAAS ionosphere model can be significantly larger than the usual 2 to 3 meter error levels during ionosphere storms. The corresponding integrity information responds well to the event suggesting that users would be properly warned about the reduced accuracy of the corrections.

In terms of the position accuracy, with dual frequency International GNSS Service (IGS), Continuously Operating Reference Station (CORS), and WAAS reference stations as rovers, the RMS position error when using WAAS was 0.7 to 1.1 meters (95 percent) in

the horizontal and 1.0 to 1.7 meters (95 percent) in the vertical (FAA 2004) Yousuf 2005). This is roughly the same level of accuracy as shown for DGPS. FAA (2005) shows a WAAS-enabled 62 to 76 percent improvement in the horizontal position error and 79 to 88 percent improvement in the vertical position errors relative to standalone GPS using WAAS-certified user equipment.

5.3 Local Base Stations

When a reference station is within a few kilometers to a user, then carrier phase methods can be used to further improve the positioning performance. Carrier phase measurements are significantly more precise than code measurements, and they are much less susceptible to multipath. Unfortunately, carrier phase measurements have an integer wavelength biases (ambiguities) that must be estimated and removed. These biases are commonly referred to as carrier phase ambiguities.

Carrier phase ambiguities are tracking biases induced by the measurement process of the carrier phase of the GPS signal. These biases have integer values (in cycles). They are random values that change with each loss of lock of the tracked signal. In other words, each satellite is assigned a random integer ambiguity that will be different every time the signal is tracked.

These biases must be estimated before the signal can be used effectively, and if possible, the ambiguities should be constrained (fixed) to their true integer values. This fixed ambiguity case will give the best possible performance when using carrier phase measurements.

There are many methods to determine the correct integer ambiguities; however, they are not relevant to this discussion. For more information on ambiguity resolution methods see Erickson (1992), Chen and Lachapelle (1995), Teunissen (1994), and Jong and Tiberius (1996).

The ability to determine the integer values of the carrier phase ambiguities is limited by the errors in the carrier phase measurements. When the reference station and user are less than 5 kilometers apart, then the carrier phase ambiguities can be reliably determined. Under these conditions the precision of the positioning solution is mainly limited by the carrier phase noise and multipath. Positioning accuracies of a few centimeters is achievable at these short distances.

As the distance between the reference station and user increases, the spatially correlated errors also gradually increase. When the errors become too large to reliably determine the carrier phase ambiguities, a less precise float ambiguity can be estimated. This distance varies depending on the magnitude of the ionosphere and troposphere errors. Under typical conditions, this distance is on the order of 20 to 30 km.

When the distance between the user and reference station increase further, the level of ionosphere error increases. The increase in ionosphere error decreases the accuracy of the float carrier phase ambiguity estimates. At this distance, a combination between the two GPS measurement frequencies can be used to completely remove the effect of the ionosphere. This ionosphere-free measurement can be used to calculate the user's

position with decimeter-level accuracy. The level of accuracy continues to increase further as the distance between the user and the reference station increases.

The ionosphere-free measurement cannot be created with single frequency receivers. In general, all of the reference station distances discussed above are slightly shorter when using only single frequency receivers instead of full dual frequency receivers.

5.4 Network-based RTK

A multiple reference station RTK is a complex, yet natural extension of single reference station RTK. A single reference station RTK actively and dynamically measures GNSS measurement errors. These measurement errors can be characterized based on spatial correlation of the error sources. The following measurement error sources are spatially correlated over tens of kilometers or more and can be useful to reduce the measurements of other GNSS users: satellite clock, satellite orbit, troposphere, and ionosphere errors.

In a single reference station RTK, the errors are assumed to be constant everywhere around the reference station. In reality, however, the quality of these error estimates degrade as a function of distance and can reach an unacceptable level for ambiguity resolution after tens of kilometers. One approach to ensure an acceptable level of measurement error over a wide geographic region is to deploy many reference stations, each operating independently. Once this infrastructure is in place, users select the reference station that will provide them with the greatest reduction of measurement errors and use the corresponding corrections in the traditional single reference station RTK approach. Unfortunately, the decision as to which reference station to use can be problematic especially when the user is located between nearby and equally spaced reference stations. The estimated measurement errors at each of the reference stations may be different, but the user is forced to discretely choose one or the other.

The solution to this problem is a multiple reference station RTK. Instead of discretely choosing the solution from one reference station or another, the multiple reference station solution allows users to combine the estimated measurement errors at each of the reference stations and smoothly transition from the errors at one reference station to another.

The multiple reference station solution is not only better because of the ease of use when transitioning between reference stations but also because the smooth combined solution is more likely to represent the user-observed measurement errors providing an even further reduction of user-measurement errors relative to the single reference station case.

An example of multiple reference station processing is illustrated in Figure 14. The red line represents the changing errors as a function of receiver location. There are two reference stations in this example. A blue reference station is located at -2, and a green reference station is located at +2 while the user in this example is located at 0 in the middle of the network. If the user were to use only the green reference station, then the residual error experienced by the user is shown by the vertical green line. Alternatively, if the user were to use the blue reference station then the error experienced by the user is represented by the blue line. When both reference stations are used, then a combined interpolated solution is shown in black and the corresponding residual error is shown as the vertical black line.

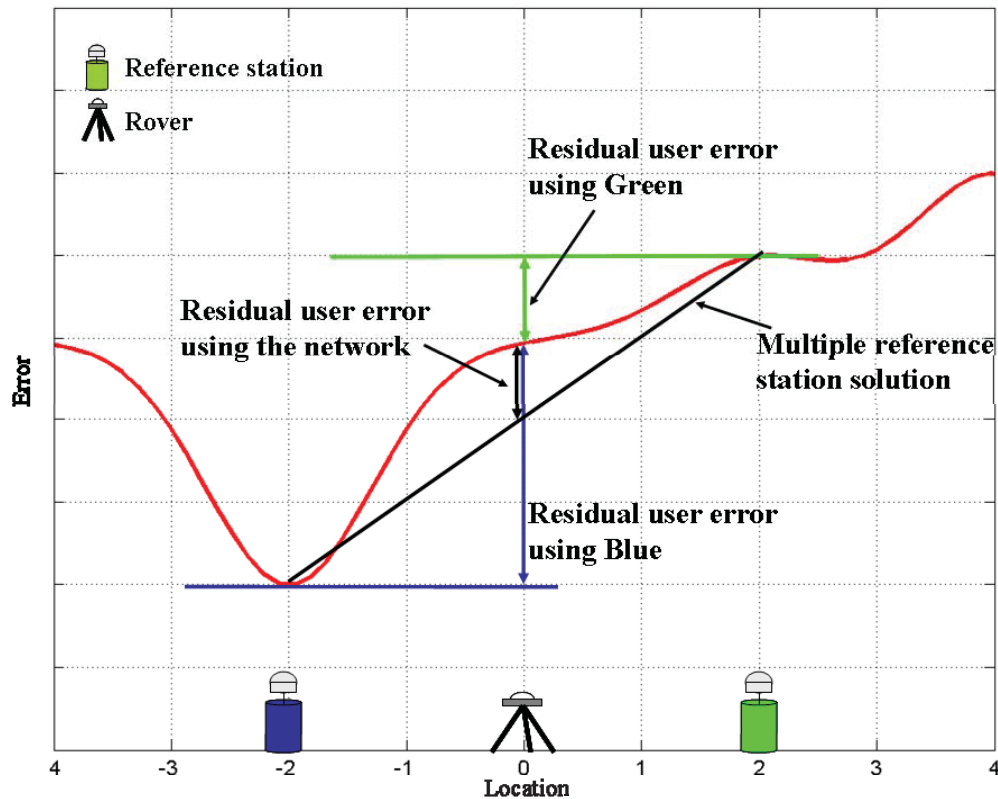


Figure 14: Example of the Measurement Error of One Satellite Across a Region (red line) (This error is measured at two locations indicated by the green and blue reference stations.)

Although there may be times when one reference station's solution is better than the network solution, the network solution is generally more likely to accurately represent the errors over the region because of the additional information gained from combining the data from all reference stations. Figure 15 and Figure 16 (produced by Leica GNSS QC Software) show comparisons of the residual dispersive and non-dispersive errors experienced by a user for both the single reference station and network reference station methods using real data. In all cases, being close to a reference station provides the best solution. The advantage of the multiple reference station model is seen between reference stations outside of the region where typical single reference station RTK processing would be acceptable.

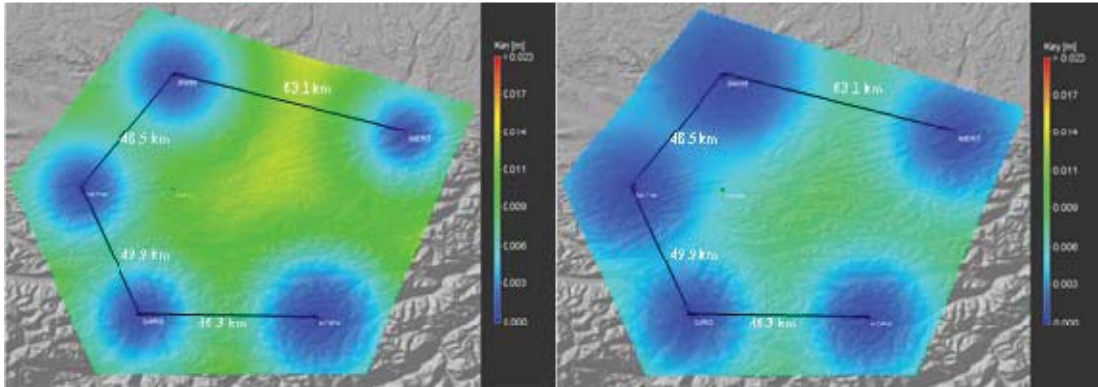


Figure 15: The Estimated Residual Dispersive (Ionosphere) Error for a Single Reference Station User (Left) and a Network Reference Station User (Right)

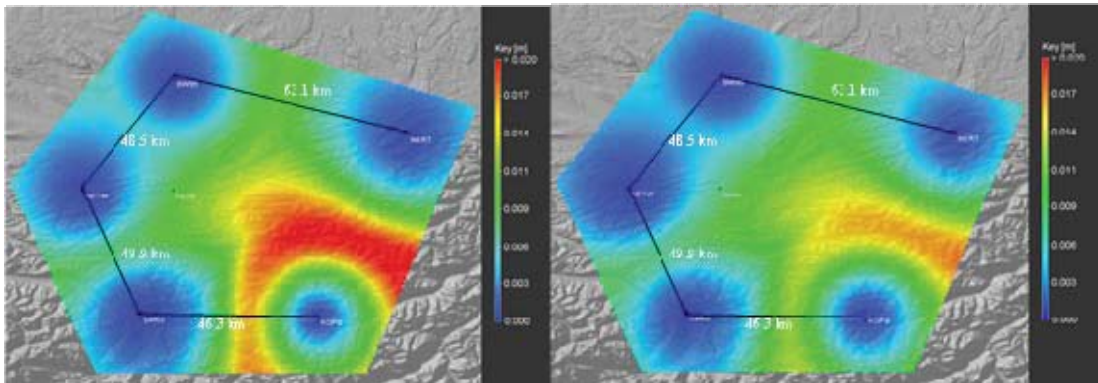


Figure 16: The Estimated Residual Non-Dispersive (Troposphere/Geometry) Error for a Single Reference Station User (Left) and a Network Reference Station User (Right)

In practice, combining the data from multiple reference stations to provide an integrated solution is more complex than the image shown in Figure 14. The following steps must be taken to create the network error model and use it effectively in the user receiver:

1. Accurately measure the relative measurement errors between the reference stations. The most accurate GNSS measurements are phase measurements; however, to use these measurements the carrier phase ambiguities must be precisely estimated and fixed to their correct integer values. To use the integer ambiguities, the double differenced form of the measurements must be used. The double differenced measurement estimates must then be undifferenced for the later steps. This adds significant complexity to the multiple reference station processing.
2. Interpolate the relative measurement errors between the stations to the location of the user.
3. Convert this information to a receiver-acceptable format. There are currently four acceptable options for transmitting network corrections:

- a. Master-auxiliary corrections. These corrections contain the absolute errors for one master reference station and the relative errors for all other auxiliary reference stations. For this format, interpolation from step two is performed by the user.
 - b. Flächen Korrektur Parameter (FKP), or area correction parameters in English. These corrections contain the absolute errors for one master station and the parameters of a regional plane model. In this case interpolation from step two is performed by the user.
 - c. Single reference station corrections. The single reference station corrections are the absolute corrections for one station combined with the relative predicted errors between that master station and the user. This format option allows for users whose receivers are older and do not support the recently developed network correction formats.
 - d. Virtual reference station (VRS). VRS corrections are the single reference station corrections (described above) that have been mathematically translated to a virtual geographic location that is closer to the user's location. This location change moves the reference station to a distance that is more representative for the new level of measurement error after applying the network error model.
4. Use the received corrections to calculate the position of the network user.

The main advantage of a multiple-reference station RTK is the improved user performance. However, the improvement in performance can also be analyzed in an opposite manner; namely, as a way to increase the spacing between reference stations while still achieving the same level of performance. The performance improvement is dependent on many factors, including the variability of the measurement errors in the region and the ability to successfully resolve network ambiguities.

A multiple-reference station RTK is more robust against station outages since a network solution can still be calculated even if individual reference station data is missing. However, due to the current trend of sparse network station spacing, the absence of any individual reference station would likely cause pockets within the network with less than desirable performance. The network, even under these conditions, is still more likely to provide a solution better than from a single-reference station.

This improvement comes at a cost of increased complexity and infrastructure. The data from all of the network reference stations must be collected in a central location for processing and then redistributed to network users. The cost of maintaining a processing centre and data communication lines for each reference station may be significant depending on the number of reference stations and the country and region of the network.

6 Review of Integration of GNSS with Inertial Navigation

This section discusses the motivation, methods and results of integrating GNSS with inertial sensors.

6.1 Introduction and Motivation

The overall motivation for integrating GNSS and inertial navigation system (INS) data is to provide a better navigation solution relative to either system alone. To this end, the key characteristics of GNSS and INS are summarized in Table 3 (e.g., Skaloud 1999).

Table 3: Key Characteristics of GNSS and INS

Characteristic	GNSS	INS
Position/Velocity Accuracy	Nearly uniform at all frequencies with higher accuracy at low-frequencies (long-term)	High accuracy at high-frequencies (short-term); errors degrade as a function of time
Attitude	Limited accuracy and requires special equipment setup	Provided as a natural byproduct with high accuracy in the short-term
Measurement Rate	Generally $\leq 10\text{-}20$ Hz	Generally ≥ 50 Hz
Autonomy	Completely reliant on signals from satellites	Self-contained sensors; fully-autonomous
Availability	Function of satellite visibility; may have temporary outages	Fully available (with degrading accuracy)
Susceptibility to Interference	Susceptible to interference	Not susceptible to interference
Gravity	Not affected by gravity	Affected by gravity

A review of Table 3 shows that GNSS and INS are highly complementary, thus making them well suited to integration with each other. Effectively, the GNSS data, when available, is used to “calibrate” the INS errors, thus allowing the INS to provide accurate navigation information when GNSS is temporarily unavailable. This has been widely recognized for many years (as reflected by the many citations provided in this section) and has thus been the focus of ongoing research to improve various aspects of navigation. The benefits of GNSS/INS integration, relative to either system alone, can be summarized as (Hartman 1988; Greenspan 1994):

- Full position, velocity, and attitude solution
- Improved accuracy and availability

- Smoother trajectories
- Greater integrity
- Reduced susceptibility to jamming and interference

Furthermore, for high accuracy applications, GNSS/INS integration can yield improved ambiguity resolution performance (Skaloud 1999; Scherzinger 2000; Scherzinger 2001; Scherzinger 2002; Petovello 2003b; Petovello et al 2003; Scherzinger 2006) and/or help to detect and correct cycle slips (Cannon 1991; Schwarz et al 1994a; Sun et al 1994; Petovello 2003b).

The following sub-sections provide a brief overview of the inertial methodology as well as the performance of various systems quoted in the literature.

6.2 Methodology

The key to understanding inertial-based navigation requires a review of the relevant methodology. This section briefly presents the key aspects of inertial navigation including the sensors involved, the error characteristics, and the methods for integrating with GNSS data. Much of the methodology is provided without mathematical derivation in order to emphasize key points, and readers are referred to the cited material for more information.

6.2.1 Inertial Navigation Basics

The fundamental sensors involved with inertial navigation are the gyroscope and accelerometer. These sensors are discussed in more detail in the sub-sections below, followed by a short discussion of what comprises an INS.

6.2.1.1 Gyroscopes

It is noted that the term “gyroscope,” or simply “gyro,” is actually a misnomer in many instances, because many current sensors do not use spinning masses (from which the name gyroscope originates). A more accurate term would be “angular rate sensor.” Nevertheless, the term “gyro” is used extensively in the literature and has thus been adopted here as well. To this end, a gyro measures the angular rate about its sensitive axis. Several types of gyros are available including, but not necessarily limited to, mechanical gyros, rate gyros, vibrating gyros, optical gyros, and cryogenic gyros (e.g., Titterton and Weston 1997; Jekeli 2000; Grewal et al 2001). Depending on the type of sensor, the errors sources may include time-varying biases, scale factors, misalignments, temperature sensitivity, magnetic sensitivities, and noise (ibid.).

6.2.1.2 Accelerometers

Counter-intuitively, accelerometers do not directly measure acceleration, but rather *specific force*, which is the vector difference of acceleration and gravitational acceleration (not gravity, which is different). As with gyros, there are several different types of accelerometers including pendulous accelerometers, vibrating accelerometers, force rebalancing accelerometers, and strain sensing accelerometers (e.g., Titterton and Weston 1997; Jekeli 2000; Grewal et al 2001). The associated errors may include time-varying

biases, scale factors, misalignments, temperature sensitivity, anisoelectricity effects, and noise (ibid.).

6.2.1.3 Inertial Measurement Unit (IMU)

The term inertial measurement unit (IMU) generally refers to orthogonal triads of accelerometers and gyros mounted in a single enclosure. It should be clear, therefore, that an IMU only measures specific force and angular rates. In contrast, an INS consists of an IMU as well as the necessary electronics to implement the mechanization equations and error equations presented in Section 6.2.2. Herein, the terms IMU and INS are, therefore, not used interchangeably, although it is warned that this does happen occasionally in the literature.

6.2.1.4 Effect of Sensor Quality

The error sources associated with inertial sensors are characterized by their magnitude and variability. The magnitude refers to how large the initial error can be, whereas the variability refers to how quickly and much the error can vary about a mean value. As will be shown later, it is the latter characteristics that are often most important in an integrated GNSS/INS system.

Several different terms have been used to classify the quality of IMUs. Table 4 gives the general classification that will be used in this report. For the time being, however, it is critical to note that lower-cost sensors, especially micro-electro-mechanical system (MEMS) sensors that are used in automotive-grade IMUs, are generally prone to larger and more variable errors. Their reduced size, cost, and power requirements are, therefore, at odds with the development of an accurate navigation system, which would ideally prefer the best quality, and thus most expensive, of sensors.

Table 4: General IMU Classifications (from Petovello 2003b)

Sensor Error	IMU Grade		
	Navigation	Tactical	Automotive
Gyro Bias (deg/h)	0.005-0.010	1-10	≥ 100
Accelerometer Bias (m/s ²)	0.050-0.100	2-4	≥ 12

6.2.2 Equations of Motion and Error Equations

This section presents, without derivation, the equations of motion and the corresponding error equations. The equations follow closely the notation in Jekeli (2000), but similar formulations are presented in, for example, Titterton & Weston (1997) and Grewal, et al. (2001).

6.2.2.1 Equations of Motion

The equations of motions, given by the following three vector differential equations describe the motion and attitude of a body as a function of time:

$$\frac{d\mathbf{p}^n}{dt} = \mathbf{T}\mathbf{v}^n \quad (1)$$

$$\frac{d\mathbf{v}^n}{dt} = \mathbf{R}_b^n \mathbf{f}^b - (2\boldsymbol{\omega}_{ie}^n + \boldsymbol{\omega}_{en}^n) \times \mathbf{v}^n + \mathbf{g}^n \quad (2)$$

$$\frac{d\mathbf{R}_b^n}{dt} = \mathbf{R}_b^n (\boldsymbol{\Omega}_{ib}^b - \boldsymbol{\Omega}_{in}^b) \quad (3)$$

where $(\bullet)^a$ is a quantity expressed in frame a ; \mathbf{p} is the position vector; \mathbf{v} is the velocity vector; \mathbf{T} relates the velocity and (possibly curvilinear) position states; \mathbf{R}_a^b is the rotation matrix (direction cosine matrix) from frame a to frame b ; \mathbf{f} is the specific force vector; $\boldsymbol{\omega}_{ab}^c$ is the angular rate vector of frame b relative to frame a expressed in frame c ; \mathbf{g} is the gravity (not gravitation) vector, and; $\boldsymbol{\Omega}_{ab}^c$ is the skew-symmetric form of $\boldsymbol{\omega}_{ab}^c$. The subscripts and superscripts refer to the coordinate frame in which the quantity is parameterized. For the purpose of this discussion, the four coordinate frames used are the body (b) frame, the Earth (e) frame, the inertial (i) frame, and the navigation (n) frame (more definitions are available in Jekeli (2000)). In the context of this report, it is assumed that the navigation frame is the local level frame, although this is not required in a general sense. For more details on equations (1) to (3) and/or the relevant coordinate frames, refer to *ibid*.

In equations (2) and (3), the specific force vector, \mathbf{f}^b , and the measured angular rate vector, $\boldsymbol{\Omega}_{ib}^b$ (in skew-symmetric form), represent the input to the system and the position, velocity, and attitude represent the output. The integration of the differential equations is performed using the *mechanization equations*, which are not discussed here.

6.2.2.2 Error Equations

Although the equations of motion relate the input and outputs of an INS, it is generally more interesting to look at the corresponding error equations. The error equations are obtained by *perturbing*, or *linearizing*, the equations of motion and are given, again without derivation, by:

$$\frac{d\delta\mathbf{p}^n}{dt} = \mathbf{T}' \cdot \delta\mathbf{p}^n + \mathbf{T} \cdot \delta\mathbf{v}^n \quad (4)$$

$$\frac{d\delta\mathbf{v}^n}{dt} = -(\mathbf{R}_b^n \mathbf{f}^b) \times \boldsymbol{\varepsilon}^n + (2\boldsymbol{\Omega}_{ie}^n + \boldsymbol{\Omega}_{en}^n) \delta\mathbf{v}^n + \mathbf{v}^n \times (2\delta\boldsymbol{\omega}_{ie}^n + \delta\boldsymbol{\omega}_{en}^n) + \delta\mathbf{g}^n + \mathbf{R}_b^n \delta\mathbf{f}^b \quad (5)$$

$$\frac{d\boldsymbol{\varepsilon}^n}{dt} = \boldsymbol{\omega}_{in}^n \times \boldsymbol{\varepsilon}^n - \delta\boldsymbol{\omega}_{in}^n + \mathbf{R}_b^n \delta\boldsymbol{\omega}_{ib}^b \quad (6)$$

where a δ in front of a quantity indicates the error in that quantity, ε is the attitude error, T' relates the position errors to their time derivatives, and the other terms are as described above. Of key importance to this report are the rightmost terms in equations (5) and (6), which contain the accelerometer (δf^b) and gyro ($\delta \omega_{ib}^b$) measurement errors, respectively. As can be seen, these errors directly contribute to the INS velocity and attitude errors respectively (and indirectly to all system errors). Recalling Section 6.2.1.4, it should now be clear why the quality of the inertial sensors is so important in defining the accuracy of the system. In particular, when GNSS data is available, the INS errors (including the IMU errors) can be effectively “calibrated” using the methods described in Section 6.2.3. However, once GNSS data is absent, the error growth of the INS is determined entirely from equations (4) to (6), of which the primary contributors are the sensor errors. As such, the smaller the variability of the errors (relative to when they were last “calibrated” using GNSS data), the better the error behavior will be.

It is also noted that the first term in equation (5) contains the true (but unknown) specific force vector. This means that the level of dynamics (i.e., accelerations) of the vehicle also has an impact on system performance in the absence of GNSS, with larger dynamics resulting in larger error growth.

From the above, to minimize *free-inertial* error of the INS (i.e., the error in the absence of GNSS data), the IMU sensor errors should be small, and the dynamics in the absence of GNSS should be low. Furthermore, the position, velocity, and attitude errors should be small prior to losing GNSS data. The extent to which this is possible will depend on the quality and frequency of the GNSS measurements used in the GNSS/INS integration and on the method of integration, as discussed in Section 6.2.3.

6.2.2.3 Other Sensor Configurations

Before continuing, it is also worth noting that considerable research has been directed at using less than a full IMU configuration of accelerometers and gyros (i.e., two triads of each). The motivation for these “reduced IMUs” is to reduce system cost at the expense of not measuring certain vehicle dynamics. However, if certain vehicle motions are not significant (e.g., roll and pitch in automotive applications), then this tradeoff may be justified, as very little information is being omitted.

Although some results obtained using reduced IMUs are discussed in Section 6.3, the details of how to implement these systems are not presented here. Suffice it to say, however, that the equations above can be modified using the appropriate assumptions to yield the relevant equations. For more details on reduced IMU systems refer, for example, to Daum, et al. (1994), Brandt & Gardner (1998), Phuyal (2004), Niu, et al. (2006), Niu, et al. (2007), Syed, et al. (2007), or Sun, et al. (2008).

6.2.3 Integration of GNSS and INS

As mentioned above, the complementary characteristics of GNSS and INS make each well suited for integration. This section discusses the main methods and considerations associated with this integration.

6.2.3.1 Integration Architectures

The concept of GNSS/INS integration is illustrated in Figure 17. As shown, the GNSS receiver and the INS are each capable of generating their own navigation solutions. However, the idea is to combine data from both systems using the “Integration Algorithm” in order to generate a hybrid solution.

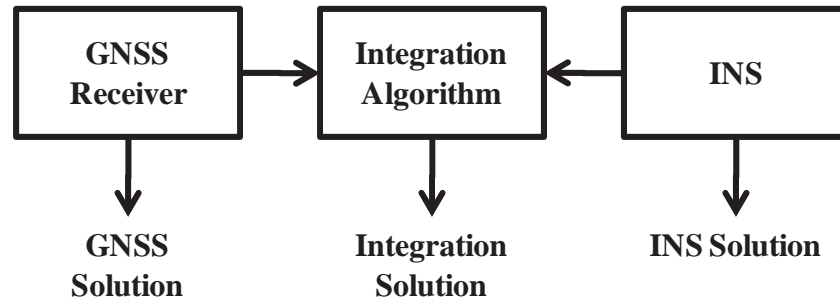


Figure 17: Concept of GNSS/INS Integration

The type of information shared between the GNSS receiver and the INS dictates the type of integration or integration architecture. There are basically three integration architectures, of which the following two are the most common (e.g., Greenspan 1994; Jekeli 2000; Petovello 2003b; Petovello, et al. 2003; Gebre-Egziabher 2007):

- *Loose integration* combines the GNSS and INS data at the position and velocity level. Although relatively simple to implement, this approach tends to exhibit poorer performance when a standalone GNSS solution cannot be computed.
- *Tight integration* combines the GNSS measurements (pseudoranges, carrier phases, and Dopplers) with the INS solution. This approach offers a good tradeoff between complexity and performance. Unlike with loose integration, a tight integration approach still allows the INS to be updated even when a standalone GNSS solution is unavailable due to lack of satellite visibility. As such, the tight integration approach tends to outperform the loose integration approach.

It is noted that some variants on the above terms/definitions are present in the literature. Regardless of the various naming conventions, however, the underlying principles are the same. Of the above two approaches, the tight integration is arguably more popular. As shown in Petovello (2003b) and Petovello, et al. (2003), the differences between the two approaches are negligible as long as GNSS data is available. However, in GNSS-denied areas, the tight integration offers better performance, with larger improvements being realized the longer GNSS data is unavailable.

In addition to the above two approaches, with the recent advent of software-defined receivers (see e.g., Borre et al 2007; Morton 2007; Scott 2007), attention has recently been given to ultra-tight (or deep) integration approaches. In this case, the INS mechanization equations are directly implemented within the tracking loops of the GNSS receiver. The two sensors, therefore, no longer operate independently of each other but rather the GNSS data is used to compensate the IMU errors and the integrated solution is used to help track the GNSS signals, particularly in the presence of high vehicle dynamics and/or interference. Ultra-tight integration strategies are not currently

commercially available and will, therefore, not be discussed further in this report. However, it is noted that ultra-tight integrations have recently been shown to offer superior carrier phase tracking performance than a “standard” GNSS receiver (O’Driscoll, et al. 2008; Petovello, et al. 2008). For more information, refer, for example, to Oppenheim, et al. (1999); Gustafson, et al. (2000); Abbott & Lillo (2003); Gustafson & Dowdle (2003); Kim, et al. (2003); Jovancevic, et al. (2004); Soloviev, et al. (2004b; 2004a); Pany, et al. (2005); Kim, et al. (2006); Groves, et al. (2007); Petovello, et al. (2007); O’Driscoll, et al. (2008); and Petovello, et al. (2008).

6.2.3.2 Integration Algorithms

Once the integration architecture is defined, the algorithm used to fuse the GNSS and INS data together must be decided (i.e., the middle box in Figure 17). The Extended Kalman Filter (EKF) is by far the most widely used algorithm used in the literature. The EKF offers an efficient and flexible implementation that suits the GNSS/INS integration problem very well, especially since the filter’s basic system model is given by equations (4) to (6) above. Details regarding Kalman filtering are available, for example, in Gelb (1974), Brown & Hwang (1992), Minkler & Minkler (1993), Maybeck 1994, and Grewal & Andrews (2008). For details on how to implement a Kalman filter for GNSS/INS integration, refer to Cannon (Cannon 1991) or Petovello (Petovello 2003b).

Other integration algorithms have also recently been proposed including the Linearized Kalman Filter (LKF) (Nassar, et al. 2005), the Unscented Kalman Filter (UKF) (Nassar, et al. 2005; Yi and Grejner-Brzezinska 2006), the Sigma Point Kalman Filter (SPKF) (Wendel, et al. 2005) and variants of the Particle Filter (PF) (Aggarwal, et al. 2006; Aggarwal 2008), to name a few. With the exception of the LKF, all other methods are based on Bayesian estimation techniques which do not assume Gaussian error distributions. These same methods are also better able to deal with non-linearities in the system model. It is noted, however, that the non-linearities in GNSS/INS systems are generally fairly small, except with very low cost MEMS sensors, and even then usually only during system initialization. As such, these approaches do not always provide significant benefits (Wendel, et al. 2005; Yi and Grejner-Brzezinska 2006). Given the relatively low use rate of these filters in the literature, their limited benefits, and their added complexity (although not necessarily computational burden), these filters are not discussed in detail in this report.

6.2.3.3 System Models

As mentioned earlier, the basic system model for any Kalman filter implementation is given by equations (4) to (6). In addition to this, however, models for the IMU sensor errors, that is, $\delta \mathbf{f}^b$ and $\delta \boldsymbol{\omega}_{ib}^b$, need to be developed. Unfortunately, there is no hard and fast rule for this process. Instead, the models will ultimately tradeoff veracity, computational efficiency, observability, and practical performance. Furthermore, all of these will likely be affected by the quality of IMU and the application under consideration. For example, a MEMS-based INS generally performs better if the scale factor and initial bias errors are estimated (Godha and Cannon 2005a). For high dynamics applications, however, scale factor errors may also have to be estimated for higher quality IMUs as well. System developers need to carefully design their filter to optimize performance according to their specific criteria.

6.2.3.4 Extra Aiding Information

Before discussing results presented in the literature, it is worth noting that other sources of aiding can sometimes be incorporated into the system for little or no cost. Three such aiding sources are discussed here. First, a barometer can be used to control the height component of the navigation solution (Lachapelle, et al. 2003), assuming all systematic errors are accounted for (e.g., Garin, et al. 2008). Although this can greatly improve the GNSS navigation solution in the horizontal and vertical directions (Lachapelle, et al. 2003), it does not directly influence the horizontal components of the INS solution (Gebre-Egziabher 2004). However, in an integrated system, the improved GNSS solution has been shown to have a positive effect on the overall system accuracy, especially in the absence of GNSS data (Godha and Cannon 2005a; Godha, et al. 2005), because the improved GNSS solutions are better able to calibrate the INS errors. Second, zero velocity updates (ZUPTs) can be used to effectively provide additional information to the system, assuming the stopping condition can be accurately and reliably identified. Third, non-holonomic constraints (NHCs) assume the vehicle travels along its longitudinal axis only. By enforcing zero accelerations in the lateral and vertical channels, improved performance can be obtained (Godha and Cannon 2005b; Godha and Cannon 2005a; Niu and El-Sheimy 2005; Syed, et al. 2007). Closely related to NHC is the use of an odometer (or wheel speed sensor) to also measure the longitudinal velocity. This approach is well suited to vehicles with anti-lock braking systems.

6.3 Review of Published Results

This section presents a summary of the key results quoted in the literature. Results are presented assuming real-time processing. In other words, the benefits of backward smoothing (Gelb 1974; Brown and Hwang 1992; Minkler and Minkler 1993; Maybeck 1994; Hide, et al. 2006; Grewal and Andrews 2008) or near real-time processing (e.g., Nassar and Schwarz 2001) are not addressed.

Given the breadth of GNSS/INS research, it is impossible to summarize all work in the literature (as an example, a search for “INS” on the U.S. Institute of Navigation (ION) website turned up over 300 papers and a search for “inertial navigation” on the IEEE Explore website turned up over 500 more). Instead, the results presented below are, in the authors’ expert opinion, a representative subset of the work that relates (directly or otherwise) to the field of vehicular navigation. Results are categorized as follows, with more attention given to the latter two categories because of their relevance to context of this work:

- Results with navigation-grade IMUs
- Results with tactical-grade IMUs
- Results with automotive-grade IMUs (i.e., MEMS)
- Results with reduced IMUs

All of the main results are presented in tabular form on pages 39 to 45, with additional information provided in the text to highlight key points. Furthermore, as needed, the various sections are augmented with references that are also relevant to this report such as

the effect of height aiding (e.g., from a barometer) or the effect of ZUPTs or other velocity constraints.

Unless otherwise stated, all IMU specifications refer to the turn-on bias stability, not the in-run stability. That said, it should be noted that IMU specifications are *not* guaranteed and differences, in some cases significant, will occur from unit to unit. Some care should, therefore, be taken when interpreting and comparing the results between citations.

6.3.1.1 Results with Navigation-Grade IMU

Results obtained with navigation-grade IMUs are summarized in Table 5. Given the quality of the IMU, the desired accuracy for these studies is at the cm-level. Nevertheless, results give initial impressions regarding the degradation of position accuracy in the absence of GNSS data. In Nassar & Schwarz (2001) different integration algorithms showed a slight improvement in the mean error when using a UKF, but given that the standard deviations of the different solutions are at the 40-55 cm level, these differences are not considered statistically significant.

6.3.1.2 Results with Tactical-Grade IMUs

Table 6 summarizes the results obtained with tactical-grade IMUs. Overall, the results are highly compatible, as should be expected with the relatively good sensors involved.

In Scherzinger (2000) and Petovello, et al. (2003) partial GPS coverage was shown to provide a considerable improvement in positioning accuracy. This illustrates the benefit of the tight integration approach, since in the same environment a loose integration would not be able to compute a GPS-only solution.

In Ford, et al. (2001b), the benefits of ZUPTs are also demonstrated. It is noted, however, that detection of zero velocity conditions is not necessarily trivial; and incorrectly identifying a ZUPT will cause large systematic errors to enter the system.

6.3.1.3 Results with Automotive-Grade IMUs

Results obtained using automotive-grade IMUs are summarized in Table 7. There are three things worth noting. First, the inclusion of a barometer does not significantly improve the overall positioning accuracy (Godha and Cannon 2005b; Godha, et al. 2005; Grejner-Brzezinska, et al. 2006). This is understandable since, in the short term, free-inertial errors are generally larger in the horizontal channel than in the vertical channel. Furthermore, since a barometer has very limited benefit to the horizontal channel in the absence of GNSS data (Gebre-Egziabher 2004), little overall benefit should be expected. Second, NHCs and odometer (or wheel pick-off) data provide an effective means of limiting error growth in vehicular applications (Ford, et al. 2004; Godha and Cannon 2005b; Niu and El-Sheimy 2005). Fortunately, the NHC requires no additional sensors, but can cause problems during turns when the underlying assumptions no longer apply. In this case, the vehicle's side slip angle has to be modeled or calculated (Gao, et al. 2007). Third, compared with the higher grade inertial units, there appears to be a larger difference in positioning performance depending on the integration algorithm used (Nassar, et al. 2005). In particular, the poor results of the LKF are the result of the feed-forward implementation, which, for low-cost IMUs, does not satisfy the inherent assumptions of the system model. That said there does not appear to be a major advantage to using a UKF over and EKF.

In addition to the citations included in Table 7, the following studies are also worth mentioning:

- When GNSS is available, the accuracy of the integrated solutions are commensurate with the quality of GNSS data provided (Wolf, et al. 1997; Farrell, et al. 2000; Yang, et al. 2000). In other words, in ideal GNSS conditions, the inertial sensors provide little, if any, accuracy benefits and serves mainly as an “interpolator” of the GNSS data.
- In Godha & Cannon (2005a), no GPS outages are simulated, but it is shown that estimation of the scale factor errors is important for MEMS-grade sensors, both during turns (even if GPS data is available) and in the absence of GNSS data. For the latter case, inclusion of the scale factor errors provides a 55 percent accuracy improvement over 30 s. Furthermore, when the scale factor estimation and NHC are combined, the positioning results are 80 percent better than when neither is used.
- Bird & Arden (2003) conducted a series of simulations to assess the positioning performance of different combinations of IMU quality (1, 100 and 3600 deg/h gyro) and GPS updates (position and/or velocity updates at 0.1 Hz or 1 Hz). Although a full recap of the results is beyond the scope of this report, the key findings were as follows (their application objective was 1 m position accuracy over 600 s):
 - A high accuracy IMU could meet the system requirements using position and velocity updates at either rate.
 - A medium accuracy IMU could meet the system requirements using position and velocity updates using only 1 Hz update (not with 0.1 Hz updates).
 - A high accuracy IMU with only velocity updates was close to meeting the 1 m requirement.
 - A medium accuracy IMU with low rate (0.1 Hz) position and velocity updates were close to meeting the requirements.

It is noted, however, that being based on simulations, the above results are likely optimistic. Nevertheless, they give a good idea as to some of the tradeoffs between IMU quality, GPS measurement quality and frequency, and positioning accuracy.

6.3.1.4 Results with Reduced IMUs

Table 8 summarizes the results obtained using reduced IMU configurations. All of the results presented involve low-cost sensors and, given the elimination of some of the IMU sensors, the error growth is more rapid than presented in the previous section. As before, however, the use of the NHC and/or odometer helps to dramatically reduce the positioning errors (Niu, et al. 2006; Syed, et al. 2007).

Table 5: Summary of Results with Navigation-Grade IMUs

Citation	IMU Biases	System Updates	Comments/Notes
Schwarz, et al. (1994b)	Accel: 5 μg (1σ) Gyro: 0.01 deg/h (1σ)	• Real-time kinematic (RTK)	• Free-inertial 3D position error of 10 cm after 30 s without GPS data.
Kumagai, et al. (2000)	Accel: 80 μg (1σ) Gyro: 0.03 deg/h (1σ)	• DGPS	• Free-inertial horizontal position error of approximately 10 m after 3 min without GPS data but with a wheel encoder (odometer).
Nassar & Schwarz (2001)	Accel: 30 μg (1σ) Gyro: 0.0035 deg/hr (1σ)	• DGPS	• Mean 3D position error over 60 s was 0.85 m, 0.75 m and 0.60 m using LKF, EKF, and UKF, respectively.

Table 6: Summary of Results with Tactical-Grade IMUs

Citation	IMU Biases	System Updates	Comments/Notes
Scherzinger (2000)	Accel: 0.5 mg Gyro: 3 deg/h	<ul style="list-style-type: none"> • RTK GPS 	<ul style="list-style-type: none"> • During full GPS outages, horizontal position error standard deviations were 0.1 m over 10 s, 0.5 m over 30 s, and 1.8 m over 60 s. • With only three GPS satellites visible, the horizontal position error standard deviations were 0.1 m, 0.25 m and 0.3 m over 10, 30 and 60 s, respectively.
Scherzinger (2001)	Accel: 1.5 mg Gyro: 3 deg/h	<ul style="list-style-type: none"> • Dual-frequency RTK • Odometer was also used 	<ul style="list-style-type: none"> • RMS horizontal position errors ranged from 0.1 m over 10 s to 1.4 m over 120 s, and even as high as 6.0 m over 600 s.
Ford, et al. (2001a)	Accel: 1 mg Gyro: 1 deg/h	<ul style="list-style-type: none"> • GPS RTK 	<ul style="list-style-type: none"> • Approximately 0.2 m RMS position errors (north and east) after 10 s GPS outage, and approximately 10-23 m over a 20 s outage.
Ford, et al. (2001b)	Accel: 1 mg Gyro: 1 deg/h	<ul style="list-style-type: none"> • GPS RTK 	<ul style="list-style-type: none"> • RMS free-inertial position error with ZUPTs was 0.22 m, 0.29 m, and 0.17 m in the north, east, and vertical directions, respectively after 30 s. After 120 s, the same values were 0.41 m, 0.39 m, and 0.34 m. • Without ZUPTs, the above errors increase to 0.29 m, 0.35 m, and 0.17 m after 30 s, and 0.53 m, 0.49 m, and 0.70 m after 120 s.
Petovello, et al. (2003)	Accel: 1 mg Gyro: 1 deg/h	<ul style="list-style-type: none"> • GPS RTK 	<ul style="list-style-type: none"> • Using a tight integration during complete GPS outages, the RMS horizontal position errors were 20 cm after 10 s and increased to 2.15 m after 40 s; 3D errors were only slightly worse. • During partial GPS outages (2-3 satellites visible), the RMS 3D position errors were reduced to ≤ 15 cm after 10 s and 1 m after

Citation	IMU Biases	System Updates	Comments/Notes
			40 s. <ul style="list-style-type: none"> • The above results are for L1 carrier phase data. Slightly worse performance was obtained when using the wide-lane linear combination. • Using a loose integration architecture, slightly worse results than above were achieved.
Nassar, et al. (2005)	Accel: 1 mg Gyro: 1 deg/h	<ul style="list-style-type: none"> • DGPS 	<ul style="list-style-type: none"> • Mean 3D position error after 60 s ranged from 1.7-3.0 m, depending on the integration algorithm (LKF was best, then EKF, then UKF).

Table 7: Summary of Results with Automotive-Grade IMUs

Citation	IMU Biases	System Updates	Comments/Notes
Salychev & Voronov (2000)	Accel: <12.5 mg Gyro: <2 deg/s (7200 deg/h)	<ul style="list-style-type: none"> Differential GPS and GLONASS 	<ul style="list-style-type: none"> Free-inertial RMS position errors were 3 m and 10 m over 30 s with constant and high vehicle dynamics, respectively. Over 20 s, the RMS errors were 10 m and 23 m, respectively.
Ford, et al. (2004)	Accel: 10 mg Gyro: 100 deg/h	<ul style="list-style-type: none"> DPGS with carrier smoothing in the position domain 	<ul style="list-style-type: none"> Free-inertial RMS position errors during 10 s of complete GPS outage were: <ul style="list-style-type: none"> 0.48 m, 0.38 m and 0.21 m in the north, east, and vertical directions, respectively. 0.43 m, 0.35 m, and 0.21 m in the north, east, and vertical directions, respectively, if the IMU misalignments and scale factors were estimated. Inclusion of wheel pick-off data improves results by an average of 30 percent in each coordinate direction.
Godha & Cannon (2005b)	Accel: 30 mg Gyro: 5400 deg/h	<ul style="list-style-type: none"> DGPS in urban canyon 	<ul style="list-style-type: none"> Horizontal RMS errors in urban canyon were: <ul style="list-style-type: none"> INS only: 5.66 m INS + Height constraint: 4.60 m INS + NHC: 3.71 m INS + Height constraint + NHC: 3.37 m
Godha, et al. (2005)	Accel: 30 mg Gyro: 5400 deg/h	<ul style="list-style-type: none"> High-sensitivity GPS Magnetometer (simulated) 	<ul style="list-style-type: none"> Horizontal RMS errors in urban canyon were: <ul style="list-style-type: none"> INS only: 16.9 m INT + Heading: 14.1 m INS + Height constraint: 12.2 m INS + Heading + Height constraint: 7.30 m
Nassar, et al.	Accel: 0.2	<ul style="list-style-type: none"> DGPS 	<ul style="list-style-type: none"> Mean 3D position error after 60 s

Citation	IMU Biases	System Updates	Comments/Notes
(2005)	mg Gyro: 0.01 deg/h		of 3071.2 m, 164.9 m, and 198.5 m using an LKF, EKF, and UKF, respectively.
Niu & El-Sheimy (2005)	Accel: 0.2 mg Gyro: 0.01 deg/s	• GPS RTK	• Mean free-inertial position error after 30 s of 28.3 m with INS alone, 10.9 m with NHC, and 3.3 m with NHC and an odometer.
Mather, et al. (2006)	Accel: N/A Gyro: 100 deg/h	• High-sensitivity GPS	• No GPS outages included. • ZUPTs are shown to reset position error to 1 m for static tests, and roughly 20 m for a simulated kinematic test. • Height error with barometer is limited only by the barometer; no impact on horizontal error.
Grejner-Brzezinska, et al. (2006)	Accel: 8.5 mg Gyro: 1 deg/s	• RTK	• Free-inertial position errors in north, east, and vertical directions of: ○ 66.9 m, 334.6 m, and 72.1 m over 30 s ○ 2472.7 m, 6542.0 m, and 1331.4 over 120 s • If a calibrated barometer and a compass are added, the results are: ○ 476.7 m, 93.8 m, and 11.3 m over 30 s • 3038.4 m, 673.3 m, and 4.8 m over 120 s

Table 8: Summary of Results with Reduced IMUs

Citation	IMU Biases	System Updates	Comments/Notes
Daum, et al. (1994)	Accel: 1 mg Gyro: 1 deg/h	• None	• Using 2 accelerometers and 1 gyro, an accuracy of 1-2.2 percent of distance traveled was demonstrated.
Syed, et al. (2007)	Accel: 0.2 mg Gyro: 0.01 deg/h	• GPS positions	<ul style="list-style-type: none"> • Considered different number of accelerometers (A) and gyros (G) with full outages. Mean errors over 60 s were (without/with NHC): <ul style="list-style-type: none"> ○ Full: 238.5 m / 62.8 m ○ 2G3A: 412.1 m / 96.3 m ○ 1G3A: 485.9 m / 110.1 m ○ 1G2A: 485.1 m / 89.9 m ○ 1G1A: 807.8 m / 439.8 m ○ 1G0A: 1042.4 m / 447.3 m
Niu, et al. (2006)	Accel: 0.2 mg Gyro: 0.01 deg/h	• SP GPS	<ul style="list-style-type: none"> • RMS position errors over a 30 s GPS outage were (full IMU/Reduced IMU consisting of 2 accelerometers and 1 gyro): <ul style="list-style-type: none"> ○ INS only: 29.8 m / 71.6 m ○ INS + NHC: 16.9 m / 22.2 m ○ INS + NHC + odometer: 6.5 m / 9.2 m
Sun, et al. (2008)	Accel: 30 mg Gyro: 5400 deg/h	• SP GPS	<ul style="list-style-type: none"> • Develops a “terrain predictor” to account of the effect of non-level terrain on systems with 2 or 3 accelerometers and 1 gyro. • Over 30 s GPS outages, the RMS horizontal position errors were (with/without terrain model): <ul style="list-style-type: none"> ○ 2A1G: 103 m / 220 m ○ 3A1G: 103 m / 221 m

7 Impact of Future GNSS and GPS Modernization

GPS modernization was described in Section 3.3. In addition to the new civil signals being deployed on GPS, several other countries and regions are developing their own global satellite navigation systems. Russia has revitalized its GNSS GLONASS constellation with a massive replenishment program. Currently, 18 satellites are operational and a further two are down for maintenance. All of the 18 operational satellites have been launched since 2005 (RSA 2009). The European Union (EU) is continuing to develop its Galileo GNSS, with two validation satellites currently in orbit; and China is developing its own GNSS, named Compass. Each system and its impact will be reviewed below. While each system is slightly different, if and when all of them are fully operational, there will be on the order of 120 navigation satellites in orbit, each broadcasting civil signals on two or three frequencies, compared to the current 49 satellites transmitting civil signals on 1 or 2 frequencies. The major implication of this is that civil users will have roughly 2.5 times as many satellites and 3 times as many signals to use in order to obtain a navigation solution.

7.1 Impact of New GPS Signals

GPS modernization will have a major effect on civil users (McDonald and Hegarty 2000). First, with the addition of L2C, it will become possible for low cost, dual frequency receivers to be deployed where presently dual frequency civil users of GPS are limited to surveying, geodetic, and scientific users with access to expensive codeless and semi-codeless receivers. The availability of this second signal will allow low cost users to form ionosphere-free observation combinations as well as form the wide-lane phase combination which is essential to RTK operation over long baselines. L2C also contains a data bit free pilot channel, which allows for improved signal acquisition in difficult environments including under foliage and indoors. L5, which will be added next, will provide a higher bandwidth and thus higher resolution pseudorange measurement and allow for improved ionosphere estimation and enable the formation of “extra-wide-lane” phase combinations (L2-L5). The combination of the higher accuracy pseudorange and the extra-wide-lane will in principle allow for instantaneous (single-epoch) ambiguity resolution on short baselines where currently the solution must be estimated over several minutes. Several methods to exploit three frequencies for ambiguity resolution have been proposed and developed (Jung, et al. 2000; Teunissen, et al. 2002; Werner and Winkel 2003; Zhang, et al. 2003; Cocard, et al. 2008; O’Keefe, et al. 2009).

7.2 Potential Use of Galileo, GLONASS, and COMPASS

The development of three additional GNSS: GLONASS, Galileo, and Compass will provide users with a GNSS constellation of up to 120 satellites with typical satellite availabilities of 40 to 48 satellites. The additional positioning geometry provided by these satellites will mean significantly lower HDOP values and improved accuracies. Each of these satellites will be transmitting up to three civil signals. There is the potential for more than 100 signals to be available to a typical civil user at any given time compared to the current 10 typically available for a L1 GPS C/A user. The advantages of employing

these signals will have to be carefully weighed against the increased receiver complexity required to acquire and track them.

Of the three GNSS currently in development, Galileo promises to be the easiest to integrate with GPS. Two of the three proposed Galileo frequencies are common with GPS L1 and L5, thus minimizing the required additional antenna and front-end hardware (HW) required. GLONASS is more problematic as it operates using a Frequency Division Multiple Access (FDMA) scheme (Takac 2009). GPS/GLONASS integration is currently used commercially in surveying applications. The main advantage of this integration is in terms of ambiguity resolution time, particularly in partially masked environments.

The effect of GPS and Galileo integration for code-based positioning has been studied by O'Keefe (2001) and many others. The general conclusion of all of these studies is that additional satellites will result in improved dilution of precision and, therefore, improved positioning accuracy.

The effect of GPS/Galileo integration for carrier phase (RTK) positioning has also been studied extensively, mainly in the context of triple-carrier-ambiguity-resolution algorithms (Lachapelle, et al. 2002; Julien, et al. 2003; Leonard, et al. 2003; Julien, et al. 2004; O'Keefe, et al. 2004; Feng and Rizos 2005; Fernández-Plazaola, et al. 2007; Ji, et al. 2007; Cao, et al. 2008b; O'Keefe, et al. 2009). The main conclusion of all of these papers is that the additional signals and satellites provided by using two systems will greatly improve ambiguity resolution time and ambiguity resolution reliability. Particularly the addition of the third frequency which is a feature of both modernized GPS and Galileo will enable almost instantaneous ambiguity resolution due to the presence of a precise pseudorange on the L5 signal and the ability to form an extra-wide-lane phase combination.

Recently, Cao, et al. (2008b) assessed the carrier phase ambiguity resolution performance of various combinations of GPS and Galileo signals. Table 9 shows the time to first fix, percent correct fix, percent incorrect fix, and percent no fix (ambiguity resolution failure) obtained on a simulated 1 km baseline with various combinations of the three common frequencies that will be available on modernized GPS and Galileo (L1, L2, and L5, which are called E1 and E5a in Galileo). In addition to the obvious results that show adding signals and systems leads to improved performance, there are two important results. First, on a short baseline like this, a dual-frequency dual-system receiver will outperform a triple frequency GPS-only receiver in terms of time to first fix (Scenarios D and F in Table 9) though in both cases ambiguity resolution will be almost instantaneous. Secondly, and more importantly for mass market applications, a single frequency dual-system receiver will outperform a dual frequency receiver (Scenarios B and C compared with E). This is very promising for mass market applications since a dual-system GPS/Galileo L1 receiver would require only one antenna and RF-front-end and simply need changes to the signal processing stage of the receiver, yet would perform considerably better than a GPS-alone system provided the baselines are short. The additional frequencies are more valuable on longer baselines where residual ionospheric error begins to become the limiting error source.

Table 9: Comparison of GPS and Galileo Ambiguity Resolution over a 1 KM Baseline (from Cao, et al. 2008b).

(MTTFF, PCF, PIF, and PNF stand for Mean Time to First Fix, Percent Correct Fix, Percent Incorrect Fix, and Percent No Fix, respectively. The measurements column indicates what observables were considered with L1, L2, and L5 representing the three GPS-phase observables and E1 and E5a the two Galileo signals that share carrier frequencies with L1 and L5, respectively.)

Scenario	Measurements	MTTFF	PCF (%)	PIF (%)	PNF (%)
A	L1	63.8	90	8.75	1.25
B	L1, L2	8.1	100	0	0
C	L1, L5	13.1	98.75	1.25	0
D	L1, L2, L5	3.4	100	0	0
E	L1, E1	3.3	98.75	1.25	0
F	L1, E1, L5, E5a	2.0	100	0	0

Very little public information about the Chinese Compass system is presently available. However, some preliminary work has been done to assess the affect of integrating this system with GPS for carrier phase applications. It is expected that the Compass system will be quite similar to the Galileo system, and thus, its usefulness for GPS augmentation will be similar (Cao, et al. 2008a).

7.2.1 Additional GNSS Constellations

GPS positioning performance can be significantly improved with the addition of signals from other GNSS. Presently the only other operational GNSS is the GLONASS system. The design GLONASS constellation consists of 24 satellites in three 64.8 degree inclined orbital planes that broadcast L1 and L2 signals. The number of GLONASS satellites has varied widely over the past 10 years between as few as 8 and as many as 20. The European Union is developing a GNSS called Galileo. Currently only two test satellites are in orbit; however, the planned constellation calls for 30 satellites in three 55 degree inclined planes. China is also developing a GNSS called Compass, very similarly to Galileo, that will also consist of 30 satellites in 3 inclined planes. The orbital characteristics of all four systems are well described in Van Diggelen (2009).

All of these systems propose to broadcast at least one civil signal near the L1 band, meaning that a single frequency receiver, or at least a single RF-front-end receiving signal from a number of systems with similar frequencies, could simultaneously track satellites from four different GNSS. In this situation, two different approaches could be taken. Either independent solutions could be computed from each system and checked against each other, or observations from all of the systems could be combined to estimate one solution. This second approach is particularly useful in urban canyon environments where it is possible that one system alone would not provide enough visible satellites, but two or more systems would. Combining observations from multiple systems requires some care to ensure that each system is operating on the same time scale and coordinate

system, or that intersystem correction values are available. These are planned for the Galileo navigation message but are not currently available in real time for GLONASS.

To demonstrate the effect of adding satellites from additional systems, median and 95th percentile values of HDOP has been computed over part of North America using the as-designed constellations for GPS, Galileo, GLONASS, and Compass. In this simulation, the effect of inter-system clock bias has been neglected and several proposed geostationary satellites in the Compass system have not been considered as well. GPS and GLONASS are assumed to have 24 satellites each, and Galileo and Compass 30 each. Figure 18, Figure 19, Figure 20, and Figure 21 are maps of 95th percentile HDOP for the GPS-only case and with the sequential addition of Galileo, GLONASS, and Compass, respectively. With only one GNSS, 5 percent of the time HDOP over North America would exceed 5, a relatively poor value, when a 20 degree elevation mask is used. The addition of a second GNSS reduces this value to around two for most of the continent, while the addition of a third and fourth GNSS further reduces the 95th percentile HDOP values to on the order of 1.5 and less than 1, respectively.

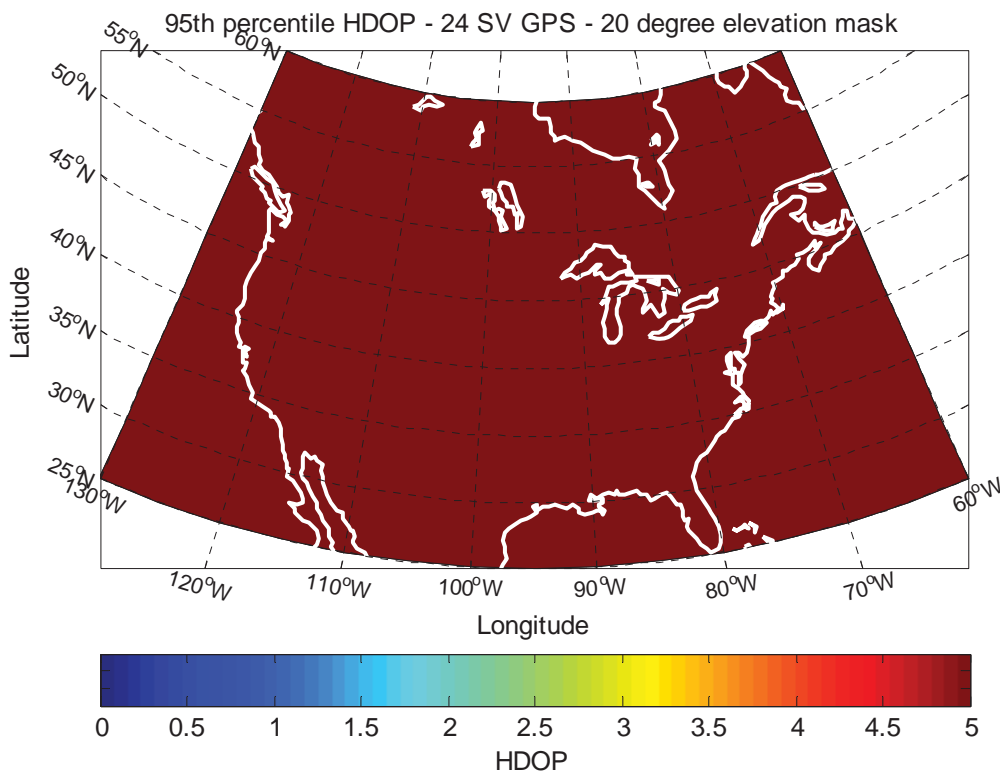


Figure 18: 95th Percentile HDOP Using a 24-Satellite GPS Constellation and a 20-Degree Elevation Mask

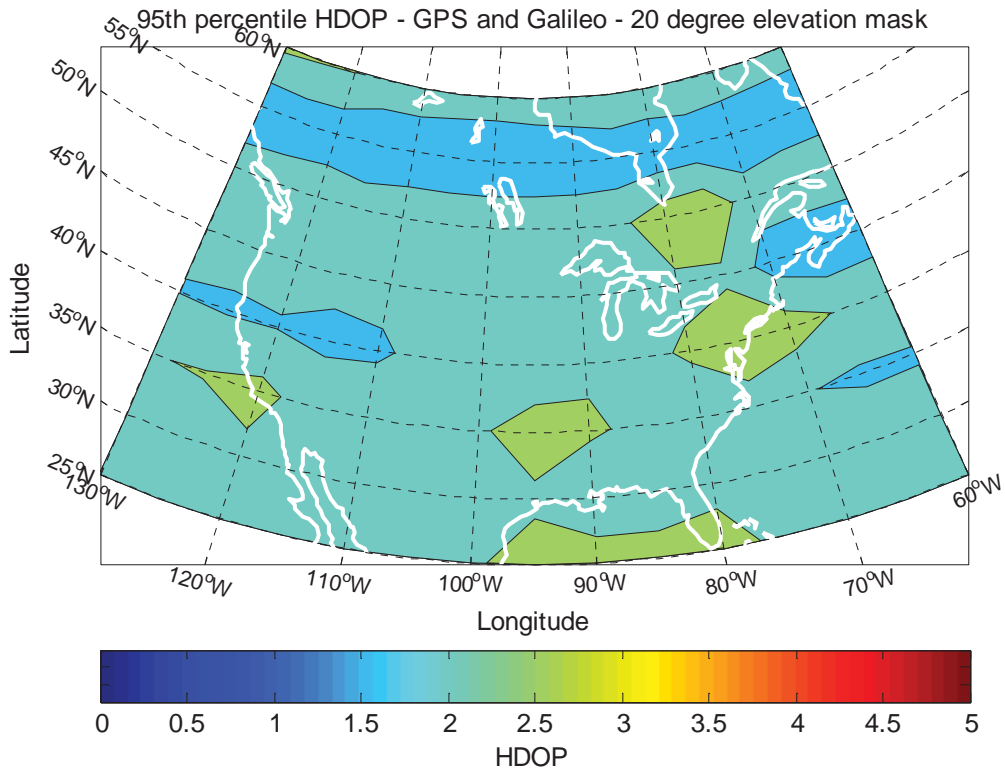


Figure 19: 95th Percentile HDOP Using a 24-Satellite GPS constellation in Conjunction with a 30-Satellite Galileo Constellation and a 20-Degree Elevation Mask

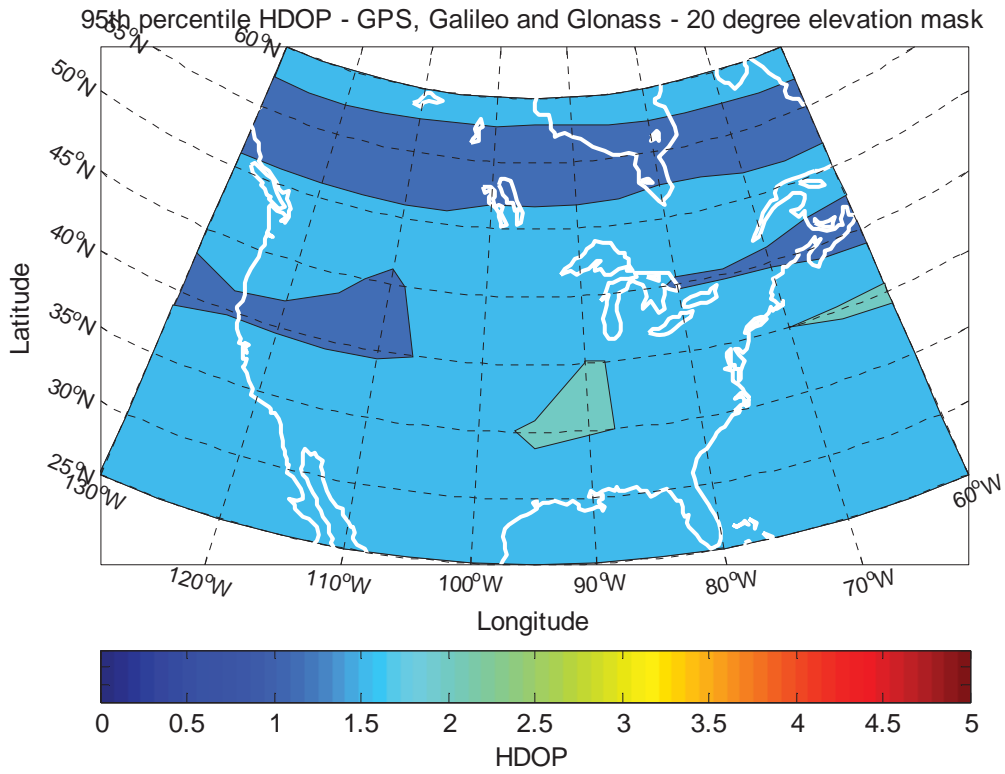


Figure 20: 95th Percentile HDOP Using GPS, Galileo, and GLONASS with a 20-Degree Elevation Mask

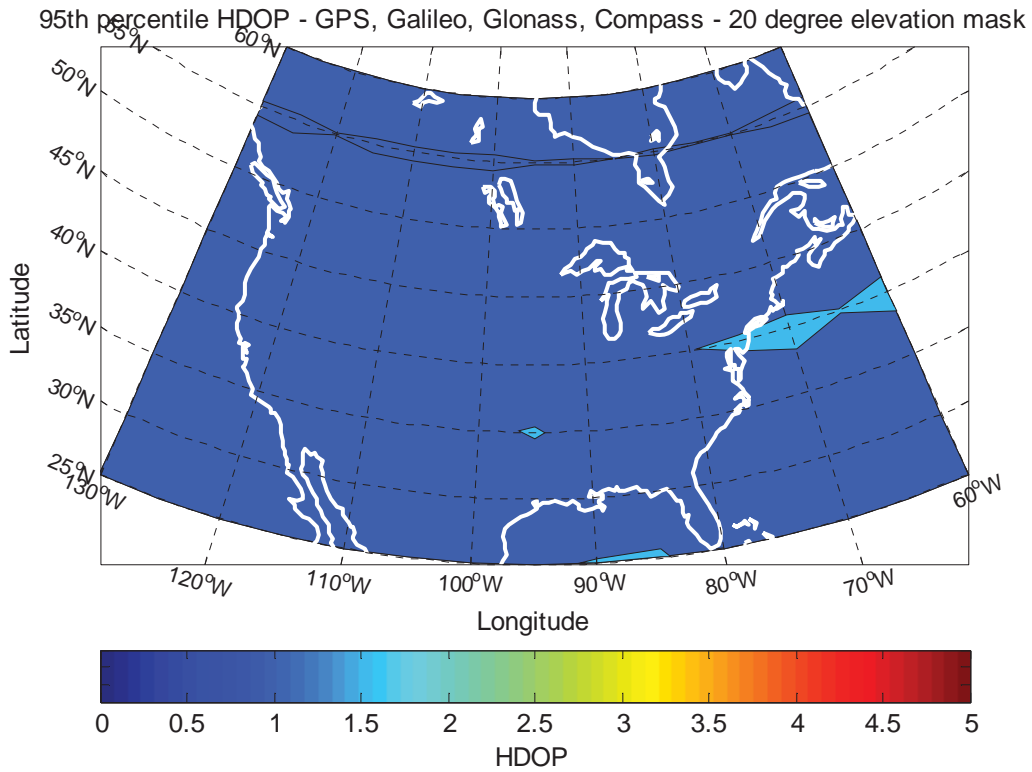


Figure 21: 95th Percentile HDOP Using GPS, Galileo, GLONASS, and Compass with a 20-Degree Elevation Mask

With a 24 satellite GPS and a 20-degree elevation mask, the typical satellite availability ranges between 5 and 8 satellites. Compare this to the 4 GNSS case where between 23 and 27 satellites are in view at all times.

8 References

- [1] Abbott, A. S. & W. E. Lillo (2003) Global Positioning Systems and Inertial Measuring Unit Ultratight Coupling Method. United States, The Aerospace Corporation: 22.
- [2] Aggarwal, P. (2008) Hybrid Extended Particle Filter (HEPF) for INS/GPS Integrated System. ION GNSS 2008, Savannah, GA, Institute of Navigation: 1600-1609.
- [3] Aggarwal, P., D. Gu & N. El-Sheimy (2006) Adaptive Particle Filter for INS/GPS Integration. ION GNSS 2006, Fort Worth, TX, Institute of Navigation: 1606-1613.
- [4] Alves (2005) *Development of Two Novel Carrier Phase-Based Methods for Multiple Reference Station Positioning*, PhD Thesis, Department of Geomatics Engineering, University of Calgary, Calgary
- [5] Bird, J. & D. Arden (2003) Simulation of Updating Requirements for MEMS-based Inertial Navigation. CASI 14th Symposium on Navigation, Montreal, QC, Canadian Aeronautics and Space Institute.
- [6] Borre, K., D. Akos, N. Bertelsen, P. Rinder & S. H. Jensen (2007) *A Software-Defined GPS and Galileo Receiver, A Single-Frequency Approach*, Birkhäuser, Boston.
- [7] Brandt, A. & J. F. Gardner (1998) Constrained Navigation Algorithms for Strapdown Inertial Navigation Systems with Reduced Set of Sensors. IEEE American Control Conference, Philadelphia, PA, IEEE: 1848-1852.
- [8] Brown, R. G. & P. Y. C. Hwang (1992) *Introduction to Random Signals and Applied Kalman Filtering*, John Wiley & Sons, Inc.
- [9] Cannon, M. E. (1991) *Airborne GPS/INS with an Application to Aerotriangulation*, Ph.D. Thesis, Geomatics Engineering, University of Calgary, Calgary
- [10] Cao, W., K. O'Keefe & M. E. Cannon (2008a) Evaluation of Compass Ambiguity Resolution Performance Using Geometric-Based Techniques with Comparison to GPS and Galileo. Proceedings of ION GNSS 2008, The Satellite Division of the Institute of Navigation 21th International Technical Meeting, September 16-19, Savannah, GA: 1688-1697.
- [11] Cao, W., K. O'Keefe & M. E. Cannon (2008b) Performance Evaluation of Combined GPS/Galileo Multi-frequency RTK Positioning Using Partial Ambiguity Fixing. Proceedings of ION GNSS 2008, The Satellite Division of the Institute of Navigation 21th International Technical Meeting, September 16-19, Savannah, GA: 2841-2849.
- [12] Chen, D. & G. Lachapelle (1995) "A Comparison of the FASF and Least-Squares Search Algorithms for Ambiguity Resolution On The Fly." *Navigation* 42(2): 371-390.
- [13] Cocard, M., S. Bourgon, O. Kamali & P. Collins (2008) "A Systematic Investigation of Optimal Carrier-phase Combinations for Modernized Triple-frequency GPS." *Journal of Geodesy* 82(9): 555-564.

- [14] Daum, P., J. Beyer & T. F. W. Kohler (1994) Aided Inertial LAnd NAvigation System (ILANA) with a Minimum Set of Inertial Sensors. IEEE-IEE Vehicle Navigation & Information Systems Conference, IEEE: 284-291.
- [15] de Jong, C. D., G. Lachapelle, S. Skone & I. A. Elema (2002) *Hydrography*, Delft University Press, Delft, The Netherlands.
- [16] de Jonge, P. & C. C. J. M. Tiberius (1996) The LAMBDA method for integer ambiguity estimation: implementation aspects. Publications of the Delft Geodetic Computing Centre.
- [17] DOD (1995) Global Positioning System Standard Positioning Service Signal Specification, 2nd Edition, Department of Defense.
- [18] DOD (2008) Global Positioning System Standard Positioning Service Performance Standard. U. Department of Defense, Assistant Secretary of Defense for Command, Control, Communications, and Intelligence.
- [19] Erickson, C. (1992) *Investigations of C/A Code and Carrier Measurements and Techniques for Rapid Static GPS Surveys*, MSc Thesis, Geomatics Engineering, University of Calgary, Calgary
- [20] FAA (2004) Wide-Area Augmentation System Performance Analysis Report, Report 11. F. A. Administration, NTSB/WAAS T&E Team.
- [21] FAA. (2007) "Wide Area Augmentation System WAAS, Fact Sheet."
- [22] Farrell, J. A., D. Givargis & M. J. Barth (2000) "Real-Time Differential Carrier Phase GPS-Aided INS." IEEE Transactions on Control Systems Technology 8(4): 709-721.
- [23] Feng, Y. & C. Rizos (2005) Three Carrier Approaches for Future Global, Regional and Local GNSS Positioning Services: Concepts and Performance Perspectives. Proceedings of ION GNSS 2005 18th International Technical Meeting of the Satellite Division of the Institute of Navigation Long Beach, CA: 2277 - 2287.
- [24] Fernández-Plazaola, U., T. M. Martín-Guerrero & J. T. Entrambasaguas-Muñoz (2007) "A New Method for Three-carrier GNSS Ambiguity Resolution." GPS Solutions.
- [25] Ford, T., J. Neumann & M. Bobye (2001a) OEM4 Inertial: An Inertial/GPS Navigation System on the OEM4 Receiver. International Symposium on Kinematic Systems in Geodesy, Geomatics and Navigation (KIS 2001), Banff, AB, Department of Geomatics Engineering, University of Calgary: 150-168.
- [26] Ford, T., J. Hamilton, M. Bobye & L. Day (2004) GPS/MEMS Inertial Integration Methodology and Results. ION GNSS 2004, Long Beach, CA, Institute of Navigation: 1587-1597.
- [27] Ford, T., J. Neumann, P. Fenton, M. Bobye & J. Hamilton (2001b) OEM4 Inertial: A Tightly Integrated Decentralized Inertial/GPS Navigation System. ION GPS 2001, Salt Lake City, UT, Institute of Navigation: 3153-3163.
- [28] GAO (2009) Significant Challenges in Sustaining and Upgrading Widely Used Capabilities, Report to the Subcommittee on National Security and Foreign Affairs, Committee on Oversight and Government Reform, House of Representatives.

- [29] Gao, J., M. G. Petovello & M. E. Cannon (2007) "GPS/Low-Cost IMU/Onboard Vehicle Sensors Integrated Land Vehicle Positioning System." EURASIP Journal on Embedded Systems 2007(Article ID 62616).
- [30] Garin, L., S. Venkatraman, P. Gupta, B. J. Kokes & T. A. Smith (2008) Enhancing Altitude Accuracy in Automotive Navigation using MEMS Barometric Sensor with GPS. ION NTM 2008, San Diego, CA, Institute of Navigation: 670-679.
- [31] Gebre-Egziabher, D. (2004) *Design and Performance Analysis of a Low-Cost Aided Dead Reckoning Navigator*, PhD Thesis, Stanford University
- [32] Gebre-Egziabher, D. (2007) What is the Difference Between 'loose', 'tight', 'ultra-tight' and 'deep' integration strategies for INS and GNSS? Inside GNSS. 2: 28-33.
- [33] Gelb, A., Ed. (1974) Applied Optimal Estimation. Cambridge, Massachusetts, The MIT Press.
- [34] Godha, S. & M. E. Cannon (2005a) Integration of DGPS with a Low Cost MEMS-Based Inertial Measurement Unit (IMU) for Land Vehicle Navigation Application. ION GNSS 2005, Long Beach, CA, Institute of Navigation: 333-345.
- [35] Godha, S. & M. E. Cannon (2005b) Development of a DGPS/MEMS IMU Integrated System for Navigation in Urban Canyon Conditions. GNSS-05, Hong Kong.
- [36] Godha, S., M. G. Petovello & G. Lachapelle (2005) Performance Analysis of MEMS IMU/HSGPS/Magnetic Sensor Integrated System in Urban Canyons. ION GNSS 2005, Long Beach, CA, Institute of Navigation: 1977-1990.
- [37] Greenspan, R. L. (1994) GPS and Inertial Navigation. Global Positioning System: Theory and Applications. B. W. Parkinson and J. J. Spilker, Jr., American Institute of Aeronautics and Astronautics, Inc. II: 187-220.
- [38] Grejner-Brzezinska, D., C. K. Toth, Y. Jwa & S. Moafipoor (2006) Seamless and Reliable Personal Navigator. ION NTM 2006, Monterey, CA, Institute of Navigation: 597-603.
- [39] Grewal, M. S. & A. P. Andrews (2008) *Kalman Filtering Theory and Practice Using MATLAB®*, John Wiley & Sons, Inc., Hoboken, NJ.
- [40] Grewal, M. S., L. R. Weill & A. P. Andrews (2001) *Global Positioning Systems, Inertial Navigations, and Integration*, John Wiley & Sons, Inc.
- [41] Groves, P. D., C. J. Mather & A. A. Macaulay (2007) Demonstration of Non-coherent Deep INS/GPS Integration for Optimised Signal-to-noise Performance. ION GNSS 2007, Fort Worth, TX, Institute of Navigation: 2627-2638.
- [42] Gustafson, D. & J. Dowdle (2003) Deeply Integrated Code Tracking: Comparative Performance Analysis. ION GPS/GNSS 2003, Portland, OR, Institute of Navigation: 2553-2561.
- [43] Gustafson, D., J. Dowdle & K. Flueckiger (2000) A Deeply Integrated Adaptive GPS-Based Navigator with Extended Range Code Tracking. IEEE PLANS, San Diego, CA, IEEE: 118-124.
- [44] Hartman, R. G. (1988) "An Integrated GPS/IRS Design Approach." NAVIGATION: Journal of Institute of Navigation 35(1): 121-134.
- [45] Hide, C., T. Moore, C. Hill & D. Park (2006) "Low Cost, High Accuracy Positioning In Urban Environments." THE JOURNAL OF NAVIGATION 59(3): 365-379.

- [46] Jekeli, C. (2000) *Inertial Navigation Systems with Geodetic Applications*, Walter de Gruyter, Berlin.
- [47] Ji, S., W. Chen, C. Zhao, X. Ding & Y. Chen (2007) "Single epoch ambiguity resolution for Galileo with the CAR and LAMBDA methods." *GPS Solutions* 11(4): 259-268.
- [48] Jovancevic, A., A. Brown, S. Ganguly, J. Noronha & B. Sirpatil (2004) Ultra Tight Coupling Implementation Using Real Time Software Receiver. ION GNSS 2004, Long Beach, CA, Institute of Navigation: 1575-1586.
- [49] Julien, O., P. Alves, M. E. Cannon & W. Zhang (2003) A Tightly Coupled GPS/GALILEO Combination for Improved Ambiguity Resolution. Proceedings of the European Navigation Conference ENC-GNSS 2003, 22-25 April, Graz, Austria: CD Rom - 14 Pages.
- [50] Julien, O., P. Alves, M. E. Cannon & G. Lachapelle (2004) Improved Triple-Frequency GPS/GALILEO Carrier Phase Ambiguity Resolution Using a Stochastic Ionosphere Modeling. Proceedings of ION NTM-04, 26-28 January, San Diego, CA: 441 - 452.
- [51] Jung, J., P. Enge & B. Pervan (2000) Optimization of Cascade Integer Resolution with Three Civil GPS Frequencies. Proceedings of the 13th International Technical Meeting of the Satellite Division of the Institute of Navigation ION GPS-2000. Salt Lake City, UT, Institute of Navigation: 2191 - 2201.
- [52] Kim, H. S., S. C. Bu, G. I. Jee & C. G. Park (2003) An Ultra-Tightly Coupled GPS/INS Integration Using Federated Filtering. ION GPS/GNSS 2003, Portland, OR, Institute of Navigation: 2878-2885.
- [53] Kim, J. W., D.-H. Hwang & S. J. Lee (2006) A Deeply Coupled GPS/INS Integrated Kalman Filter Design using Linearized Correlator Output. ION Annual Meeting/IEEE PLANS, San Diego, CA, Institute of Navigation and IEEE: 300-305.
- [54] Klobuchar, J., P. Dorherty & M. B. El-Arini (1995) "Potential Ionospheric Limitations to GPS Wide-Area Augmentation System (WAAS)." *Navigation* 42(2): 353-379.
- [55] Kumagai, H., T. Kindo & S. Sugimoto (2000) DGPS/INS/VMS Integration for High Accuracy Land-Vehicle Positioning. ION GPS 2000, Salt Lake City, UT, Institute of Navigation: 1845-1853.
- [56] Lachapelle, G., M. E. Cannon, K. O'Keefe & P. Alves (2002) "How will Galileo Improve Positioning Performance?" *GPS World* 13(9): 38-48.
- [57] Lachapelle, G., O. Mezentsev, J. Collin & G. MacGougan (2003) Pedestrian and Vehicular Navigation Under Signal Masking Using Integrated HSGPS and Self Contained Sensor Technologies. World Congress, International Association of Institutes of Navigation, Berlin.
- [58] Leick (2004) *GPS Satellite Surveying*, John Wiley and Sons.
- [59] Leonard, A., H. Krag, G. Lachapelle, K. O'Keefe, C. Huth & S. C (2003) Impact of GPS and Galileo Orbital Plane Drifts on Interoperability Performance Parameters. Proceedings of GNSS03, Graz, Austria: Session C-2, 11 pages.
- [60] Leva, J., M. W. de Haag & K. Van Dyke (1996) Performance of Standalone GPS. *Understanding GPS Principles and Applications*. E. D. Kaplan. Boston, Artech House.

- [61] MacGougan, G. (2003) *High Sensitivity GPS Performance Analysis in Degraded Signal Environments*, MSc Thesis, Department of Geomatics Engineering, University of Calgary, Calgary
- [62] Mather, C. J., P. D. Groves & M. R. Carter (2006) A Man Motion Navigation System Using High Sensitivity GPS, MEMS IMU and Auxiliary Sensors. ION GNSS 2006, Fort Worth, TX, Institute of Navigation: 2704-2714.
- [63] Maybeck, P. S. (1994) *Stochastic Models, Estimation and Control*, NavtechGPS.
- [64] McDonald, K. & C. Hegarty (2000) Post-Modernization GPS Performance Capabilities. ION AM 2000 Proceedings of the Institute of Navigation 56th Annual Meeting, San Diego, California: 242-249.
- [65] Minkler, G. & J. Minkler (1993) *Theory and Application of Kalman Filtering*, Magellan Book Company, Palm Bay, FL.
- [66] Misra, P. & P. Enge (2001) *Global Positioning System, Signals, Measurements, and Performance*, Ganga-Jamuna Press, Lincoln, Massachusetts.
- [67] Morton, J. (2007) "Expert Advice: Software Defines Future." GPS World System Design and Test News.
- [68] Nassar, S. & K.-P. Schwarz (2001) Bridging DGPS Outages in Kinematic Applications Using A Simple Algorithm for INS Bias Modeling. International Symposium on Kinematic Systems in Geodesy, Geomatics and Navigation (KIS 2001), Banff, AB, Department of Geomatics Engineering, University of Calgary: 401-408.
- [69] Nassar, S., E. W. Shin, X. Niu & N. El-Sheimy (2005) Accurate INS/GPS Positioning with Different Inertial Systems Using Various Algorithms for Bridging GPS Outages. ION GNSS 2005, Long Beach, CA, Institute of Navigation: 1401-1410.
- [70] Niu, X. & N. El-Sheimy (2005) The Development of a Low-cost MEMS IMU/GPS Navigation System for Land Vehicles Using Auxiliary Velocity Updates in the Body Frame. ION GNSS 2005, Long Beach, CA, Institute of Navigation: 2003-2012.
- [71] Niu, X., S. Nassar, C. Goodall & N. El-Sheimy (2007) "A Universal Approach for Processing any MEMS Inertial Sensor Configuration for Land-Vehicle Navigation." *The Journal of Navigation*: 233–245.
- [72] Niu, X., S. Nassar, Z. Syed, C. Goodall & N. El-Sheimy (2006) The Development of A MEMS-Based Inertial/GPS System for Land-Vehicle Navigation Applications. ION GNSS 2006. Fort Worth, TX, Institute of Navigation: 1516-1525.
- [73] O'Driscoll, C., M. G. Petovello & G. Lachapelle (2008) Impact of Extended Coherent Integration Times on Weak Signal RTK in an Ultra-Tight Receiver. NAV08 Conference. London, UK, Royal Institute of Navigation.
- [74] O'Keefe, K. (2001) Availability and Reliability Advantages of Galileo/GPS Integration. Proceedings of ION GPS2001, The Satellite Division of the Institute of Navigation 14th International Technical Meeting, Salt Lake City, Utah: 2096-2104.
- [75] O'Keefe, K., S. Ryan & G. Lachapelle (2002) "Global Availability and Reliability Assessment of the GPS and Galileo Global Navigation Satellite Systems." *Canadian Aeronautics and Space Journal* 48(2): 123-132.

- [76] O'Keefe, K., O. Julien, M. E. Cannon & G. Lachapelle (2004) Evaluation of the Availability, Accuracy, Reliability and Carrier-Phase Ambiguity Resolution Capabilities of the Galileo GNSS in Conjunction with Modernized GPS. Proceedings of IAC 2004, the 2004 International Astronautical Congress, Vancouver, British Columbia: 12 Pages.
- [77] O'Keefe, K., M. Petovello, W. Cao, G. Lachapelle & E. Guyader (2009) "Comparing of Multi-carrier Ambiguity Resolution methods for Geometry-Based GPS and Galileo Low Earth Orbiting Satellite Attitude Determination." International Journal of Navigation and Observation 2009(Article ID 592073): 15 pages.
- [78] Olynik, M. (2002) *Temporal Characteristics of GPS Error Sources and Their Impact on Relative Positioning*, MSc Thesis, Geomatics Engineering, University of Calgary, Calgary
- [79] Oppenheim, A. V., R. W. Schaffer & J. R. Buck (1999) *Discrete-Time Signal Processing*, Prentice Hall, Upper Saddle River, NJ.
- [80] Pany, T., R. Kaniuth & B. Eissfeller (2005) Deep Integration of Navigation Solution and Signal Processing. ION GNSS 2005, Long Beach, CA, Institute of Navigation: 1095-1102.
- [81] Parkinson, B. W. (1996) Introduction and Heritage of NAVSTAR, the Global Positioning System. Global Positioning System: Theory And Applications. B. W. Parkinson and J. J. Spilker, Jr. Washington, American Institute of Aeronautics and Astronautics. 1.
- [82] Parkinson, B. W. & J. J. Spilker, Jr., Eds. (1996) Global Positioning System: Theory and Applications. Profess in Astronautics and Aeronautics. Washington, American Institute of Aeronautics and Astronautics.
- [83] Petovello, M. (2003a) *Real-Time Integration of a Tactical-Grade IMU and GPS for High-Accuracy Positioning and Navigation*, PhD Thesis, Department of Geomatics Engineering, University of Calgary, Calgary
- [84] Petovello, M. G. (2003b) *Real-Time Integration of a Tactical-Grade IMU and GPS for High-Accuracy Positioning and Navigation*, Ph.D. Thesis, Geomatics Engineering, University of Calgary, Calgary
- [85] Petovello, M. G., M. E. Cannon & G. Lachapelle (2003) "Benefits of Using a Tactical Grade INS for High Accuracy Positioning." NAVIGATION: Journal of Institute of Navigation 51(1): 1-12.
- [86] Petovello, M. G., C. O'Driscoll & G. Lachapelle (2007) Ultra-Tight GPS/INS for Carrier Phase Positioning In Weak-Signal Environments. NATO RTO SET-104 Symposium on Military Capabilities Enabled by Advances in Navigation Sensors. Antalya, Turkey, NATO: 18.
- [87] Petovello, M. G., C. O'Driscoll & G. Lachapelle (2008) Weak Signal Carrier Tracking Using Extended Coherent Integration with an Ultra-Tight GNSS/IMU Receiver. European Navigation Conference. Toulouse, France: 11.
- [88] Phuyal, B. (2004) An Experiment for a 2-D and 3-D GPS/INS Configuration for Land Vehicle Applications. IEEE PLANS 2004, IEEE: 148-152.
- [89] Raquet, J. (1998) *Development of a Method for Kinematic GPS Carrier-Phase Ambiguity Resolution Using Multiple Reference Receiver*, PhD Thesis, Department of Geomatics Engineering, University of Calgary, Calgary

- [90] Ray, J. (2000) *Mitigation of GPS Code and Carrier Phase Multipath Effects Using a Multi-Antenna System*, PhD Thesis, Department of Geomatics Engineering, University of Calgary, Calgary
- [91] RSA. (2009) "Russian Space Agency Information Analytical Centre - GLONASS Status." Retrieved June 24, 2009.
- [92] Salychev, O. S. & V. V. Voronov (2000) Low Cost INS/GPS Integration: Concepts and Testing. ION NTM 2000, Anaheim, CA, Institute of Navigation: 98-205.
- [93] Scherzinger, B. M. (2000) Precise Robust Positioning with Inertial/GPS RTK. ION GPS 2000, Salt Lake City, UT, Institute of Navigation: 155–162.
- [94] Scherzinger, B. M. (2001) Robust Inertially Aided RTK Position Measurement. International Symposium on Kinematic Systems in Geodesy, Geomatics and Navigation (KIS 2001), Banff, AB, Department of Geomatics Engineering, University of Calgary: 265–272.
- [95] Scherzinger, B. M. (2002) Robust Positioning with Single Frequency Inertially Aided RTK. ION GPS 2002, Portland, OR, Institute of Navigation: 911–917.
- [96] Scherzinger, B. M. (2006) "Precise Robust Positioning with Inertially Aided RTK." NAVIGATION: Journal of Institute of Navigation 53(2): 73-83.
- [97] Schleppe, J. (2006) The Suitability of the u-blox LEA-4T for Heading Determination. PLAN Group Internal Document. Calgary, University of Calgary.
- [98] Schwarz, K.-P., N. El-Sheimy & Z. Liu (1994a) Fixing GPS Cycle Slips by GPS/INS - Methods and Experience. International Symposium on Kinematic Systems in Geodesy, Geomatics and Navigation (KIS 1994), Banff, AB, Department of Geomatics Engineering, University of Calgary: 265–275.
- [99] Schwarz, K.-P., N. El-Sheimy & Z. Liu (1994b) Fixing GPS Cycle Slips by INS/GPS - Methods and Experiences. International Symposium on Kinematic Systems in Geodesy, Geomatics and Navigation (KIS 1994), Banff, AB, Department of Geomatics Engineering, University of Calgary: 265-275.
- [100] Scott, L. (2007) "Directions 2008: Software-Defined Radio Role to Grow." GPS World System Design and Test News, Retrieved January 7, 2008.
- [101] Shrestha (2003) *Investigations into the Estimation of Tropospheric Delay and Wet Refractivity Using GPS Measurements*, MSc Thesis, Department of Geomatics Engineering, University of Calgary, Calgary
- [102] Skaloud, J. (1999) *Optimizing Georeferencing of Airborne Survey Systems by INS/DGPS*, Ph.D. Thesis, Geomatics Engineering, University of Calgary, Calgary
- [103] Soloviev, A., F. van Grass & S. Gunawardena (2004a) Implementation of Deeply Integrated GPS/Low-Cost IMU for Reacquisition and Tracking of Low CNR GPS Signals. ION National Technical Meeting, San Diego, CA, Institute of Navigation: 923-935.
- [104] Soloviev, A., S. Gunawardena & F. Van Grass (2004b) Deeply Integrated GPS/Low-Cost IMU for Low CNR Signal Processing: Flight Test Results and Real Time Implementation. ION GNSS 2004, Long Beach, CA, Institute of Navigation: 1598-1608.
- [105] Spilker, Jr., J. J. (1996a) Satellite Constellation and Geometric Dilution of Precision. Global Positioning System: Theory And Applications. B. W. Parkinson

- and J. J. Spilker, Jr. Washington, American Insistute of Aeronautics and Astronautics. 1.
- [106] Spilker, Jr., J. J. (1996b) GPS Signal Structure and Theoretical Performance. Global Positioning System: Theory And Applications. B. W. Parkinson and J. J. Spilker, Jr. Washington, American Insistute of Aeronautics and Astronautics. 1.
- [107] Sun, D., M. G. Petovello & M. E. Cannon (2008) "GPS/Reduced IMU with a Local Terrain Predictor in Land Vehicle Navigation." International Journal of Navigation and Observation 2008.
- [108] Sun, H., M. E. Cannon, T. E. Owen & M. A. Meindl (1994) An Investigation of Airborne GPS/INS for High Accuracy Position and Velocity Determination. ION NTM 2004, Institute of Navigation: 801–809.
- [109] Syed, Z., P. Aggarwal, X. Niu & N. El-Sheimy (2007) Economical and Robust Inertial Sensor Configuration for a Portable Navigation System. ION GNSS 2007, Fort Worth, TX, Institute of Navigation: 2129-2135.
- [110] Takac, F. (2009) GLONASS interfrequency-biases and ambiguity resolution. Inside GNSS. March/April: 24-28.
- [111] Teunissen, P., P. Joosten & C. Tiberius (2002) A Comparison of TCAR, CIR and LAMBDA GNSS Ambiguity Resolution. Proceedings of the 15th International Technical Meeting of the Satellite Division of the Institute of Navigation ION GPS 2002. Portland, OR, Institute of Navigation: 2799 - 2808.
- [112] Teunissen, P. J. G. (1994) A new method for carrier phase ambiguity estimation. Proceedings of IEEE Plans '94, Las Vegas, NV: 862-873.
- [113] Titterton, D. H. & J. L. Weston (1997) *Strapdown Inertial Navigation Technology*, Peter Peregrinus Ltd.
- [114] Van Diggelen, F. (2009) *A-GPS, Assisted GPS, GNSS, and SBAS*, Artech House, Boston.
- [115] Ward, P. (1996) GPS Satellite Signal Characteristics. Understanding GPS Principles and Applications. E. D. Kaplan. Boston, Artech House.
- [116] Wells (1999).
- [117] Wendel, J., J. Metzgar, R. Moenikes, A. Maier & G. F. Trommer (2005) A Performance Comparison of Tightly Coupled GPS/INS Navigation Systems Based on Extended and Sigma Point Kalman Filters. ION GNSS 2005, Long Beach, CA, Institute of Navigation: 456-466.
- [118] Werner, W. & J. Winkel (2003) TCAR and MCAR Options With Galileo and GPS. ION GPS/GNSS 2003 Portland, OR, Institute of Navigation: 790 - 800.
- [119] Wolf, R., B. Eissfeller & G. Hein (1997) A Kalman Filter for the Integration of a Low Cost INS and an Attitude GPS. International Symposium on Kinematic Systems in Geodesy, Geomatics and Navigation (KIS 1994), Banff, AB, Department of Geomatics Engineering, University of Calgary: 143-150.
- [120] Yang, Y., J. A. Farrell & M. J. Barth (2000) High-Accuracy, High-Frequency Differential Carrier Phase GPS Aided Low-Cost INS. IEEE PLANS 2000, IEEE: 148-155.
- [121] Yi, Y. & D. Grejner-Brzezinska (2006) Performance Comparison of the Nonlinear Bayesian Filters Supporting GPS/INS Integration. ION NTM 2006, Monterey, CA, Institute of Navigation: 977-983.

- [122] Yousuf, R. (2005) *Evaluation and Enhancement of the Wide Area Augmentation System*, MSc Thesis, Geomatics Engineering, University of Calgary, Calgary
- [123] Zhang, J. H. (1999) *Investigations into the Estimation of Residual Tropospheric Delays in a GPS Network*, MSc Thesis, Department of Geomatics Engineering, University of Calgary, Calgary
- [124] Zhang, W., M. E. Cannon, O. Julien & P. Alves (2003) Investigation of Combined GPS/GALILEO Cascading Ambiguity Resolution Schemes. Proceedings of the 16th International Technical Meeting of the Satellite Division of the Institute of Navigation ION GPS/GNSS 2003, Portland, Oregon: 2599 - 2610.

VSC-A Final Report: Appendix E-3
GPS Service Availability Study Final Report

Prepared by
PLAN Group
University of Calgary

List of Acronyms

AT	Along Track (component of the IVV)
CAMP	Crash Avoidance Metrics Partnership
CICAS-V	Cooperative Intersection Collision Avoidance System – Violation
CCIT	Calgary Center for Innovative Technology
CD	Cumulative Distribution
CDF	Cumulative Distribution Function
DOP	Dilution of Precision as HDOP, VDOP, PDOP, TDOP, GDOP (Horizontal, Vertical, Position, Time, Geometric)
DPOS	Difference in Position
DSRC	Dedicated Short Range Communications
ECEF	Earth Centered Earth Fixed
ENU	East North Up (Local Frame)
FHWA	Federal Highway Administration
GDOP	Geometric Dilution of Precision
GLONASS	Global Navigation Satellite System
GNSS	Global Navigation Satellite System
GPS	Global Positioning System
HW	Hardware
INS	Inertial Navigation System
ITS	Intelligent Transportation Systems
IVV	Inter-Vehicle Vector
NHTSA	National Highway Traffic Safety Administration
RAIM	Receiver Autonomous Integrity Monitoring
RMS	Root Mean Squared
RTK	Real-Time Kinematic
SP	Single Point
SW	Software
USDOT	United States Department of Transportation
VSC2	Vehicle Safety Communications 2
VSC-A	Vehicle Safety Communications – Applications

V2V	Vehicle-to-Vehicle
V2I	Vehicle to Infrastructure
V2I-B	V2I where both vehicles are inside the Infrastructure zone
V2I-S	V2I where only one vehicle is inside the Infrastructure zone
WAAS	Wide Area Augmentation System
XT	Across Track (component of the IVV)

Table of Contents

List of Acronyms.....	E-3-ii
1 Introduction.....	E-3-1
2 Abbreviations.....	E-3-1
2.1 Test Receivers	E-3-1
2.2 Availability Measures.....	E-3-1
3 Field Test Description	E-3-2
3.1 Vehicle Setup	E-3-2
3.2 V2I Setup.....	E-3-4
3.3 Data Collected	E-3-5
4 Data Processing.....	E-3-6
4.1 Reference Solutions.....	E-3-8
4.2 Vehicle to Vehicle (V2V) Processing Methods	E-3-9
4.2.1 Difference in Position (DPOS) Method	E-3-9
4.2.2 Moving Base-Station RTK.....	E-3-9
4.3 Vehicle to Infrastructure (V2I) Processing Method	E-3-10
5 Performance Measures	E-3-11
5.1 Accuracy.....	E-3-11
5.2 Availability.....	E-3-11
6 Predictive Measures	E-3-13
6.1 Dilution of Precision	E-3-13
6.2 Number of Satellites.....	E-3-14
7 Data Collection Summary	E-3-14
8 Vehicle-to-Vehicle Test Results.....	E-3-15
8.1 Reference IVV Statistics	E-3-16
8.2 Effects of Positioning Method.....	E-3-18
8.2.1 Availability.....	E-3-18
8.2.2 Number of Satellites.....	E-3-20
8.2.3 Dilution of Precision	E-3-20
8.2.4 Accuracy	E-3-20
8.2.5 Environment Types	E-3-24
8.3 Effects of Receiver Quality	E-3-25
8.3.1 Availability.....	E-3-25

8.3.2	Number of Satellites.....	E-3-27
8.3.3	Dilution of Precision	E-3-28
8.3.4	Accuracy	E-3-28
8.3.5	Environment Type.....	E-3-29
8.4	Effects of WAAS.....	E-3-29
8.4.1	Availability.....	E-3-30
8.4.2	Number of Satellites.....	E-3-30
8.4.3	Dilution of Precision	E-3-30
8.4.4	Position Accuracy	E-3-30
8.4.5	Environment Types	E-3-32
8.5	Effects of Constellation Limitations.....	E-3-33
8.5.1	Availability.....	E-3-34
8.5.2	Number of Satellites.....	E-3-34
8.5.3	Dilution of Precision	E-3-34
8.5.4	Accuracy	E-3-34
8.5.5	Environment Types	E-3-36
9	Characterization of Errors.....	E-3-37
9.1	Number of Satellites.....	E-3-38
9.2	Dilution of Precision	E-3-40
9.3	Inter-Vehicle Distance.....	E-3-42
9.4	Vehicle Speed.....	E-3-44
10	Vehicle-to-Infrastructure Test Results	E-3-47
11	Conclusions	E-3-51
12	References	E-3-55
13	Supplementary Material	E-3-56
13.1	Photos Illustration of The Data Collection Routes.....	E-3-56
13.1.1	Deep Urban	E-3-56
13.1.2	Major Urban Throughway	E-3-58
13.1.3	Major Rural Throughway.....	E-3-61
13.1.4	Major Road (Urban and Rural)	E-3-64
13.1.5	Freeway/Interstate.....	E-3-66
13.1.6	Mountain Roads	E-3-68
13.1.7	Local Roads.....	E-3-69

13.2 Heading Accuracy	E-3-72
13.3 Analysis of RTK Processing Packages	E-3-73

List of Figures

Figure 3-1: Receiver, Computer and Antenna Setup of Vehicle 1	E-3-2
Figure 3-2: Receiver, Computer and Antenna Setup of Vehicle 2	E-3-3
Figure 3-3: Photograph of Test Vehicles	E-3-4
Figure 3-4: Equipment Setup on the Roof of Vehicle 2	E-3-4
Figure 3-5: Tripod Mounted Antenna and Receiver Used in V2I Tests.....	E-3-5
Figure 4-1: Definition of the Along Track (AT) and Across Track (XT) Components of the Inter Vehicle Vector (IVV).....	E-3-7
Figure 4-2: Schematic Showing the Antenna Geometry on One Vehicle	E-3-8
Figure 5-1: Availability Definitions.....	E-3-12
Figure 8-1: CDF for the Horizontal Error for RTK and DPOS Processing of all (AW- AW) Data	E-3-23
Figure 8-2: CDF for the AT and XT Errors for RTK and DPOS Processing of all (AW-AW) Data	E-3-23
Figure 8-3: CDFs of the AT and XT Errors in the IVV Solutions Using (AW-AW) and (BW-BW), RTK.....	E-3-29
Figure 8-4: Effects of WAAS on the Number of Satellites and DOP	E-3-31
Figure 8-5: CDF of the Horizontal Error for (BW-BW) and (BW-BN) Combinations Over All Environments	E-3-31
Figure 8-6: CDF of Horizontal Errors in the Local Road Environment for (BW-BW) and (BW-BN), DPOS.....	E-3-33
Figure 8-7: Dilution of Precision and Satellite Number Histograms for (BW-BW) and (B24W-B24W).....	E-3-35
Figure 8-8: CDF of Horizontal Errors for (BW-BW) and (B24W-B24W) - Effect of Limited Constellation.....	E-3-36
Figure 8-9: CDF of Horizontal Errors for (BW-BW) and (B24W-B24W) in Mountain Environment.....	E-3-37
Figure 9-1: Horizontal RMS Error in IVV versus the Number of Satellites for (AW- AW), DPOS, for each Environment	E-3-38
Figure 9-2: Horizontal RMS Error in IVV versus the Number of Satellites for (AW- AW), RTK, for each Environment.....	E-3-39
Figure 9-3: Horizontal RMS Error in IVV versus the Number of Satellites for (BW-BW), DPOS, for each Environment.....	E-3-39
Figure 9-4: Horizontal RMS Error in IVV versus the Number of Satellites for (BW-BW), RTK, for each Environment.....	E-3-40
Figure 9-5: Horizontal RMS Error in IVV versus HDOP for (AW-AW), DPOS, for each Environment	E-3-41
Figure 9-6: Horizontal RMS Error in IVV versus HDOP for (BW-BW), DPOS, for each Environment	E-3-41
Figure 9-7: Horizontal RMS Error in IVV versus the Inter-Vehicle Distance for (AW-AW), DPOS, for each Environment.....	E-3-42
Figure 9-8: Horizontal RMS Error in IVV versus the Inter-Vehicle Distance for (BW-BW), DPOS, for each Environment	E-3-43
Figure 9-9: Horizontal RMS Error in IVV versus the Distance for (AW-AW), RTK, for each Environment.....	E-3-43

Figure 9-10: Horizontal RMS Error in IVV versus the Inter-Vehicle Distance for (BW-BW), RTK, for each Environment..... E-3-44

Figure 9-11: Horizontal RMS Error in IVV versus the Speed for (AW-AW), DPOS, for each Environment..... E-3-45

Figure 9-12: Horizontal RMS Error in IVV versus the Speed for (BW-BW), DPOS, for each Environment..... E-3-45

Figure 9-13: Horizontal RMS Error in IVV versus Speed for (AW-AW), RTK, for each Environment E-3-46

Figure 9-14: Horizontal RMS Error in IVV versus the Speed for (BW-BW), RTK, for each Environment E-3-46

Figure 10-1: V2I Time Series for (AW-AW) for an Interstate Environment E-3-47

Figure 10-2: CDF of Horizontal Errors in V2I Estimate of IVV, (AW-AW) E-3-48

Figure 10-3: CDF of Horizontal Errors in V2I Estimate of IVV, (BW-BW)..... E-3-49

List of Tables

Table 3-1: RTK Combinations Processed.....	E-3-6
Table 7-1: Data Collection Summary	E-3-15
Table 8-1: Reference IVV Statistics for each of the V2V Data Collections	E-3-17
Table 8-2: Availability Statistics for Selected Receiver Pairs Comparing the RTK and DPOS Positioning Methods	E-3-18
Table 8-3: Data Gap Statistics for Selected Receiver Pairs Comparing the RTK and DPOS Positioning Methods	E-3-19
Table 8-4: Mean Number of Satellites used by Selected Receiver Pairs Comparing the RTK and DPOS Positioning Methods	E-3-20
Table 8-5: Along and Across Accuracy for Selected Receiver Pairs with the RTK and DPOS Positioning Methods	E-3-21
Table 8-6: Availability of Solutions with Less than 20 m for Selected Receiver Pairs with the RTK and DPOS Positioning Methods	E-3-22
Table 8-7: Availability Statistics for (AW-AW) using RTK and DPOS in each of the Environments	E-3-24
Table 8-8: Availability Statistics for (BW-BW) Using RTK and DPOS in each of the Environments	E-3-25
Table 8-9: Availability Statistics for all Data for (AW-AW) and (BW-BW) Receiver Pairs.....	E-3-26
Table 8-10: Availability Statistics for all Deep Urban Data for (AW-AW) and (BW-BW) Receiver Pairs	E-3-26
Table 8-11: Data Gap Statistics for all Data of the AW and BW Receivers in SP Mode.....	E-3-27
Table 8-12: Data Gap Statistics for all Data of the AW and BW Homogeneous Receiver Pairs	E-3-27
Table 8-13: Mean Number of Satellites for all Data of the AW and BW Homogeneous Receiver Pairs	E-3-27
Table 8-14: Availability Statistics for all Data for Selected Receiver Pairs Showing the Effect of WAAS.....	E-3-30
Table 8-15: Availability Statistics for Deep Urban Data for Selected Receiver Pairs Showing the Effect of WAAS.....	E-3-32
Table 8-16: Availability Statistics for all Data for (BW-BW) and (B24W-B24) - Effect of Limited Constellation	E-3-34
Table 10-1: Discontinuities in the IVV Estimate at Zone Transitions for (AW-AW) Combination.....	E-3-50
Table 10-2: Discontinuities in the IVV Estimate at Zone Transitions for (BW-BW) Combination.....	E-3-50
Table 11-1: Availability Statistics for All Receiver Combinations and V2V Processing Methods.....	E-3-51
Table 11-2: Data Gap Statistics for all Receiver Combinations and V2V Processing Methods.....	E-3-54

1 Introduction

This study was conducted as a part of the Positioning Technology Development task of the Crash Avoidance Metrics Partnership (CAMP) Vehicle Safety Communications 2 (VSC2) consortium Vehicle Safety Communications – Applications (VSC-A) Project. A prototype positioning system was designed, developed, and evaluated as a part of the overall VSC-A Project. This study was designed to investigate the accuracy and availability of positioning information from a VSC-A-like system under various conditions and configurations.

The report is organized as follows. Sections 3 and 4 describe the data collection and processing, respectively. Section 5 introduces metrics that are used to compare the various methods of relative positioning, while Section 6 discusses measures that may be used to infer system performance in real-time. Section 7 summarizes the data that was collected, subdivided down into multiple environments. The major component of the report is Section 8 in which the results from the Vehicle-to-Vehicle (V2V) study are used to make various comparisons of the methods and receiver types utilized. In Section 9, the dependency of errors on various quantities, including the predictive measures discussed in Section 6, is analyzed. The results of the Vehicle-to-Infrastructure (V2I) tests are presented and discussed in Section 10. This is followed by conclusions and recommendations.

2 Abbreviations

2.1 Test Receivers

- AW: High quality L1 “geodetic” type receiver (uses Wide Area Augmentation System (WAAS) ranges and corrections in internal solution).
- BW: High sensitivity, “low cost” receiver (uses WAAS ranges and corrections in internal solution).
- BN: Same as BW with no WAAS use
- B24W: High sensitivity “low-cost” receiver configured to use only a limited 24 satellite constellation (first four satellites in each of the six planes) in the navigation solution. Also uses WAAS (ranging and corrections).
- B: Refers to any/all of BW, BN, and B24.

2.2 Availability Measures

Refer to Section 5.2 for the definitions of these measures.

- AWR: Availability with Certain Reference
- AWOR: Availability without Certain Reference

- FA: Full Availability
- FAWE(n): Full Availability with Error Less than n m

3 Field Test Description

This section describes the field test setup in detail, including the hardware (HW) setup and the data collected.

3.1 Vehicle Setup

Two vehicles were used for the data collection. The HW and data flow configurations for these vehicles are shown in Figure 3-1 and Figure 3-2. The equipment, as mounted on the test vehicles, is shown in Figure 3-3 and Figure 3-4.

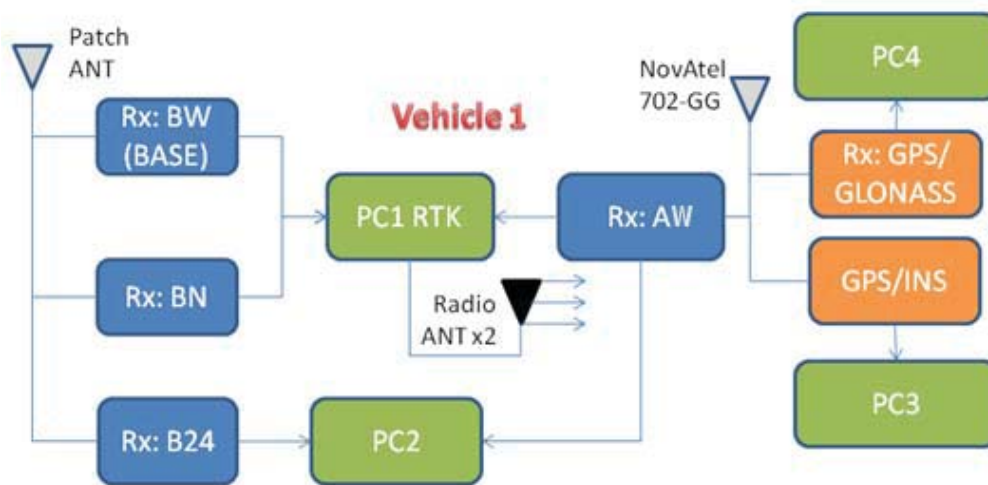


Figure 3-1: Receiver, Computer and Antenna Setup of Vehicle 1

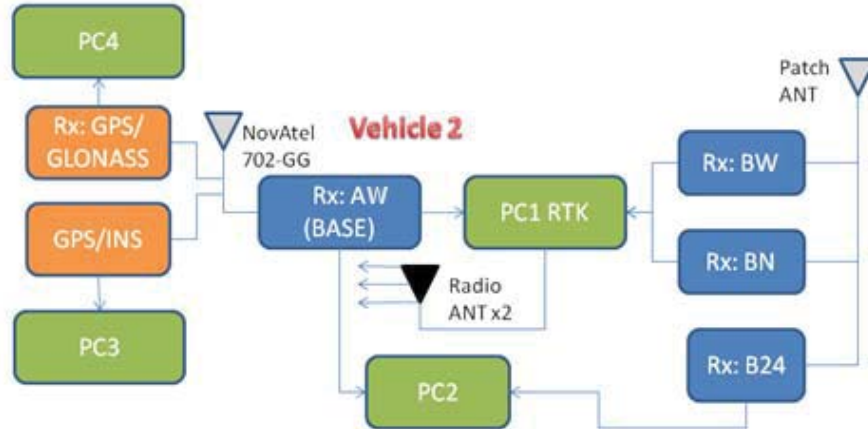


Figure 3-2: Receiver, Computer and Antenna Setup of Vehicle 2

In each vehicle, receiver AW (labeled Rx: AW in Figure 3-1 and Figure 3-2) is attached to a high quality dual-frequency Global Positioning System (GPS)+Global Navigation Satellite System (GLONASS) antenna, while receivers BW, BN, and B24W are connected to a common, low-cost patch antenna which was fixed to an aluminum plate on top of a wooden pedestal, as shown in Figure 3-4. The pedestal served the purposes of bringing the antenna to roughly the same height as the dual-frequency antenna and preventing signal shading from the equipment on the vehicle roof-racks. The aluminum plates served as ground planes for the antennas, improving their performance. The separation between the antennas on each vehicle, which was accounted for as described in Section 4, was measured to be 360 mm in each case. The antennas were positioned as closely as possible to the centerline of the vehicle.

In addition to the “test receiver,” each vehicle was outfitted with additional equipment to provide reference trajectories. In particular, each vehicle had both an integrated dual frequency GPS/Inertial Navigation System (INS) system and a geodetic grade receiver configured to use both GPS and GLONASS satellites. Both systems used the aforementioned dual-frequency GPS+GLONASS antenna. The reference systems were completed with two stationary base stations located on the Calgary Center for Innovative Technology (CCIT) rooftop of the University of Calgary at precisely known WGS84 positions.

Transmission and reception of data between the two vehicles required for the Inter-Vehicle Vector (IVV) Real-Time Kinematic (RTK) calculations were achieved using Wave Radio Modules with two magnetically mounted 802.11p antennas on each vehicle for redundancy. During testing, Vehicle 1 generally followed Vehicle 2. In order to minimize the potential interference of the roof mounted instruments on the between-vehicle communications, the antennas on Vehicle 1 were located close to the front of the roof, while those on Vehicle 2 were located close to the rear of the roof. In each case, 15 cm of roof space was left to provide ground planes for the antennas.



Figure 3-3: Photograph of Test Vehicles



Figure 3-4: Equipment Setup on the Roof of Vehicle 2

3.2 V2I Setup

For the V2I data collections, the vehicle setup described in the previous section was complemented by a survey grade receiver with data logging capability attached to a

tripod mounted antenna as shown in Figure 3-5. This served the purpose of the infrastructure point required for V2I calculations.



Figure 3-5: Tripod Mounted Antenna and Receiver Used in V2I Tests

3.3 Data Collected

Each of the computers, PC1 through PC4 shown in Figure 3-1 and Figure 3-2, ran specific software (SW) to facilitate calculations and data logging as follows:

- **PC1:** Commercially available RTK SW
- **PC2:** Two SW packages dedicated to AW and B type receivers
- **PC3 and PC4:** Data logging software for the reference solutions

In addition to raw measurements used for post processing, data collected by the computers on each vehicle included:

- Single Point (SP) navigation solutions for AW and B receivers: Latitude, Longitude, and Height of the relevant antenna in WGS84
- Horizontal Dilution of Precision (HDOP) and number of satellites used in the SP navigation solution for AW and B receivers
- Velocity solutions for AW and B24 receivers
- Moving base-station RTK solutions (combinations described below): Easting, Northing, and Up between the relevant antennas in units of meters

- Geometric Dilution of Precision (GDOP)⁶ and number of satellites used in the moving base-station navigation solutions

All data was logged at 2 Hz. This rate was chosen as a reasonable balance between time resolution, equipment capability, and resulting data volume. As indicated in Figure 3-1 and Figure 3-2, each vehicle had a base (or host) receiver for RTK calculations. For Vehicle 1, it was BW; and for Vehicle 2, it was AW. Excluding B24W on each vehicle allowed the receiver combinations shown in Table 3-1. Thus, the RTK SW running on Vehicle 1 calculated (and logged) the moving base-station RTK solution for the AW, BW, and BN receivers on Vehicle 2 relative to the BW receiver on Vehicle 1, while the SW running on Vehicle 2 calculated and logged the solutions of the AW, BW, and BN receivers in Vehicle 1 relative to the AW receiver on Vehicle 2.

Table 3-1: RTK Combinations Processed

Vehicle 1	Vehicle 2
BW (host)	AW
	BW
	BN
AW	AW (host)
BW	
BN	

4 Data Processing

The major aim of the project was to determine the relative merits of various GPS based methods of estimating the IVV from a reference point on Vehicle 1 to a reference point on Vehicle 2 (the reference points that were used are discussed below). Thus, before describing the specific methods that were used to determine the vector, it is important to understand its definition and the frame in which it was calculated.

This IVV was obtained in one of two ways depending upon whether the method was an RTK-based method, which yields the IVV directly in terms of a local East-North-Up (ENU) frame (defined relative to the host/base), or a method based upon the absolute positions of the two vehicles, in which case the geodetic coordinates of each vehicle were transformed into the Earth-Centered-Earth-Fixed (ECEF) frame and the location of Vehicle 1 was used as the reference point to express the location of Vehicle 2 in the local ENU frame. Once obtained by one of these methods, the IVV in the ENU frame was resolved into three more physically meaningful components, namely Along Track (AT), Across Track (XT), and Up, defined relative to Vehicle 1. The first two components are generally of more interest since they position the vehicles relative to each other in the horizontal plane, as shown in Figure 4-1. During the calculations, the orientation of the Across, Along, and Up axes of Vehicle 1 was always determined using the reference GPS/INS system. Doing so ensured consistent resolution of the components for all IVV determination methods.

⁶ HDOP was not available from the output of the RTK SW.

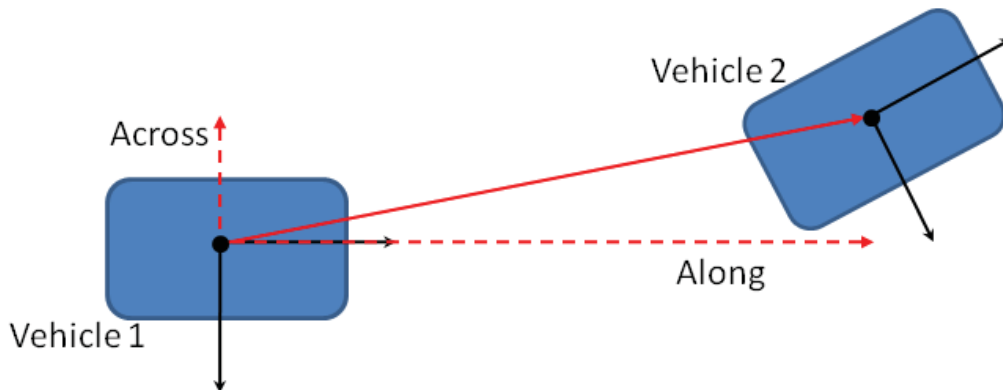


Figure 4-1: Definition of the Along Track (AT) and Across Track (XT) Components of the Inter Vehicle Vector (IVV)

A slight complication to the processing scheme just described arises because the resulting IVV depends upon the locations of the receiver antennas used in the calculations. As was mentioned in Section 3.1, the antennas used by the A and B receivers on each vehicle were separated by 36 cm and placed on the centerline of the vehicle. Since the analysis requires the comparison of the IVV calculated using different receiver pairs, common reference points on each vehicle were required. Thus, in the calculations, the heading and pitch of each vehicle's GPS/INS reference system was used to effectively account for the location of the antenna for the B receivers, so that the reference points for the IVV could always be considered to be the phase centers of the antennas for the A receivers. The basic method by which this was achieved is shown schematically in Figure 4-2. In the figure, A_{Ant} and B_{Ant} are the locations of the phase centers of the antennas used by the A and B type receivers--the points at which the navigation solutions from the two receiver types are defined. The unit vector, \mathbf{u} , in the vehicle's direction of travel is determined using the GPS/INS integrated system on the vehicle. As is shown, the navigation solutions from the B receivers can be translated back to A_{Ant} by subtracting $0.36\mathbf{u}$.

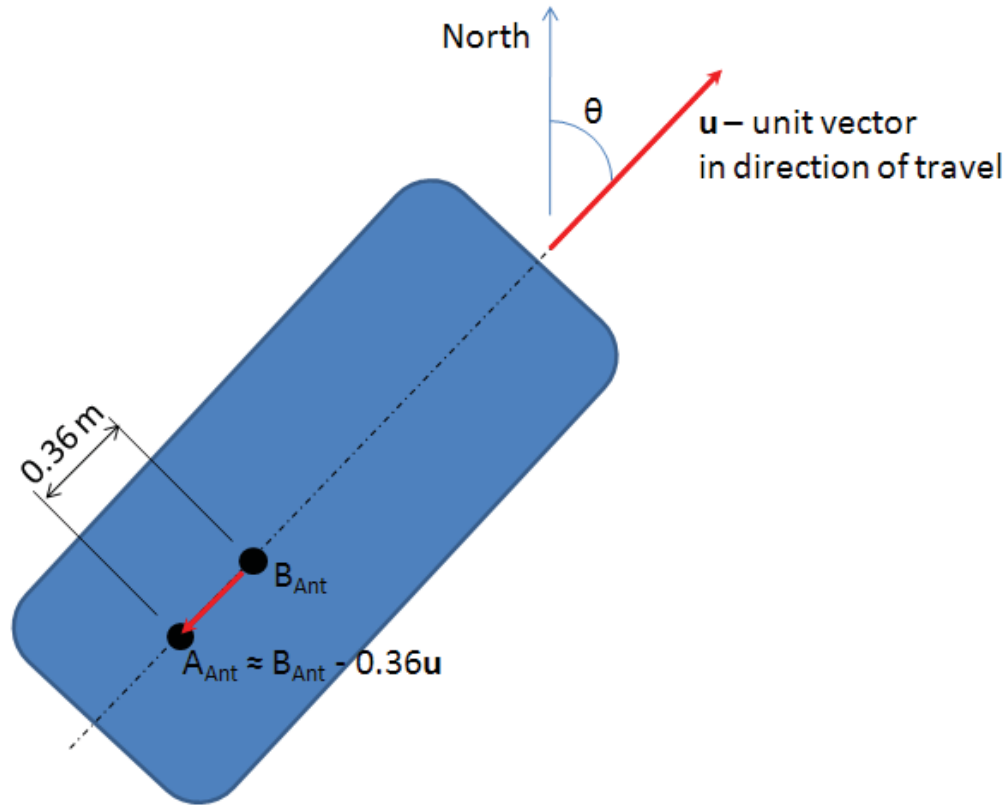


Figure 4-2: Schematic Showing the Antenna Geometry on One Vehicle

4.1 Reference Solutions

As mentioned in Section 3.1, dedicated Global Navigation Satellite System (GNSS) receivers and a GPS/INS system were included on each vehicle so that reference values of the IVV could be determined. For all environments except Deep Urban, multiple reference IVVs, at least three, were determined for redundancy. Once they were calculated, the solutions were compared visually for each data collection. Based on these comparisons, one of the references was chosen as the standard for that particular data collection, and a second was chosen for comparative purposes. The difference between the reference and comparison IVVs gives an indication of the confidence in the reference, particularly when different methods are used to calculate them. If the reference and comparison IVV differed by too much for a certain portion of a data set, that segment was marked as having an uncertain reference. The threshold for the difference was set at 1 m for all environments except Deep Urban; but as is shown in Section 8.1, this level was very rarely crossed. The root mean squared (RMS) difference between the chosen and comparison IVVs was usually much less than 20 cm.

As mentioned above, this multiple reference approach was not used for the Deep Urban environment. This was because the GNSS-based approaches could not be relied upon in the urban canyons--the GPS/INS derived IVV was used exclusively.

The methods by which the various reference solutions were calculated are now described. Commercially available GPS/INS SW was used to process the dual frequency GPS/INS

data in a tightly coupled integration scheme using the base stations at CCIT. The geodetic positions of the two vehicles obtained from the SW were combined in the manner described above to obtain the AT, XT, and Up components of the reference IVV solutions.

Post-processing RTK estimates of the IVV in the local ENU frame were obtained using three SW packages. Two of the packages were developed within the PLAN group, one of which allowed either GPS only or GPS/GLONASS configurations. The third package was obtained from a commercial vendor.

The estimates of the IVV obtained were transformed into Along Track, Across Track, and Up components using the attitude of Vehicle 1 as determined by the GPS/INS system on that vehicle.

4.2 Vehicle to Vehicle (V2V) Processing Methods

Two methods of calculating the IVV solutions solely from the measurements of the test receivers were evaluated. These methods and their characteristics are described below.

4.2.1 Difference in Position (DPOS) Method

The SP navigation solution of each of the test receivers (AW, BW, BN, B24) on each vehicle was recorded. These navigation solutions were transformed using the method described with reference to Figure 4-1 to determine the AT, XT, and Up components of the IVV. This method is referred to as the Difference in Position Method (DPOS).

The major advantage of DPOS is its simplicity; it requires only that the receiver be able to calculate positions in real-time, and vehicles in the same area share their calculated positions. It may also be useful to transmit quality values along with this position estimate, including the number of satellites, the HDOP, or any other built-in quality indicators.

In DPOS, as long as measurement errors or biases affect both receivers in the same way, they will not affect the relative positions between the receivers. Although maximizing the number of satellites in view is the best strategy for calculating the best possible individual, SP position, it is not the best strategy for calculating the best possible relative position. For best results in terms of the relative position accuracy between two receivers, the use of common satellites is the most important condition.

4.2.2 Moving Base-Station RTK

As discussed in Section 3.3, RTK SW was used to calculate and log the six receiver baselines specified in Table 3-1. The solutions from this SW can be transformed to the desired components of the IVV using the method outlined at the beginning of Section 4. It should be mentioned that the solutions using the AW receiver on Vehicle 2 as base needed to have the direction of the IVV reversed.

With conventional RTK systems, one stationary receiver is used as the base station and is positioned at a known location. With a Moving Base-Station RTK, one receiver, the “host,” is selected as the base station for each baseline; however, the location of the host is updated at every epoch using SP processing. Since the recommended operating range of the radios used in the V2V tests is 300 m (Bai & Krishnan 2006) [1] and the expected

SP position error is less than 10 m, the error that might be introduced in the IVV due to the above SP error is at the mm level (Luo & Lachapelle 2003) [3] and inconsequential in the present case.

Moving Base-Station RTK, generally referred to in the following simply as RTK unless clarification is required, has some significant advantages over the DPOS approach described previously. Only satellites that are visible to both receivers are utilized in RTK solutions, because a differencing method between measurements is used to reduce errors. This increases the likelihood that measurement errors that affect one receiver will affect both receivers similarly and will, therefore, not adversely affect the estimate of the IVV. RTK also makes full use of precise carrier phase measurements. The use of carrier phase measurements is described in the Literature Review document. It is important to reiterate that it may not always be possible to validate the estimated integer ambiguities, which would limit the precision of the position solution. Changes in the fixed or estimated integer carrier phase ambiguities also create changes in the estimated positions. Changes from float to fixed ambiguities or changes between fixed ambiguities can also cause discontinuities in the position solution.

4.3 Vehicle to Infrastructure (V2I) Processing Method

The implementation of position-assisted infrastructure is intended to improve positioning accuracy around key intersections or other critical locations. The Concept of Operation in the Cooperative Intersection Collision Avoidance System-Violations (CICAS-V) prototype system is an example of the use of this concept. In deployment, the infrastructure locations would broadcast reference station corrections in a zone surrounding a broadcasting point. When vehicles enter the infrastructure zone, they could switch their positioning methods from unassisted SP to kinematic mode relative to the reference point.

In this project, a broadcasting infrastructure point with a 300 m range was simulated using post-processing. The first part of the processing involved determining the location of the stationary tripod mounted antenna shown in Figure 3-5. This location was obtained by processing the measurements collected by the stationary receiver and base receivers at CCIT using commercial RTK-network SW. This SW estimated that the obtained RTK solution was accurate to 5 mm (1 sigma). Next, the GPS/INS position solution for each vehicle was used to identify the times at which the vehicle crossed the circle of 300 m centered on the infrastructure point. Using the stationary infrastructure receiver as base, commercial post-processing RTK SW was then used to determine RTK solutions for each of the test receivers (AW, BW, BN, B24W) on each vehicle for the times at which the vehicle was inside the circle. It is important to note that the processing for each time segment during which the vehicle passed through the circle was initiated at exactly the instant the vehicle crossed the circle, and the SW generally took a few epochs to converge or provide a solution. This was done because it emulates the conditions that will occur in future possible deployment (i.e., communication will only be possible within the specified range (here 300 m)), and this is when calculations could begin. The RTK solutions for each test receiver were transformed into geodetic positions using the previously determined location of the infrastructure point. Outside of the time segments during which a vehicle is within range of the infrastructure point, and for times during

which no V2I solution is available, the derived geodetic position for each of the test receivers is replaced with that obtained from the receiver running in SP mode. Determination of the IVV from a pair of such padded V2I-aided solutions follows the same protocol as described for DPOS.

5 Performance Measures

The performance of the three methods of estimating the IVV, namely RTK, DPOS, and V2I, is analyzed for the multiple receiver combinations using two main measures of accuracy and availability. The precise meanings of these terms as used in this project are described below.

5.1 Accuracy

The accuracy of a particular method (RTK, DPOS, or V2I) and receiver combination for a particular data set is determined using the error in the determination of the IVV as a function of time relative to the reference chosen for that data set (refer to Section 4.1). The AT and XT components of the error time series are presented in plots, while their means and standard deviations are tabulated. Histograms and Cumulative Distribution (CD) plots of the error components and CD plots of the magnitude of the horizontal errors are also presented. Errors in the vertical component of the IVV are not shown in this study because they are not a concern for vehicles on the same roadway⁷.

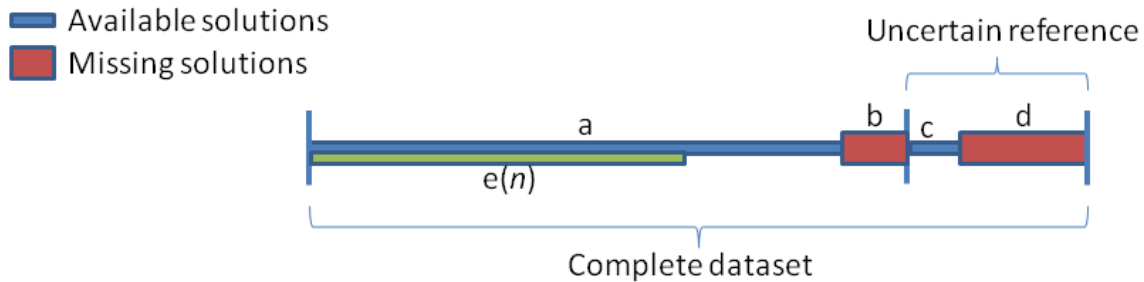
The mean of the AT or XT errors is an indication of possible biases relative to the reference IVV, while the standard deviation is an indication of the variability of the errors. These values are quoted based upon data that have less than 20 m error (relative to the reference IVV) in either component. The 20 m limit was chosen because errors of this magnitude should be able to be detected and eliminated using Receiver Autonomous Integrity Monitoring (RAIM), vehicle sensors such as inertial sensors or wheel speed sensors or possibly map-matching techniques. Removing data with large errors ensures that outliers, which may be in error by more than 1 km, do not bias the means and standard deviations, thereby allowing for better comparison and interpretation.

5.2 Availability

Availability used in this project is defined with reference to Figure 5-1. In this figure Missing Solutions,” sections “b” and “d,” occur at epochs when either a solution cannot be computed due to poor satellite geometry or when, for RTK calculations, there is a communications failure between the two vehicles. It was not possible to unambiguously determine the reason for the absence of solutions from inspection of the RTK logs because both radio failure and the inability to calculate a solution simply resulted in missing epochs in the log file. The section marked “uncertain reference” represents the epochs for which the either the reference or comparison IVVs (refer to Section 4.1) are missing or their difference between was beyond a threshold. As is discussed in Section 8.1, the RMS of the difference between the reference and comparison IVVs was

⁷ For applications in which vehicles are on an interchange, the vertical component of the IVV may be useful to determine which vehicles are on the same road.

generally less than 20 cm, and less than 10 cm in environments permitting open sky views.



- a Epochs with available solutions and certain reference
- b Epochs with no solution and certain reference
- c Epochs with available solutions but uncertain reference
- d Epochs with no solution and uncertain reference
- e(*n*) Available with error less than *n* meters (and certain reference)

Figure 5-1: Availability Definitions

The three most important availability measures for a given method⁸ (RTK or DPOS) and a given receiver combination are:

- Full Availability (FA): The percentage of the time a solution is available (with no regard to the quality of that solution).

$$FA = \frac{(a + c)}{(a + b + c + d)}$$

- Availability With Certain Reference (AWR): The percentage of the time a solution is available *and* the reference is of certain quality with respect to the time a reference of certain quality is available.

$$FA = \frac{a}{(a + b)}$$

This quantity specifies the availability of solutions of which it is possible to determine the accuracy.

⁸ Availability calculations for the V2I method were not performed, because the intermittent nature of the solutions renders the results meaningless.

- Availability Without Certain Reference (AWOR): The percentage of the time a solution is available, but its accuracy cannot be quantified because the reference is of uncertain quality.

$$AWOR = \frac{c}{(a + b + c + d)}$$

Since the availability metrics just discussed do nothing to quantify the accuracy of the solutions, an additional measure was defined. Suppose “ $e(n)$ ” in Figure 5-1 is the number of epochs for which the error (the AT or XT component) is less than n meters, then the following useful metric can be defined:

- Full Availability with Error Less than n m (FAWE(n)): The percentage of time a solution with error less than n meters is available.

$$FAWE(n) = \frac{e(n)}{(a + b + c + d)}$$

This quantity is obviously bounded above by the FA. There is some uncertainty in the quantity due to the presence of the “ c ” portion of Figure 5-1, which represents epochs for which solutions exist; but their accuracy is not quantifiable, since the reference is of uncertain quality. For this reason, when FAWE(n) is quoted, it is increased by half of AWOR and has an uncertainty of the same amount (i.e., it is quoted as $FAWE(n) + \frac{1}{2} AWOR \pm \frac{1}{2} AWOR$).

FAWE(n) is quoted for $n = 1.5$ m and $n = 5$ m, since these distances are those considered sufficient to position (relatively) a vehicle at the lane and road level, respectively.

6 Predictive Measures

Under actual operation, no reference solution is available, and the accuracy of the IVV estimate cannot be known. For this reason it is of interest to determine if there are quantities, easily derivable from the measurements of a GNSS receiver, which can be correlated with the accuracy. If such quantities existed, they could be shared between vehicles to provide an estimate of the accuracy of the instantaneous IVV solutions.

6.1 Dilution of Precision

The DOP is an indicator of the satellite geometry. This is directly linked with the position accuracy, because an improvement in satellite geometry (represented by a lower value of DOP) for a constant level of measurement error results in improved position accuracy. The HDOP at each receiver in a pair is used for DPOS, while a single GDOP value is presented for the RTK method.

6.2 Number of Satellites

The number of satellites used in the calculation of position is also an indicator of the expected positioning accuracy and reliability. The more satellites used in the calculation of a position solution, the more position errors can be averaged, resulting in an overall improvement in accuracy. While this is true of SP solutions for DPOS as mentioned previously, it is important that common satellites be used. Thus, a direct correlation between number of satellites used in the position solution at each vehicle (i.e., a pair of numbers) and IVV accuracy is not likely for DPOS. For RTK, since common satellites are used in the solution, such a correlation could be expected.

7 Data Collection Summary

V2V data was collected in and around Calgary, Canada, between August 4, 2009 and August 25, 2009. In the majority of the tests, Vehicle 1 followed Vehicle 2 with a distance of less than 300 m, and generally between 30 and 150 m. Some driving environments forced modifications of the default behavior (e.g., on highways vehicles moved in between the two test vehicles necessitating lane changes). Approximately 52 hours of data was collected, but reduced to just over 45 hours of usable data.

The data was collected in the seven test environments listed below, which were selected in accordance with Federal Highway Administration (FHWA) descriptions [2]. Photos in each of the environments are shown in Section 13. The amount of data collected in each of these environments is summarized in Table 7-1.

Deep Urban Canyons: Streets deep within the city surrounded by many tall buildings are an example of the Deep Urban Canyon environment. These roads are characterized by high mask angles. Driving in this environment is at low speeds, typically 25 mph, with frequent starts and stops. For this study, streets in downtown Calgary were used. The mask angles were typically 20 to 40 degrees but occasionally reached 80 degrees.

Major Urban Thruway: This environment contains roads with 40 to 50 mph speed limits. The roads are surrounded by 3- to 4-storey buildings on both sides with approximately 20 degree elevation masks. Examples of this environment are Telegraph Road in Michigan or parts of Crowchild Trail in Calgary.

Major Rural Thruway: This environment also contains roads with 40 to 50 mph speed limits; but in distinction to the Major Urban Thruway area environment, the sides of the roads have only occasional 3- to 4-storey buildings and have an otherwise open view of the sky. Examples of this environment are US12 around Irish Hills in Michigan and parts of Sarcee Trail in Calgary.

Major Roads: Routes in this environment have speed limits of 30 to 40 mph and mask angles ranging from 5 degrees in rural sections to 20 degrees in urban sections. Examples of these types of roads include Mound Road in Warren, Michigan, or Shaganappi Trail in Calgary.

Local Roads: Local Roads are typical neighborhood roads with speed limits of approximately 25 mph. These roads are typically narrower than those in the Major Road

environment and often have substantial numbers of trees that will limit the sky-view. Driving on Local Roads is generally characterized by frequent stops and cornering.

Interstate/Freeway: This environment comprises divided highways with at least 2 lanes in each direction with speed limits of 55 to 70 mph. Examples of this environment include Highway 1 outside of 16th Avenue between Shaganappi and Deerfoot Trails in Calgary. The environment is mostly open sky with 5 degree elevation masks with a few overpasses.

Mountains: The final environment type is on roads that would otherwise be described as Major Roads or Interstate/Freeway, that pass through tree covered and mountainous areas. The speed limit on these roads is similar to the interstate/freeway environment; however, the mask angle is significantly higher due to the trees and mountains.

Table 7-1: Data Collection Summary

Category	Time Collected	%
Deep Urban	1:39:54	3.7%
Major Urban Thruway	9:50:03	21.8%
Major Rural Thruway	8:40:09	19.2%
Major Road	8:10:40	18.1%
Local Road	6:30:48	14.4%
Interstate/Freeway	9:04:51	20.1%
Mountains	1:08:32	2.5%
Total	45:04:57	

V2I data was collected on August 26, 2009, and August 27, 2009. Collections were performed in five environments—those that were used for V2V tests with the exception of Deep Urban and Mountains. These two environments were excluded for reasons of safety. Three types of “coordinated pass” were performed in each environment:

- **Following:** Vehicle 1 followed Vehicle 2 past the infrastructure point.
- **Approaching:** The vehicles approached the infrastructure point from opposite directions attempting to pass it at approximately the same time.
- **Intersection:** The vehicles approached the infrastructure point from roadways separated by approximately 90 degrees. In the Freeway tests, an overpass was used; Vehicle 1 drove on the overpass, while Vehicle 2 drove on the Freeway underneath.

At least two passes of each type were collected in each environment.

8 Vehicle-to-Vehicle Test Results

This section contains presentation and discussion of the results of the field tests described in Section 7. It focuses on comparing data that isolates factors that may impact V2V performance, namely the effect of receiver type and quality, the effects of WAAS, the effect of a limited constellation size, and the IVV calculation method (RTK versus

DPOS). For each of these comparisons, tabulated data and figures obtained using specific receiver combinations are chosen to support arguments.

Each comparison contains the same subsections:

- A discussion of availability using the measures presented in Section 5.2 (FA and FAWE) and/or data gap statistics.
- Comments regarding the number of satellites and DOP using each method/receiver combination with a view as to whether these are effective accuracy predictors.
- Analysis of the accuracy allowed for each method/receiver combination.
- Comments regarding the performance of all method/receiver combinations in different environments.

8.1 Reference IVV Statistics

Before making comparisons between various methods of determining the IVV, it is essential that one has confidence in the reference values used to determine the vector. As was discussed in Section 4.1, the reference IVV was calculated using a variety of different methods, HW, and SW. Visual comparisons of plots of the magnitudes of the differences between the various reference IVV solutions were then used to select the reference IVV and the second best solution to assess the agreement between the two solutions. Table 8-1 summarizes the important statistics for the selected reference and comparison IVVs for each of the V2V data collections. The columns of this table have the following interpretation.

- **Total RMS:** The RMS of the differences between the reference and IVVs selected over the entire duration of the test.
- **Post-Reject RMS:** The RMS of the difference between the reference and comparison IVVs after the data has been rejected (see below).
- **Missing:** The percentage of the duration of the test during which the reference or comparison IVV is absent.
- **Rejected:** The percentage of the duration of the test during which the difference between the reference and comparison IVVs is greater than 1 m, so the reference is of uncertain quality.

As was discussed in Section 5.2, portions of data where there are rejected or missing reference IVVs add slightly to the uncertainty in the specification of availability measures.

When interpreting the data in Table 8-1, it is important to note that there was no data rejection in the Urban Canyon environments, despite the fact that the RMS values are on the order of 10 m. This is because GNSS-only techniques cannot be used reliably in this particular environment. The IVV obtained using the integrated GPS/INS system on each vehicle was used as the reference IVV. The only other number standing out in the table is the high level of missing data for the August 12, 2009 data collection. The local roads

environment, and this test run in particular, involves frequent heavy tree cover, making it a challenging environment for GNSS.

Aside from the aforementioned Urban Canyon results, the RMS of the differences between the reference and comparison IVVs is generally less than 20 cm, with the largest differences occurring on the local roads, for the reason discussed above. For the environments involving mainly open sky, the RMS of the differences is generally below 10 cm, indicating excellent agreement.

Table 8-1: Reference IVV Statistics for each of the V2V Data Collections

Date	Test	Environment	Total RMS (m)	Post- Reject RMS (m)	Missing (%)	Rejected (%)
04Aug	A	Interstate	0.08	0.08	0.2	0.0
	C	Mountain	0.16	0.16	1.4	0.0
	D	Interstate	0.02	0.02	0.0	0.0
05Aug	A	Urban Canyon	9.47	9.47	0.0	0.0
	B	Urban Canyon	12.24	12.24	0.0	0.0
06Aug	A	Interstate	1.52	0.07	2.3	0.3
12Aug	A	Local Roads	0.28	0.22	20.9	1.5
13Aug	A	Interstate	0.04	0.04	1.5	0.0
	B	Local Roads	0.03	0.03	1.1	0.0
14Aug	A	Major Roads	0.09	0.05	3.2	0.1
	C	Interstate	0.70	0.22	5.1	3.5
17Aug	A	Local Roads	0.20	0.17	0.0	0.4
	B	Local Roads	0.36	0.27	1.5	2.9
19Aug	A	Major Roads	1.04	0.04	4.0	0.2
	B	Major Roads	6.93	0.19	4.1	3.1
	C	Major Roads	0.19	0.12	5.4	0.4
20Aug	A	Urban Thruway	0.15	0.15	1.2	0.1
	B	Major Roads	0.05	0.05	0.0	0.0
21Aug	A	Urban Thruway	0.20	0.08	0.9	0.3
	B	Urban Thruway	0.05	0.04	2.1	0.0
	C	Urban Thruway	0.07	0.06	2.8	0.1
24Aug	A	Urban Thruway	0.06	0.06	3.9	0.0
	B	Urban Thruway	0.09	0.05	0.4	0.2
	C	Rural Thruway	0.02	0.02	1.8	0.0
	D	Rural Thruway	0.29	0.06	0.6	0.6
25Aug	A	Rural Thruway	0.05	0.05	1.2	0.0
	B	Rural Thruway	0.09	0.06	3.7	0.2
	C	Rural Thruway	0.04	0.04	0.5	0.0
	D	Rural Thruway	0.06	0.06	0.5	0.0

8.2 Effects of Positioning Method

The DPOS and RTK positioning methods are compared in this section. Two homogeneous receiver pairs (AW-AW) and (BW-BW) and two mixed pairs (AW-BW) and (BW-AW) were chosen for comparison.

8.2.1 Availability

As shown in Table 8-2, the FA (see Section 5.2) of the RTK positioning method, ranging from 82 percent to 92 percent is significantly lower than the DPOS method, which ranges from 97 percent to 100 percent. A very small percentage of missing RTK solutions are due to failure of the real-time radio link, which does not affect the DPOS methods for this analysis (as discussed in Section 4.2.1, DPOS was calculated in post-mission). It should be noted that it was not possible to unambiguously determine the cause of a data gap in the RTK solutions; but out of the 45 hours of data, there were only 6 minutes during which there was a communication failure, as was determined through comparison of locally and remotely logged data.

Table 8-2: Availability Statistics for Selected Receiver Pairs Comparing the RTK and DPOS Positioning Methods

Receivers		Proc. (D)POS/(R)TK	FA (%)	FAWE (1.5 m)		FAWE (5 m)		UNC. (%)
Host	Remote			AT (%)	XT (%)	AT (%)	XT (%)	
AW	AW	R	92	91	91	91	91	<1
		D	97	93	92	96	95	1
	BW	R	84	68	69	83	83	<1
		D	98	62	66	95	95	1
BW	AW	R	84	81	80	84	83	<1
		D	98	59	68	94	95	1
	BW	R	82	74	71	81	81	<1
		D	100	89	88	97	97	2

While the FA of DPOS is considerably higher than that of RTK for all considered receiver pairs, the same cannot be said for the FAWE values. The DPOS and RTK FAWE (1.5 m) values for (AW-AW) are almost identical. Indeed, the fact that FAWE (1.5 m) for the (AW-AW) pair is only 1 percent less than the FA for RTK means that when a RTK solution is available from the pair, it is almost certain to have an error less than 1.5 m. The FAWE (1.5 m) values for both mixed pairs are higher for RTK than they are for DPOS.

The low FA for (BW-BW) in RTK is likely because the RTK SW rejects more BW measurements than AW measurements. This would be caused by the increased noise and multipath errors present in the measurements of the B receivers that is a consequence of their high-sensitivity signal tracking. The Type A receiver phase lock loops are also expected to be of a higher quality, resulting in better carrier phase measurements that contain a lower number of cycle slips.

Table 8-2 and the availability and accuracy tables that follow show there is usually very little difference between the magnitude of the errors in AT and XT components of the IVVs. There is indeed little theoretical reason to support a difference in accuracy of these components in the general case. Cases where one might expect a higher accuracy for one of the components include those where the environment (tall buildings/trees) reduces the observable satellite constellation to a strip parallel with the direction of travel. Assuming sufficient satellites are available to calculate the IVV, one would expect greater accuracy for the AT component in such a case.

Finally, Table 8-2 shows incongruous FAWE(1.5) values for the (AW-BW) and (BW-AW) pairs using RTK. Since the receivers involved are the same, one would expect similar performance. The discrepancy, which is no longer apparent at the 5 m level, is likely due to the RTK SW treating the two receiver types, or the host and remote, differently.

Table 8-3 shows that RTK has more and longer data gaps than DPOS. This is most pronounced in the (BW-BW) where there are approximately 1500 more data gaps for RTK than with the same receiver pairs using DPOS. While a small number of the data gaps are due to communications failures, the majority is because of the aforementioned rejection of measurements from the high-sensitivity receivers and because the number of satellites used in the RTK solution is bounded by the smaller of the two numbers of satellites observed by receiver pair. This bound exists because, as mentioned previously, RTK can only use observations common to both receivers.

When the vehicles enter environments that limit the number of satellites in view, the satellites rejected by the RTK processing software cause the RTK solution to have too few satellites to calculate and output a solution. It may be possible to tune the RTK processing software so that it does not reject as many measurements, which would increase availability but would also impact position accuracy.

Table 8-3: Data Gap Statistics for Selected Receiver Pairs Comparing the RTK and DPOS Positioning Methods

Receivers		Proc. (D)POS/(R)TK	# Gaps	Gaps < 15 s		15s < Gaps < 30 s		Gaps > 30 s	
Host	Remote			%	Ave (s)	%	Ave (s)	%	Ave (s)
AW	AW	R	1459	90	5	6	21	4	72
		D	1123	97	2	2	19	2	77
	BW	R	1375	56	7	31	20	13	67
		D	894	96	2	2	20	2	58
BW	AW	R	1377	56	6	31	20	13	9
		D	829	97	2	2	20	2	1
	BW	R	1455	53	6	33	20	14	71
		D	8	100	3	0	-	0	-

8.2.2 Number of Satellites

The number of satellites used in DPOS solutions⁹ is significantly higher than that in RTK solutions for all receiver combinations, as is shown in Table 8-4. For (BW-BW), the 30 percent increase in the number of satellites used is, at least in part, why the DPOS positioning method performs better than the RTK method for this receiver combination.

Table 8-4: Mean Number of Satellites used by Selected Receiver Pairs Comparing the RTK and DPOS Positioning Methods

Receivers		Proc. (D)POS/(R)TK	Mean # Satellites
Host	Remote		
AW	AW	R	7.7
		D	9.0
	BW	R	7.1
		D	9.6
BW	AW	R	7.1
		D	9.6
	BW	R	7.0
		D	10.1

8.2.3 Dilution of Precision

It is not possible to compare the DOP values for the RTK and DPOS methods because, as mentioned previously, the RTK SW only output GDOP, while DPOS yielded two HDOP values.

8.2.4 Accuracy

The accuracy of the various receiver and processing methods combinations can be determined with reference to Table 8-2, which shows the availability of solutions with specified levels of accuracy (1.5 m and 5 m), and Table 8-5, which tabulates the means and standard deviations of the AT and XT errors. As mentioned in Section 5.1, the means and standard deviations are presented for the data that has had errors (relative to the reference IVV) larger than 20 m in each of the components removed. The 20 m limit was chosen since errors of this magnitude should be detectable using RAIM and/or additional vehicle sensors or map-matching. The FAWE(20) values, which are shown in Table 8-6, indicate the percentage of the data with AT or XT component errors less than 20 m (i.e., the percentage of the data used in the calculation of the means and standard deviations). Note that the FA, FAWE(20 m) values, and the means and standard deviations are split in two tables (Table 8-5 and Table 8-6) for clarity.

As could have been expected from Table 8-2, Table 8-6 shows that when an RTK solution is available, it has, to the resolution of the table at least, an error less than 20 m. The DPOS method generally shows a presence of 1 percent - 2 percent of solutions with more than 20 m error in the AT or XT components. It should be remembered, however,

⁹ In this and subsequent tables, the numbers of satellites for DPOS are found by averaging those used by the two receivers involved so that a single number is produced for each receiver pair.

that the DPOS combinations have a significantly higher FA than the RTK combinations, as was discussed above.

Table 8-5 shows that the standard deviations for the DPOS pairs are consistently higher than those for the corresponding receivers using RTK, indicating that the RTK method has greater precision than DPOS for the same receiver pairs. The absolute values of the means for the RTK pairs are also generally smaller than the corresponding DPOS pairs, the one exception being the (BW-BW) pair where the mean of the XT error is the same for both methods and that of the AT error is less for DPOS. The difference in the means of the errors, which corresponds to a difference in accuracy, is most pronounced for the mixed pairs (i.e., (BW-AW) and (AW-BW)). This is because the RTK method only uses satellites that are common to both receivers and, therefore, the common measurement errors cancel. The DPOS method uses whichever satellites are available at each individual receiver and does not ensure that only common satellites are used. The use of different satellites, particularly those at low elevation, will introduce biases that are not common between the vehicles and, thereby, degrade the relative position accuracy. This effect is more pronounced as the number of different satellites increases.

The fact that (BW-BW) DPOS shows slightly better accuracy (as judged by the magnitude of the mean of the error) than (BW-BW) RTK is not regarded as very significant; the DPOS method still results in a lower precision (large standard deviations). The reason that the performance of the pair using RTK is not substantially better than the pair using DPOS in terms of mean and standard deviation is likely linked to the low quality phase measurements from the B receivers, as compared to the AW receivers. This is supported by the fact that for all pairs involving an AW receiver, the means and standard deviations are less, often significantly so, for RTK compared to DPOS.

Table 8-5: Along and Across Accuracy for Selected Receiver Pairs with the RTK and DPOS Positioning Methods

Receivers		Proc (D)POS/(R)TK	Along Errors		Across Errors	
Host	Remote		Mean (m)	S.D. (m)	Mean (m)	S.D. (m)
AW	AW	R	0.01	0.42	0.01	0.57
		D	-0.02	0.78	0.02	0.99
	BW	R	0.05	1.37	-0.02	1.45
		D	-0.17	1.97	0.09	1.92
BW	AW	R	-0.02	0.74	0.05	0.91
		D	0.22	1.96	-0.15	1.79
	BW	R	-0.06	1.10	0.15	1.35
		D	0.02	1.41	0.15	1.59

Table 8-6: Availability of Solutions with Less than 20 m for Selected Receiver Pairs with the RTK and DPOS Positioning Methods

Receivers		Proc. (D)POS/(R)TK	FA (%)	FAWE (20 m)	
Host	Remote			AT (%)	XT (%)
AW	AW	R	92	92	92
		D	97	96	96
	BW	R	84	84	84
		D	98	96	96
BW	AW	R	84	84	84
		D	98	97	97
	BW	R	82	82	82
		D	100	98	98

Figure 8-1 and Figure 8-2 show two graphical representations of the difference in accuracy between the RTK and DPOS positioning methods for the AW-AW pair.

When interpreting these cumulative distribution function (CDF) plots and others in this report, it is important to note that the percentages on the vertical scale are defined relative to the times when the solution and the reference is available. The following hypothetical example highlights the problem that may arise through incorrect interpretation of this kind of plot. Suppose for a certain data set using a certain receiver pair that:

- The reference is available 100 percent of the time.
- RTK is available only 40 percent of the time; but when available, its solution has an error always less than 5 m.
- DPOS is available 90 percent of the time; but when available, the error is only less than 5 m 50 percent of the time.

In this case the CDF comparing RTK and DPOS will show RTK reaching 100 percent within 5 m while DPOS will only reach 50 percent at the same point, making the performance of RTK look much better than that of DPOS. A different style of CDF might show the total percentage of solutions on the vertical axis, in which case RTK would reach only 40 percent and DPOS 45 percent by the 5 m mark, making their performance appear much closer. The CDFs adopted herein give a good indication of the distribution of errors for the *available solutions* for each method.

In the case of Figure 8-1 and Figure 8-2 the situation is not as extreme as in the hypothetical situation just discussed, because the full availability of the RTK and DPOS solutions for the (AW-AW) pair are reasonably close, 92 percent and 97 percent respectively. Even with these FA values, incorrect interpretation of the CDFs is possible. Figure 8-2 would seem to indicate that the (AW-AW) pair using RTK has a higher availability of solutions with component-wise errors smaller than 1.5 m than for DPOS, whereas Table 8-2 shows that the opposite is true. What the figures do show is that the quantifiable *available solutions* from (AW-AW) RTK almost all have a horizontal error of less than 1 m; more than 90 percent have a horizontal error less than 0.5 m. As for (AW-AW) DPOS, Figure 8-1 indicates that of the available solutions, just under 90 percent have a horizontal error less than 1 m.

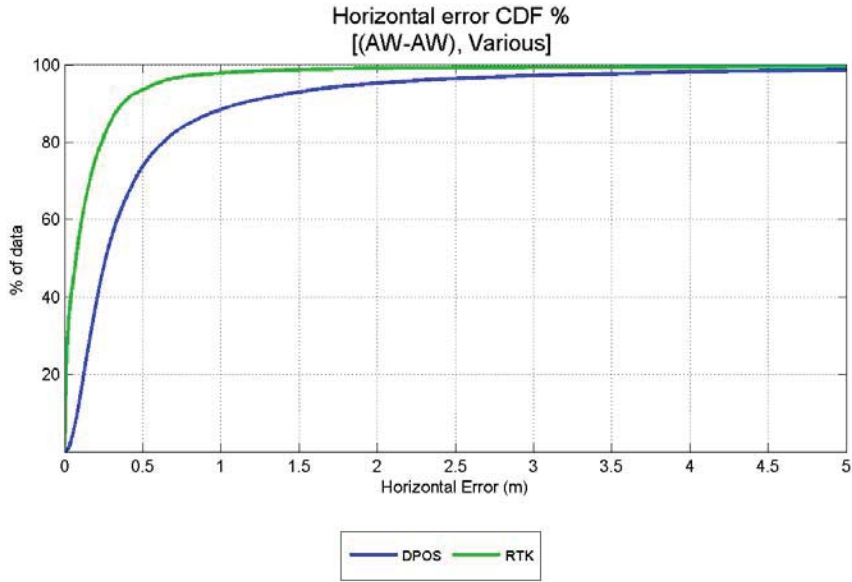


Figure 8-1: CDF for the Horizontal Error for RTK and DPOS Processing of all (AW-AW) Data

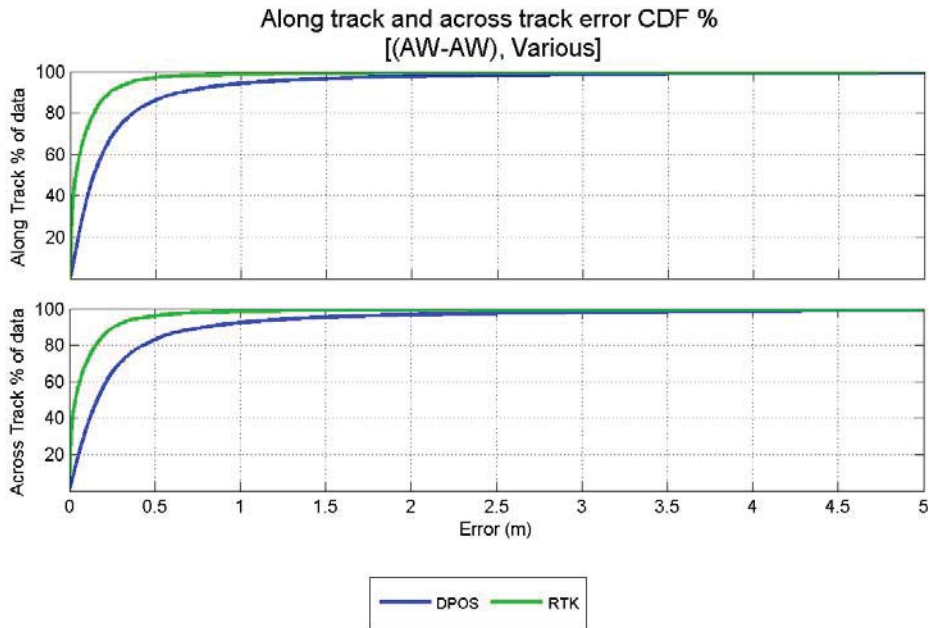


Figure 8-2: CDF for the AT and XT Errors for RTK and DPOS Processing of all (AW-AW) Data

8.2.5 Environment Types

Table 8-7 shows the availability of solutions with 1.5 m and 5 m accuracy from the (AW-AW) pair using both RTK and DPOS for each of the test environments. When using the DPOS, it shows that the FA is always greater than that for RTK (i.e., DPOS yields a solution more often than RTK). The difference in availability is greatest in the areas that are traditionally challenging for GNSS, Deep Urban, and Local Roads, the latter often being associated with heavy tree cover. With the exception of these environments, the availability of solutions using both DPOS and RTK is greater than 90 percent. The availability of solutions with less than 1.5 m error is almost the same for RTK and DPOS in each environment; the exception being Local Roads, where RTK yields solutions of this quality 8 percent less often. In all environments, FAWE(5 m) is essentially equal to FA for RTK, indicating that practically all available solutions have a component-wise error smaller than 5 m. This is also true for DPOS, with the exception of the Deep Urban environment where the approximate difference between FA and FAWE(5) is 11 percent.

Table 8-7: Availability Statistics for (AW-AW) using RTK and DPOS in each of the Environments

Environment	Proc. (D)POS/(R)TK	FA (%)	FAWE(1.5 m)		FAWE(5)		Unc.
			AT (%)	XT (%)	AT (%)	XT (%)	%
Deep Urban	R	47	39	37	45	42	0
	D	60	39	34	50	48	0
Interstate/ Freeway	R	95	95	95	95	95	<1
	D	99	96	95	95	95	<1
Local Roads	R	84	81	81	82	82	<1
	D	97	89	88	93	93	3
Major Roads	R	94	93	93	93	93	<1
	D	98	95	92	97	96	1
Mountain Roads	R	99	99	99	99	99	<1
	D	100	99	97	99	99	<1
Rural Thruways	R	97	97	96	97	97	<1
	D	99	98	98	99	99	<1
Urban Thruways	R	95	95	95	95	95	<1
	D	99	95	96	98	98	<1
Various	R	92	91	91	91	91	<1
	D	97	93	92	96	95	1

Table 8-8 shows the same information as Table 8-7 but for the (BW-BW) pair instead of the (AW-AW) pair. The availability for DPOS is considerably higher than that for RTK for all environments except Interstate and Mountain Roads where the differences are 5 percent and 8 percent, both in favor of DPOS. Solutions at the lane level (1.5 m) are always more available with DPOS than RTK, with the largest differences being in the Deep Urban and Local Roads environments. Perhaps the most surprising entries at the 1.5 m level are those for RTK in the Interstate environment. Here the difference between FA and FAWE(1.5 m) is 13 percent indicating that 13 percent of the solutions available

from RTK in this environment have errors larger than 1.5 m. This is in contrast to the (AW-AW) pair using RTK in the same environment where all available solutions have errors less than 1.5 m, as was shown in Table 8-7. Given that this environment is characterized by open sky views, this relatively poor accuracy must be attributed to either the lower quality measurements from the B receivers or sub-optimal treatment of the measurements by the RTK SW. Not too much weight should be given to the fact that the FAWE(1.5 m) values are almost equal to the FA for the Mountain Roads environments when using RTK; this was a short data set comprising only 2.5 percent of the total data (refer to Table 7-1). As was the case for the (AW-AW) pair, the FAWE(5 m) values are almost equal to the corresponding FA values, indicating that regardless of environment and processing method, almost all available solutions have component-wise errors smaller than 5 m. The obvious exception is the Deep Urban environment, where the differences between FA and FAWE(5 m) are approximately 5 percent for RTK and more than 30 percent for DPOS.

Table 8-8: Availability Statistics for (BW-BW) Using RTK and DPOS in each of the Environments

Environment	Proc. (D)POS/(R)TK	FA (%)	FAWE(1.5)		FAWE(5)		Unc.
			AT (%)	XT (%)	AT (%)	XT (%)	%
Deep Urban	R	34	21	21	29	28	0
	D	100	40	31	72	60	0
Interstate/ Freeway	R	95	82	82	95	95	<1
	D	100	97	98	99	99	1
Local Roads	R	64	54	47	63	62	<1
	D	100	80	79	96	96	3
Major Roads	R	81	78	74	81	80	<1
	D	100	88	86	98	97	2
Mountain Roads	R	92	91	91	91	91	<1
	D	100	94	94	99	99	<1
Rural Thruways	R	88	80	75	87	87	<1
	D	100	93	93	99	99	<1
Urban Thruways	R	84	78	76	84	83	<1
	D	100	82	86	99	99	<1
Various	R	82	74	71	81	81	<1
	D	100	89	88	97	97	1

8.3 Effects of Receiver Quality

The effect of receiver quality is evaluated by comparing the performance of homogeneous pairs of AW and BW receivers.

8.3.1 Availability

As shown in Table 8-9, the BW receivers have slightly higher availability than the AW receivers when using the DPOS positioning method. The difference in availability

between these receiver combinations is more pronounced in the Deep Urban environment, as shown in Table 8-10. In this environment the high sensitivity B receivers using DPOS have much higher FA than the AW using DPOS, but the availability of solutions with an accuracy of 1.5 m is about the same.

The (AW-AW) receiver combination has a higher availability than the (BW-BW) combination when both pairs used RTK for all environments except for Interstate/Freeway. This is likely because the RTK SW rejects a significant number of measurements from the BW receivers.

Table 8-9: Availability Statistics for all Data for (AW-AW) and (BW-BW) Receiver Pairs

Receivers		Proc. (D)POS/(R)TK	FA (%)	FAWE (1.5 m)		FAWE (5 m)		UNC. (%)
Host	Remote			AT (%)	XT (%)	AT (%)	XT (%)	
AW	AW	R	92	91	91	91	91	<1
		D	97	93	92	96	95	1
BW	BW	R	82	74	71	81	81	<1
		D	100	89	88	97	97	1

Table 8-10: Availability Statistics for all Deep Urban Data for (AW-AW) and (BW-BW) Receiver Pairs

Receivers		Proc. (D)POS/(R)TK	FA (%)	FAWE (1.5 m)		FAWE (5 m)		UNC. (%)
Host	Remote			AT (%)	XT (%)	AT (%)	XT (%)	
AW	AW	R	47	39	37	45	42	0
		D	60	39	34	50	48	0
BW	BW	R	34	21	21	29	28	0
		D	100	40	31	72	60	0

The data gaps associated with the AW and BW receivers can be quantified in two ways. Table 8-11 shows statistics for the gaps in the receivers' solutions when running in SP mode. There are two orders of magnitude difference in the numbers of gaps between the AW and BW receivers. The majority of the gaps for the AW receivers have a duration of less than 15 seconds, but there are a non-negligible number, nearly 20, of gaps that are longer than 30 seconds. These occur in the Deep Urban environment.

Table 8-11: Data Gap Statistics for all Data of the AW and BW Receivers in SP Mode

Receivers		#Gaps	Gaps < 15 s		15 s < Gaps < 30 s		Gaps > 30 s	
Type	Vehicle		%	Ave (s)	%	Ave (s)	%	Ave (s)
AW	1	893	96.0	2.0	2.0	21.5	2.0	58.0
	2	825	96.5	2.2	1.8	20.1	1.7	57.6
BW	1	7	100.0	2.1	0.0	-	0.0	-
	2	3	100.0	2.3	0.0	-	0.0	-

The second way to quantify data gaps is shown in Table 8-12. As would be expected from the data in Table 8-11, (AW-AW) DPOS has significantly more data gaps than (BW-BW) DPOS. The new information that Table 8-12 adds is that the gaps for (BW-BW) RTK are longer (on average) than those for (AW-AW) RTK. While 97 percent of the gaps for (AW-AW) RTK are shorter than 15 seconds, only 53 percent of the gaps for (BW-BW) RTK fall in this range. This is, again, due to the rejection of poor quality measurements from the BW receivers by the RTK SW. The WAAS measurements have no effect on the above as they are not used in the RTK solutions.

Table 8-12: Data Gap Statistics for all Data of the AW and BW Homogeneous Receiver Pairs

Receivers		Proc. (D)POS/(R)TK	# Gaps	Gaps < 15s		15s < Gaps < 30s		Gaps > 30s	
Host	Remote			%	Ave (s)	%	Ave (s)	%	Ave (s)
AW	AW	R	1459	90	5	6	21	4	72
		D	1123	97	2	2	19	2	77
BW	BW	R	1455	53	6	33	20	14	71
		D	8	100	3	0	-	0	-

8.3.2 Number of Satellites

Table 8-13 shows that, on average, the (BW-BW) combination uses one more satellite than the (AW-AW) combination in DPOS, but that the margin is effectively reversed for RTK. Again this can be explained by the fact that the BW receivers have a high sensitivity; and, therefore, track more satellites in SP mode. While the measurements they provide will be of lower quality than the AW receivers, a large number of them are consequently rejected by the RTK SW.

Table 8-13: Mean Number of Satellites for all Data of the AW and BW Homogeneous Receiver Pairs

Receivers		Proc. (D)POS/(R)TK	Mean # Satellites
Host	Remote		
AW	AW	R	7.7
		D	9.0

Receivers		Proc. (D)POS/(R)TK	Mean # Satellites
Host	Remote		
BW	BW	R	7.0
		D	10.1

8.3.3 Dilution of Precision

The average RTK DOPs for the (AW-AW) and (BW-BW) pairs are 2.0 and 2.8 respectively, implying that the IVV estimates calculated using the AW receivers should have higher accuracy. The average DOPs¹⁰ of the receivers in SP mode (as used in DPOS) are approximately 1.3 for the AW receivers and 0.9 for BW receivers. This indicates that if the measurements from the two receivers were of the same quality, the BW receivers should have more accurate SP solutions.

8.3.4 Accuracy

Table 8-9 shows that (AW-AW) in RTK yields nearly 20 percent more solutions capable of positioning vehicles at the “lane level” (1.5 m) than (BW-BW) using the same processing method. At the 5 m accuracy level, the difference is approximately 10 percent still in favor of the AW pair. The superior accuracy of the AW pair is supported by a higher number of satellites, lower DOP values, and more accurate measurements. What the FAWE numbers do not show, but Figure 8-3 illustrates, is that the AW pair offers substantially more solutions that are accurate to the sub-meter level. When interpreting Figure 8-3, the discussion preceding Figure 8-1, the meaning of the percentages on the vertical axis should be considered.

The accuracy of the IVV estimates from the receiver pairs when using DPOS is nearly the same with AW at 92 percent versus BW at 89 percent, at least as far as the availability of solutions at the 1.5 m level is concerned. While the DOP is lower for the BW pair, this does not translate into noticeably more accurate IVV solutions for a number of reasons, including the fact that the measurements from the B receivers have larger errors than those from the A receivers. As discussed previously, the accuracy of the SP solution is a function of the satellite geometry (DOP) and the measurement errors. As was the case for RTK when using DPOS, (AW-AW) offers more solutions that are accurate to the sub-meter level than the (BW-BW) pair.

¹⁰ These values are the averages of the DOP values at each of the two receivers.

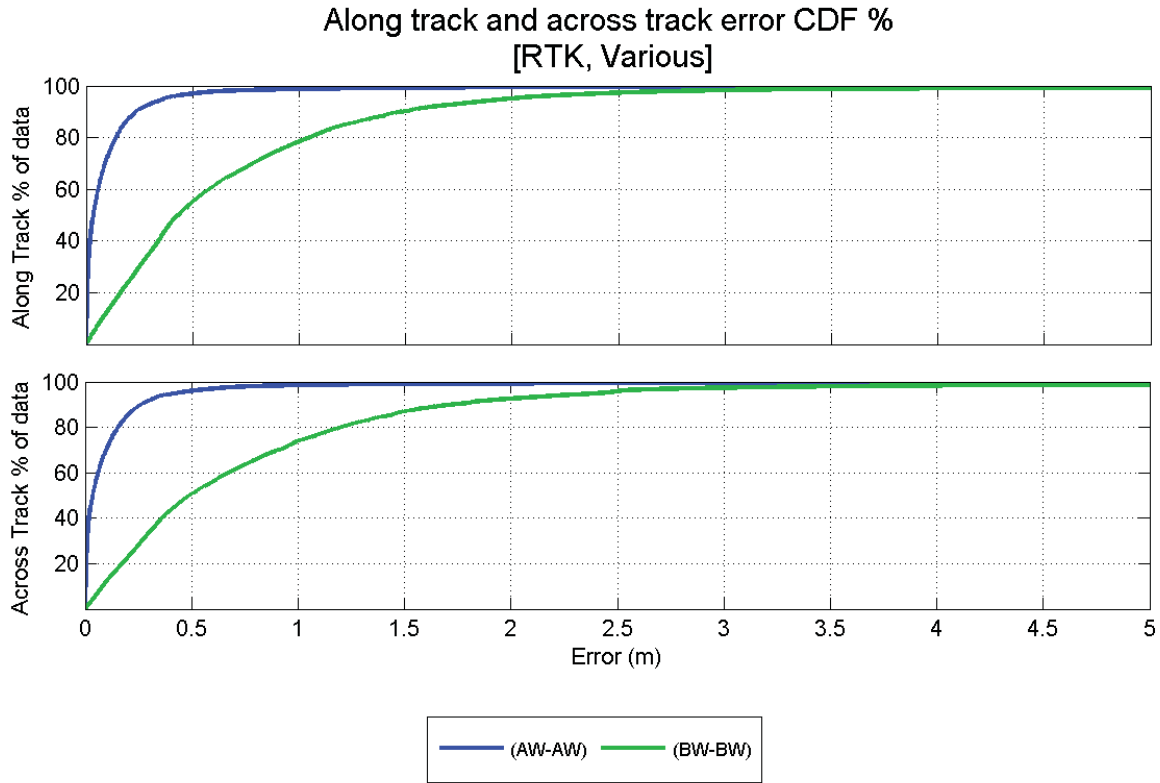


Figure 8-3: CDFs of the AT and XT Errors in the IVV Solutions Using (AW-AW) and (BW-BW), RTK

8.3.5 Environment Type

The points discussed in the previous section regarding the accuracy of receiver pairs and methods generally apply for all tested environments. The greatest difference in the performance of the receiver pairs when using RTK occurred in the Local Roads environment where the FAWE (1.5 m) for (BW-BW) was around 50 percent while it was 81 percent for (AW-AW).

8.4 Effects of WAAS

This section evaluates the effect of WAAS on the B receivers. The BW (like AW and B24W) receivers used both WAAS ranging and differential corrections, while BN used neither. Three receiver pairs are considered, namely two homogeneous pairs (BW-BW) and (BN-BN) and one mixed pair, (BW-BN). Since the RTK SW does not use WAAS measurements, only the performance of DPOS is discussed.

8.4.1 Availability

Table 8-14 shows the effect of WAAS on the FA is negligible. The most obvious difference in the table is that between the mixed pair (BW-BN) and the homogeneous pairs for FAWE (1.5 m), the reasons for which are discussed in Section 8.4.4.

Table 8-14: Availability Statistics for all Data for Selected Receiver Pairs Showing the Effect of WAAS

Receivers		Proc. (D)POS/(R)TK	FA (%)	FAWE (1.5 m)		FAWE (5 m)		UNC. (%)
Host	Remote			AT (%)	XT (%)	AT (%)	XT (%)	
BN	BN	D	100	90	89	97	97	1
BW	BN	D	100	82	84	97	97	1
	BW	D	100	89	88	97	97	1

8.4.2 Number of Satellites

As illustrated in Figure 8-4, on average, the BW receivers track approximately 1.4 satellites more than the BN receivers. This is due to the two WAAS satellites. On average, both receiver types use over 8 satellites in their navigation solutions, hence the addition of 1.4 satellites is not very significant.

8.4.3 Dilution of Precision

Figure 8-4 also shows the DOP for each of the receivers used in the pairs under consideration. As would be expected, since the BW receivers use a larger number of satellites, their DOP value is lower than that of the BN receivers. The difference, however, is small at approximately 0.1 on average.

8.4.4 Position Accuracy

As was shown in Table 8-14, the effect of WAAS satellites on position accuracy is negligible when the receiver pair is homogeneous. While the WAAS satellites and differential corrections make a SP solution more accurate, there is no visible benefit for the estimation of the IVV. The likely reason is that the position errors for each of the BN receivers will be similar and, therefore, cancelled when the IVV is calculated. For the (BW-BN) pair, such canceling does not occur. The BW receiver will have a more accurate SP solution, principally due to the available differential corrections. Since the BN receiver solution does not use these, the accuracy of the corresponding IVV solution decreases. Table 8-14 shows that these effects are confined to the sub 5-meter level. Figure 8-5 shows that the errors in the IVV solutions incurred by having only one WAAS-enabled receiver are generally below 3 m in the horizontal plane. When ionospheric activity increases, this error will increase.

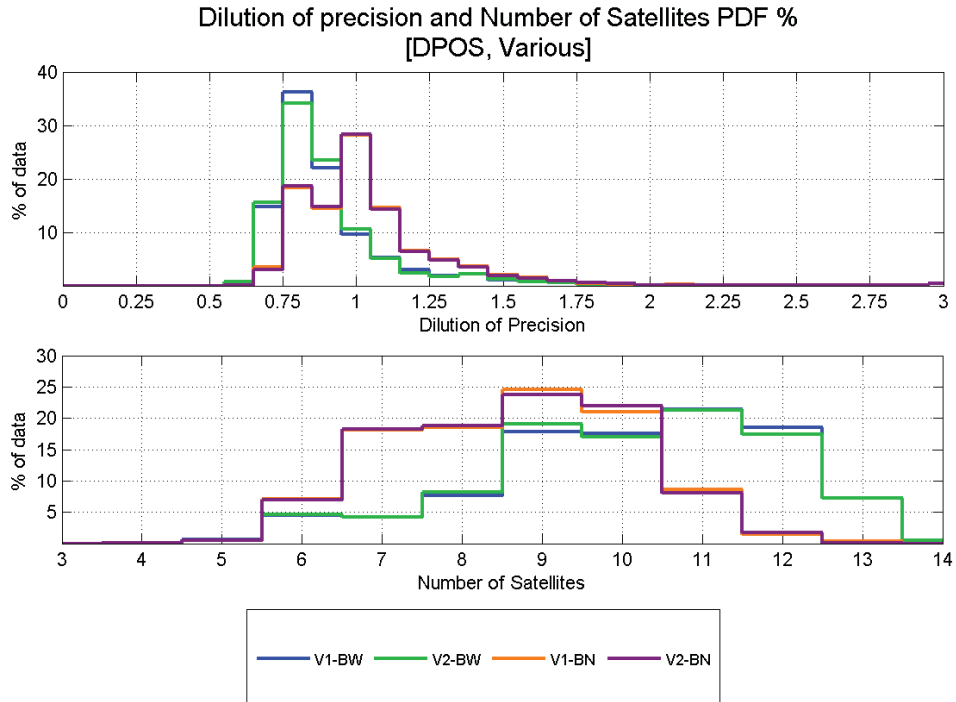


Figure 8-4: Effects of WAAS on the Number of Satellites and DOP

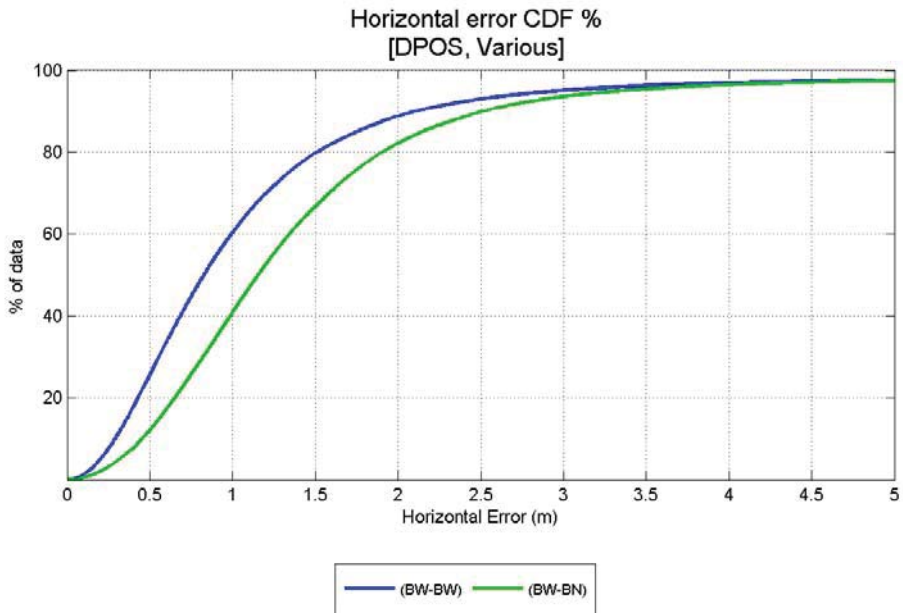


Figure 8-5: CDF of the Horizontal Error for (BW-BW) and (BW-BN) Combinations Over All Environments

8.4.5 Environment Types

The points discussed above, namely that two homogeneous pairs are more accurate than the mixed pair and the homogeneous pairs have similar accuracy, apply almost regardless of the environment. The exceptions to this are the Local and Mountain environments where (BN-BN) is more accurate than (BW-BW). The case for the Local Environment is shown in Figure 8-6. The reason is that in these two environments, which are both characterized by frequent turns and signal blockage due to trees and topography, one of the receivers in the pair (BW-BW) is intermittently denied access to the WAAS corrections, essentially rendering it the same as (BW-BN). In the other environments involving more open sky views and less frequent turns, with the exception of Deep Urban, the receivers will normally have access to the same satellites and corrections. In the Deep Urban case, there is little difference in the performance of (BW-BW), (BN-BN), and (BW-BN), as shown in Table 8-15. What is interesting to note in this table is the pronounced difference in the availability of solutions in the along and across track directions. This is likely due to the previously mentioned reduction of the visible GPS constellation caused by the presence of tall buildings.

Table 8-15: Availability Statistics for Deep Urban Data for Selected Receiver Pairs Showing the Effect of WAAS

Receivers		Proc. (D)POS/(R)TK	FA (%)	FAWE (1.5 m)		FAWE (5 m)		UNC. (%)
Host	Remote			AT (%)	XT (%)	AT (%)	XT (%)	
BN	BN	D	100	39	33	69	63	0
BW	BN	D	100	37	30	69	63	0
	BW	D	100	40	31	72	60	0

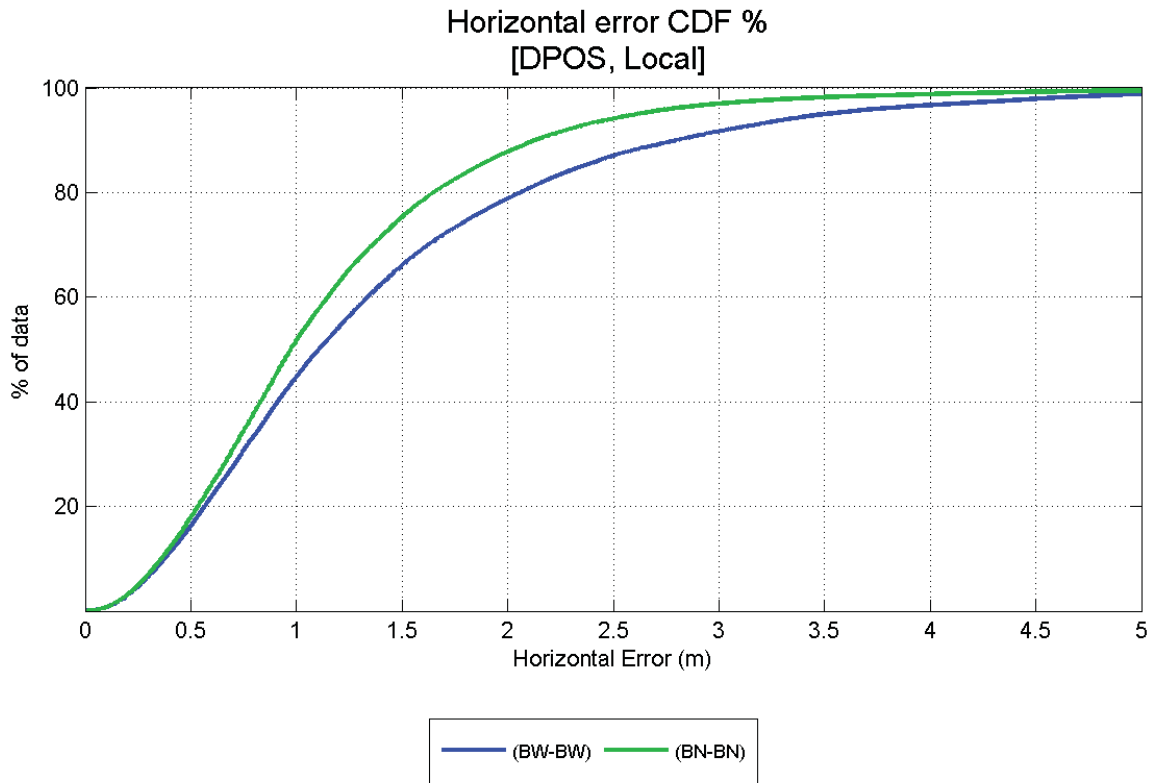


Figure 8-6: CDF of Horizontal Errors in the Local Road Environment for (BW-BW) and (BN-BN), DPOS

8.5 Effects of Constellation Limitations

The effects of a limited constellation, as would result if the US Government allowed the GPS constellation to drop to the minimum guaranteed, are shown by comparing the performance of the (BW-BW) and (B24W-B24W) pairs. This choice of pairs is logical since the receivers are of the same type (i.e., high sensitivity), and both have WAAS satellites and corrections enabled. The difference in their performance should be entirely due to the smaller constellation of satellites that the B24W receivers can use in their navigation solutions. Since the measurements of the B24W receivers were not processed using RTK, the comparison is limited to performance using the DPOS method.

It is noted that while the comparison used here isolates the effect of the limited constellation, more dramatic results may be obtained through the comparison of the high-sensitivity (BW-BW) pair with a standard receiver pair using a limited constellation in the navigation solution. This was not part of the objectives of this project.

8.5.1 Availability

As shown in Table 8-16, there is negligible difference in the availability of solutions between (BW-BW) and (B24W-B24W). Both yield solutions 100 percent of the time, and these are accurate to the lane level approximately 90 percent of the time.

Table 8-16: Availability Statistics for all Data for (BW-BW) and (B24W-B24) - Effect of Limited Constellation

Receivers		Proc. (D)POS/(R)TK	FA	FAWE (1.5 m)		FAWE (5 m)		UNC.
Host	Remote			AT	XT	AT	XT	
BW	BW	D	100	90	89	97	97	1
B24W	B24W	D	100	89	89	97	96	1

The B24W pair has 21 data gaps compared to 8 for the BW pair. In both cases, all gaps are less than 15 seconds. The increased number of gaps of the B24W pair is not very significant when it is considered that the (AW-AW) pair has in excess of 1000 data gaps over the same data, when using DPOS, and that 19 of 21 data gaps for the B24W pair occur in the Deep Urban environment.

8.5.2 Number of Satellites

As shown in Figure 8-7, the BW pair, as would be expected, uses more satellites in their calculation of the IVV solutions than the B24W pair. The difference is, on average, approximately 1.3. The difference is larger in open sky environments (e.g., 2.0 for the Interstate/Freeway environment). This being the case, the difference of 2 satellites is unlikely to correspond to a noticeable degradation in performance, since in these environments the B24W receivers typically use nearly 10 satellites in the computation of the navigation solutions.

8.5.3 Dilution of Precision

Figure 8-7 also shows the DOPs of the receivers involved in the calculation of the IVV solutions using the DPOS method for the BW and B24W pairs. On average, the DOPs of the limited constellation pair are within 0.05 of those for the BW pair.

8.5.4 Accuracy

As would be expected from an examination of the DOPs, the accuracy of the (BW-BW) and (B24W-B24W) pairs are very similar. The FAWE values in Table 8-16 and the CDF of horizontal errors in Figure 8-8 show that the performance is almost identical. The largest difference in accuracy occurs in the Deep Urban environment, where both perform poorly.

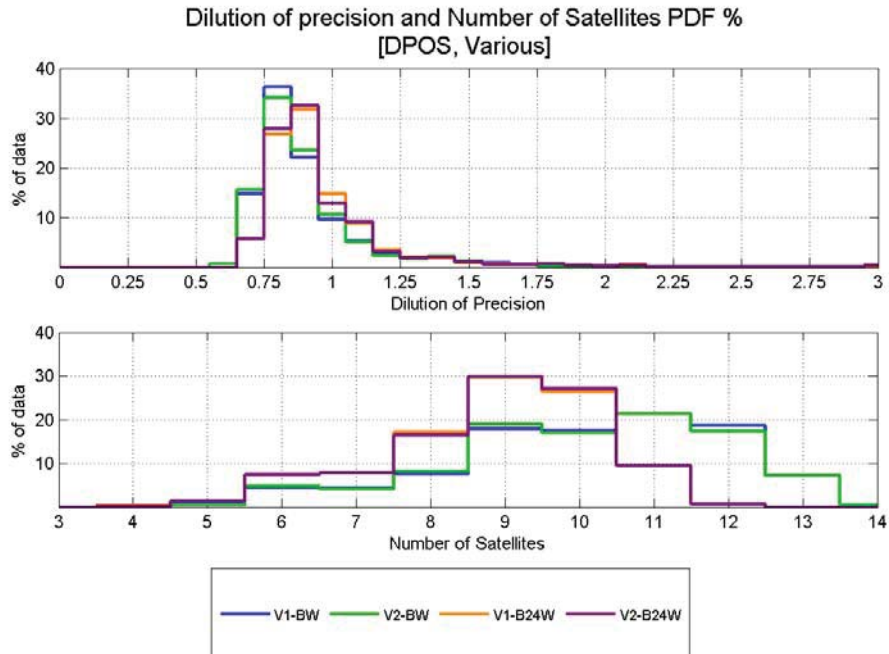


Figure 8-7: Dilution of Precision and Satellite Number Histograms for (BW-BW) and (B24W-B24W)

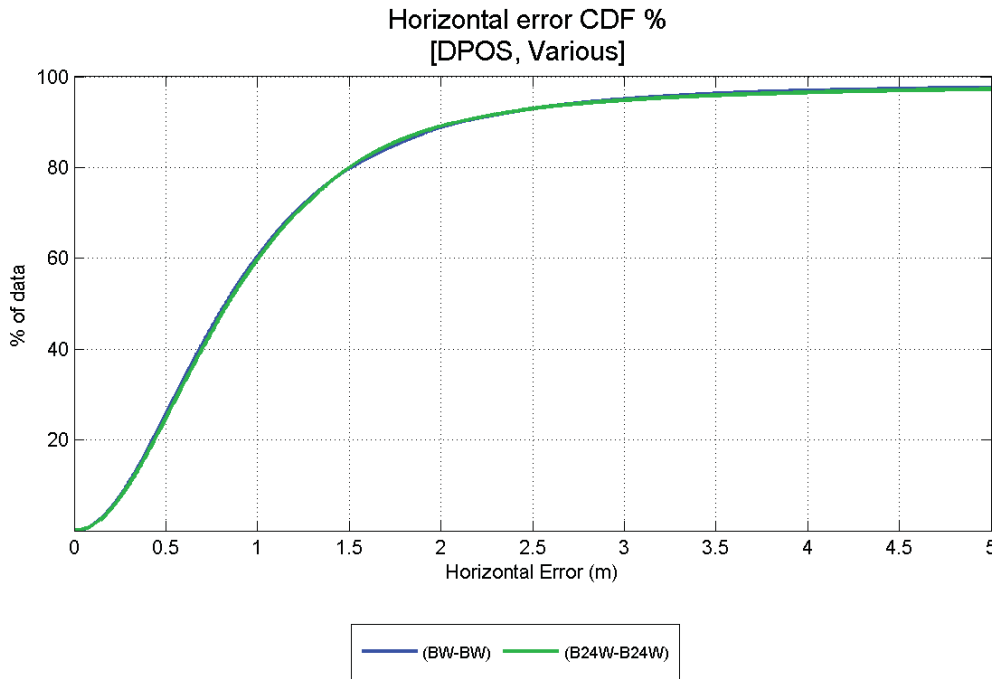


Figure 8-8: CDF of Horizontal Errors for (BW-BW) and (B24W-B24W) - Effect of Limited Constellation

8.5.5 Environment Types

It was noted above that the accuracy of the BW pair was noticeably better than the B24W pair in the Deep Urban environment. This observation is reversed in the Mountain environment, as is shown in Figure 8-9. It should be noted that the portion of data in the mountain environment was just over an hour, so the results shown in Figure 8-9 should not be taken to suggest that B24W will always perform better than BW in the mountains.

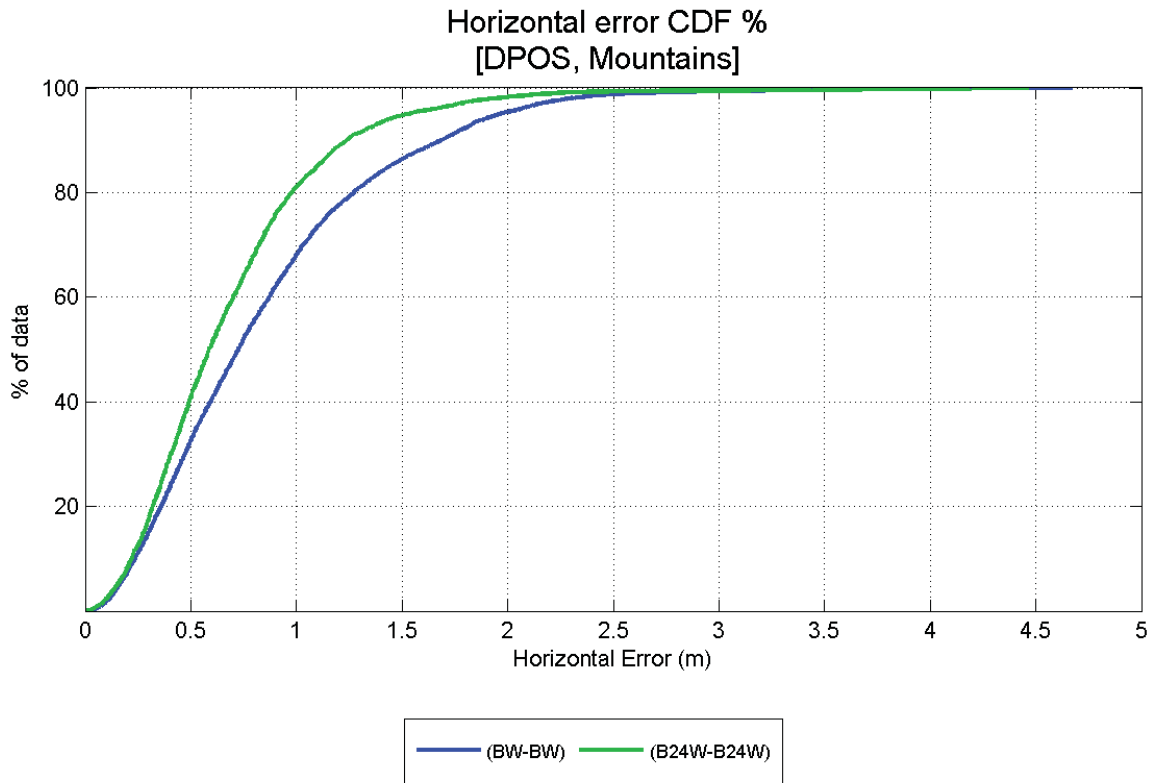


Figure 8-9: CDF of Horizontal Errors for (BW-BW) and (B24W-B24W) in Mountain Environment

9 Characterization of Errors

As mentioned in Section 6 where DOP and the number of satellites were introduced as potential predictive measures of the accuracy of the estimate of the IVV, it is desirable that the expected accuracy of the IVV be able to be determined in real-time. In this section, the efficacy of the two aforementioned predictive measures are discussed for (AW-AW) and (BW-BW) pairs. In addition to these predictive metrics, possible dependence of the accuracy of the IVV estimate on vehicle kinematics is explored. In particular, potential correlation between the errors in the IVV estimate and both inter-vehicle distance and vehicle speed were investigated. The potential dependence of the error on vehicle heading was also explored, but the figures are not included in this document as no conclusive results were obtained.

It should be noted that data from the Deep Urban environment was not used for this analysis for the following reasons. Firstly, the magnitudes of the errors in this environment are substantially larger than those in the other environments, meaning that the characterization of the errors in the other environments might be masked. Secondly,

the Deep Urban environment was not the major focus of the present study; only 2 percent of the data collected was in this environment. To more fully characterize the environment may require a dedicated study.

9.1 Number of Satellites

It is well known that SP position accuracy is a function of the number of satellites in view. In general, the more satellites used in the navigation solution, the better the position accuracy.

The correlation between position accuracy and the number of satellites is very consistent for the (AW-AW) pairs (i.e., an increase in the number of satellites is accompanied by an increase in accuracy, and the accuracy is similar for each environment). Figure 9-1 and Figure 9-2 indicate that, on average, when using (AW-AW) in DPOS or RTK, if 7 satellites are used in the navigation solution, a horizontal RMS accuracy of 1.5 m or better can be expected in the estimate of the IVV. The figures also show that the RTK accuracy continues to improve as the number of satellites is increased while the DPOS positioning method appears to remain at the 1 m level.

Figure 9-3 and Figure 9-4 show that the correlation between accuracy and number of satellites used in the navigation solution is weaker for the (BW-BW) combination, particularly for the DPOS method. For example, the RMS error in the Local Roads environment is similar for 5 and 12 satellites. For the majority of the environments, the (BW-BW) receiver combination requires 8 or more satellites to achieve a horizontal position RMS of 1.5 m. The RTK position accuracy for the Interstate environment does not improve beyond 1.5 m even with a further increase in the number of satellites.

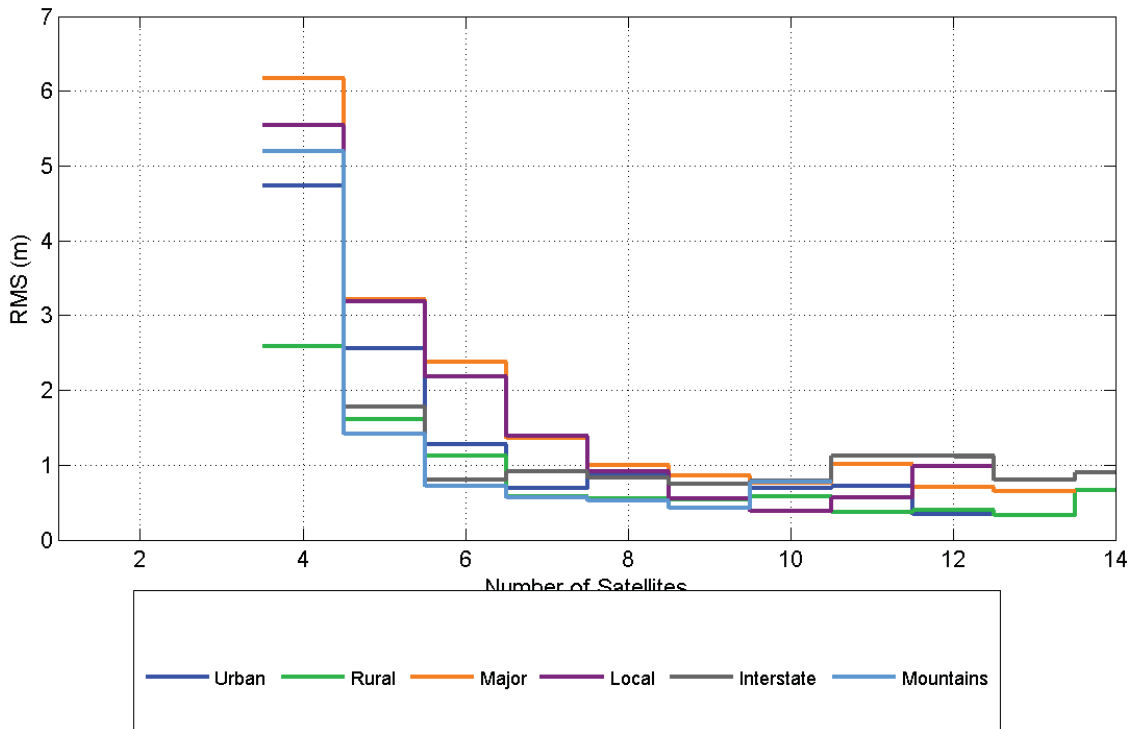


Figure 9-1: Horizontal RMS Error in IVV versus the Number of Satellites for (AW-AW), DPOS, for each Environment

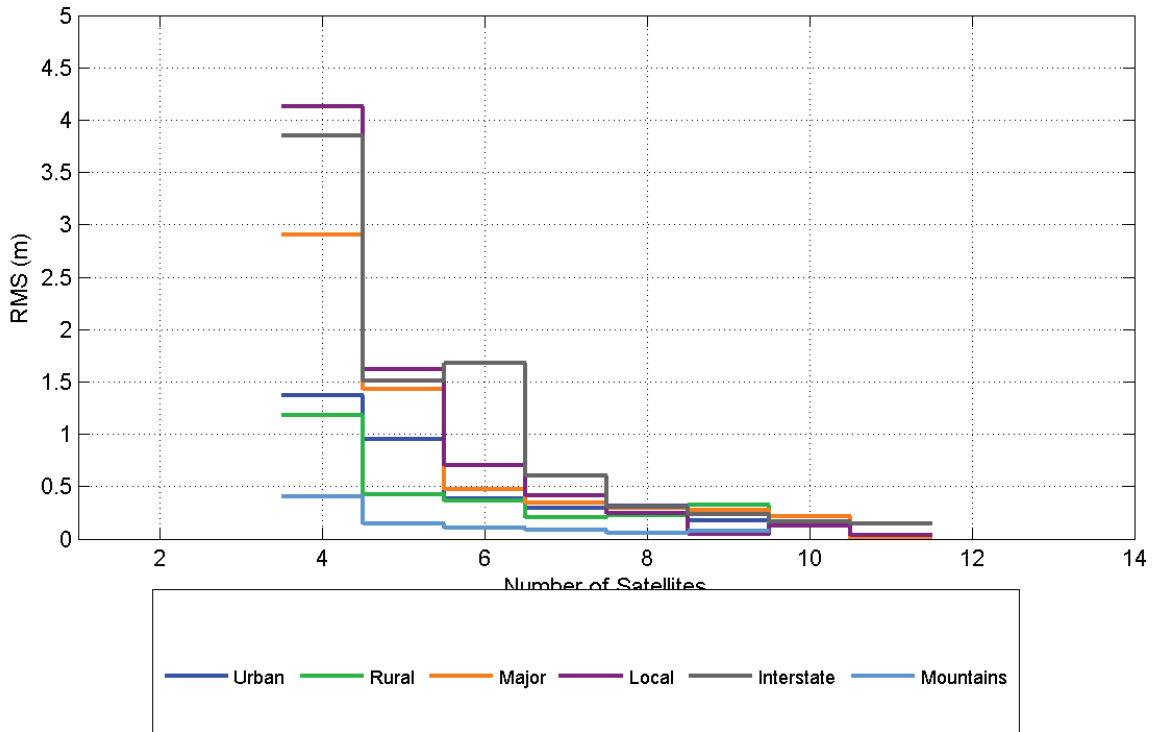


Figure 9-2: Horizontal RMS Error in IVV versus the Number of Satellites for (AW-AW), RTK, for each Environment

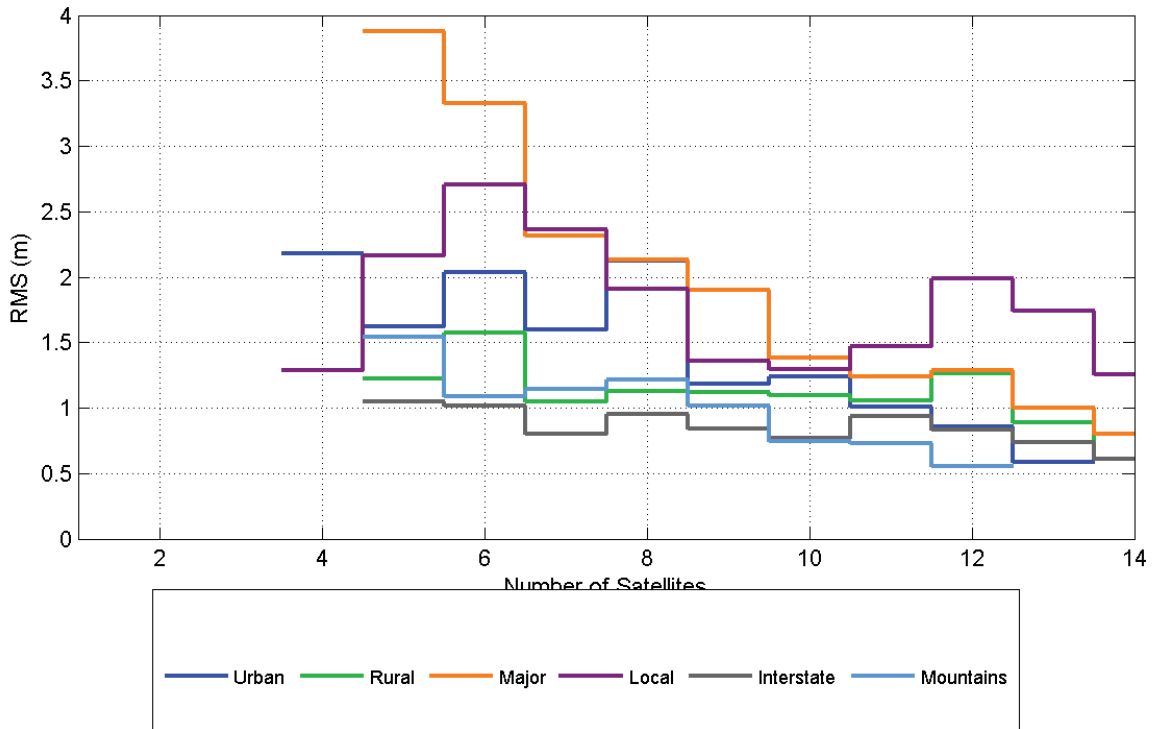


Figure 9-3: Horizontal RMS Error in IVV versus the Number of Satellites for (BW-BW), DPOS, for each Environment

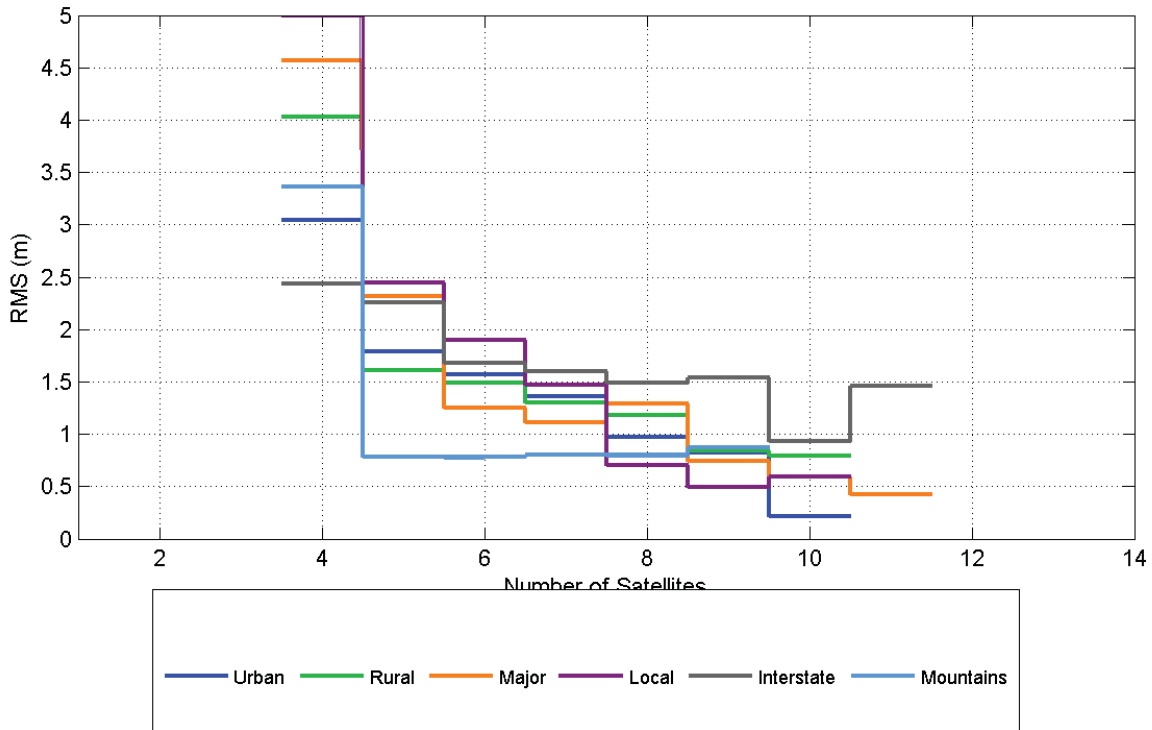


Figure 9-4: Horizontal RMS Error in IVV versus the Number of Satellites for (BW-BW), RTK, for each Environment

9.2 Dilution of Precision

As discussed in Section 5.1 of Alves, et al. (2009), the DOP is a measure of the geometry of satellites used in the navigation solution that can be related to the accuracy of the obtained solution. In general, the greater the geometrical dispersion of the satellites, the lower the DOP and the better the position accuracy. The HDOP for the RTK is not available. Therefore, only the DPOS positioning method is analyzed in this section.

Figure 9-5 shows that a horizontal RMS position error of 1.5 m or less was achieved for all considered environments for HDOP less than approximately 1.1 for the (AW-AW) receiver combination. With the exception of the Local Roads environment, a generally monotonic relationship exists between the HDOP and the error.

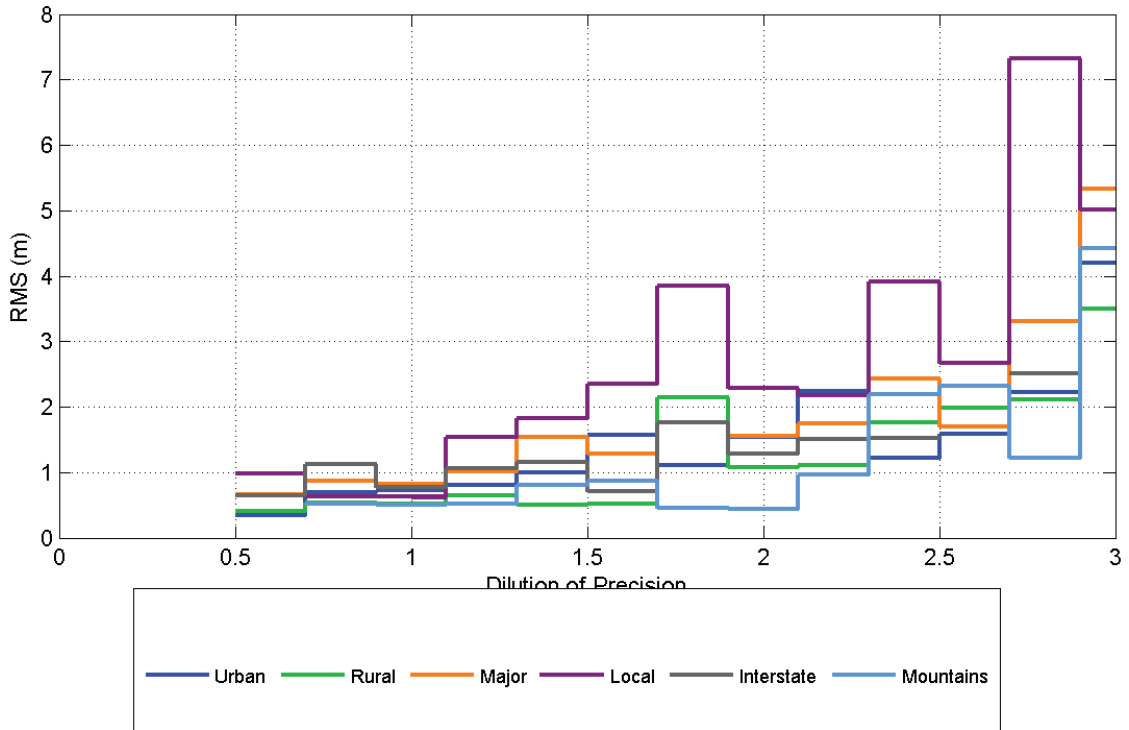


Figure 9-5: Horizontal RMS Error in IVV versus HDOP for (AW-AW), DPOS, for each Environment

Figure 9-6 shows that, as for the number of satellites, the correlation between DOP and accuracy is much weaker for (BW-BW) than it is for (AW-AW).

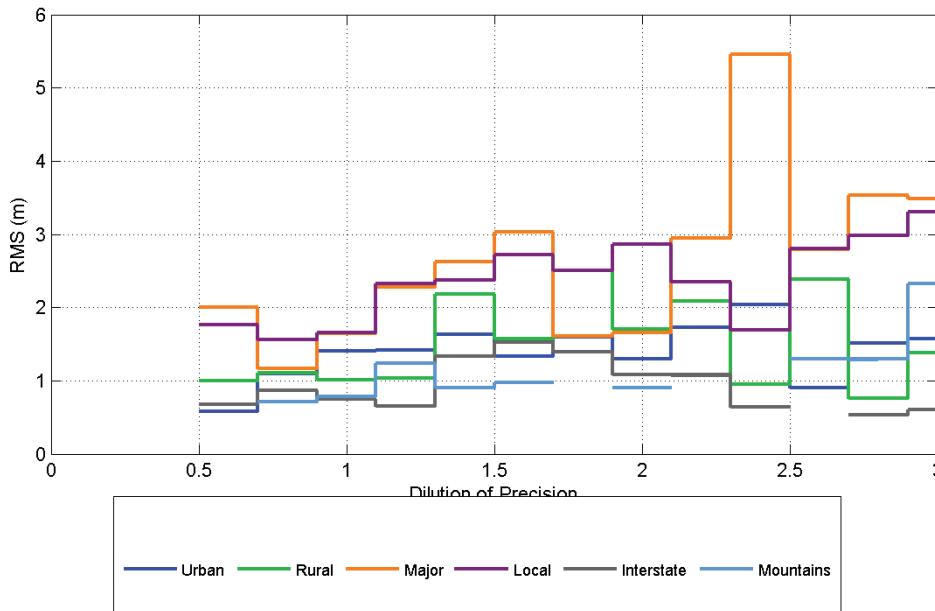


Figure 9-6: Horizontal RMS Error in IVV versus HDOP for (BW-BW), DPOS, for each Environment

9.3 Inter-Vehicle Distance

The distance between antennas is commonly used to estimate position accuracy obtained using some form of differential processing; however, this is typically reported as parts per million in applications where antenna separation is on the order of kms. The antenna separation for V2V positioning in this project was always less than 300 m.

Figure 9-7 and Figure 9-8 show the horizontal position error as a function of the distance between the vehicles for the DPOS method and the (AW-AW) and (BW-BW) receiver combinations, respectively. Figure 9-9 and Figure 9-10 show the horizontal position error as a function of the distance between the vehicles for the RTK method and the (AW-AW) and (BW-BW) receiver combinations, respectively. The typical vehicle separations were less than 100 m; therefore, the number of samples in each bin of the data where the vehicle separation is greater than 100 m are limited.

The figures indicate that there is no substantial and definitive correlation between vehicle separation and the accuracy of the IVV estimate for the typical inter-vehicle distances used herein. To truly determine the presence or absence of a correlation would require extensive dedicated tests.

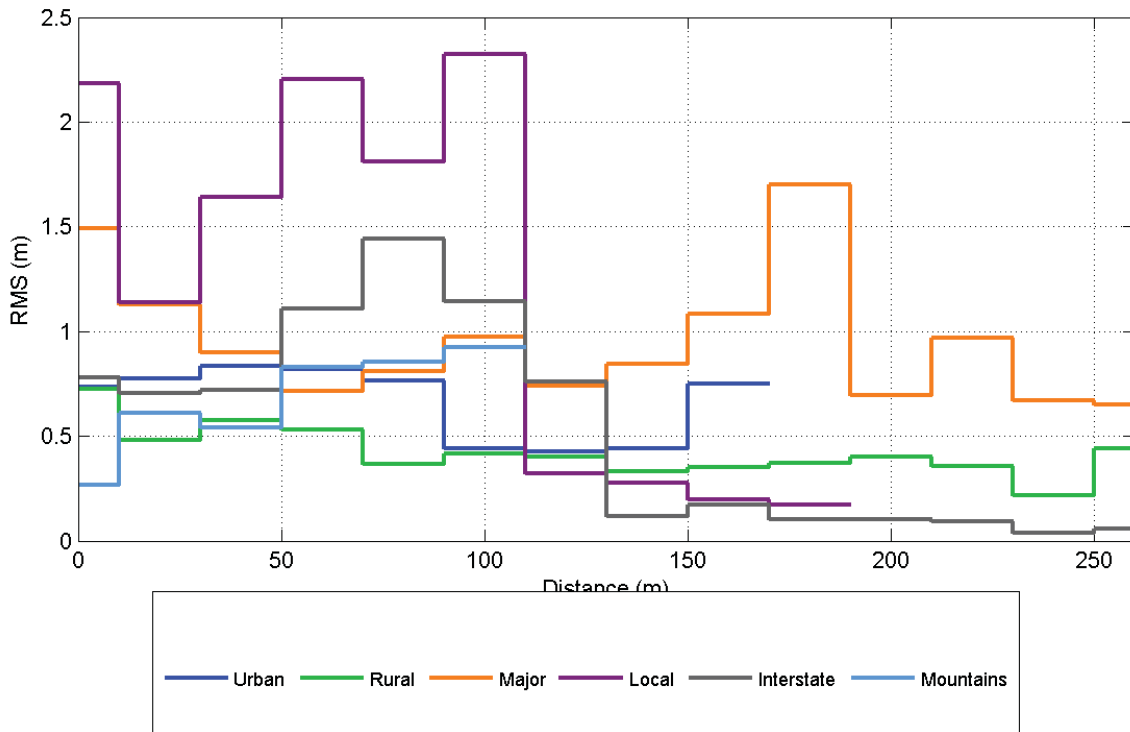


Figure 9-7: Horizontal RMS Error in IVV versus the Inter-Vehicle Distance for (AW-AW), DPOS, for each Environment

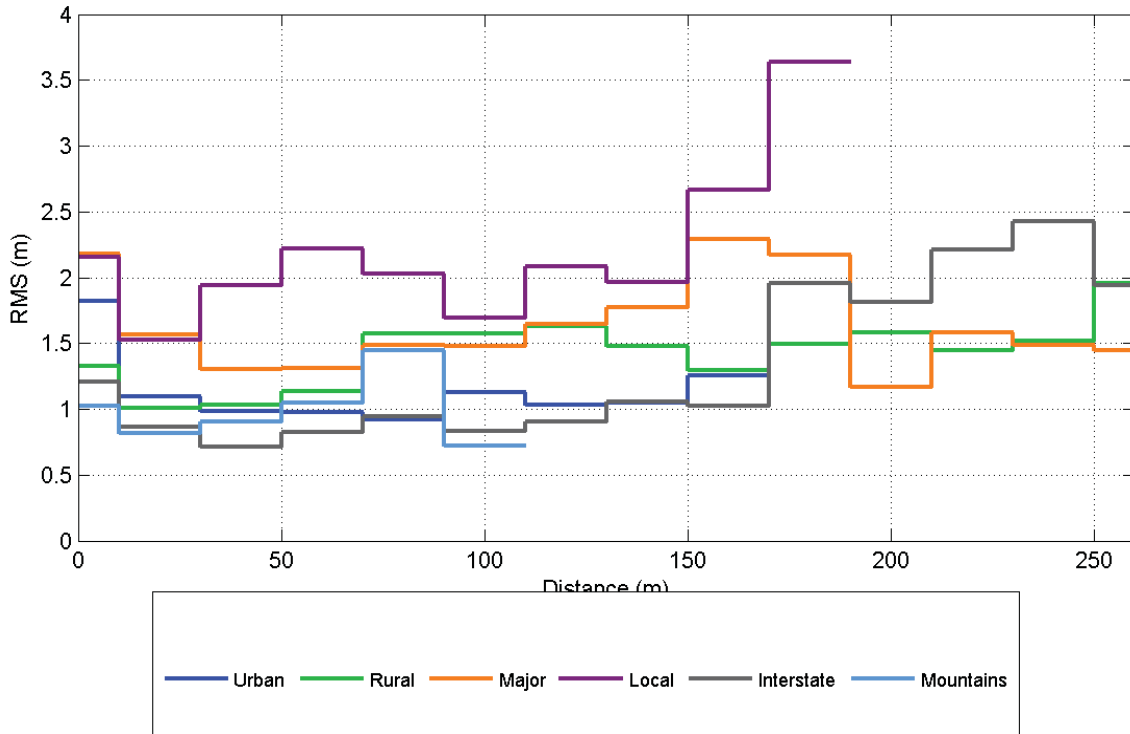


Figure 9-8: Horizontal RMS Error in IVV versus the Inter-Vehicle Distance for (BW-BW), DPOS, for each Environment

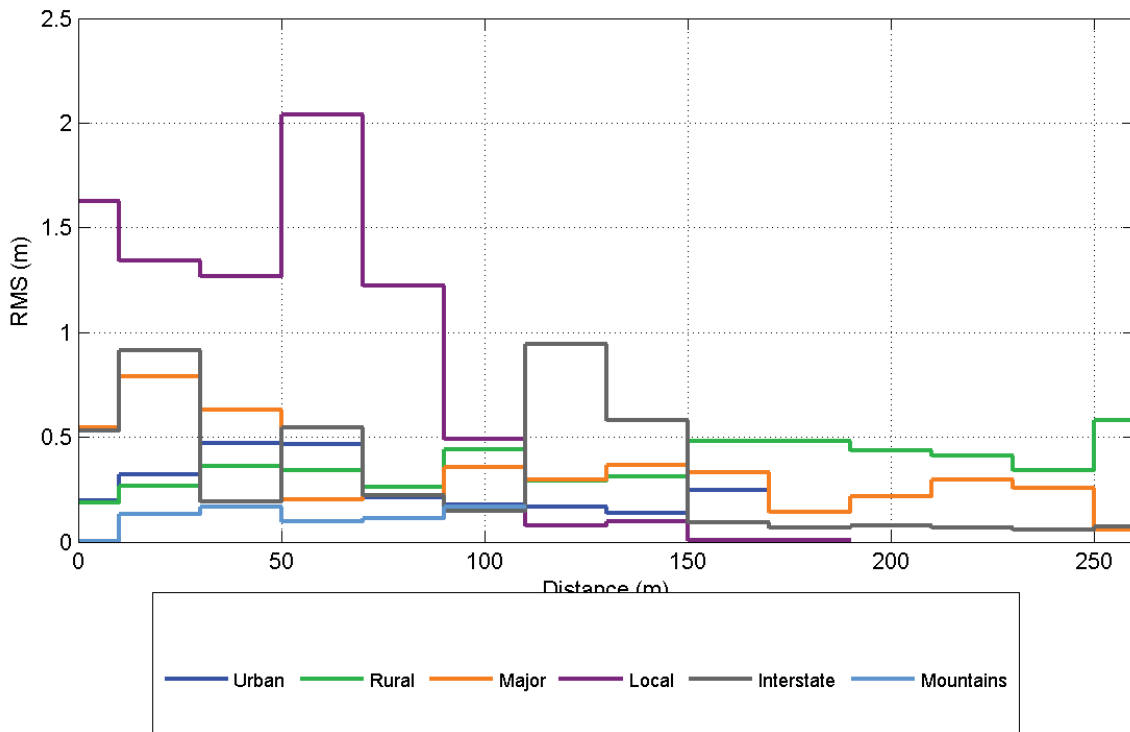


Figure 9-9: Horizontal RMS Error in IVV versus the Distance for (AW-AW), RTK, for each Environment

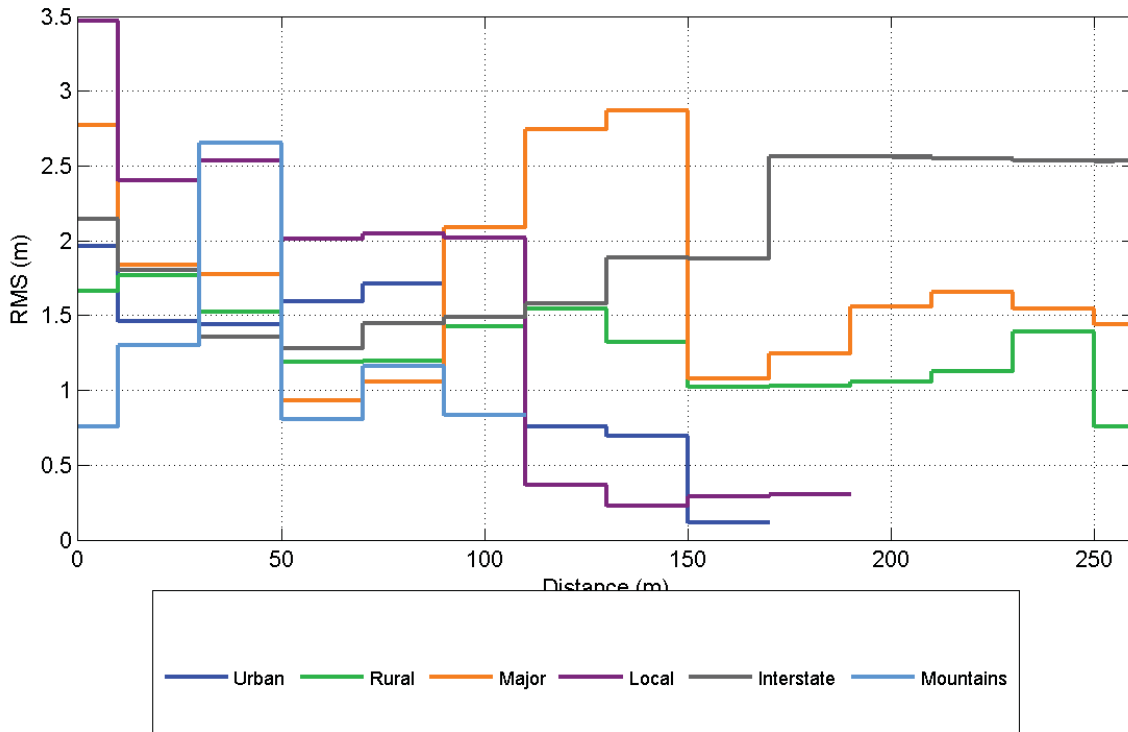


Figure 9-10: Horizontal RMS Error in IVV versus the Inter-Vehicle Distance for (BW-BW), RTK, for each Environment

9.4 Vehicle Speed

Figure 9-11 and Figure 9-12 show the horizontal error in the IVV as a function of the vehicle speed for the DPOS method using (AW-AW) and (BW-BW) combinations, respectively. Figure 9-13 and Figure 9-14 show the same relationships for the RTK method.

The speed limits for each environment set the maximum range of speeds. The distribution of samples for each environment is different depending on the speeds on each of the roads. For example vehicles travelling on an interstate road will rarely be below 50 miles per hour, conversely vehicles were not travelling faster than 40 miles per hour on local roads. This distribution of samples is important to consider when deriving conclusions based on these plots. Sampling of data from different environments was subjected to constraints in those environments. Therefore, comparison of performance in two environments in the same speed range may include effects of sampling.

There is no strong correlation between vehicle speed and position accuracy evident from the results. However, it may be possible to ascertain the environment type that the vehicle is in based on its vehicle speed and other variables, which would help to predict the current relative position accuracy. For example, the slight tendency (observable in Figure 9-11 to Figure 9-14 to a varying degree) for decreasing errors with increasing speeds, is potentially due to an increased likelihood of higher speeds in open areas which tend to have higher speed limits and less traffic.

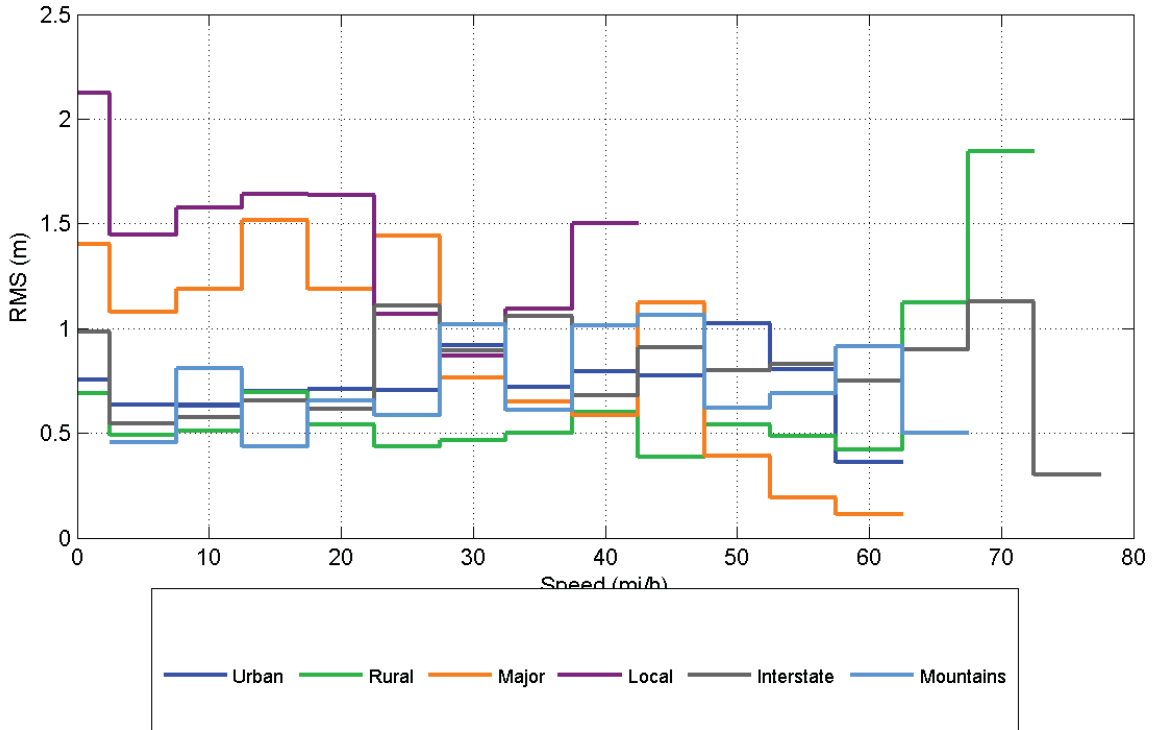


Figure 9-11: Horizontal RMS Error in IVV versus the Speed for (AW-AW), DPOS, for each Environment

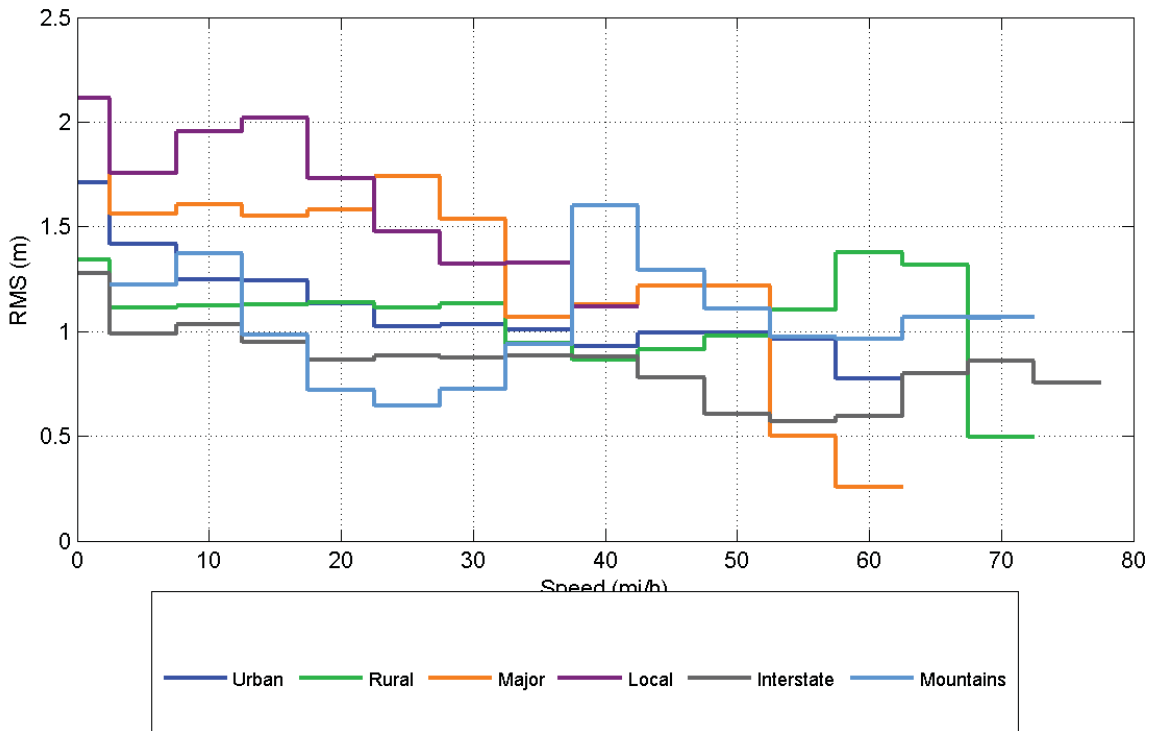


Figure 9-12: Horizontal RMS Error in IVV versus the Speed for (BW-BW), DPOS, for each Environment

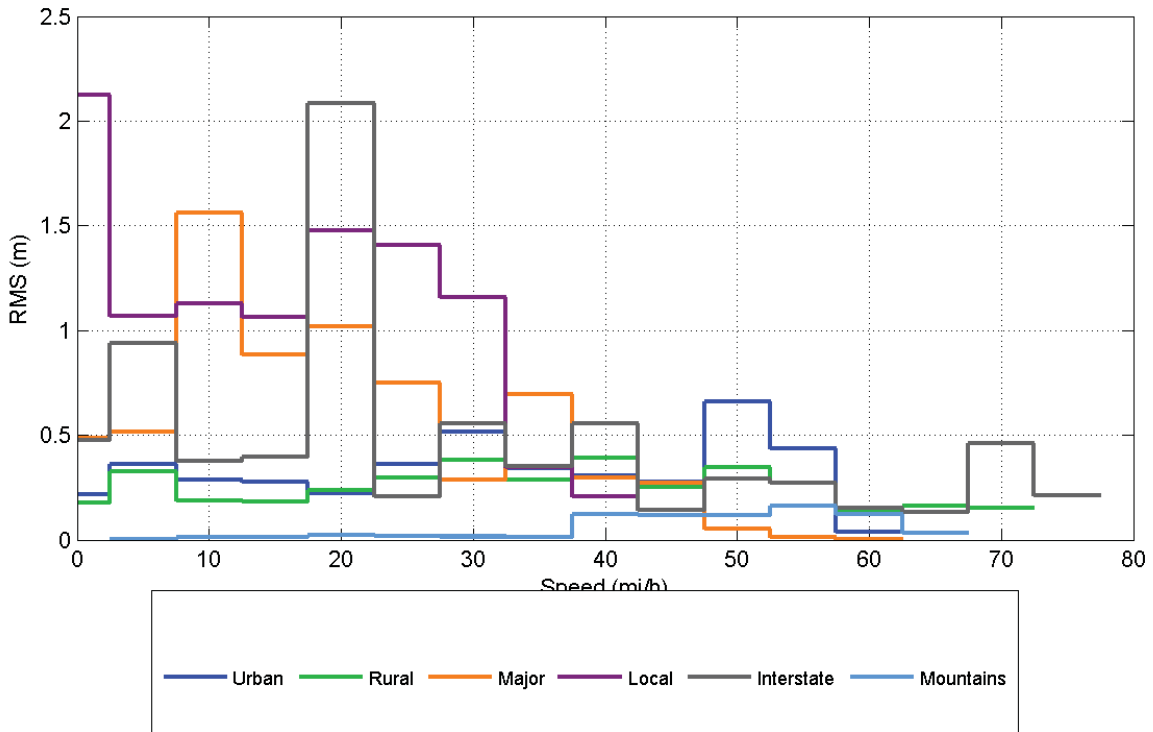


Figure 9-13: Horizontal RMS Error in IVV versus Speed for (AW-AW), RTK, for each Environment

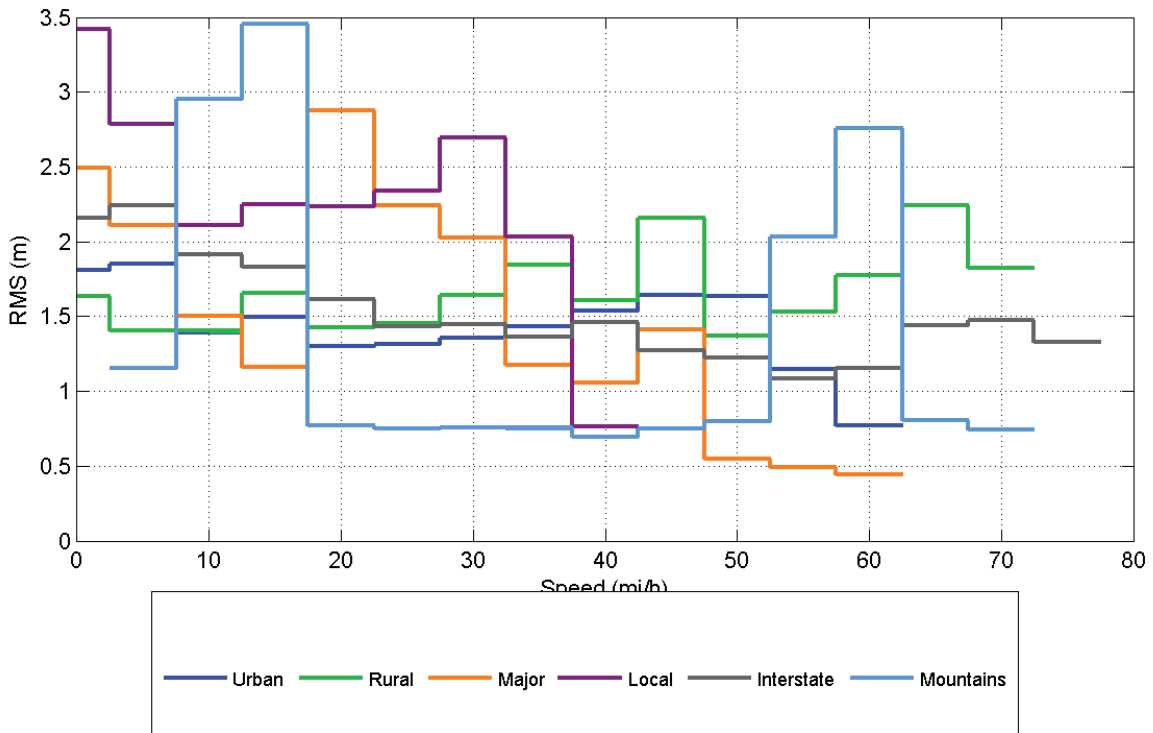


Figure 9-14: Horizontal RMS Error in IVV versus the Speed for (BW-BW), RTK, for each Environment

10 Vehicle-to-Infrastructure Test Results

As discussed in Section 7, V2I data was collected in 5 environment types over 2 days. The requirements for the V2I reference trajectories were much stricter than V2V. This is because any errors in the reference trajectory larger than a few centimeters would be noticeable due to the high accuracy of the (AW-AW) V2I solution. While more than 40 V2I passes were recorded, the accuracy requirements means that they were reduced to 20 V2I passes that are used for the statistics and analysis discussed here. The 20 passes include the 3 coordinated types described in Section 7 in which the vehicles are following each other, approaching each other, and approaching an instrumented intersection with roughly orthogonal directions.

A typical time series plot of the AT and XT components of the errors in the IVV estimate during a V2I pass is shown in Figure 10-1. The errors in four IVV solutions are shown in the figure:

- V2I Single (V2I-S): Solution in which only one of the two vehicles has a V2I solution (only one vehicle within the zone).
- V2I Both (V2I-B): Solution when both vehicles have V2I solutions.
- DPOS: The alternative solution when V2I is unavailable (i.e., when outside the V2I zone, the receivers work in SP mode).
- RTK: Shown for comparative purposes.

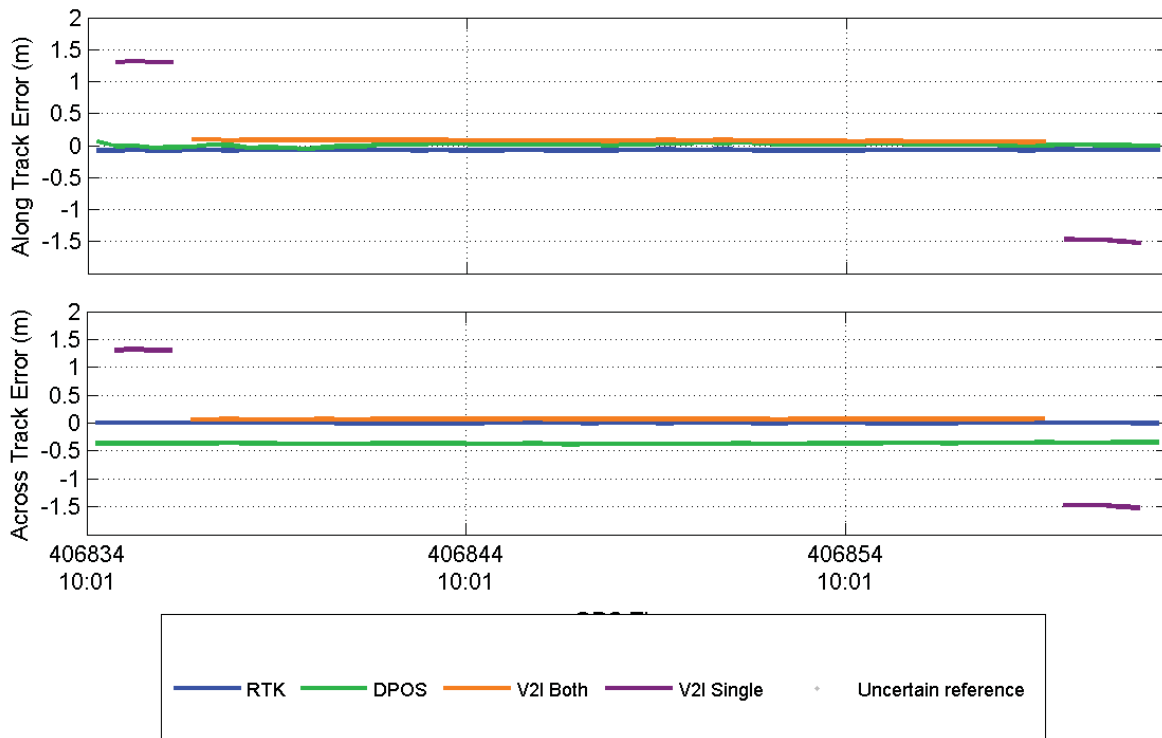


Figure 10-1: V2I Time Series for (AW-AW) for an Interstate Environment

Here, the focus is on three important characteristics of the V2I tests:

- The accuracy of V2I-S
- The accuracy of V2I-B
- The discontinuity in the IVV estimate when one of the vehicles enters or leaves a zone

Only the (AW-AW) and (BW-BW) receiver combinations are discussed in the following sections; although in the accompanying document, figures are presented for each of the receiver combinations used in the V2V DPOS analysis.

Figure 10-2 and Figure 10-3 show the CDFs of horizontal errors in the IVV estimate for the (AW-AW) and (BW-BW) receiver combinations, respectively. Each vehicle pass has a very short duration, usually lasting less than 2 minutes depending on the driving environment and the vehicle speed. A pass was chosen to start and end a few seconds before and after the first and last vehicle entered and left the V2I zone so that all transitions would be apparent. Due to these short durations, the total number of epochs for each of the solutions of interest is very low, especially for the V2I-S solutions. The small number of samples should be considered when interpreting Figure 10-3 and Figure 10-2. With this caveat, the figures show that for both receiver combinations, the RTK and V2I-B solutions are very similar. The V2I-S solutions offer the poorest IVV accuracy. This is because the vehicle with the V2I solution will have an accurate position while the other will have larger errors. In the DPOS case, the errors for the SP solutions are similar and are effectively canceled when the IVV is calculated.

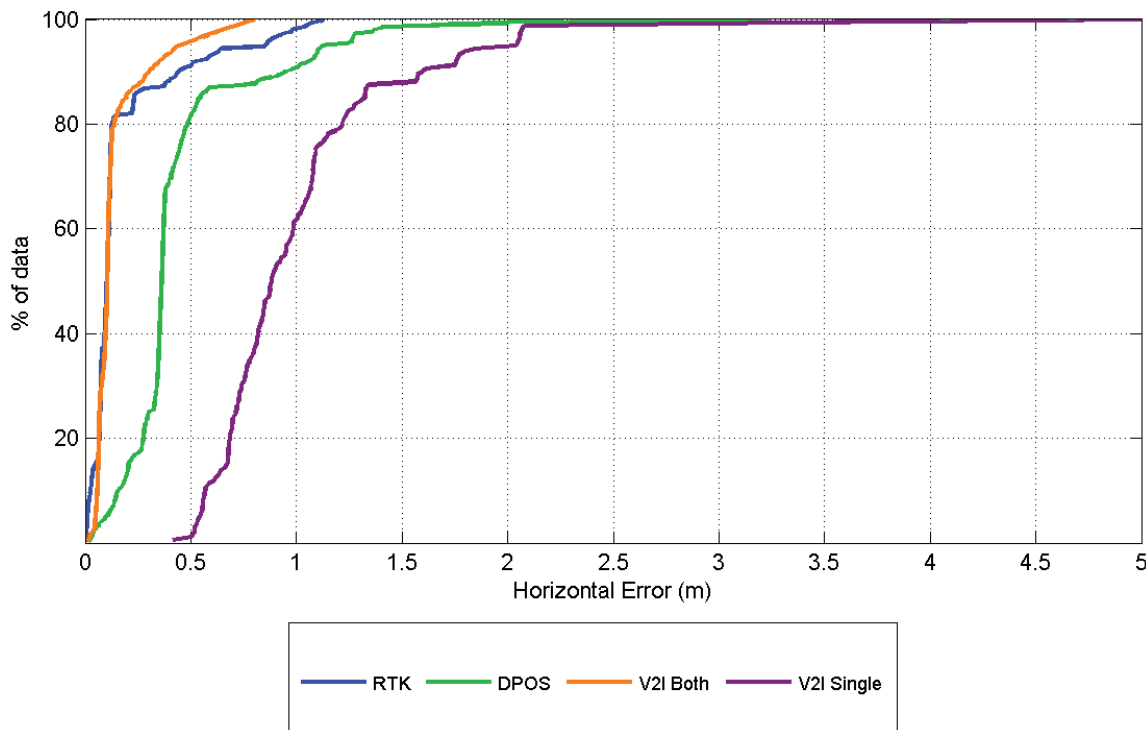


Figure 10-2: CDF of Horizontal Errors in V2I Estimate of IVV, (AW-AW)

The poor V2I-S performance suggests that each vehicle should only switch to the infrastructure solution when both vehicles are using the infrastructure solution. If both the V2I-B and RTK solutions are available, then it may not be necessary to switch from RTK to V2I-B solutions because of their similar accuracy performances.

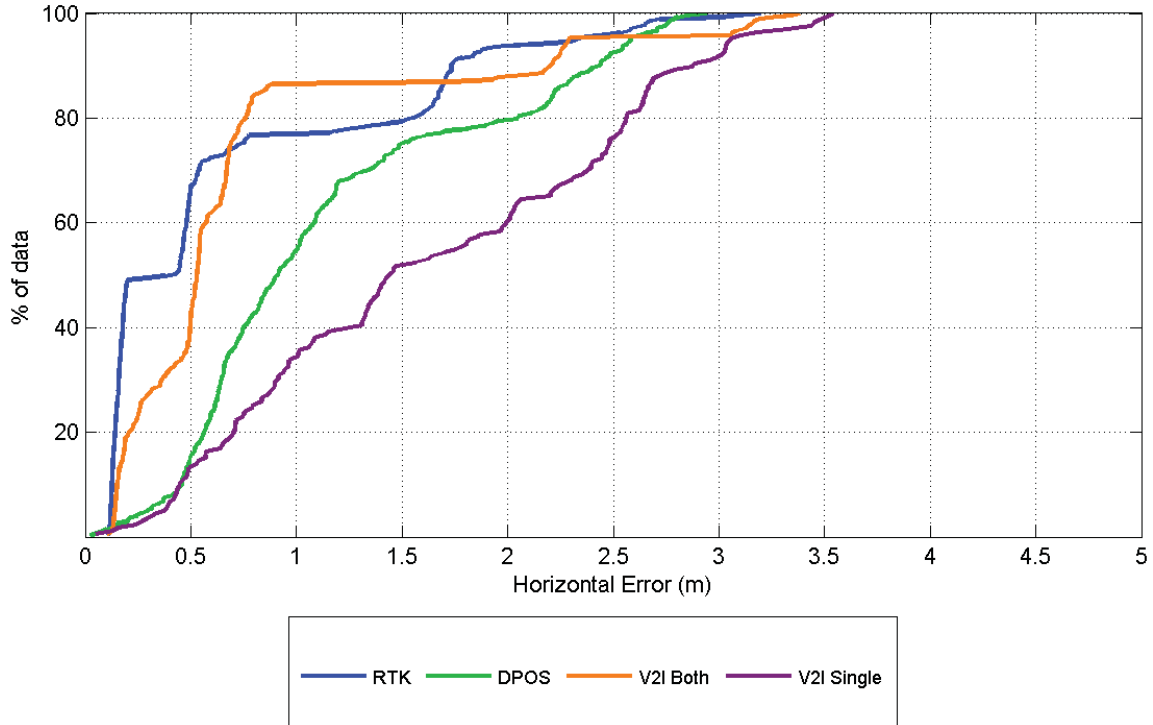


Figure 10-3: CDF of Horizontal Errors in V2I Estimate of IVV, (BW-BW)

The discontinuities in the IVV estimate that occur when switching between modes (e.g., DPOS to V2I-S), are tabulated for the analyzed passes for (AW-AW) in Table 10-1 and (BW-BW) in Table 10-2. The magnitudes of discontinuity show large variability even for the runs in the same environment using the same receivers. For example, in transitions from DPOS to V2I-S using the (BW-BW) combination in the Major Urban Thruway, the magnitudes range from 0.3 m to more than 5 m (AT) and from 0.8 m to more than 5 m (XT). Discontinuities of 5 m obviously make relative position at the lane level (1.5 m) a difficult proposition. Aside from the variability and magnitude of possible discontinuities in the IVV estimate, the major conclusion that can be drawn from inspection of Table 10-1 and Table 10-2 is that the discontinuities are generally smaller for (AW-AW) than for (BW-BW). While it is of questionable value to quote statistics from this small sample size with such large variability, the average magnitudes for the (AW-AW) and (BW-BW) combinations are 0.77 m and 1.47 m, respectively. That the (AW-AW) pair has smaller discontinuities is to be expected since the discontinuity is approximately bounded¹¹ by the error in the SP solution, and the AW receivers generally have smaller errors than the BW receivers. One would expect the discontinuities for the BN receivers would be even larger, since these receivers do not have the benefit of the WAAS differential corrections.

¹¹ This bound is only strict if the V2I-B is solution is considered to be exact.

Table 10-1: Discontinuities in the IVV Estimate at Zone Transitions for (AW-AW) Combination

Environment	DPOS → V2I S		V2I S → V2I B		V2I B → V2I S		V2I S → DPOS	
	AT (m)	XT (m)	AT (m)	XT (m)	AT (m)	XT (m)	AT (m)	XT (m)
Major Urban Thruway	0.49	0.99	-0.06	-0.40	-0.05	0.26	0.33	-0.14
	-0.18	-0.09	0.15	0.24	0.63	0.46	-0.38	-0.40
					-0.62	-0.82	0.69	0.88
Major Rural Thruway	-0.53	-0.40	-0.21	0.43	-0.86	-0.67	-0.45	-0.38
	0.24	0.01	-0.43	-0.13	-0.65	-0.87	0.72	0.85
	-1.37	-1.39	1.40	1.43	0.61	0.53	-0.54	-0.53
Local Roads			-1.02	-0.83	-1.05	-1.16	1.01	0.35
					0.91	0.44	-1.18	-1.15
	1.32	0.71	-0.40	-0.28	-0.77	-0.38	-0.58	0.82
Freeway	-0.28	-0.79	0.44	0.47	1.75	1.69	-1.84	-1.37
	1.80	2.30	-1.97	-1.99	-0.56	-0.58	1.77	0.36
	-1.24	-1.66	1.21	1.24	1.53	1.55	-1.52	-1.18
	1.24	0.96	-0.42	-0.58	-0.89	-0.98	0.76	1.02
	-1.28	-1.05	0.27	0.78	0.31	0.56	-0.21	-0.21
	-1.11	-1.03	-0.19	0.52			0.40	-1.14
Major Roads	-0.08	0.25	-0.08	-0.29	-0.93	-0.90	1.11	1.56
			0.35	0.53	-0.79	-0.98	-0.12	0.09
	1.36	0.60	0.16	-0.96	0.24	-0.40		

Table 10-2: Discontinuities in the IVV Estimate at Zone Transitions for (BW-BW) Combination

Environment	DPOS → V2I S		V2I S → V2I B		V2I B → V2I S		V2I S → DPOS	
	AT (m)	XT (m)	AT (m)	XT (m)	AT (m)	XT (m)	AT (m)	XT (m)
Major Urban Thruway	> 5	>5			0.39	1.08	-0.65	-0.87
	-0.77	-0.88	2.67	0.85	1.33	2.97	-1.78	-3.11
	0.30	1.07	-0.82	-0.99	-1.03	0.07	-0.84	0.18
	1.29	1.42	-5.44	-3.55	3.58	2.09	-3.13	-1.02
Major Rural Thruway	0.80	1.95	-0.82	-1.89	-0.34	1.81	-0.97	-1.37
	1.18	1.35	0.17	-0.49	1.13	2.15	-1.84	-1.94
			1.95	1.03	-1.08	-0.47	-2.26	0.09
Local Roads			0.96	1.88	-1.86	-3.46	0.19	2.20
	-1.85	-0.66					-1.44	1.05
	0.13	-0.09			0.82	1.66	-0.99	-0.26
Freeway	-1.74	-2.61	5.38	4.79	2.31	3.29	-2.33	-2.94
	-0.88	0.15	0.88	-0.25	0.18	0.66	-0.01	-0.78
	-2.02	-2.48	2.71	2.83	1.00	1.70	-1.75	-2.04

Environment	DPOS → V2I S		V2I S → V2I B		V2I B → V2I S		V2I S → DPOS	
	AT (m)	XT (m)	AT (m)	XT (m)	AT (m)	XT (m)	AT (m)	XT (m)
	-0.33	-0.10	-0.44	-0.08	-1.62	-1.44	0.90	1.22
	1.71	-1.20					-0.83	0.40
	0.74	-2.33	-0.42	-0.12	-0.57	-0.58	0.76	-1.14
Major Roads	2.05	2.68	0.40	-1.25	-2.18	0.04	1.13	-0.04
	1.26	-0.69	-1.14	-1.25	-2.59	-1.62	3.02	1.98
	-1.83	-2.64	3.16	3.51	0.80	0.20	-0.86	1.30

11 Conclusions

The conclusions presented below are based on the extensive, multi-environment tests and equipment conducted in accordance with the requirements of the project.

The availability of each positioning method as a function of the receiver combination, constellation utilized, use of WAAS, and accuracy threshold is given in Table 11-1. Although the results are self-explanatory, a few important conclusions are in order. Note that the availability numbers presented here are dependent on the particular mix of environments specified for this testing. For example, increasing the proportion of challenging GNSS environments, such as deep urban, would decrease the availability values. The environment mix was designed to represent the road use of an average driver as given in the FHWA publication on *Our Nation's Highways* (FHWA 2008) [2].

Table 11-1: Availability Statistics for All Receiver Combinations and V2V Processing Methods

Receivers		Proc. (D)POS/(R)TK	FA (%)	FAWE (1.5 m)		FAWE (5 m)		UNC (%)
Host	Remote			AT (%)	XT (%)	AT (%)	XT (%)	
AW	AW	R	92	91	91	91	91	<1
		D	97	93	92	96	95	1
	BW	R	84	68	69	83	83	<1
		D	98	62	65	95	95	1
	BN	R	84	73	73	84	83	<1
		D	98	62	70	95	95	1
BW	AW	R	84	81	80	84	83	<1
		D	98	59	68	94	95	1
	BW	R	82	74	71	81	81	<1
		D	100	89	88	97	97	1
	BN	R	80	71	68	79	79	<1
		D	100	82	84	97	97	1
BN	BN	D	100	90	89	97	97	1
B24W	B24W	D	99	89	89	97	96	1

Explanation of acronyms utilized in the table:

- FA: Full Availability
 - FAWE (1.5 m): Full Availability With Errors < 1.5 m
 - FAWE (5 m): Full Availability With Errors < 5 m
 - UNC: UNCertainty (%) in availability due to uncertain reference inter-vehicle vector
 - AT: Along Track
 - XT: Across Track
 - AW: Type A Receiver with WAAS
 - BW: Type A Receiver with WAAS
 - BN: Type A Receiver without WAAS
1. Full availability percentages with errors less than 1.5 m in both along and across track using the RTK method involving one or two Type B receivers are lower than those using two Type A receivers by up to 20 percent. The experience of the Team suggests this discrepancy is caused by a difference in the quality of the phase lock loops (PLL). The higher quality PLLs of Type A receivers results in a lower number of carrier phase cycle slips and a higher probability of obtaining high accuracy carrier phase ambiguity fixed or partly fixed solutions. Higher numbers of cycle slips in receiver Type B contribute to frequent ambiguity resets resulting in relatively poorer solutions.
 2. The best availability percentages with errors less than 1.5 m, namely 90 percent or slightly more, occur with pairs of Type AW receivers in either RTK or DPOS mode or with pairs of Type B receivers, both with WAAS or both with no WAAS, in DPOS mode. When mixing the WAAS and no WAAS options, the availability drops because WAAS satellites provide not only an additional signal but also differential corrections for GPS satellites to improve absolute accuracy. However, unless corrections are applied at both receivers, the IVV accuracy decreases significantly.
 3. Full availability percentages with errors less than 1.5 m using the DPOS method with pairs of identical receivers is significantly better than corresponding values using pairs of mixed receivers. The different internal settings used by receivers, such as measurement acceptance criteria, can lead to mismatched satellites between non-homogeneous receiver pairs, while different ionospheric and tropospheric models can lead to dissimilar biases in their navigation solutions.
 4. At the 5 m accuracy level, the DPOS method for each of the considered receiver combinations has availability level of at least 95 percent. The detrimental effects of receiver non-homogeneity are not observable at this lower accuracy. For RTK, the availability measures at the 5 m accuracy level are lower and essentially equal to the associated full availability values. These full availability values are highly receiver combination dependent.

5. The RTK SW utilized in the tests did not use WAAS satellites and, therefore, the impact of WAAS on RTK cannot be assessed. However the use of these satellites would theoretically improve all RTK performance parameters.
6. Type B receiver pairs with WAAS generally perform the same as those with no WAAS in the DPOS mode. Under the test conditions prevailing during July-August 2009 when a GPS constellation of 31 satellites was available, the addition of WAAS satellites did not add significantly to the geometry of the satellites. As discussed in Point 2 above, mixing the type B WAAS and no WAAS receivers decreased availability. In DPOS mode, WAAS signals without differential corrections would generally be better to maintain high IVV solution accuracy, although absolute vehicle location accuracy would decrease and, under poor satellite geometry, an IVV solution accuracy might also decrease.
7. Certain anomalous results in Table 11-1, such as the difference in performance between the AW-BW and BW-AW combinations using RTK which is limited to availability of solutions with 1.5 m accuracy, are thought to be attributable to the proprietary RTK SW. Other incongruous results include the availability of solutions with 1.5 m accuracy for the AW-BW and AW-BN combinations using RTK, which since the RTK SW did not use WAAS in the calculations, should be identical. Without precise knowledge of the algorithms used within the receivers and the RTK SW, it is not possible to conclusively state the reasons for these discrepancies.
8. The difference in availability between the 24-satellite nominal constellation and the 31-satellite constellation available during the August 2009 tests was negligible using Type B receivers in DPOS mode. While the B24W-B24W pair used, on average, 1.3 satellites fewer than the BW-BW pair in the calculation of the navigation solution, the average HDOP values for the two pairs were within 0.05 of each other, supporting the similar availability of accurate results. The discrepancy between the two receiver pairs would likely be more evident if a larger portion of the test duration was spent in the Deep Urban environment where satellite availability was limited.
9. Data gap statistics for the roughly 45 hours of collected data are given in Table 11-2. A gap in the data is defined as a time interval when no solution is available due to the lack of measurements. This can be due to transmission problems (for RTK only), insufficient number of measurements, or a combination thereof. Most gaps are less than 15 s and have average durations of 2 to 7 s. The statistics in the table are dependent upon the mix of environments used in the data collection; the majority of gaps occurred in the Deep Urban environment, which accounted for less than 4 percent of the total testing duration.

Table 11-2: Data Gap Statistics for all Receiver Combinations and V2V Processing Methods

Receivers		Proc. (D)POS/(R)TK	# Gaps	Gaps < 15 s		15s < Gaps < 30 s		Gaps > 30 s	
Host	Remote			%	Ave (s)	%	Ave (s)	%	Ave (s)
A	A	R	1459	90	5	6	21	4	72
		D	1123	97	2	2	19	2	77
	BW	R	1375	56	7	31	20	13	67
		D	894	96	2	2	20	2	58
	BN	R	1303	54	6	32	20	14	68
		D	894	96	2	2	20	2	58
BW	A	R	1377	56	6	31	20	13	9
		D	829	97	2	2	20	2	1
	BW	R	1455	53	6	33	20	14	71
		D	8	100	3	0	-	0	-
	BN	R	1601	53	8	33	20	14	68
		D	11	100	2	0	-	0	-
BN	BN	D	9	100	4	0	-	0	-

10. Data gaps for RTK generally occur more often and last longer than those for DPOS using the same receiver combinations. This is particularly evident for the BW-BW pair. While it was not possible to determine the cause for each individual RTK data gap, the Dedicated Short Range Communications (DSRC) radio link between the vehicles was found to be operating properly 99.8 percent of the time suggesting that the majority of gaps were due to insufficient common measurements from the receivers after rejection. The number and duration of gaps could likely be reduced by tuning the SW, although this may lead to a decrease in accuracy and reliability.
11. The dependency of the RTK method on the SW prescribed for the project was not investigated herein. However, the previous experience of the investigators suggests that reputable, independently developed L1-only RTK SW packages used over short inter-receiver distances, such as the 300 m as was the case for this test, will generally give similar results.
12. Discontinuities in the IVV estimates at transitions between DPOS and V2I modes have great variability, but potentially have magnitudes that may make relative positioning at the lane (1.5 m) or road (5 m) identification level difficult.

12 References

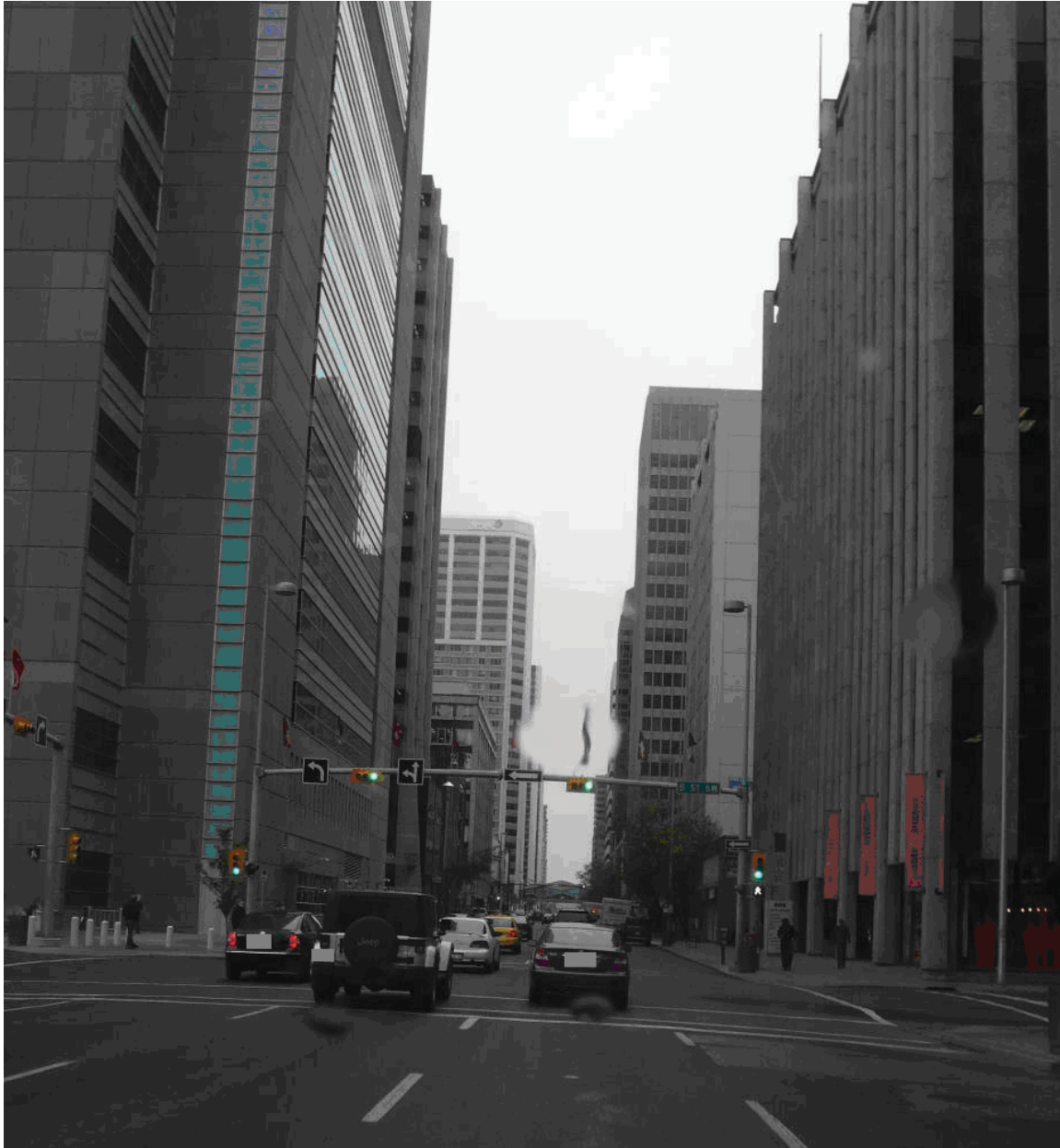
- [1] Bai, F. and H. Krishnan, “*Reliability Analysis of DSRC Wireless Communication for Vehicle Safety Applications*,” Proceeding of the 9th International Conference of Intelligent Transportation System, 2006.
- [2] U.S. Department of Transportation, Federal Highway Administration, “*Our Nation's Highways*,” FHWA-PL-08-021, 2008.
- [3] Luo, N., and G. Lachapelle, “*Relative Positioning of Multiple Moving Platforms using GPS*,” IEEE Transactions on Aerospace and Electronic Systems, 39, 3, 936-948, 2003.

13 Supplementary Material

13.1 Photos Illustration of The Data Collection Routes

High definition video was collected for each of the data segments (V2V and V2I) of the final field study. The video camera was positioned on the rear vehicle, facing the lead vehicle. This appendix contains representative photos showing each of the data collection environments.

13.1.1 Deep Urban



Urban Canyon with 20-30 Storey Buildings



Urban Canyon with 20-40 Storey Buildings

13.1.2 Major Urban Throughway



**Major Urban Throughway Road with Overpass and Sloped Road Banks
Creating A Natural 10 Degree Elevation Mask**



**Major Urban Throughway with a Pedestrian Overpass and 1-4
Storey Buildings**



**Major Urban Throughway Representative of Natural Elevation
Mask (5-10 Deg)**



**Major Urban Throughway Representative of Overpass and High Elevation
Mask on Right Side of the Vehicle**



Major Urban Throughway Representative of Multiple (2) Overpasses and Road within 5-15 Degree Elevation Mask



Major Urban Throughway Representative of a Parallel-to-Trajectory Overpass, with Increased Wall to Create Poor Across Track Satellite Observability

13.1.3 Major Rural Throughway



Major Rural Throughway Representative of Occasional High Rise Buildings, Electrical Fixtures, and Foliage to Only One Side of the Vehicle



Major Rural Throughway Representative of Typical Open Sky Conditions, but Containing Signs and Lamp Fixtures



Major Rural Throughway Representative of Low Elevation Masking Trees - Also Shows Test Vehicle Passing GPS Infrastructure Station



Major Rural Throughway Representative of Typical Open Sky Conditions



Major Rural Throughway Experiencing Signal Shading On Left Side of the Road

13.1.4 Major Road (Urban and Rural)



Major Road Containing Foliage Signal Shading On the Vehicle's Right, and Less Substantial Foliage Signal Masking on Vehicle's Left



Major Road with Mostly Open Road Conditions and Parking Lot to the Right, with a 2 Story Building



Major Rural Road Containing Only Sporadic Foliage Signal Masks



Major Road Containing Single Story Buildings Near V2I Station

13.1.5 Freeway/Interstate



Freeway with Open Sky Conditions



V2I Station Near a Freeway Exit with Excellent Open Sky Visibility



Freeway Road Selection Showing Open Sky Nature



Freeway Road Selection Showing Open Sky Nature

13.1.6 Mountain Roads



Mountain Road Selection Showing with Foliage Signal Masking 5-25 Degrees



Mountain Road Approaching Rocky Mountains, Which Includes Natural Signal Masking of 10-25 Degrees

13.1.7 Local Roads



Local Residential Streets with 10-40 Degree Foliage Signal Masking



Local Residential Streets with Asymmetric Foliage Signal Masking



Local Residential Streets with High Signal Masking



Local Roads with Very High Foliage Signal Masking (> 60 Degrees) and Location of a V2I Station



Local Road Intersection Showing One Test Vehicle Approaching the Intersection and the Other Traveling Through the Intersection



Local Road Intersection with Near 90 Degree Foliage Signal Mask

13.2 Heading Accuracy

The heading accuracy relative to the Inertial Explorer heading is shown for the AW and B24W receivers. The heading has only been processed for a sample of the data that includes all environments except for the Deep Urban and Mountain Roads environments. All heading differences were removed if the speed of the vehicle was less than 5 miles per hour.

Figure 13-1 and Figure 13-2 show histograms of the heading errors for B24W and AW, respectively. The overall RMS heading error of the AW and B24W receivers is 1.4 and 1.6 degrees, respectively.

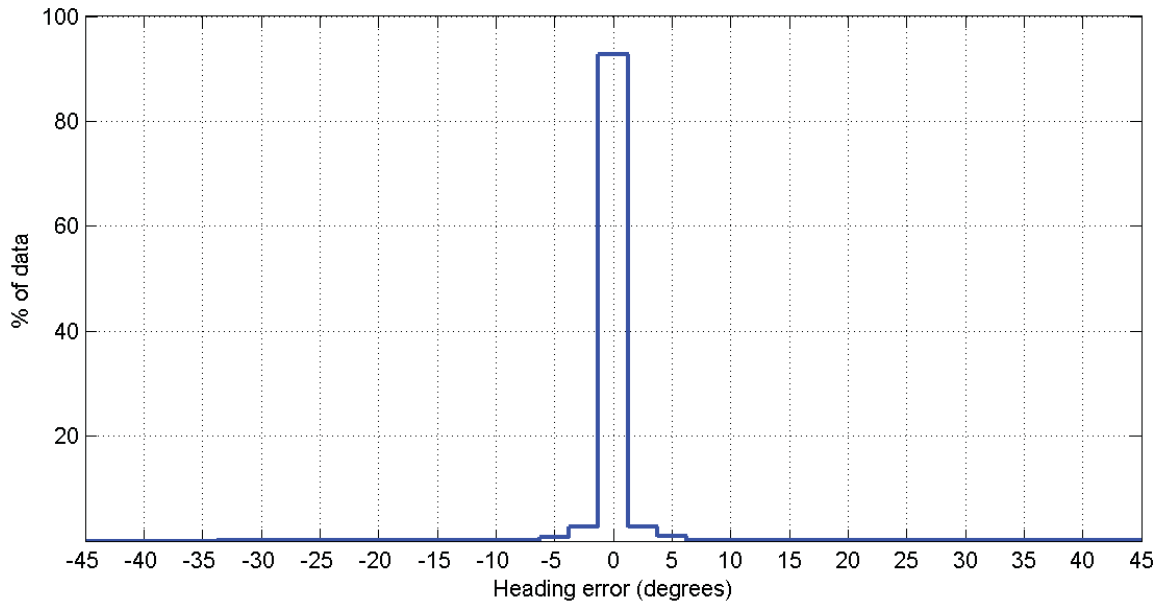


Figure 13-1: Histogram of the Heading Errors for B24W in All Environments

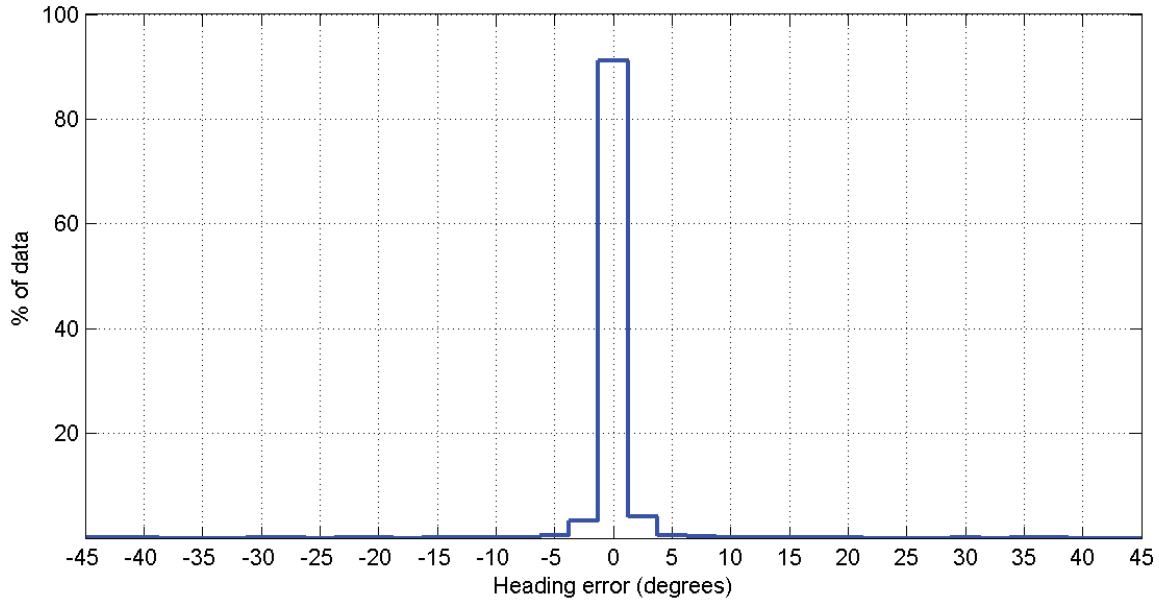


Figure 13-2: Histogram of the Heading Errors for AW in All Environments

13.3 Analysis of RTK Processing Packages

A select dataset is used to outline the difference in performance between various RTK SW packages. The RTK solutions show significant inconsistencies in combinations that in theory should provide the same level of accuracy (i.e., (BW-BN) and (BW-BW) (since WAAS is not used), (AW-BW) and (BW-AW)). Further investigation into these inconsistencies could not identify the reason for the differences. It may be due to nonlinear processes in the SW, including ambiguity resolution.

The PLANSoft SW is compared to the RTK results for the Mountain Road environment. This data segment was chosen because the RTK time-series plot is atypical.

Figure 13-3 shows the time series of the RTK and PLANSoft processing methods, and Figure 13-4 shows a histogram comparison for 04AUG09 Data Segment C for the (AW-AW) receiver combination. The RMS position errors for the RTK and PLANSoft positioning SW is 0.10 m (AT), 0.11 m (XT) and 0.02 m (AT), 0.03 m (XT), respectively. The PLANSoft solution performs consistently better than the RTK solution for this data segment.

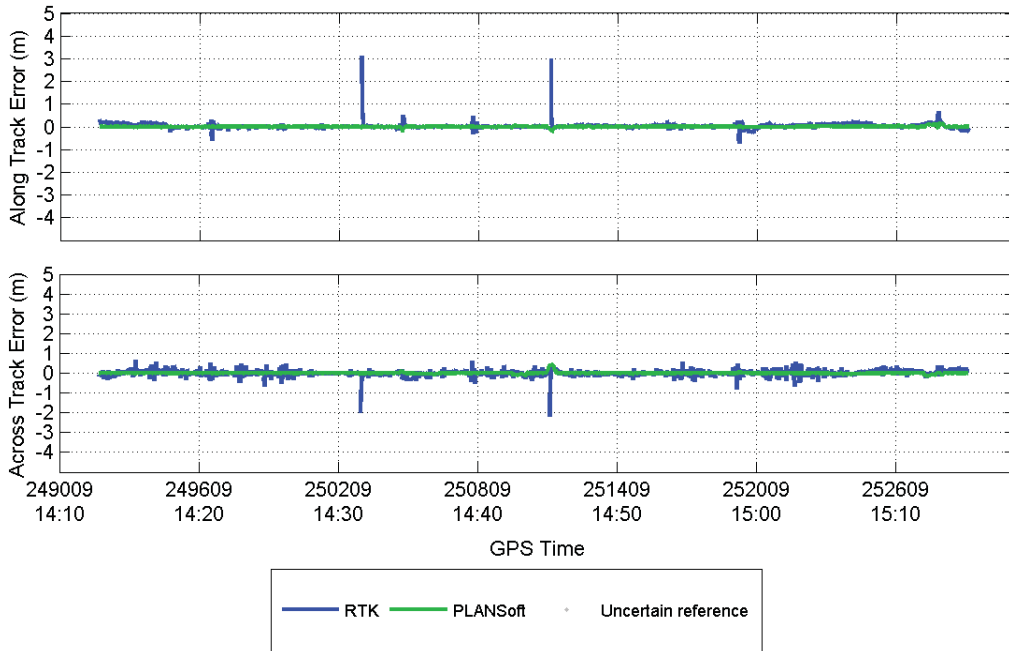


Figure 13-3: Time Series Comparing (AW-AW) for RTK and PLANSOFT Processing Methods for 09AUG09 Mountain Road Environment

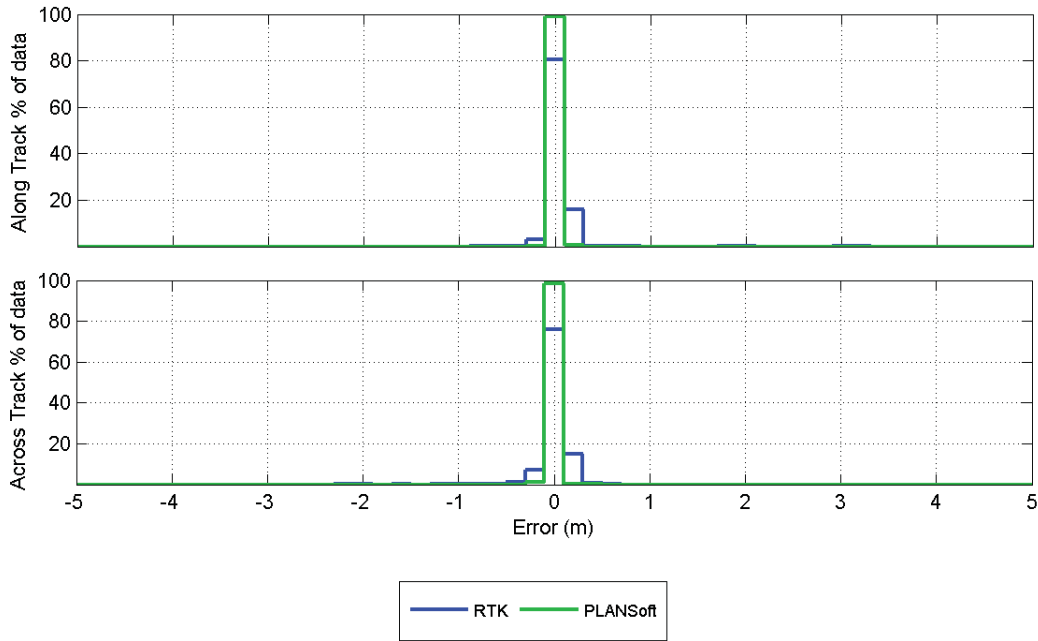


Figure 13-4: Histogram Comparing (AW-AW) for RTK and PLANSOFT Processing Methods for 09AUG09 Mountain Road Environment

Figure 13-5 shows the time series of the RTK and PLANSOFT processing methods, and Figure 13-6 shows a histogram comparison for 04AUG09 Data Segment C for the (BW-BW) receiver combination. The RMS position errors for the RTK and PLANSOFT positioning SW is 0.73(AT), 1.80(XT) and 0.62(AT), 0.56(XT), respectively. The RTK

solution has biases in the along track direction that are not present in the PLANSOFT processing SW. This suggests that the results may be slightly different if a different SW package is used or if the current SW package were tuned for the characteristics of the BW data.

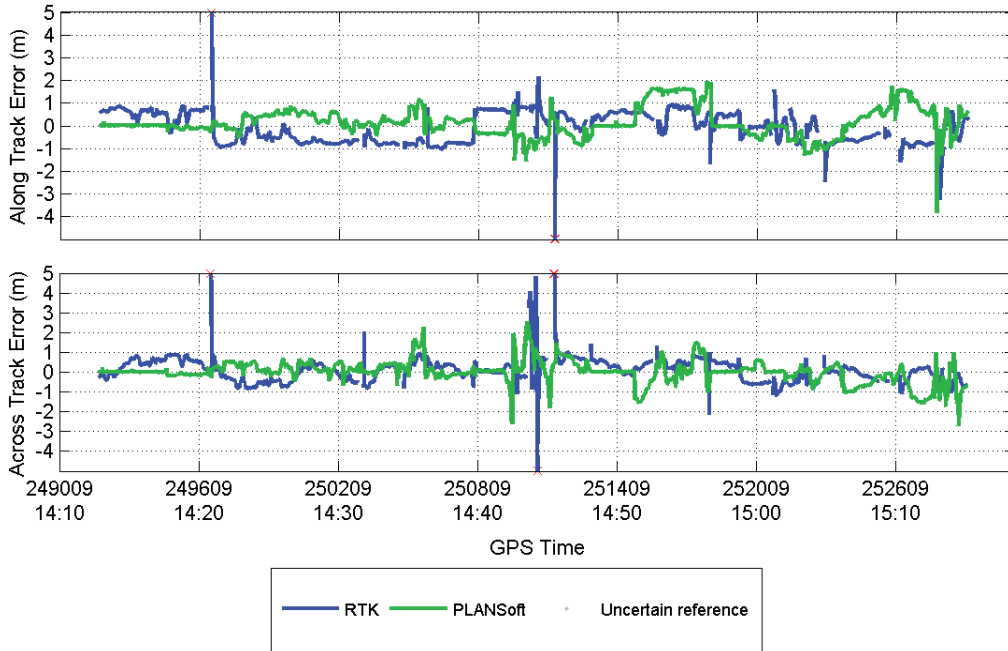


Figure 13-5: Time Series Comparing (BW-BW) For RTK and Plansoft Processing Methods for 09AUG09 Mountain Road Environment

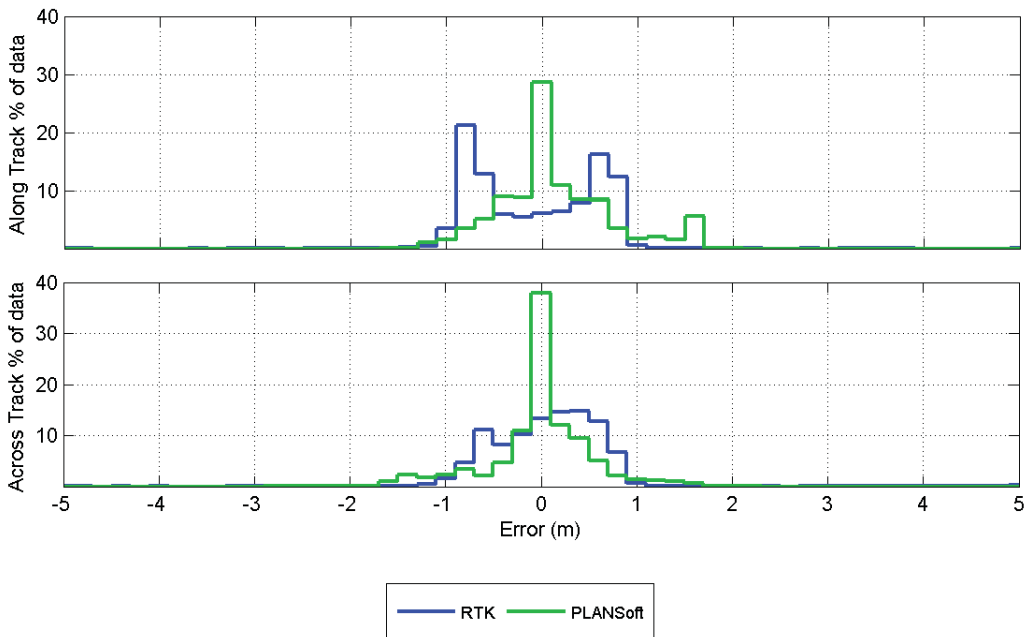


Figure 13-6: Histogram Comparing (BW-BW) For RTK and Plansoft Processing Methods for 09AUG09 Mountain Road Environment

VSC-A Final Report: Appendix I
Multiple-OBE Scalability Testing Results

List of Acronyms

CAMP	Crash Avoidance Metrics Partnership
HV	Host Vehicle
IPG	Inter-Packet Gap
ITS	Intelligent Transportation Systems
JPO	Joint Program Office
NHTSA	National Highway Traffic Safety Administration
OBE	On-Board Equipment
OTA	Over-the-Air
PER	Packet Error Rate
RITA	Research and Innovative Technology Administration
RSS	Receive Signal Strength
RTCM	Radio Technical Commission for Maritime Services
RTK	Real-Time Kinematic
RV	Remote Vehicle
USDOT	United States Department of Transportation
VSC2	Vehicle Safety Communications 2
VSC-A	Vehicle Safety Communications – Applications
V2V	Vehicle-to-Vehicle

Table of Contents

List of Acronyms.....	I-ii
1 Introduction.....	I-1
2 Baseline Scalability Test Results	I-1
2.1 PER vs. Range for Vehicle Pairs.....	I-2
2.2 PER vs. RSS and PER vs. Range for Multiple RVs.....	I-3
2.3 IPG Distribution	I-6
3 Non-Baseline Static Scalability Test Results	I-8
3.1 PER vs. Message Size	I-8
3.2 PER vs. Message Transmit Rate	I-9
3.3 PER vs. Data Transmit Rate.....	I-10
3.4 PER vs. Data Transmit Rate vs. Range	I-12
3.5 PER vs. Data Transmit Rate vs. RSS	I-13
4 Moving Scalability Test Results	I-14
4.1 Interpreting the Charts.....	I-16
4.2 PER Comparison for Channel Configuration C2 vs. C3.....	I-17
4.3 Cumulative PER for Moving HV with Moving Blocking RV	I-18
4.4 Cumulative PER for Moving HV w/ Moving Semi-Blocking RV	I-20
4.5 Cumulative PER for Stationary HV	I-22
4.6 PER Comparison for Stationary vs. Moving Vehicle Tests.....	I-23
4.7 Moving Test Results Summary and Next Steps.....	I-24

List of Figures

Figure 1: PER vs. Range for an HV / RV Combination – Ch. Cfg. 1, 2, 3, & 4 – 24, 48, 36, & 60 Tx Radios	I-3
Figure 2: PER vs. Range for Multiple RVs – Example Plot for 24 Tx Radios	I-4
Figure 3: PER vs. Range & PER vs. Avg. RSS for Multiple RVs – Ch. Cfg. 1, 3, & 2 – 60 Tx Radios	I-5
Figure 4: IPG Distribution – Ch. Cfg. 1, 3, & 2 – 48, & 60 Tx Radios.....	I-7
Figure 5: PER vs. OTA Packet Length – Ch. Cfg. 2 & 3 – 60 Tx Radios.....	I-9
Figure 6: PER vs. Message Transmit Rate – Ch. Cfg. 2 & 3 – 60 Tx Radios	I-10
Figure 7: PER vs. Data Transmit Rate at the Center of Radio Coverage – Ch. Cfg. 2 & 3 – 60 Tx Radios	I-11
Figure 8: PER vs. Data Transmit Rate at the Edge of Radio Coverage – Ch. Cfg. 2 & 3 – 60 Tx Radios	I-12
Figure 9: PER vs. Data Transmit Rate vs. Range – Ch. Cfg. 2 & 3 – 60 Tx Radios.....	I-13
Figure 10: PER vs. Data Transmit Rate vs. RSS – Ch. Cfg. 2 & 3 – 60 Tx Radios.....	I-14
Figure 11: Vehicle and Pod Moving Deployment Configuration.....	I-15
Figure 12: PER vs. Range for Moving Vehicles – Example Plot for 60 Tx Radios.....	I-17
Figure 13: PER vs. Range for Moving Vehicles – C2 vs. C3 – 60 Tx Radios	I-18
Figure 14: PER vs. Range for Multiple RVs – Moving HV w/ Blocking RV – Ch. Cfg. 2 – 60 Tx Radios	I-19
Figure 15: PER vs. Range for Principle RV – Moving HV w/ Blocking RV – Ch. Cfg. 2 – 60 Tx Radios	I-20
Figure 16: PER vs. Range for Multiple RVs – Moving HV w/ Semi-Blocking RV – Ch. Cfg. 2 – 60 Tx Radios	I-21
Figure 17: PER vs. Range for Principle RV – Moving HV w/ Semi-Blocking RV – Ch. Cfg. 2 – 60 Tx Radios	I-22
Figure 18: PER vs. Range for Multiple RVs – Stationary HV – Ch. Cfg. 2 – 60 Tx Radios	I-23
Figure 19: Stationary vs. Moving Vehicle Test Comparison – Ch. Cfg. 2 – 60 Tx Radios	I-24

List of Tables

Table 1: Channel Configurations for Scalability TestingI-1

1 Introduction

As noted in the main body of the Final Report under the data analysis of the multiple-On-Board Equipment (OBE) scalability testing, gathering the necessary data in order to analyze the Packet Error Rate (PER) and the Inter-Packet Gap (IPG) distribution was of primary interest. In addition to the results provided in the main body of the Final Report, this appendix will provide additional test results and analysis for the baseline and other tests, both static and moving, that were run as part of the preliminary scalability testing effort for the different channel configurations tested which are listed in Table 1 below.

Table 1: Channel Configurations for Scalability Testing

Configuration #	Channel Configuration Description
C1	IEEE 1609.4 channel switching mode
C2	Channel 172 dedicated safety channel (i.e., no channel switching)
C3	IEEE 1609.4 channel switching mode with messages submitted for transmission at a random time during each control channel interval
C4	IEEE 1609.4 channel switching mode with messages submitted for transmission via a time-shifting algorithm in an attempt to evenly space transmissions out during the intended channel

2 Baseline Scalability Test Results

In the main body of the Final Report, the Cumulative PER results and Average IPG results at a particular host vehicle (HV) for the baseline test configuration are presented. The results include the data for channel configurations C1 (1609.4–Timer Based), C3 (1609.4–Random Control Channel Interval Transmit), and C2 (Dedicated Safety Channel 172) for the 24, 48, and 60 radio scaling increment tests and show that the configuration method used for message transmission has a strong correlation to PER and IPG encountered. As expected, collisions at the beginning of a channel interval result in higher PER and correspondingly IPG for C1, which has the worst performance. Taking advantage of knowing when the channel interval begins and ends and implementing countermeasures in an attempt to avoid collisions as in C3 and C4 (1609.4–Time-shifted Control Channel Interval Transmit) provided better results than C1, which made no such attempt. C2, which provided full-time access to the channel, had the best PER and IPG performance and did not appear to be as affected as the other configurations as the scaling increments increased.

In addition to the PER and IPG test results discussed in the main body of the Final Report, other baseline test analysis looked at the PER versus Range, the PER versus Receive Signal Strength (RSS), and the IPG distribution for each of the channel configurations. For each of these tests, C2 outperformed C3 and C4, which in turn,

outperformed C1 as in the previous test results. These test results are provided in the following sections.

2.1 PER vs. Range for Vehicle Pairs

Figure 1 below shows the test results for PER versus range for different HV / remote vehicle (RV) combinations. The results are shown for each of the channel configurations and radio scaling increments. For each HV / RV combination, the HV remains constant while a different RV is chosen at an increasing range (9m, 55m, 165m, and 260m) from the HV. Note that for each of the HV / RV combinations there is not a data point (indicated by a dot on the chart) for each and every scaling increment. This has to do with some of the RVs not participating in a particular scaling increment (e.g., green Prius for the 24 radio scaling increment) or due to the data not being collected for a particular scaling increment (e.g., 36 radio scaling increment for channel configurations C3 and C4).

For each scaling increment the results show that C1 has the highest PER while C2 has the lowest PER. C3 and C4 perform in between C1 and C2 and have similar results with one another.

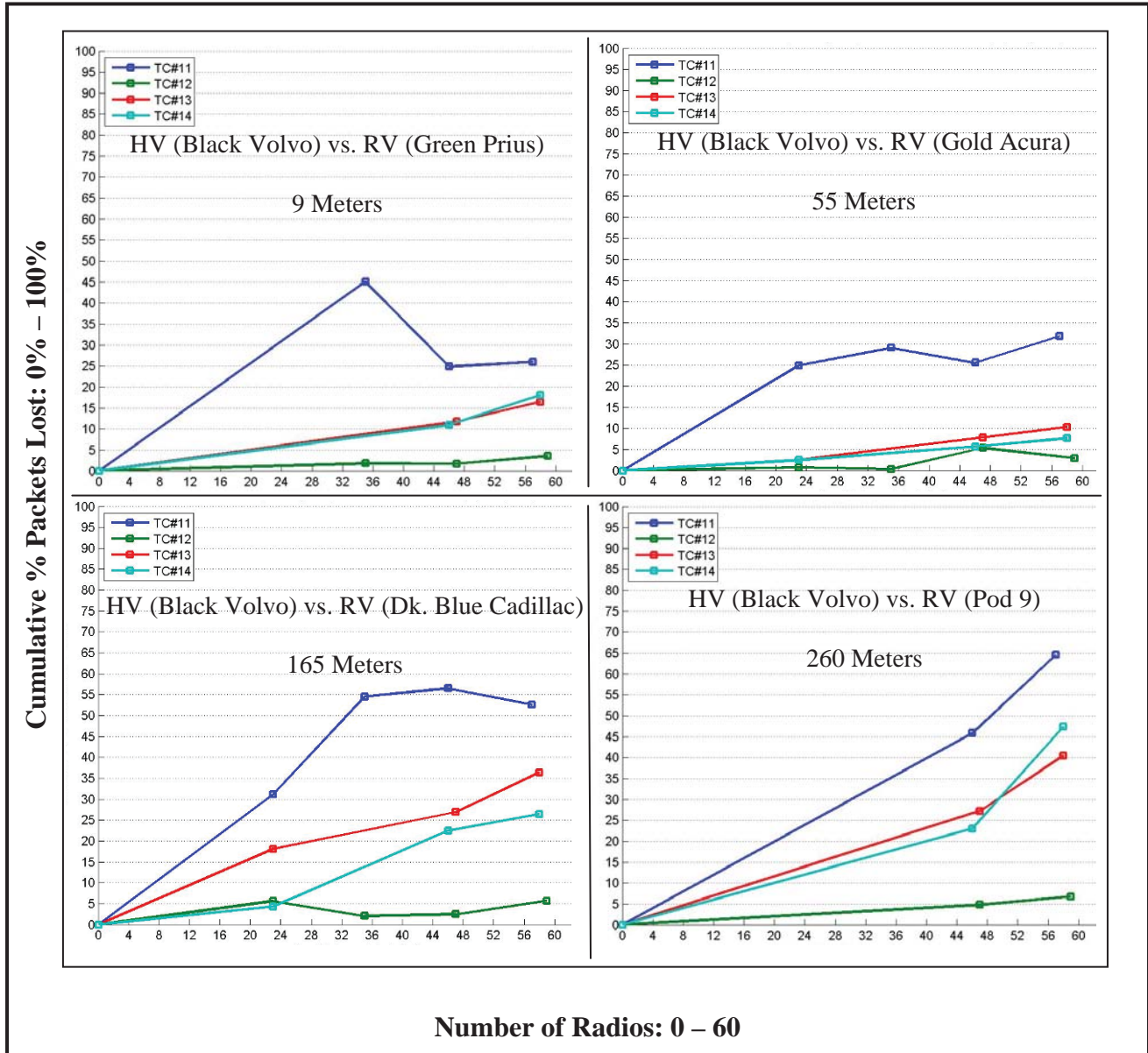


Figure 1: PER vs. Range for an HV / RV Combination – Ch. Cfg. 1, 2, 3, & 4 – 24, 48, 36, & 60 Tx Radios

2.2 PER vs. RSS and PER vs. Range for Multiple RVs

The PER versus RSS and the PER versus range for multiple RVs is presented as a scatter plot. Figure 2 provides an example of this type of plot for the 24 radio scaling increment along with some details on how to interpret the data contained in plot using the Pod 2 data as an example. Multiple HVs are shown on the same plot to evaluate overall test performance for the entire network.

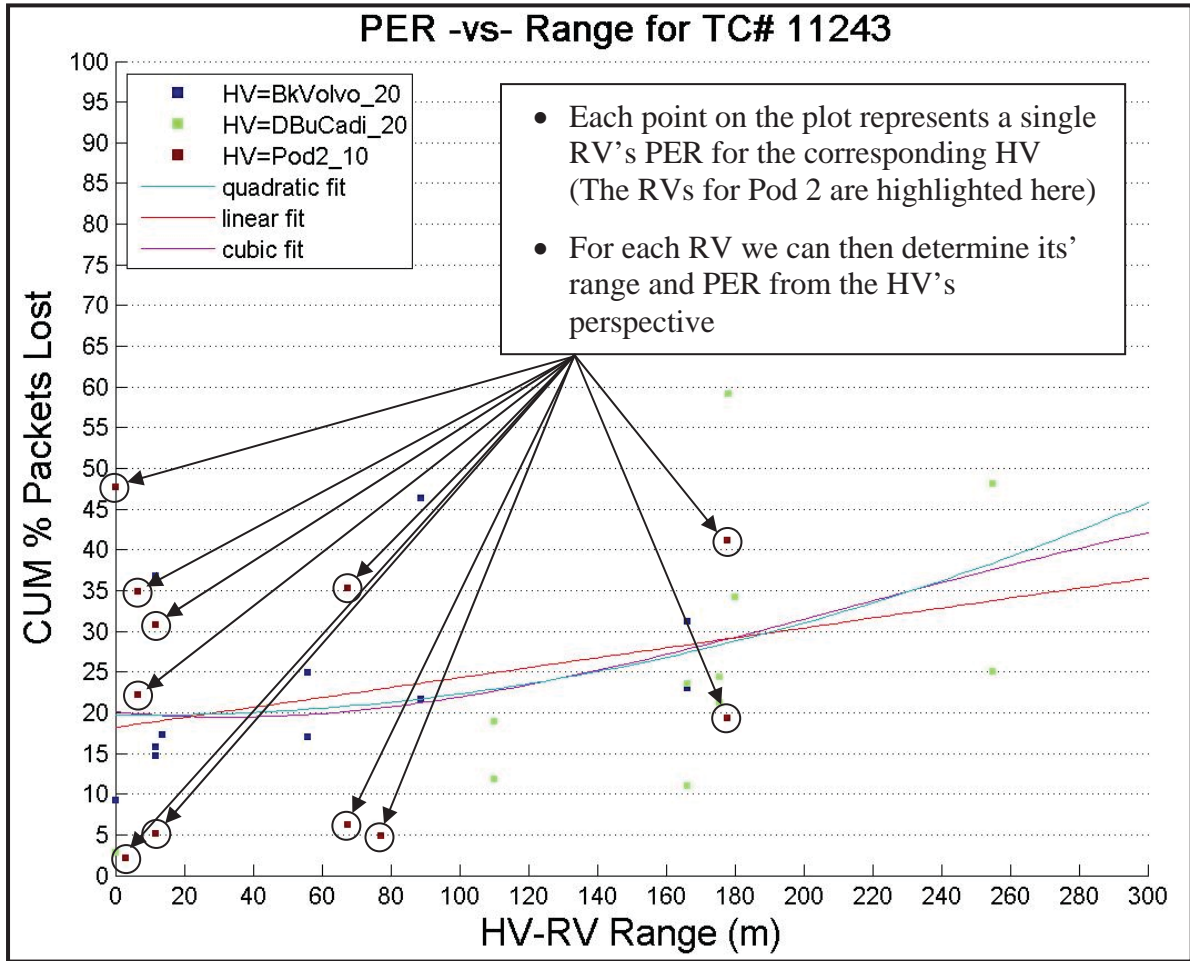


Figure 2: PER vs. Range for Multiple RVs – Example Plot for 24 Tx Radios

The left-side column of Figure 3 shows the PER versus HV / RV range for channel configurations C1, C3, and C2 for the 60 radio scaling increment. Note that these plots exclude the results of the second radio of each OBE due to it having a lower transmit power than the first radio of the OBE. Based on the large scattering of points, the channel configurations C1 and C3 charts indicate that PER is weakly correlated to range potentially due to varying signal strengths. Channel configuration C2, which minimizes packet collisions, appears to have a strong correlation between PER and range and allows better packet reception at greater ranges which was also shown to be the case in Section 2.1.

The right-side column of Figure 3 shows the PER versus average RSS for the same channel configurations and radio scaling increment as the HV / RV range charts. These charts indicate that PER is more strongly correlated to RSS for all channel configurations. Minimizing packet collisions allows better packet reception at weaker signal strengths, as shown with channel configuration C2 (dedicated safety channel).

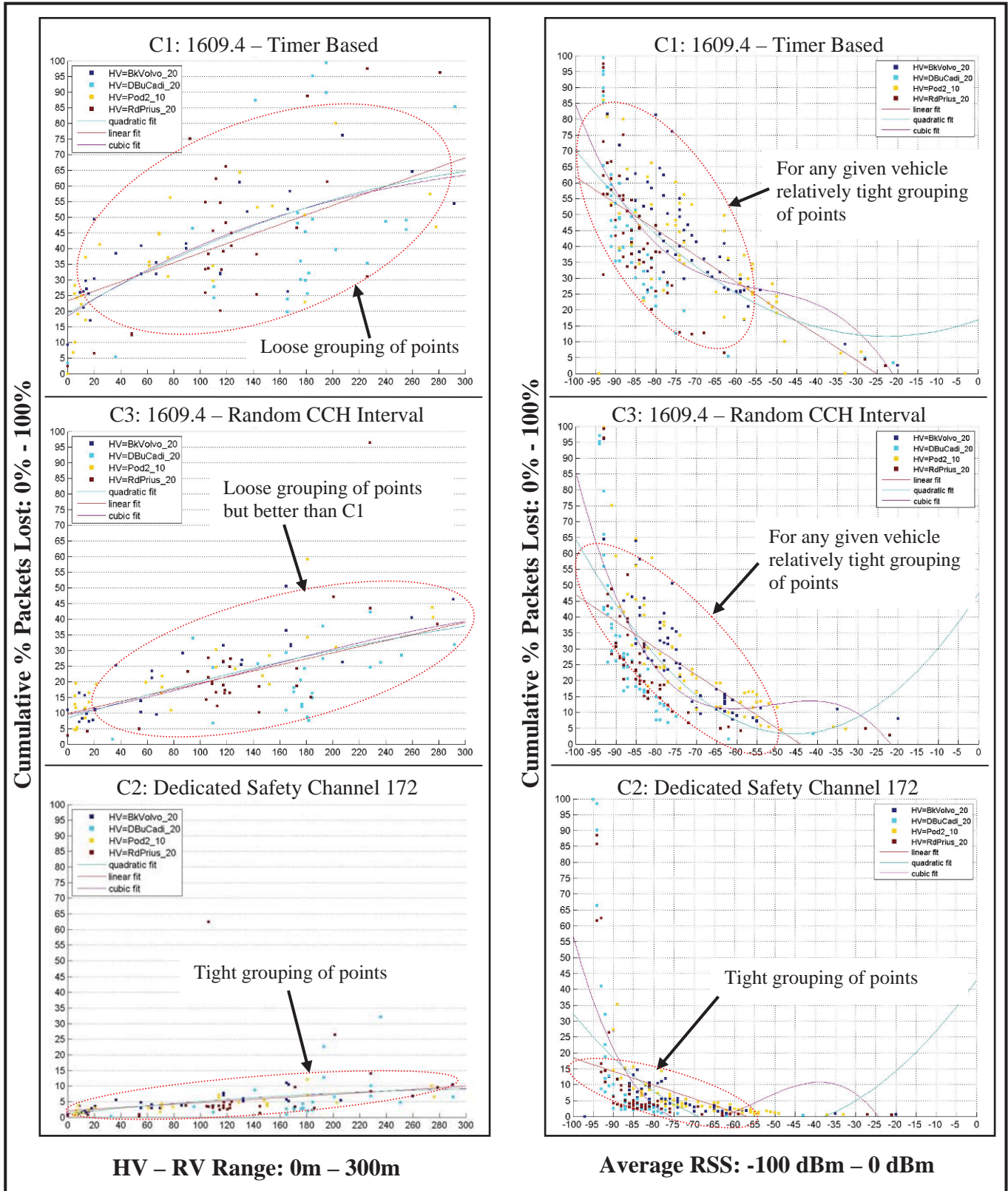


Figure 3: PER vs. Range & PER vs. Avg. RSS for Multiple RVs – Ch. Cfg. 1, 3, & 2 – 60 Tx Radios

2.3 IPG Distribution

Figure 4 shows the IPG distribution of all the packets received at V2 (black Volvo) which was part of the center cluster of radios. The IPG distribution shows that for channel configuration C1 some RVs were not heard from for periods of 400ms – 500ms while for channel configuration C2 the worst case was 200ms – 300ms. For future testing it would be useful to analyze the number of vehicles that fell within each of these bins due to the vehicles with the lower PER (and thus more received packets) potentially skewing these results.

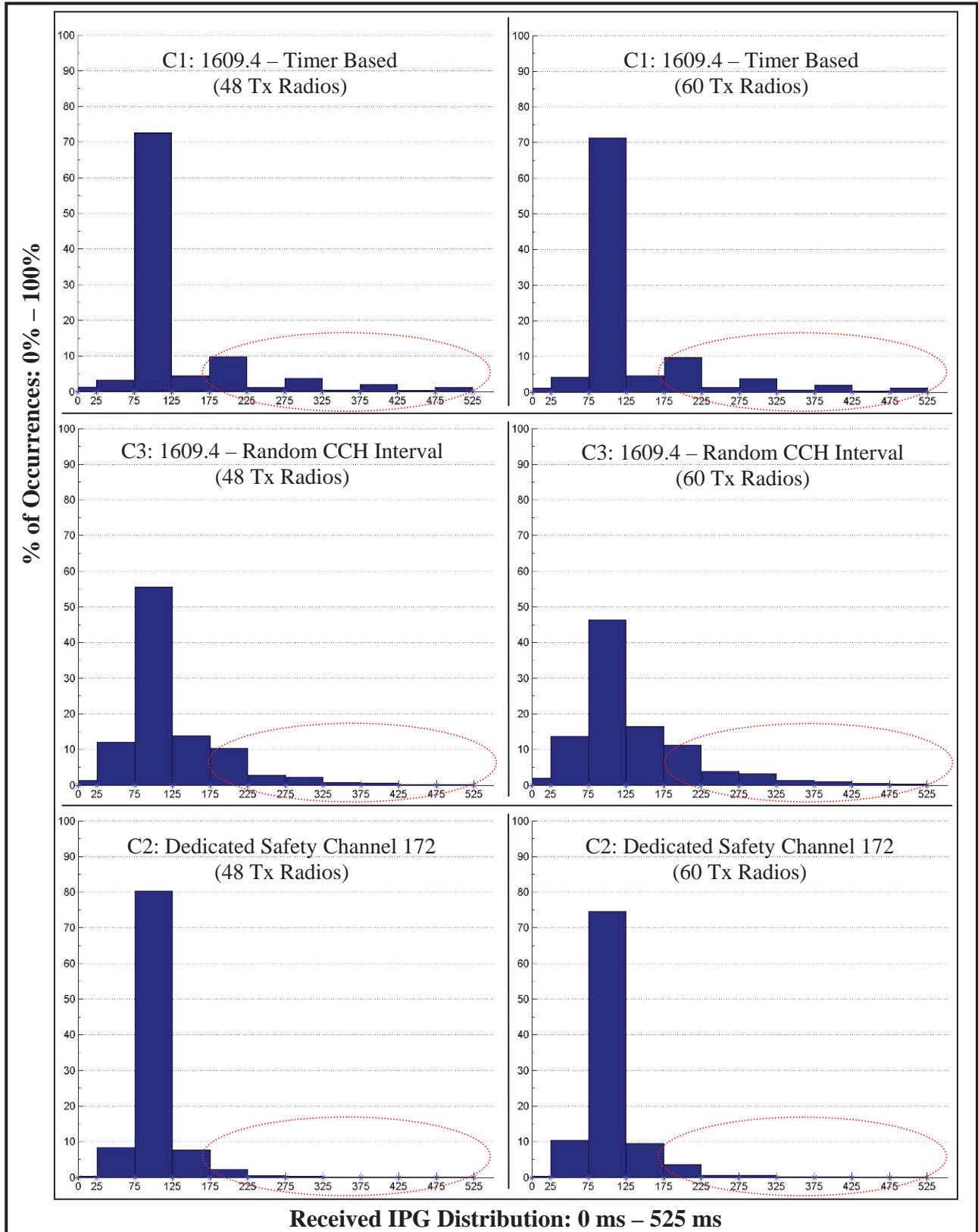


Figure 4: IPG Distribution – Ch. Cfg. 1, 3, & 2 – 48, & 60 Tx Radios

3 Non-Baseline Static Scalability Test Results

The baseline test results indicate that 1609.4 channel switching with no countermeasures to address the synchronized collision issue is not a viable channel configuration for V2V safety DSRC. Because of this, the non-baseline static tests focused on channel configurations C2 and C3 for the data gathering and analysis. The data analysis for these tests primarily looked at the PER and included PER versus message size, PER versus message transmit rate, and PER versus data transmit rate for the 48 and 60 radio scaling increments. These test results are provided in the following sections along with the baseline results for comparison. In addition, for the data transmit rate analysis the PER versus Range and PER versus RSS for baseline and non-baseline tests is provided. For all of these tests, due to the results being similar for both scaling increments, only the 60 radio scaling increment results are provided.

3.1 PER vs. Message Size

For this test, 86 bytes of padding were added to the Over-the-Air (OTA) message when compared to the baseline configuration for a total of 464 OTA bytes. These bytes represent (approximately) the Radio Technical Commission for Maritime Services (RTCM) 1002 data that would be present if Real-Time Kinematic (RTK) positioning was enabled and seven satellites were in view. The results show (Figure 5) that increasing the OTA packet length increased the PER for both channel configurations. This is caused from a higher OTA congestion level when using larger packet sizes.

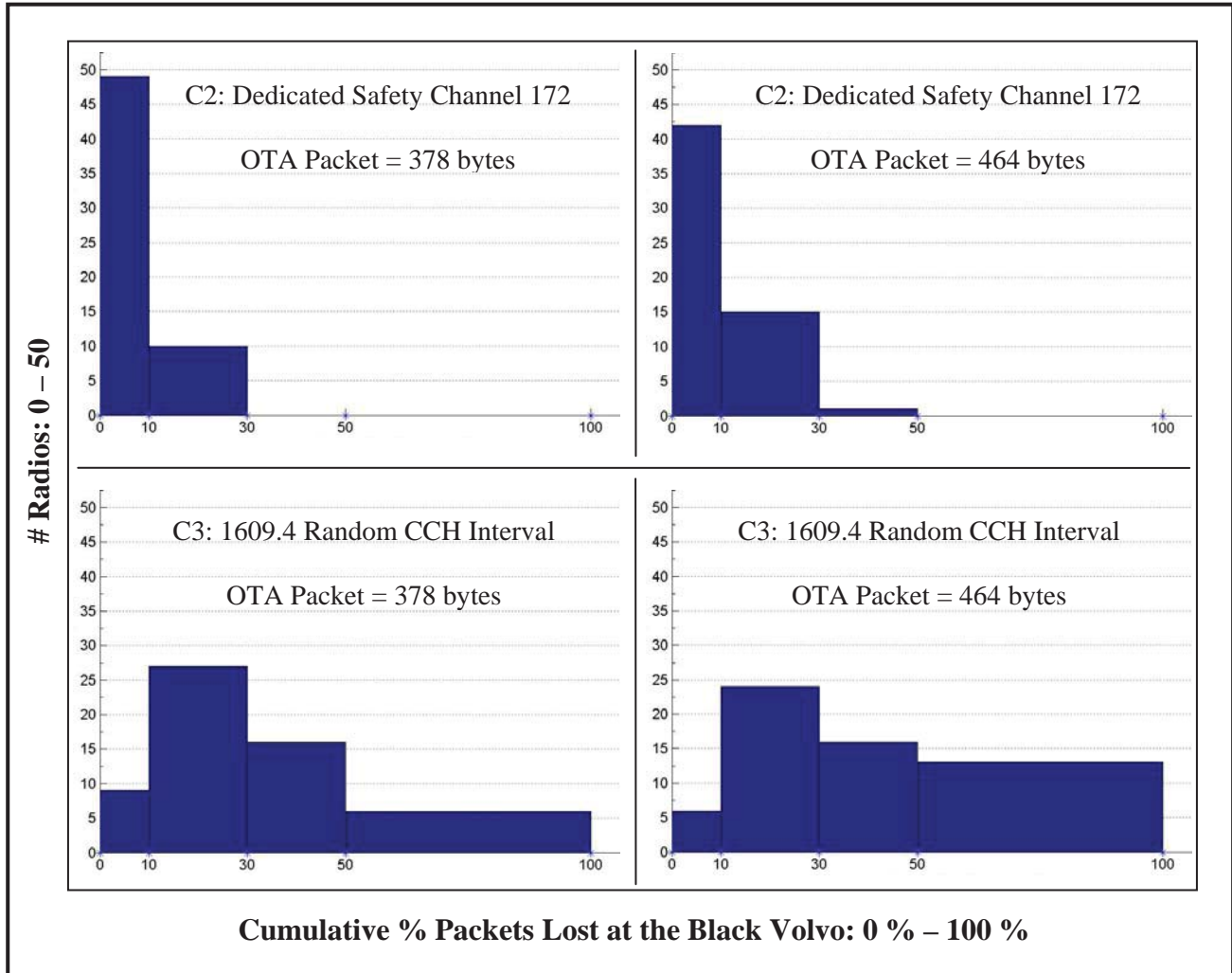


Figure 5: PER vs. OTA Packet Length – Ch. Cfg. 2 & 3 – 60 Tx Radios

3.2 PER vs. Message Transmit Rate

For this test, a 5 Hz message transmit rate was used as opposed to the 10 Hz rate used in the baseline test. Decreasing the transmit rate from 10Hz to 5Hz decreased the PER for both configurations (Figure 6). This was expected and is caused from a lower congestion level when RVs are transmitting less frequently.

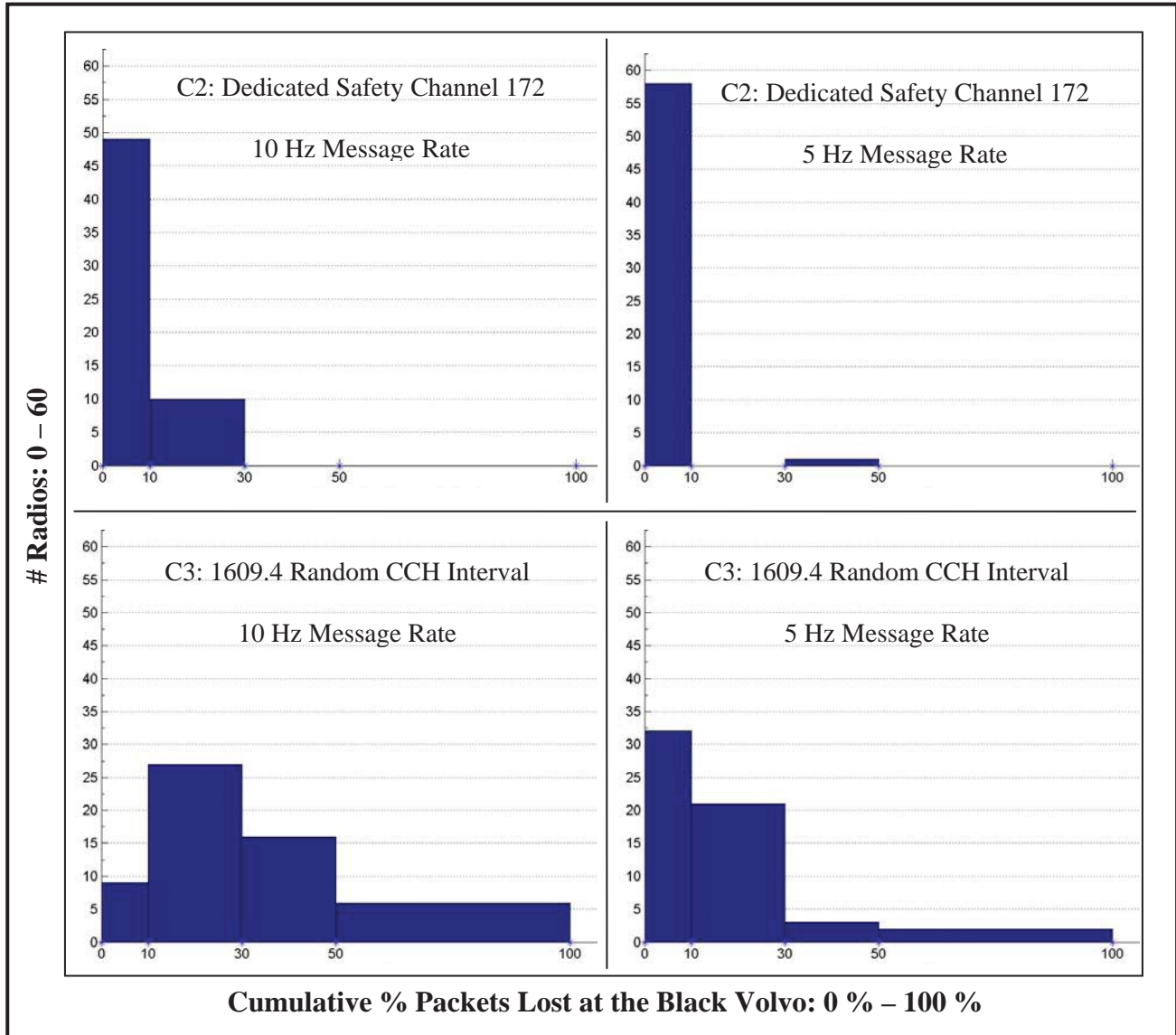


Figure 6: PER vs. Message Transmit Rate – Ch. Cfg. 2 & 3 – 60 Tx Radios

3.3 PER vs. Data Transmit Rate

For this test, a 12 Mbps data rate was used as opposed to the 6 Mbps rate used in the baseline test. Two sets of data are presented below. The first data set is for the black Volvo (V2) which was part of the center cluster of pods and vehicles and in communication range with all of the other radios. The second data set is for the dark blue Cadillac (V3) which was positioned at the far edge of the radio communication and was not in communication range with all of the other radios.

For the black Volvo, which was in the center of radio communication, increasing the data transmit rate from 6 Mbps to 12 Mbps decreased the overall PER for both configurations but appears to have had a larger affect on transmit configuration C3 (Figure 7) perhaps because the results for C2 were already quite good and there was not a lot of room for improvement.

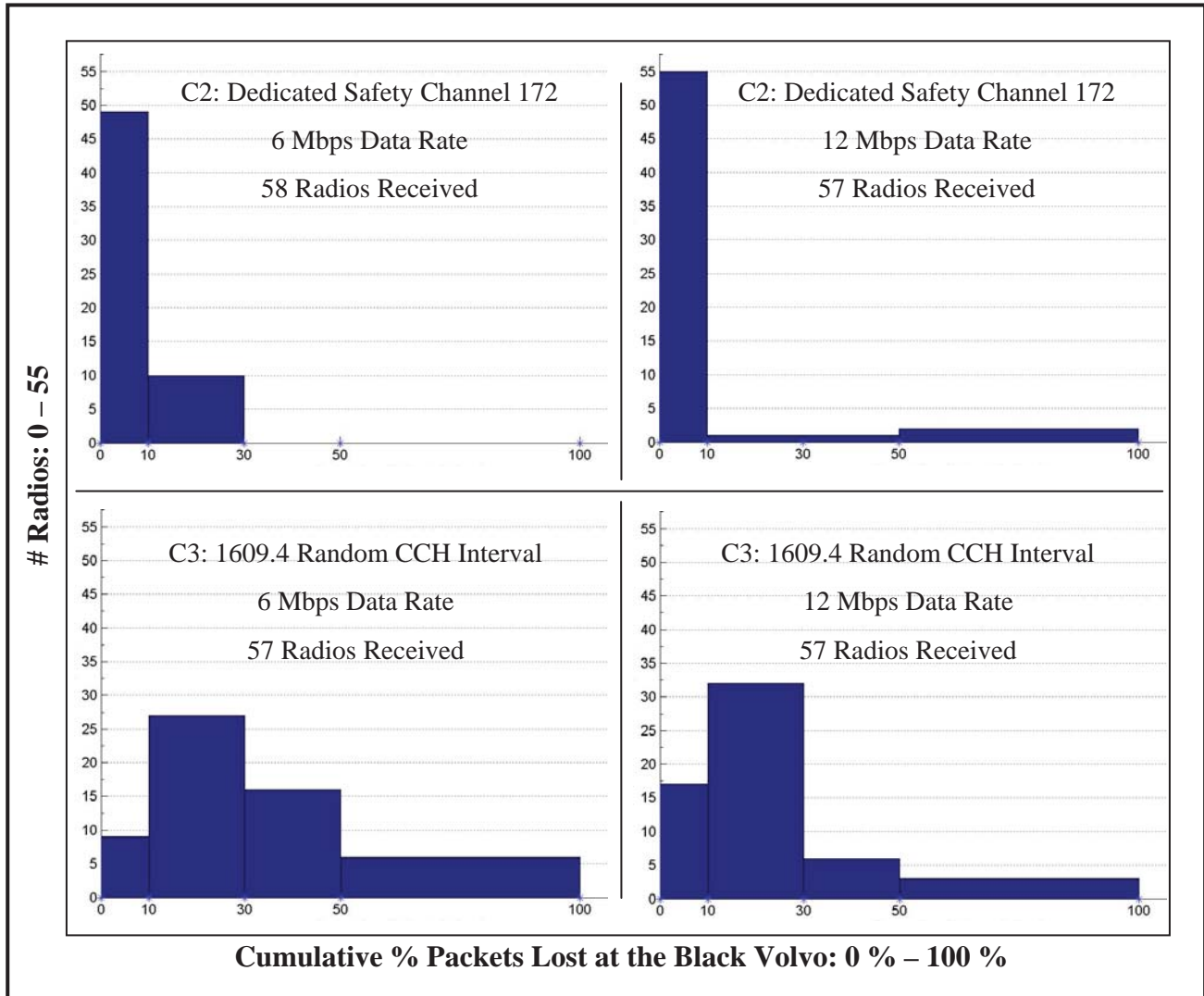


Figure 7: PER vs. Data Transmit Rate at the Center of Radio Coverage – Ch. Cfg. 2 & 3 – 60 Tx Radios

For the dark blue Cadillac, which was on one of the far edges of radio communication, increasing the data transmit rate from 6 Mbps to 12 Mbps increased the overall PER for both configurations, but less so for transmit configuration C3. It also reduced the number of RVs it could communicate with by about ten (Figure 9).

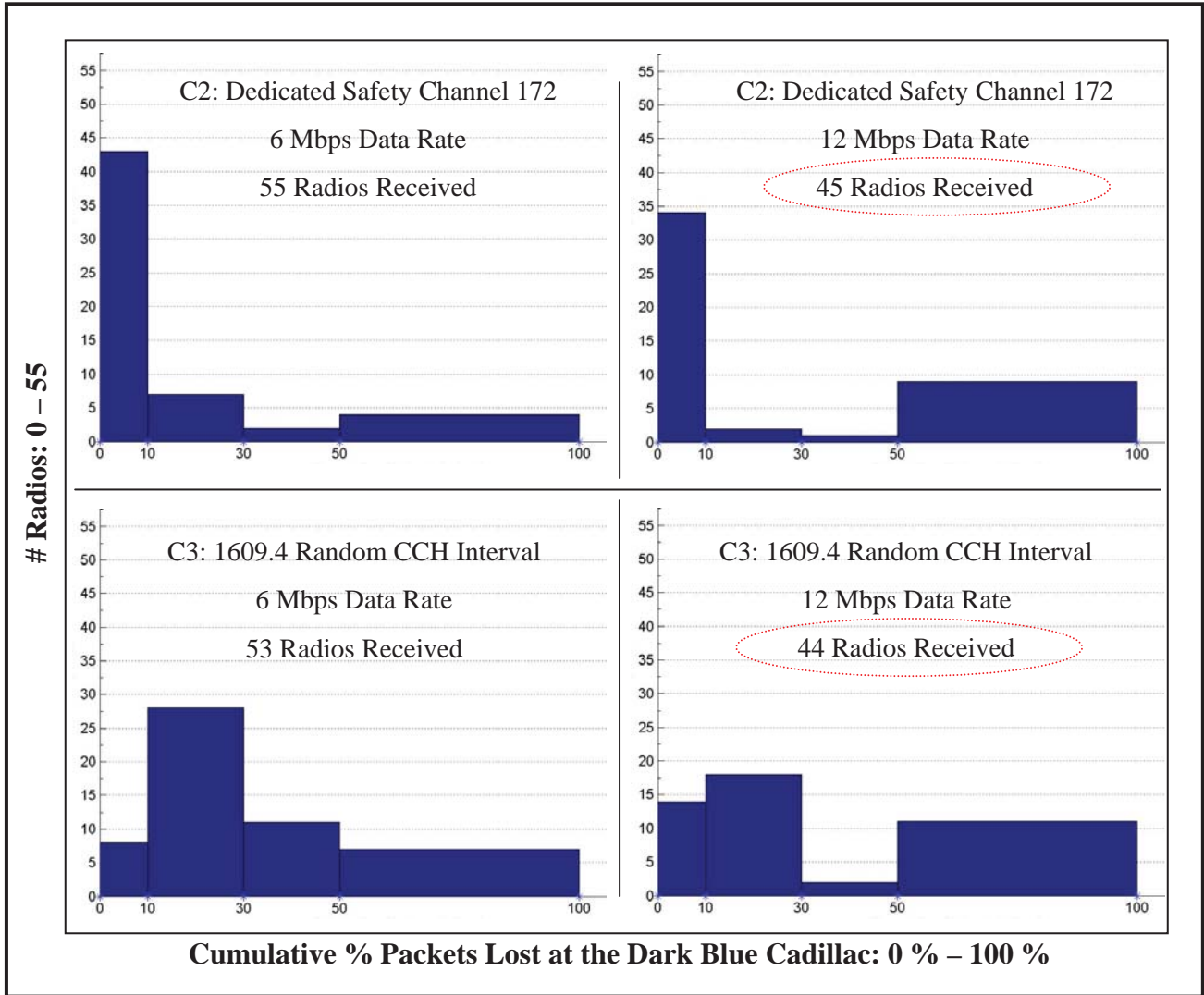


Figure 8: PER vs. Data Transmit Rate at the Edge of Radio Coverage – Ch. Cfg. 2 & 3 – 60 Tx Radios

3.4 PER vs. Data Transmit Rate vs. Range

The following charts show the PER versus range for a 6 Mbps data rate and a 12 Mbps data rate for radios with the same transmit power. Figure 9 shows that increasing the data rate appears to negatively affect some percentage of RVs PER beyond 100m, although low PER is still observed in many RVs up to 300m. As previously noted, transmitting at 12 Mbps appears to have had a more positive affect on transmit configuration C3 than C2. Note that in the Figure 9 range plots, as was the case with the PER versus range results in Section 2.2, the results of the second radio of each OBE unit are excluded due to it having a lower transmit power than the first radio of the OBE.

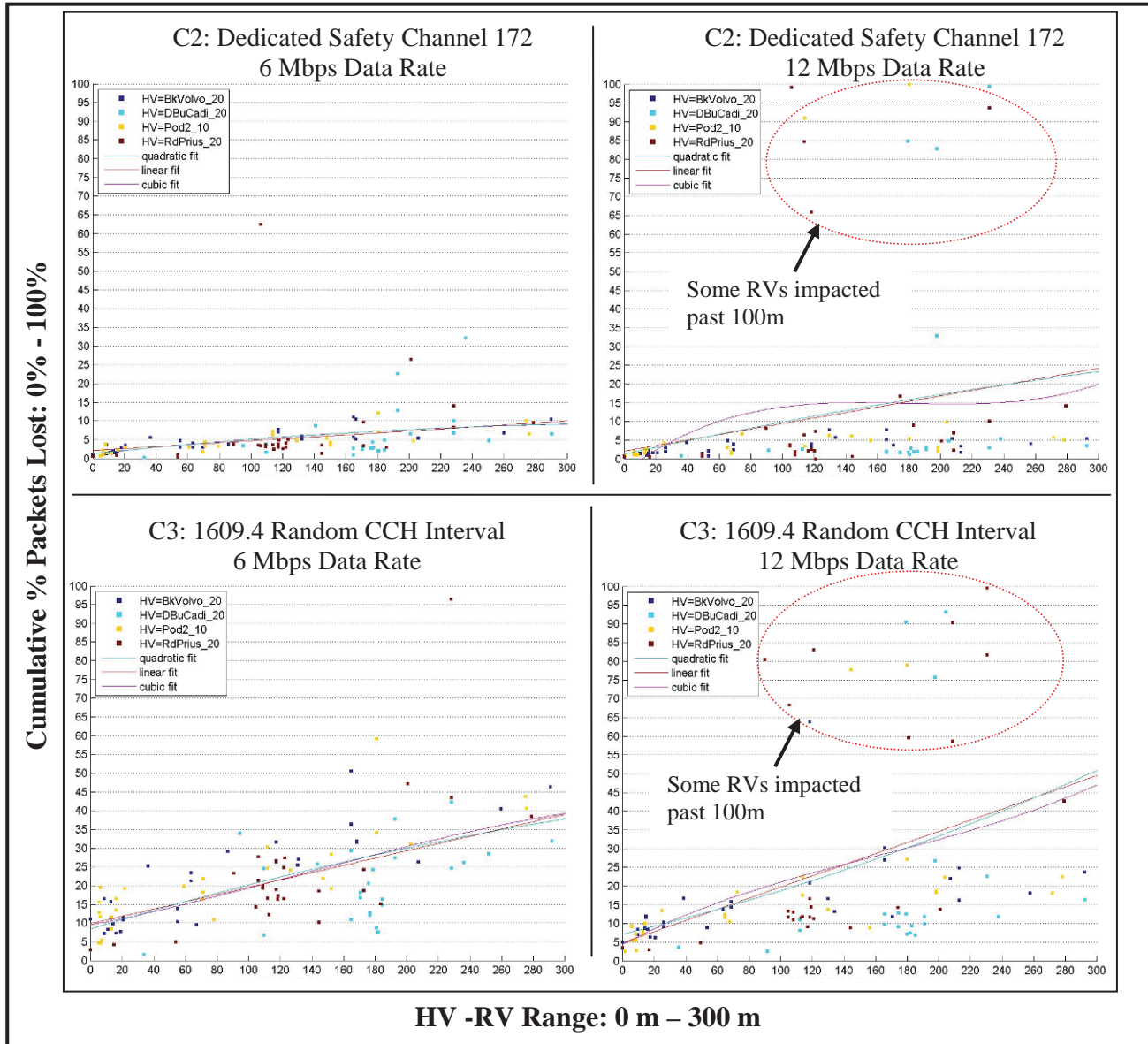


Figure 9: PER vs. Data Transmit Rate vs. Range – Ch. Cfg. 2 & 3 – 60 Tx Radios

3.5 PER vs. Data Transmit Rate vs. RSS

Finally, Figure 10 below shows the PER versus average RSS results presented as a scatter plot for both data transmit rates. Increasing the transmit data rate from 6 Mbps to 12 Mbps decreased the PER for RVs with equivalent stronger signals but reduced the ability to communicate with RVs with weaker signals. At 6 Mbps, packets were received at approximately a minimum -94 dBm, but at 12 Mbps, they were only received at approximately a minimum -90 dBm.

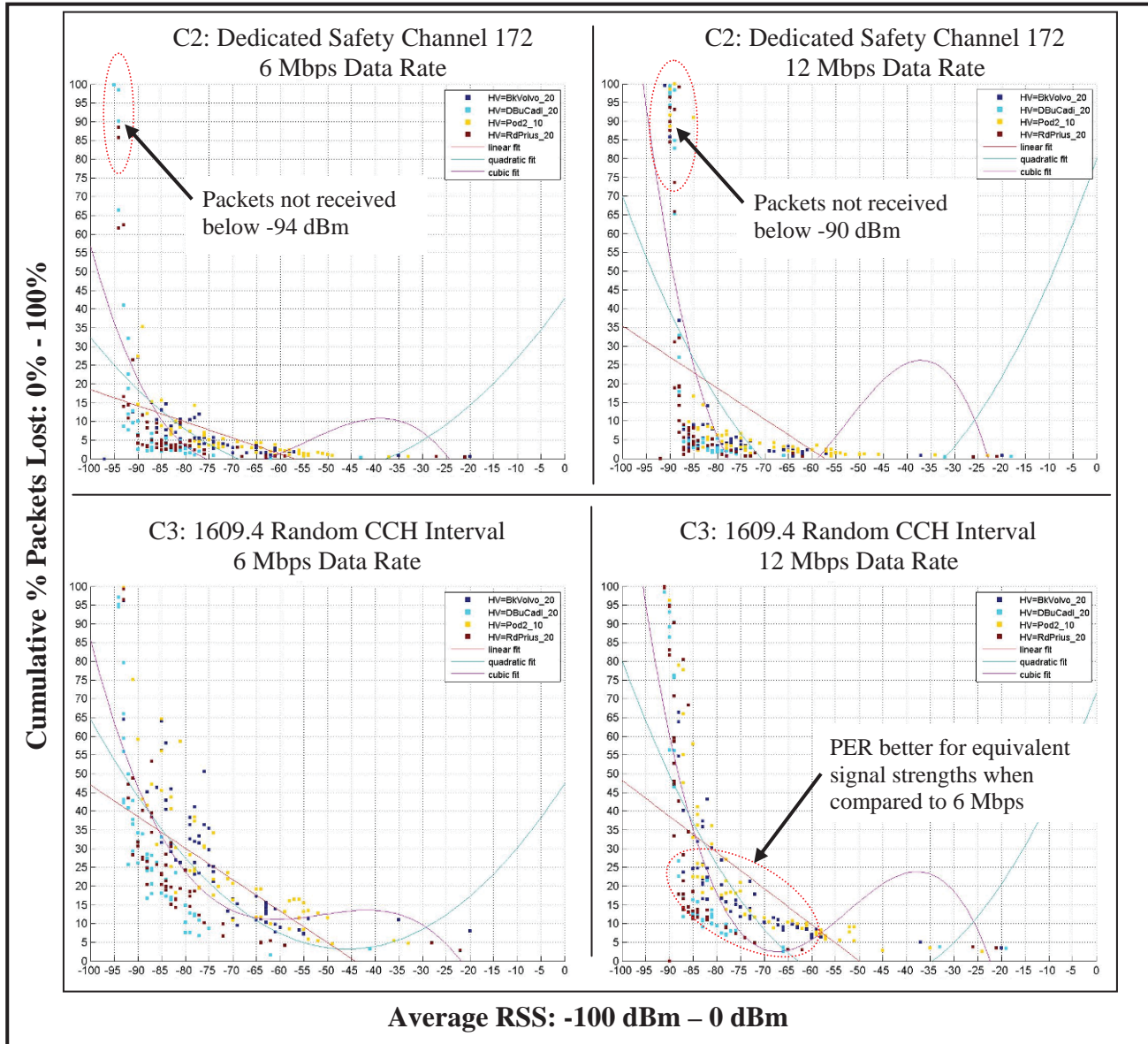


Figure 10: PER vs. Data Transmit Rate vs. RSS – Ch. Cfg. 2 & 3 – 60 Tx Radios

4 Moving Scalability Test Results

In addition to the static deployment tests, a number of moving tests were run to analyze the effects of PER versus distance in a moving environment. For consistency, the pod / vehicle layout for the pods and vehicles that remained static did not change considerably from the all-static tests. It consisted of a center cluster of four pods and four vehicles with the remaining pods placed at varying distances up to 275m from the center cluster. Unlike the static tests all vehicles outside of the center cluster were moving for these tests. Figure 11 provides a diagram identifying the location of each of the pods and

vehicles that were used in the tests and identifies which vehicles were static and which were moving.

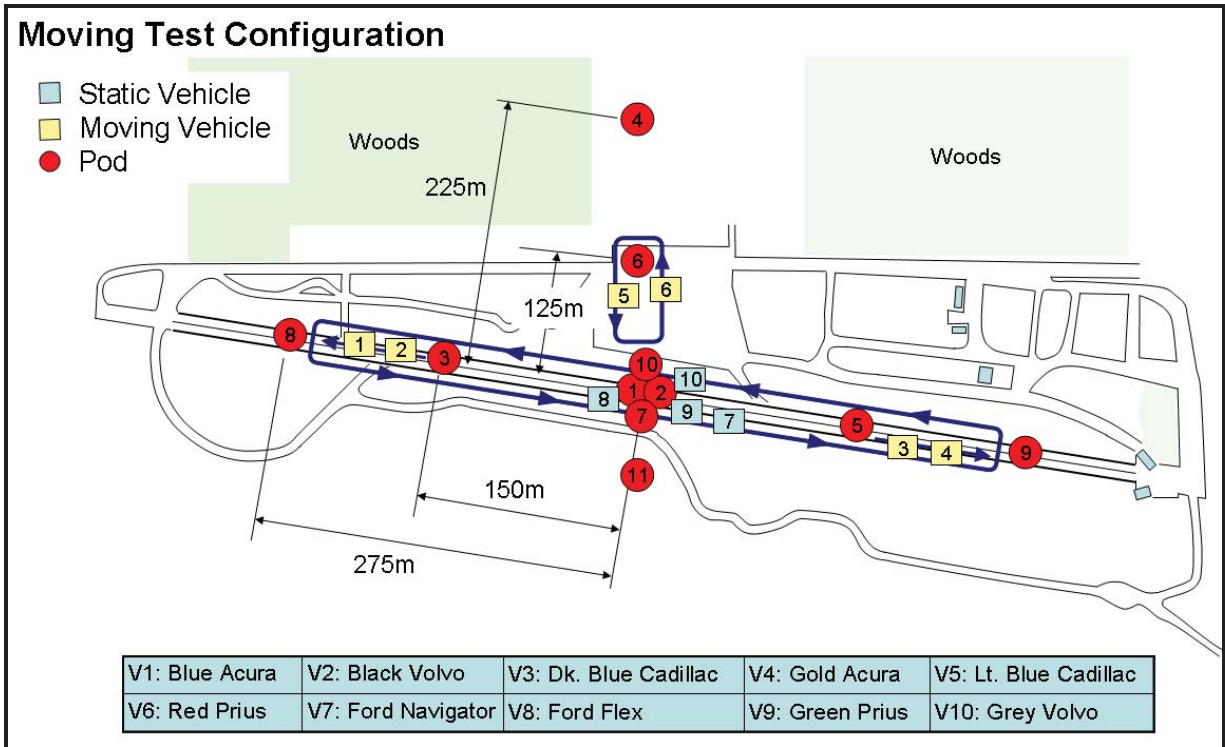


Figure 11: Vehicle and Pod Moving Deployment Configuration

Vehicles V2 (HV) and V1 (RV) traveled together with V2 following relatively close behind V1. Similarly vehicles V3 (HV) and V4 (RV) traveled together with V3 following relatively close behind V4. All four vehicles traveled in a big loop thru main track. Vehicles V6 (HV) and V5 (RV) made a smaller loop outside of the track with each one attempting to remain at opposite ends of the loop.

Channel configurations C2 and C3 were tested for three radio scaling increments consisting of 24, 48, and 60 radios. Other than having moving vehicles, the test configuration was the same as the baseline test configuration. Logs were captured on moving vehicles V2, V3, V6, and stationary Pod2 which were considered to be the HVs for these tests.

The data analysis for these tests primarily looked at the PER versus distance from both an increasing range to the RV(s) and a decreasing range to the RV(s) from the HV's perspective. This included looking at the PER among all of the other radios (RVs) in the test in addition to the PER with the principle other moving vehicle (RV) in the test (i.e., V1 for V2, V4 for V3, and V5 for V6). Only the data from the 60 radio scaling increment will be presented.

The following data analysis sections start with a comparison between channel configurations C2 and C3 to show that, similar to the static tests, C2 performs better than C3 from a PER analysis perspective. The remaining data analysis sections only provide the data for channel configuration C2. Since the data is similar for V2 and V3, which

were both traveling in a big loop through the main track, only the data from V2 will be presented in order to allow for a comparison between the static and moving test results. This section ends with a PER comparison between the static and moving results and some conclusions drawn from the results of the moving tests.

4.1 Interpreting the Charts

Figure 12 shows the charts that were developed to analyze the PER versus range from the HV perspective for all of the RVs the HV was in communication with. Additional charts are also presented in the analysis sections that show the PER versus range from the HV perspective for the principle RV that the HV was traveling with. To aid in the plotting of the data, the ranges were grouped into 3m bins. Two types of charts were developed:

1. A chart to plot the number of packets received at each range grouping
2. A chart to plot the percentage of packets lost or PER for each range grouping

Each of these charts has multiple plots:

- Blue lines / dots show the # packets / PER for all of the RVs
- Red lines / arrows show the # packets / PER when the HV to RV distance was decreasing
- Green lines / dots show the # packets / PER when the HV to RV distance was increasing or unchanged

For the PER charts linear (solid line) and quadratic fit (dashed line) curves are provided based on the plotted points.

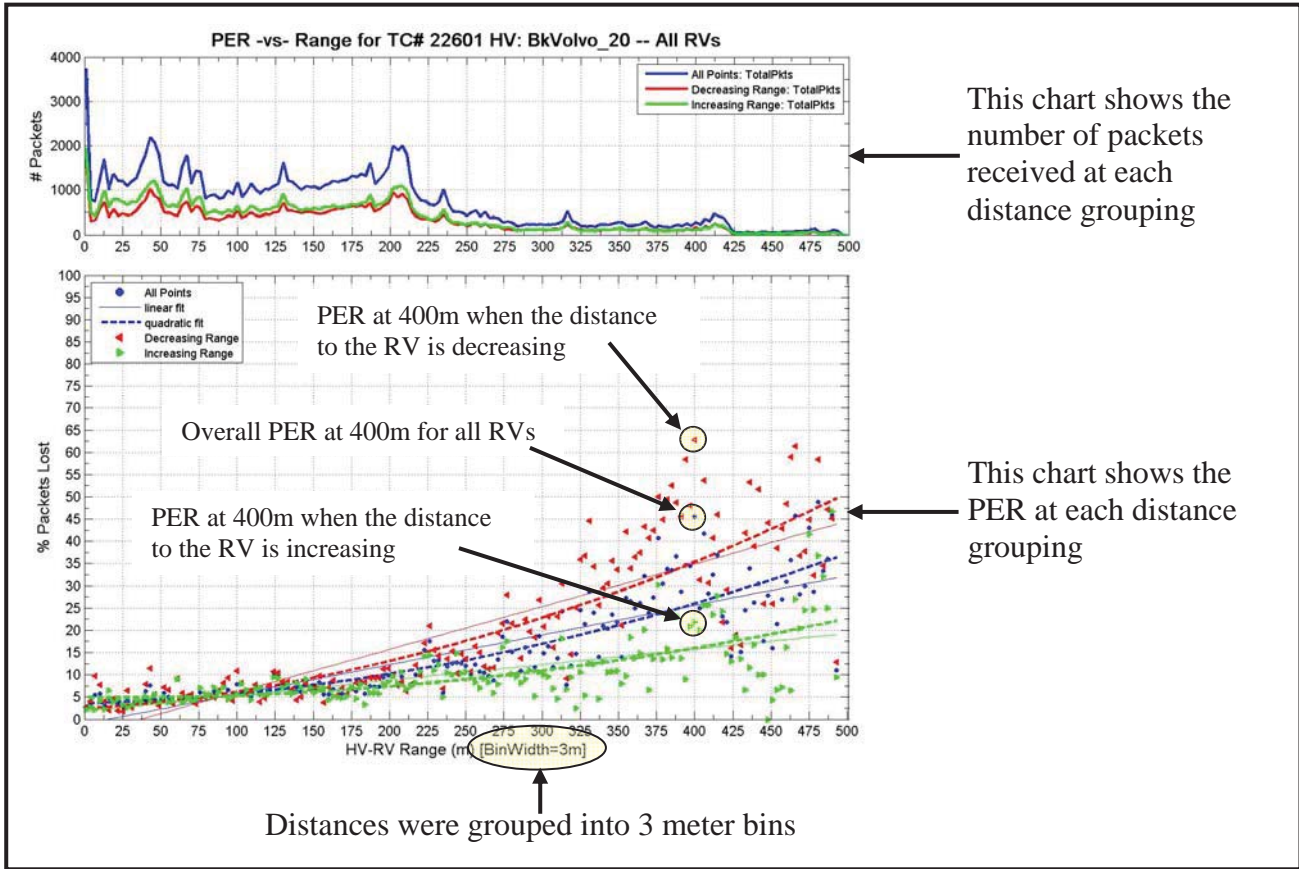


Figure 12: PER vs. Range for Moving Vehicles – Example Plot for 60 Tx Radios

4.2 PER Comparison for Channel Configuration C2 vs. C3

Figure 13 shows a comparison of the results between channel configuration C2 and channel configuration C3 from the perspective of V2 (black Volvo). Similar to the stationary tests, C2 has better PER versus range performance than C3. The results from the perspective of V3 (dark blue Cadillac) are similar and thus not presented. The remaining data analysis sections will go into more details on what the charts show.

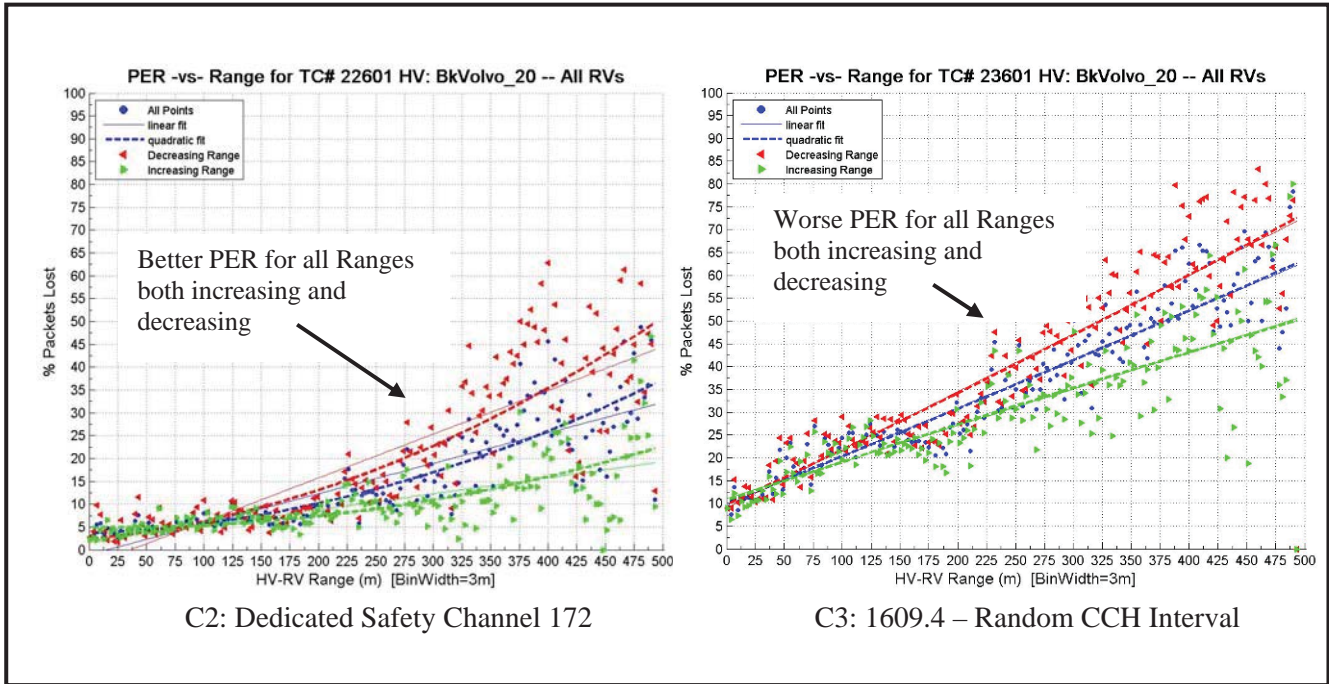


Figure 13: PER vs. Range for Moving Vehicles – C2 vs. C3 – 60 Tx Radios

4.3 Cumulative PER for Moving HV with Moving Blocking RV

Figure 14 shows the PER versus range for a moving HV (V2 black Volvo) with a moving blocking RV (V1 blue Acura) for all of the RVs the HV was in communication with. The top chart shows that packets were received from other vehicles at all distances from 0-500m, but most vehicles were within 250m due to the test layout and driving patterns (Figure 11). The bottom chart shows that the PER from RVs located in front of the HV (decreasing range) is worse than from RVs located behind (increasing range). This difference is more noticeable at greater distances. This may be caused from the RV being located in front of the HV, reducing the ability for the HV to receive messages from the forward direction.

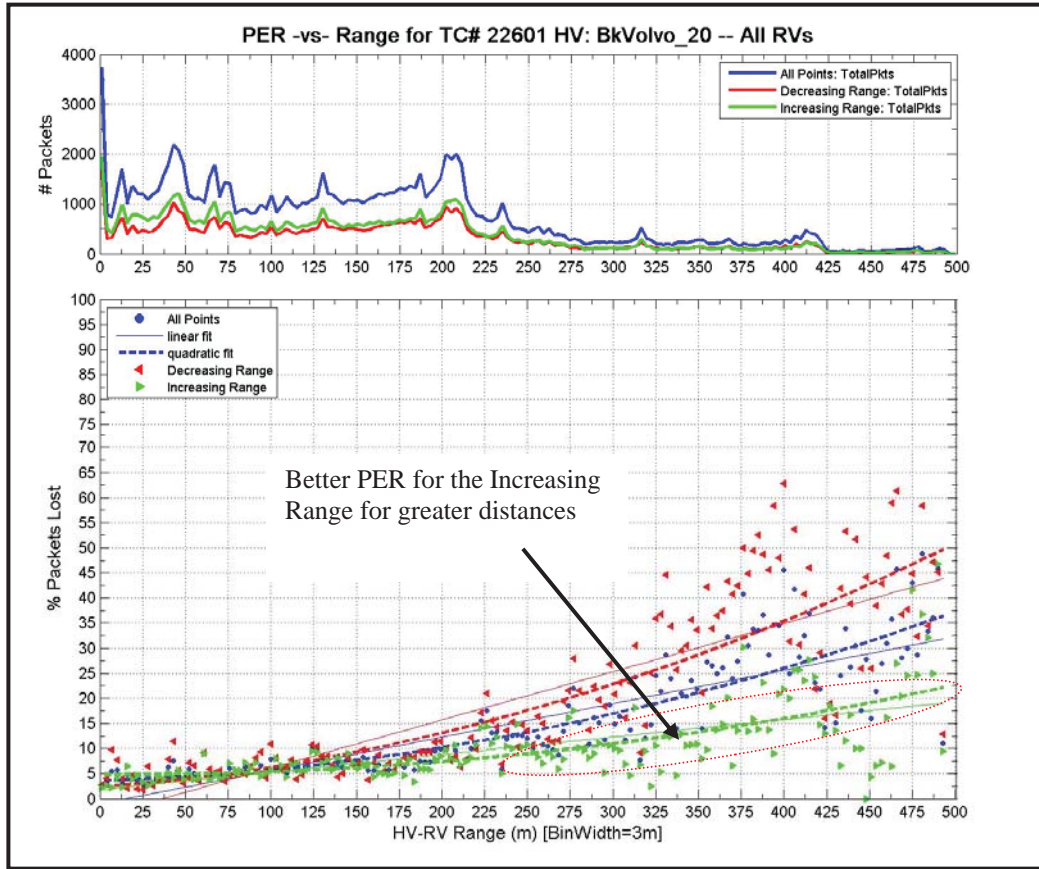


Figure 14: PER vs. Range for Multiple RVs – Moving HV w/ Blocking RV – Ch. Cfg. 2 – 60 Tx Radios

Figure 15 shows the PER versus range from the HV perspective for the principle moving RV that the HV was traveling behind. The top chart shows the distance between the HV and RV ranged between 10m to 60m while the bottom chart shows that the PER from the leading RV to the following HV was less than 10% for most of the distances measured. The congestion level of 60 transmitting radios did not appear to affect the PER of the RV at these relatively close distances.

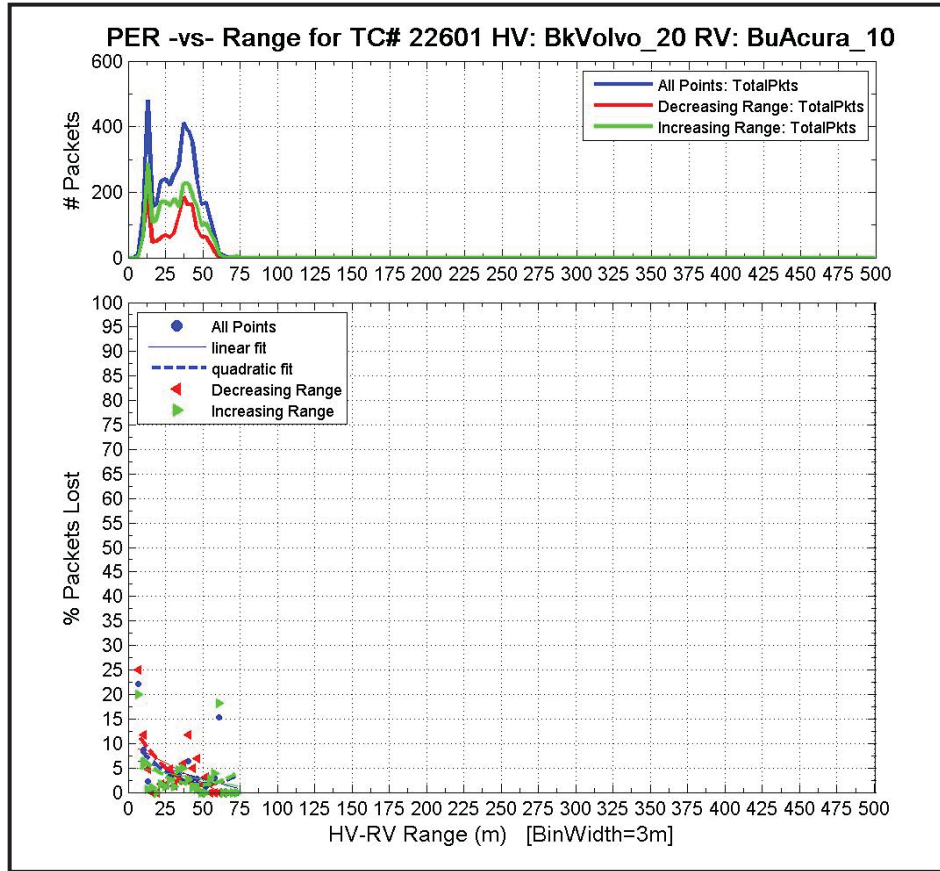


Figure 15: PER vs. Range for Principle RV – Moving HV w/ Blocking RV – Ch. Cfg. 2 – 60 Tx Radios

4.4 Cumulative PER for Moving HV w/ Moving Semi-Blocking RV

Figure 16 shows the PER versus range for a moving HV (V6 red Prius) with a moving semi-blocking RV (V5 light blue Cadillac) for all of the RVs the HV was in communication with. The top chart shows that packets were received from other vehicles at all distances from 0-325m. However, most vehicles were within 225m due to the test layout and driving patterns (Figure 11). The bottom chart shows that the PER from RVs located in front (decreasing range) and behind (increasing range) the HV appears similar. Unlike the previous test, due to the HV and RV driving at opposite ends of the loop in this test, the RV did not continuously block the HV. This may account for the loose grouping of points between 175m and 300m for both the increasing and decreasing range. The slightly better PER observed at the 275-325m range is caused from communication with Pods 8 and 9 which were generally line of sight.

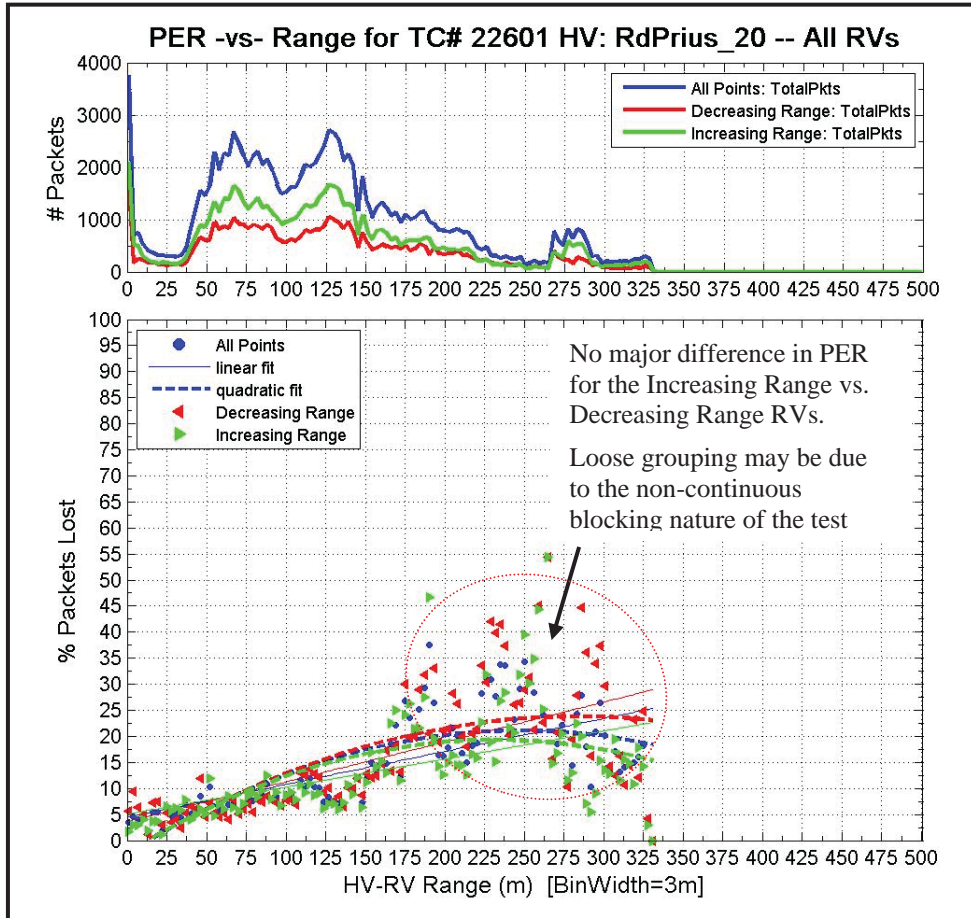


Figure 16: PER vs. Range for Multiple RVs – Moving HV w/ Semi-Blocking RV – Ch. Cfg. 2 – 60 Tx Radios

Figure 17 shows the PER versus range from the HV perspective for the principle moving RV that the HV was traveling with. The top chart shows the distance between the HV and RV ranged between 5m to 100m while. The bottom chart shows the PER of the RV, measured at the HV, was better from the forward direction than the rear. Since the vehicles were relatively close and there were not any obstructions between the two vehicles, the difference in PER may have been caused by antenna placement or vehicle roof curvature.

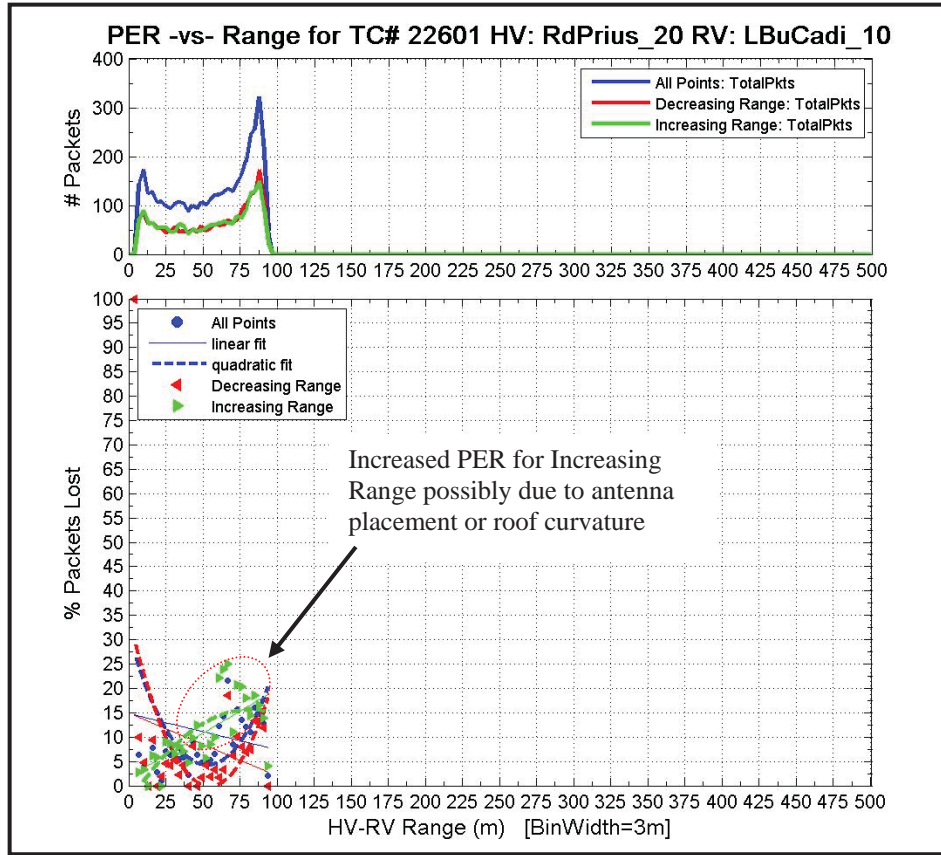


Figure 17: PER vs. Range for Principle RV – Moving HV w/ Semi-Blocking RV – Ch. Cfg. 2 – 60 Tx Radios

4.5 Cumulative PER for Stationary HV

Figure 18 shows the PER versus range for a stationary HV (pod 2) for all of the RVs the HV was in communication with. The top chart shows that most packets received by the HV were at specific distances. Since the HV was stationary these correspond to the stationary RVs (pods and vehicles) in the test. The packets from the moving RVs were received at distances from 0-225m with the furthest stationary pod being at 275m. Recall that packets received from an RV where there is no change in the distance are categorized as “Increasing Range,” thus, the green spikes for each of RVs that are stationary with respect to the HV. The bottom chart shows that the PER from all RVs moving towards or away from the stationary HV appears similar. Additional PER results (not shown) between pod 2 and specific RVs also do not show any clear difference in either direction.

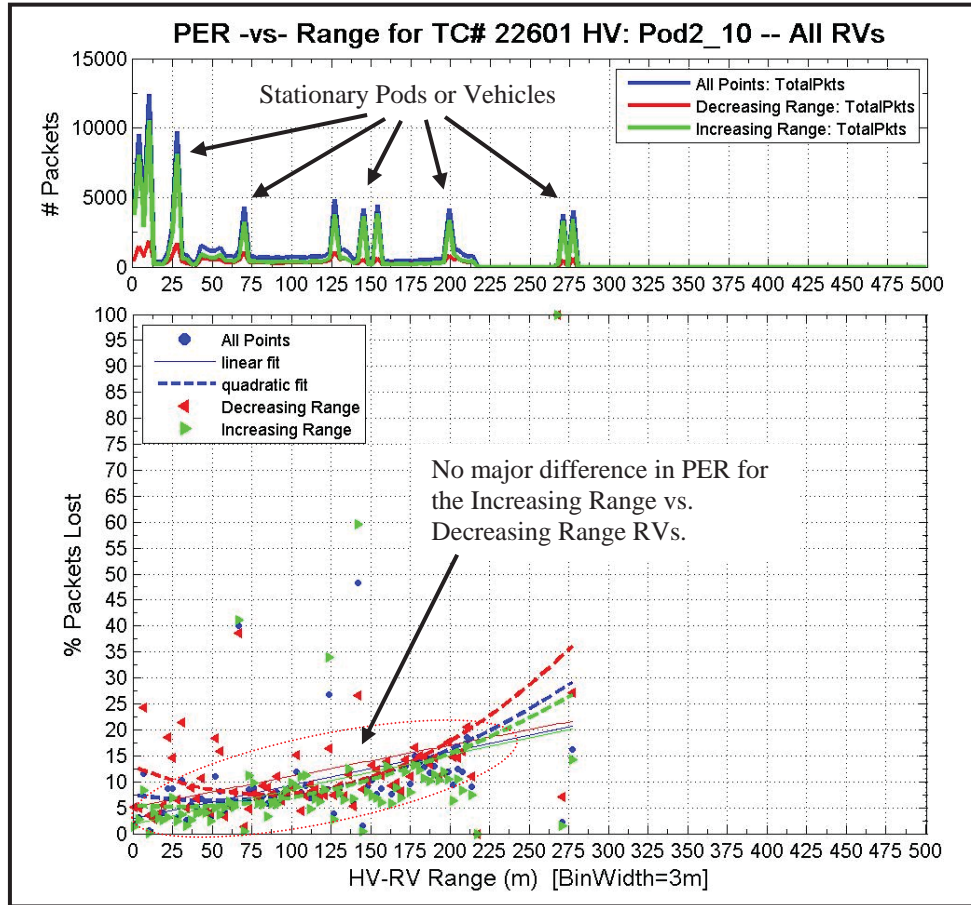


Figure 18: PER vs. Range for Multiple RVs – Stationary HV – Ch. Cfg. 2 – 60 Tx Radios

4.6 PER Comparison for Stationary vs. Moving Vehicle Tests

Figure 19 below shows a comparison of the PER versus range for the stationary test compared to the moving tests. While the stationary tests have less coverage across all possible ranges, the stationary PER results show somewhat better performance than the moving results. The increasing range moving results, with a moving HV and blocking moving RV, have similar performance to the static test results for corresponding ranges out to approximately 300m which was the maximum tested range for the all-static configuration. The increasing range moving results with a moving HV and semi-blocking RV are somewhat worse when compared to the static test which may be caused by the RV periodically blocking the HV.

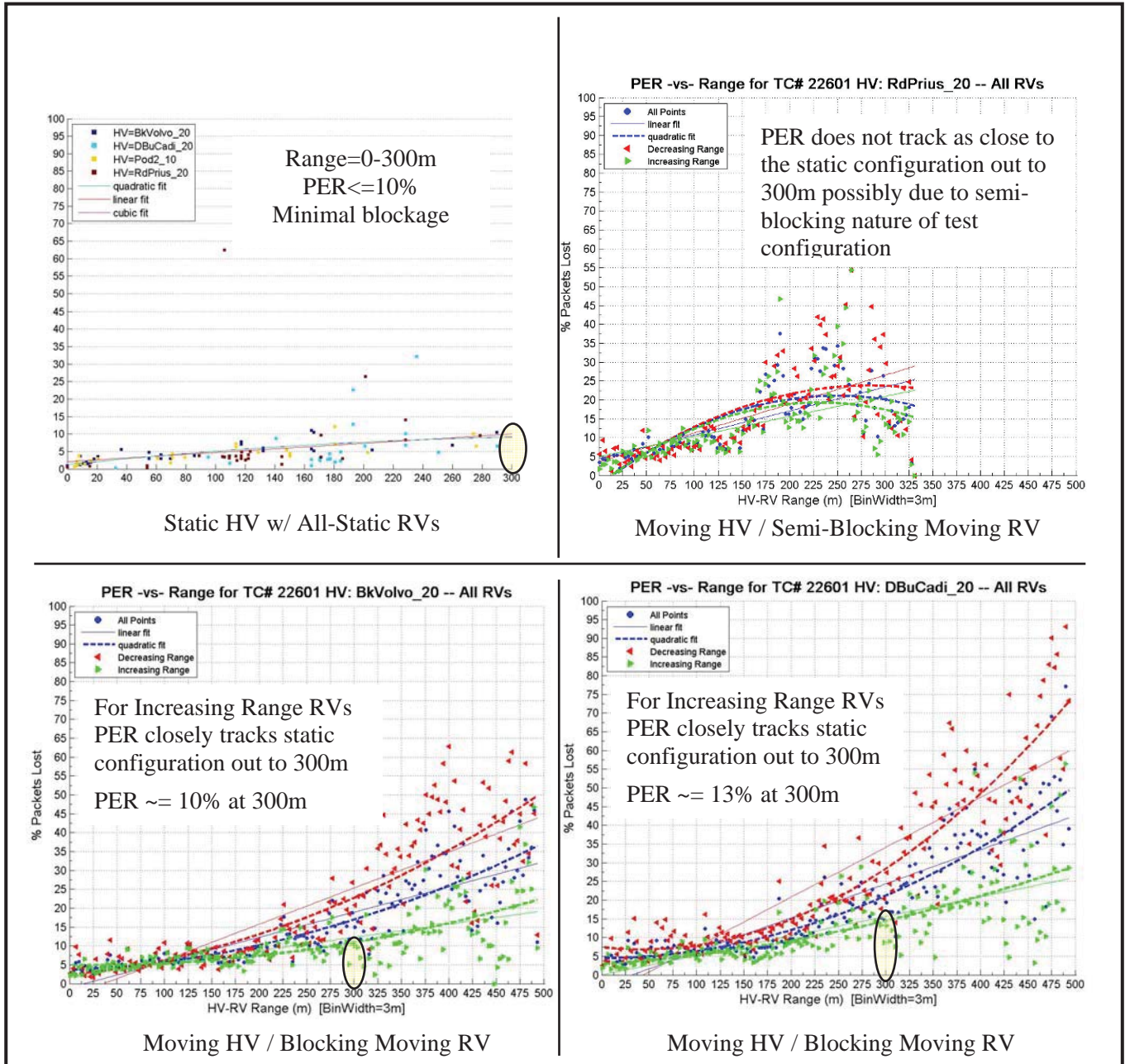


Figure 19: Stationary vs. Moving Vehicle Test Comparison – Ch. Cfg. 2 – 60 Tx Radios

4.7 Moving Test Results Summary and Next Steps

In general the following summarizes the conclusions that can be drawn from the preliminary moving scalability test results:

1. Like the stationary test results, the dedicated safety channel configuration (C2) results in superior performance, when considering PER, compared to using the CCH interval (C3) for transmitting periodic safety messages.

2. The moving test results show a greater range of best case and worse case PER. While not conclusive, the difference in PER appears to be caused from blockage from other vehicles, both moving and stationary.
3. The PER between adjacent moving vehicles (less than 60m apart) was less than 10% with 60 RVs when using the dedicated safety channel (C2). Antenna placement on some vehicles may have also affected the PER.
4. The stationary PER test results were overall better than the moving test results, but the “better case” moving PER test results (i.e., presumed without blockage) were similar to the stationary results.

The results in this appendix are a good start for beginning to understand the effects that combinations of moving and static vehicles may have on PER at a particular HV. More analysis needs to be done on the affect a blocking vehicle may have on the PER at a particular HV as well as combinations of blocking vehicles (e.g., multiple vehicles blocking the HV, vehicle blocking the RV, etc.).

As was mentioned in the main body of the final report, some of the next steps include incorporating lessons learned into future projects where Vehicle-to-Vehicle (V2V) system scalability has to be proven beyond the achievable total number of units within this project (i.e., 60). This includes lessons learned in test bed design and development, SW design and stability, and scalability testing logistics.

DOT HS 811 492C
September 2011



U.S. Department
of Transportation
**National Highway
Traffic Safety
Administration**

